CRUSTAL THICKNESS VARIATION IN SOUTH CENTRAL ALASKA:

RESULTS FROM BROADBAND EXPERIMENT ACROSS THE ALASKA RANGE

A

THESIS

Presented to the Faculty

Of the University of Alaska Fairbanks

In Partial Fulfillment of the Requirements

For the Degree of

DOCTOR OF PHILOSOPHY

By

Elizabeth Veenstra, B.Sc., M.Sc.

Fairbanks, Alaska

December 2009

ProQuest LLC
789 East Eisenhower Parkway
P.O. Box 1346
Ann Arbor, MI 48106-1346

CRUSTAL THICKNESS VARIATION IN SOUTH CENTRAL ALASKA:

RESULTS FROM BROADBAND EXPERIMENT ACROSS THE ALASKA RANGE

By

Elizabeth Veenstra

RECOMMENDED:

Roger A. Hansen

Jeffrey T. Freymueller

Rebecca K. Wallace

D. B. Stone

Douglas H. Christensen

Advisory Committee Chair

Michael T. Williams

Chair, Department of Geology and Geophysics

APPROVED:

Dean, College of Natural Science and Mathematics

Lawrence K. Duffy

Dean of the Graduate School

Nov 30, 2009

Date

Abstract

The Broadband Experiment Across the Alaska Range (BEAAR) was a passive source seismic study in which 36 three-component broadband seismic stations were deployed over a period of 27 months to collect high quality data to study the Alaska Range and perhaps elucidate tectonic processes. The wavetrain of a teleseismic body wave may be interpreted in terms of reflection and transmission of waves converted at discontinuities. The recorded signal may be regarded as a convolution of the source-time function, the receiver function, and the instrument response. A receiver function is the contribution to the seismic waveform recorded at a single station due to the response of local crustal structure, and can be inverted for vertical velocity structure beneath the three-component broadband seismic station. Receiver function analyses reveal typical crust beneath the lowlands north of the Alaska Range is 26 km thick, while beneath the mountains typical crust is 35–45 km thick. Receiver function analysis of ~15,000 teleseismic waveforms recorded by BEAAR broadband seismometers provided over 100 crustal thickness data points. Similarity between crustal thicknesses determined from receiver function analysis and crustal thicknesses predicted from topography assuming Airy isostasy indicate the observed crustal root is sufficient to support the Alaska Range. North of the range, however, the crust is systematically thinner than predicted by simple Airy isostasy. A crustal density contrast of 4.6% across the Hines Creek Fault, 2700 kgm^{-3} to the north and 2830 kgm^{-3} to the south, explains the observed difference between the crustal thicknesses predicted by simple Airy isostasy and the crustal thicknesses determined by receiver function analysis. Our results indicate that variations in both crustal thickness and density are required to explain the seismic and gravity data. Crustal thicknesses across the central Alaska Range suggest that these mountains are supported by a crustal root developed due to contractional thickening. Crustal thickness data reveal differences in terrane thickness: a thin Yukon-Tanana terrane north of the Hines Creek fault and thicker Kahiltna/Wrangellia terranes to the south. Finally, the pattern of thin crust to the north and thicker crust to the south appears to be modified by late Cenozoic structures such as the Denali fault, with contractional thickening in the Alaska Range, including areas north of the Hines Creek fault in the northern foothills fold and thrust belt. BEAAR crustal thickness data suggest that major faults extend to the base of the crust.

Table of Contents

List of Figures

Page

List of Tables

List of Appendices

Acknowledgments

This work benefited from contributions by many individuals, including intense physical labor during the field deployment. Instrumentation was provided by the Program for the Array Seismic Studies of the Crustal Lithosphere of the Incorporated Research Institutions for Seismology. Thanks to friends at the Alaska Earthquake Information Center for field assistance, and University of Alaska Fairbanks Office of Land Management personnel for assistance obtaining land use permits. Figures were made using Generic Mapping Tool (Wessel and Smith, 1995). The National Science Foundation financially supported BEAAR under award EAR-9725168. Reviews by committee members Wes Wallace and Jeff Freymueller helped significantly in the final stages of writing. Finally, thanks to Mom, Dad, and Little One.

Chapter 1 - Introduction

Continental deformation and wide plate boundary zones represent a departure from the simple rigid plate model of plate tectonics. The simplest rigid plate tectonic model assumes no interior deformation of the plate, and boundaries between plates are sharp and distinct. The majestic mountains that we observe associated with plate boundaries, and the relatively diffuse nature of actual plate boundaries, indicate that the simple rigid plate model is incomplete. In addition, little is known about the relative importance of dynamic and structural mechanisms of uplift in creating and sustaining the topography above subduction zones. Numerical experiments suggest that topography above subduction zones is due to plate coupling and the transmission of horizontal compressive stress (e.g. England and McKenzie, 1982) resulting in structural thickening. Other studies suggest that topography above subduction zones results from dynamic forces acting on the base of the crust (e.g. Melosh and Raefsky, 1980). Dynamic forces could include buoyancy due to high heat flow, heat introduced from the mantle or perhaps even magma trapped beneath the crust. Alternatively, one might postulate support provided by an underlying buoyant subducted slab. Observations of crustal thickness help us discriminate between models to provide a better understanding of how mountains are supported.

The Broadband Experiment Across the Alaska Range (BEAAR) project was a passive source seismic study undertaken to collect high quality data that could be used by a number of scientists to better understand the Alaska Range in particular and tectonic processes in general. This goal of amassing a high quality seismic database with unrivaled coverage, completeness, and detail in the Alaska Range has been achieved. The raw seismic data are available to the public through the Incorporated Research Institutions for Seismology (IRIS) Data Management Center. This thesis provides details of the receiver function analysis, constraining crustal thickness across the Alaska Range.

To begin, I introduce the tectonic setting of south-central Alaska, followed by previous crustal thickness studies and the BEAAR project.

Physiographic and Tectonic Setting

The North American Cordillera, less commonly known as the Pacific Mountain system of North America, runs from Alaska to Central America. Between the Pacific Ocean and the interior plains of North America are two rugged mountain belts with an intermontane lowland. In Alaska, the northern cordillera includes the Brooks Range, which connects to the Rocky Mountain System, while the southern cordillera includes the Aleutian Range - Alaska Range, which broadly arcs around to the southeast to connect to the Boundary Ranges (Figure 1). The intermontane region in our study area includes the Yukon-Tanana upland as well as the Tanana-Kuskokwim lowland. The southern cordillera forms a broad arc as it changes from southwest trending topography in the Aleutian Range, to complex arcuate east-west trending

topographic belts in the central interior Alaska Range, to predominantly northwest trending topographic belts in the Alaskan panhandle and Canada. The southern cordillera in south central Alaska may be considered two arcuate mountain ranges with an intervening lowland: the Alaska-Aleutian province to the north and the Pacific Border Ranges (Kenai-Chugach-St. Elias) to the south with Coastal Trough (Cook Inlet – Susitna lowland – Copper River lowland) in between. The Talkeetna Mountains interrupt the lowland between the Alaska-Aleutian province and the Pacific Border Ranges, all part of the southern mountain belt of the North American Cordillera in south central Alaska.

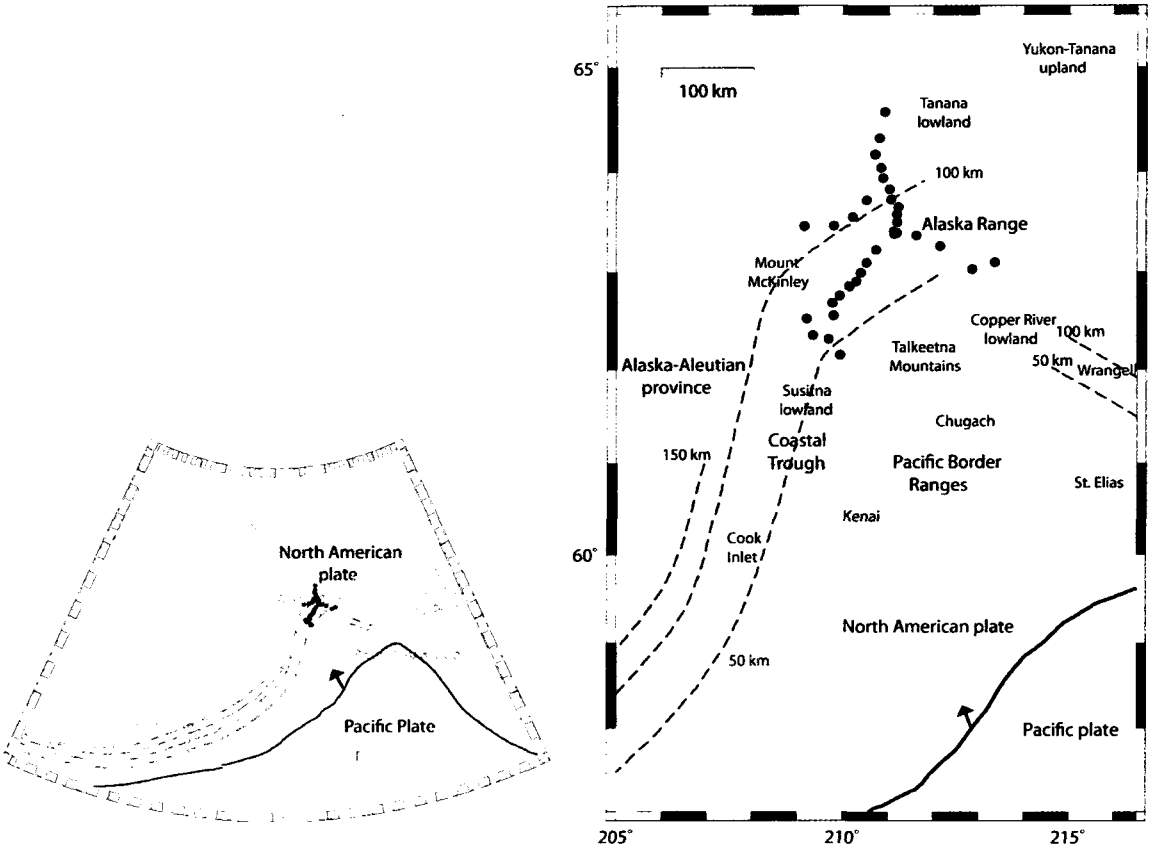

Figure 1: Physiographic and tectonic setting. Shading indicates land surface topography. Dashed lines represent Wadati-Benioff zone isopleths at 50km intervals down to 200 km. Solid line locates North American - Pacific plate boundary, arrow represents 5.5 cm/yr Pacific plate motion vector. Dots indicate BEAAR station locations.

The complex tectonics of southern Alaska are produced by the interaction of the North American and Pacific plates (Figure 1). Active seismicity indicates the Pacific plate is subducting beneath the North American plate (Gedney, 1970; van Wormer et al., 1974; Lahr, 1975; Davies, 1975). Seismicity abates at approximately 200 km depth, interpreted to be the down-dip reflection of the Pacific plate. Reconstructions (Delong et al., 1978; Wallace and Engebretson, 1984; Engebretson et al., 1985; Ridgway

et al., 2002) include relative motion vectors between Alaska (North America + accreted terranes) and the Farallon, Kula, and Pacific plates. The Pacific plate is currently moving northwest relative to Alaska, with dominantly dextral strike slip along the Queen Charlotte and Fairweather transform fault system to the east, and normal to oblique subduction along the Aleutian megathrust. Gently dipping subduction is observed beneath south-central Alaska (Jacob et al., 1977; Davies and House, 1979; Ratchkovski and Hansen, 2002b). The plate boundary at the transition between transform fault and megathrust is complex (Von Huene, 1972; van Wormer et al., 1974; Lahr and Plafker, 1980; Perez and Jacob, 1980; Stone, 1983; Lahr et al., 1988; Fletcher and Freymueller, 1999; Gulick et al., 2007; Wallace, 2008). In south central Alaska most of these complexities are associated with the Yakutat collision zone (Chapman et al., 2008; Fuis et al., 2008; Wallace, 2008). Current convergence rates between the Pacific and North American plates in southern Alaska and along the Aleutian arc increase from 5.5 cm/yr in the east to 7.5 cm/yr in the west (DeMets et al., 1990).

Active seismicity of the Aleutian Wadati-Benioff zone (Biswas, 1973; van Wormer et al., 1974; Davies, 1975; Lahr, 1975; Engdahl and Scholz, 1977; Davies and House, 1979; Pulpan and Frohlich, 1985; Gedney and Davies, 1986; Page et al., 1989; Kissling and Lahr, 1991; Page et al., 1991; Zhao et al., 1995) disappears to the east beneath the Alaska Range. A seismicity map (Figure 2) with epicentral locations of historic events, and a larger scale map of seismicity in interior Alaska (Figure 3) illustrate that seismic activity is common across most of the state (Biswas and Tytgat, 1988; Page et al., 1991; Taber et al., 1991; Ratchkovski and Hansen, 2002a). Isopleths clearly define the Aleutian Wadati-Benioff zone to the west, which changes strike near Mount McKinley, perhaps indicating segmentation of the subducting plate (Kienle et al., 1983; Page et al., 1989; Lu and Wyss, 1996; Ratchkovski, 2001; Ratchkovski and Hansen, 2002b). The Wadati-Benioff zone clearly indicates gently dipping subduction beneath south central Alaska. Abrupt termination of intermediate and deep focus earthquakes near 212° E longitude (Davies, 1975; Stone, 1977; Agnew, 1980; Fuis et al., 2008) leaves the eastern section of the Wadati-Benioff zone beneath south-central Alaska open to interpretation. The weakly defined Wrangell-St. Elias Wadati-Benioff zone (Stephens et al., 1984; Page et al., 1989) is enigmatic.

Active arc volcanism also disappears to the east beneath the Alaska Range (Jacob et al., 1977; Nye et al., 2002). Coats (1962) noted the volcanic front is roughly 110 km above the seismic zone, and similarly Jacob et al. (1977) recognized the coincidence of the surface projection of the 100 km depth contour of the Wadati-Benioff zone and arc volcanoes (Figure 4). The kinematically defined trench-volcano distance widens as subduction shallows, as occurs in south central Alaska. Alaskan volcanoes associated with Aleutian trench subduction near the study area include (south to north) Augustine, Iliamna, Redoubt, Spurr, and Hayes (Kienle et al., 1983). The Buzzard Creek Volcanics (Figure 4) are just

tiny cinder cones, but this 3,000 year old small volume monogenetic volcanism is located near the surface projection of the 100 km isopleth, and has recently been shown to have the unique and unmistakable geochemical trace-element signature of arc volcanism (Nye, 1999; Nye et al., 2002). The absence of long-lived volcanoes from the north-easternmost 320 km of the seismically defined subduction zone has been called the Denali Volcanic Gap (Nye et al., 2002). The Wrangell volcanoes are similar to Aleutian volcanoes in composition and age, but differ in form and eruptive behavior (Nye, 1983; Miller and Richter, 1994). Wrangell volcanoes are much larger than Aleutian volcanoes. Wrangell volcanoes are more shield-like and appear non-explosive. The numerous volcanoes in south central Alaska are related to underthrusting of Pacific plate beneath North American continental crust.

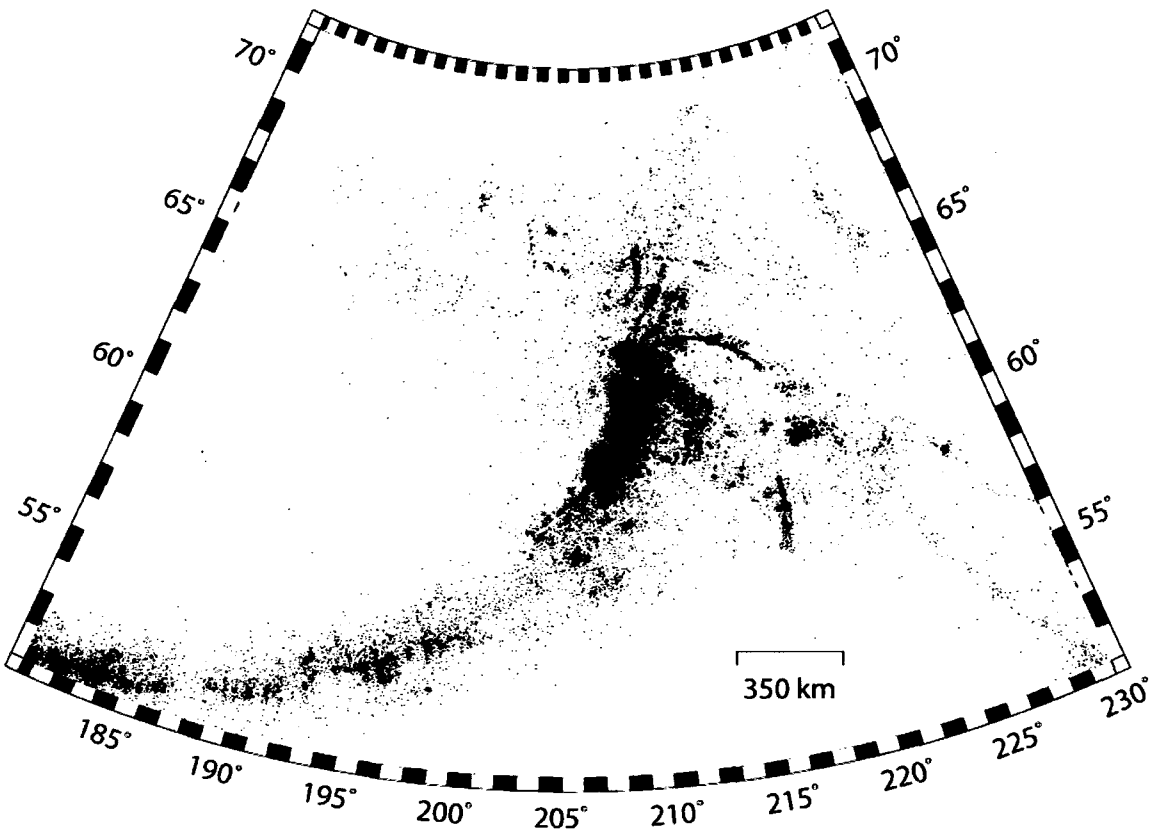

Figure 2: Historical seismicity showing epicentral locations of earthquakes with magnitude ≥2.0, 0-350 km depth, between 1898 and May 2008. Land surface shading indicates topography with lighter colors indicating mountainous regions.

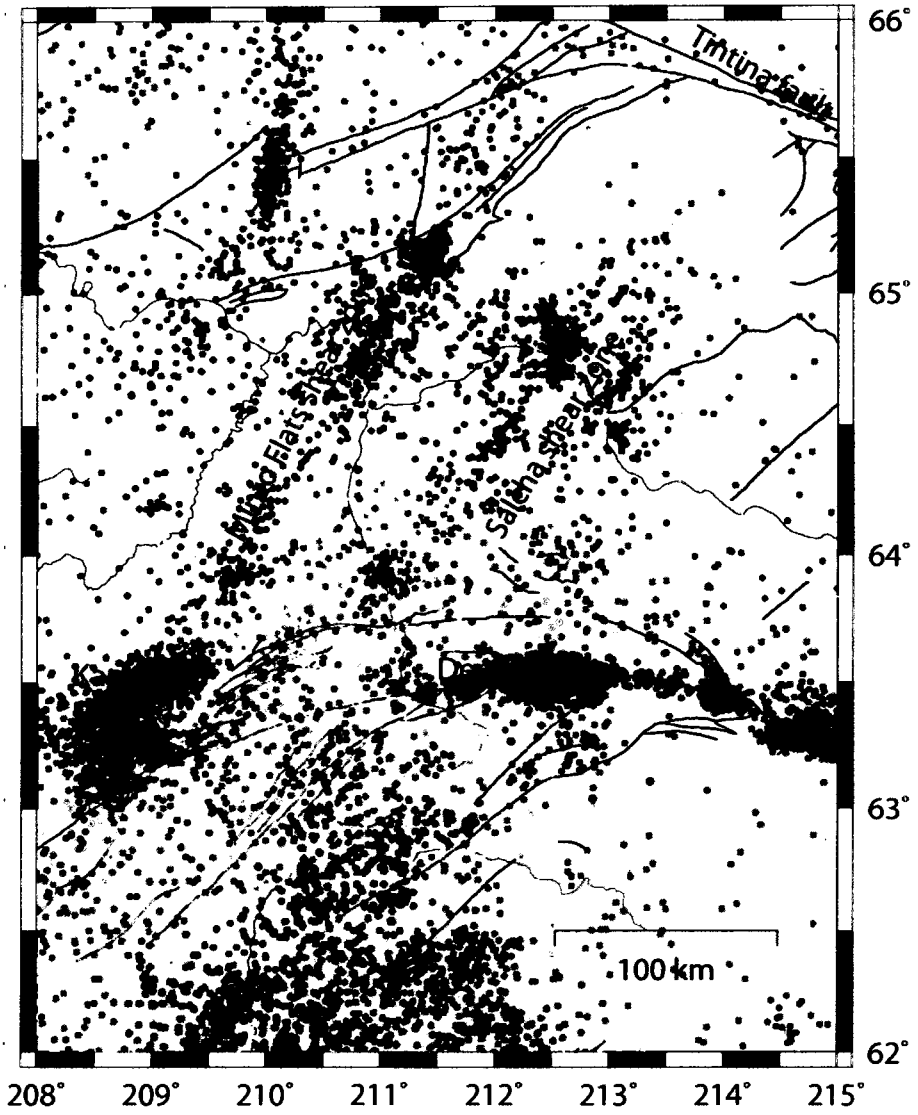

Figure 3: Map of interior Alaska seismicity (historic events 1898 - May 2008). Crustal events (0-35 km) are located with blue dots and reveal seismic zones (e.g. Minto Flats seismic zone and Salcha seismic zone) and clusters of seismicity (e.g. Kantishna seismic cluster [Burris, 2007]). Intermediate to deep events, plotted with green (35-75 km), yellow (75-125 km) and red (125-350 km), locate the Wadati-Benioff zone where the Pacific slab is subducting beneath the North American plate. Black dots indicate BEAAR station locations, blue lines represent rivers, and black curvilinear lines represent mapped faults. (Some information is obscured by the abundance of seismic event locations.)

There are many interesting facets of interior Alaska seismicity. For example, between the Denali fault and the Tintina fault, both dominantly right lateral strike slip fault systems, we observe dominantly left lateral shear zones such as Minto Flats and Salcha seismic zones, roughly linear features in the shallow crustal seismicity. This shallow crustal seismicity pattern reflecting transpression and block rotation

between 63°N and 66°N contrasts sharply with the deeper seismicity pattern to the south which is dominated by collision and subduction.

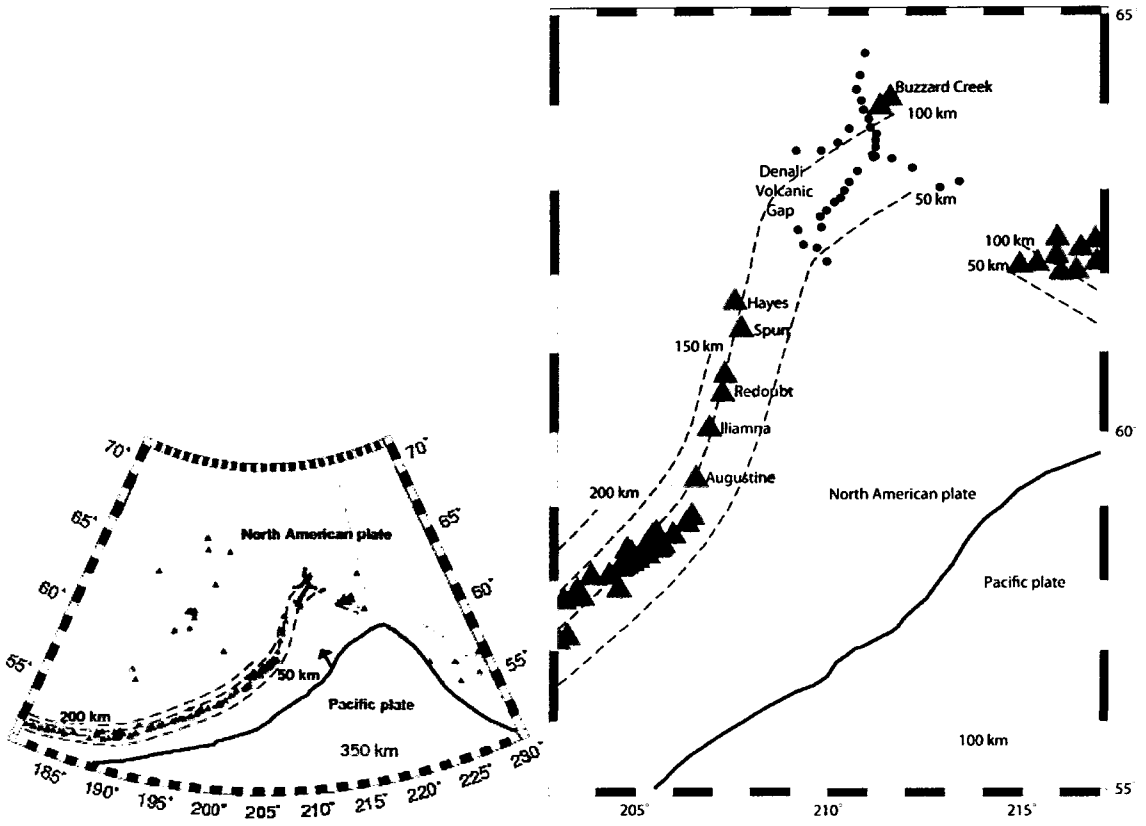

Figure 4: Map of volcanic centers. Solid line indicates plate boundary, dashed lines represent Wadati-Benioff zone 50 km contours, and triangles indicate the location of volcanic centers. Arc volcanoes typically coincide with surface projection of the 100 km Wadati-Benioff zone depth contour. Notice the lateral distance between plate boundary and volcanic centers. Volcanic centers such as Augustine, Iliamna, Redoubt, Spurr, Hayes, and Buzzard Creek illustrate wider trench-volcano distance across this region of gently dipping subduction.

Terranes

South-central Alaska is recognized as an accumulation of numerous allochthonous tectonostratigraphic terranes (Jones et al., 1972, 1977, 1982, 1987; Packer and Stone, 1972, 1974; Coney et al., 1980; Panuska and Stone, 1981, 1985; Howell, 1985; Stone et al., 1982; Panuska, 1985; Monger and Berg, 1987; Stone and Wallace, 1987; Ridgway et al., 2002) that reflect a complex tectonic history. The terranes were detached from the subducting slabs as the dense oceanic Pacific/Kula/Farallon plates subducted beneath North America, and then shoved about and rearranged considerably over the past 200+ Ma. In general, the present structural configuration of south-central Alaska was created as a result of large scale translations and rotations in the Cretaceous and Tertiary (Plafker and Berg, 1994).

Tectonic affinities of terranes across the Alaska Range include a metamorphosed continental margin, turbidite basins, and displaced magmatic arcs (Plafker and Berg, 1994). Relatively large expanses are covered by the Yukon-Tanana terrane to the north, Wrangellia and Peninsular terranes to the south, and Kahiltna terrane in between (Silberling et al., 1994). The Yukon-Tanana composite terrane consists of dominantly continental rocks metamorphosed during collision with North America, which were later extended in the mid- to late-Mesozoic. The Wrangellia and Peninsular terranes have evolved arc affinities. The Wrangellia and Peninsular terranes collided outboard of the Yukon-Tanana during mid- to late-Mesozoic time in a complex multi-phase process. The Kahiltna is a deep marine basinal terrane, tectonically collapsed between the metamorphosed continental margin affinity rocks of the Yukon-Tanana, and the outboard arc affinity rocks of the Wrangellia and Peninsular terranes (Wallace and Engebretson, 1984; Pavlis et al., 1993; Plafker and Berg, 1994; Ridgway et al., 2002).

Figure 5 shows BEAAR station locations plotted with respect to terranes identified in the literature. The three most extensive major terranes are the Yukon-Tanana, Wrangellia, and Kahiltna terranes. In addition to these major terranes in our study area, several small narrow terranes are adjacent to the Denali fault in the central and eastern Alaska Range, including the Aurora Peak (Aleinikoff, 1984; Aleinikoff et al., 1987; Brewer, 1982; Nokleberg et al., 1985, 1989, 1992b; Ridgway et al., 1997), McKinley (Reed and Nelson, 1980; Jones et al., 1981, 1982, 1983, 1984, 1987; Gilbert et al., 1984), Mystic (Jones et al., 1982, 1983, 1984, 1987; Reed and Nelson, 1980), Pingston (Jones et al., 1981, 1982, 1983, 1984, 1987; Gilbert et al., 1984; Nokleberg, et al., 1994; Reed and Nelson, 1980), Windy (Jones et al., 1984, 1987; Nokleberg and Aleinikoff, 1985; Nokleberg et al., 1985, 1986, 1989, 1992a, b, 1994; Stanley et al., 1990), and Dillinger terranes (Jones et al., 1982; Gilbert and Bundtzen, 1984; Patton et al., 1989, 1994; Ridgway et al., 1997). In addition to those terranes adjacent to the Denali fault, a number of other smaller terranes are in our study area (Jones and Silberling 1979; Silberling et al., 1994). Those that occur south of the Denali fault, tectonically intermixed with the Kahiltna assemblage as rootless nappes or steeply dipping fault bound units, include the Chulitna (Nichols and Silberling, 1979; Jones and Silberling, 1979; Jones et al., 1980; Nokleberg et al., 1994), Susitna (Jones et al., 1980, 1982; Nokleberg et al., 1994), West Fork (Jones et al., 1982; Csejtey et al., 1986), Broad Pass (Jones et al., 1982; Csejtey et al, 1986; Nokleberg et al., 1994), Maclaren (Smith and Lanphere, 1971; Turner and Smith, 1974; Smith, 1981; Nokleberg et al., 1982, 1985, 1989, 1992ab; Csejtey et al., 1986; Dusel-Bacon, 1991, 1994; Dusel-Bacon et al., 1994; Forbes et al., 1973a, b; Smith et al., 1974; Eisbacher, 1976; Stout and Chase, 1980; Ridgway et al., 1997), and Clearwater terranes (Jones et al., 1984; Nokleberg et al., 1985, 1992ab; Csejtey et al., 1986; Dusel-Bacon et al., 1994).

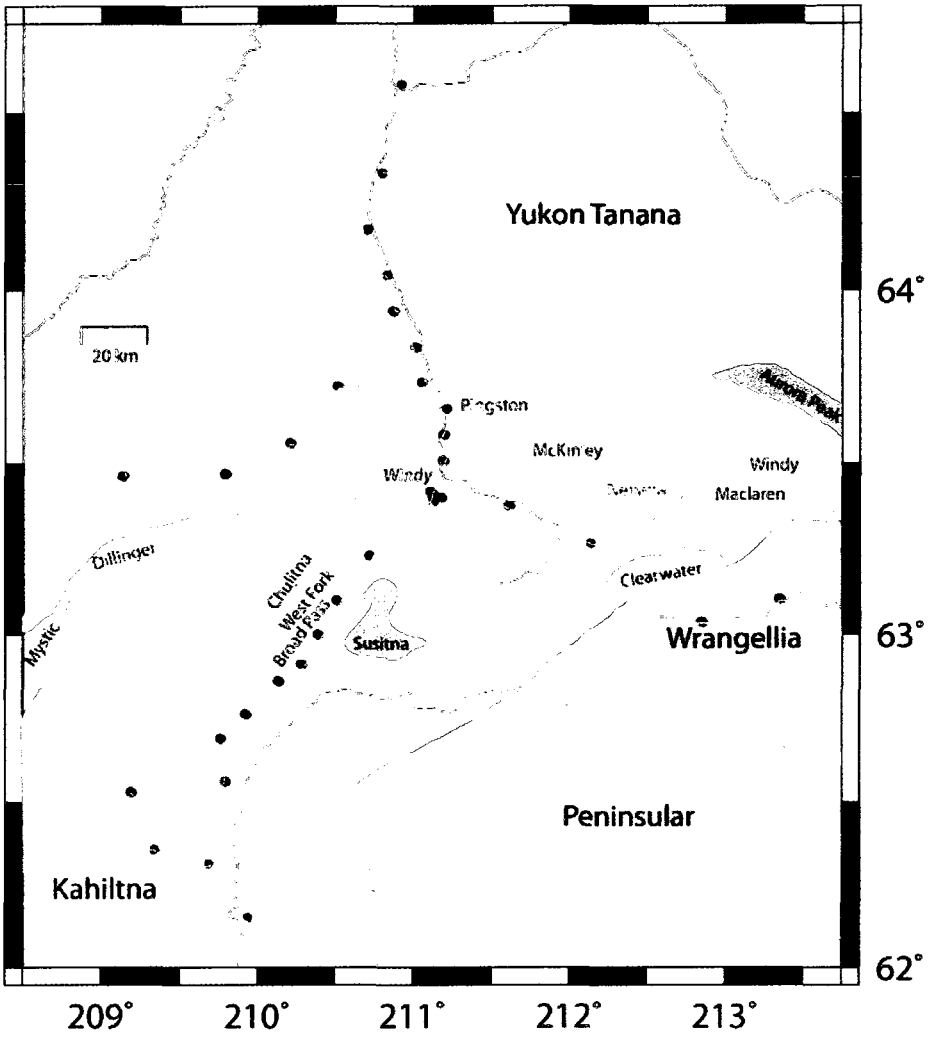

Figure 5: Terrane map. The Yukon-Tanana, Wrangellia, Peninsular, and Kahiltna terranes are major terranes. Narrow terranes identified adjacent to the Denali fault in the central and eastern Alaska Range include Aurora Peak, McKinley, Mystic, Pingston, Windy, and Dillinger terranes. Chulitna, Susitna, West Fork, Broad Pass, Maclaren, Nenana, and Clearwater terranes are tectonically intermixed with Kahiltna. Dots indicate BEAAR station locations.

Evidence suggests substantial displacements along major faults and significant dismemberment of terranes, but details of the tectonic history of terranes in south-central Alaska remain elusive. The origin of many of the smaller terranes is speculative, and to complicate interpretation of existing data, discrepancies and apparent contradictions between different types of data are common. For example, different sets of paleomagnetic data (van der Voo et al., 1980; Yole and Irving, 1980; Hillhouse and Gromme, 1984; Haeussler et al., 1989; Gardner et al., 1988; Plafker et al., 1989; Stamatakos et al., 2001) and paleontologic data (Newton, 1983; Silberling, 1985; Detterman, 1988) suggest different timing and

amounts of terrane displacement and amalgamation. The tectonic activity along the continental margin has been recorded via deposition of sedimentary rocks, emplacement of plutonic rocks and eruption of volcanic rocks, as well as metamorphic overprinting, most of which have been structurally rearranged by relative motion along the plate margin.

Structure

South-central Alaska is made up of terranes, fault-bounded allochthonous fragments added to a craton at an active margin by accretion, which are displaced laterally by strike-slip motion (Ridgway et al., 2002; Nokleberg and Richter, 2007; Pavlis and Roeske, 2007; Haeussler, 2008). It is important to recognize that the seismically active and named faults are in general not original terrane emplacement faults. Weak zones are reactivated and recycled in response to changes in stress. In a region of transpression with many small blocks, a single fault plane will likely accommodate pure strike-slip, thrust, or oblique slip at varying times in its history.

The seismically active Denali fault is one of the most obvious structural features in the Alaska Range having cut an arcuate path through the mountains (Figure 6). The Denali fault is a dominantly dextral strike-slip fault consisting of many individual fault segments (Sainsbury and Twenhofel, 1954; St. Amand, 1954, 1957; Twenhofel and Sainsbury, 1958; Grantz, 1966; Denton and Stuiver, 1967; Hickman, 1971; Richter and Matson, 1971; Stout et al., 1973; Reed and Lanphere, 1974; Brogan et al., 1975; Wahrhaftig et al., 1975; Packer et al., 1975; Hickman et al., 1977; Plafker et al., 1977, 1989, 1994; Lanphere, 1978; Clague, 1979; Stout and Chase, 1980; Savage et al., 1981; Csejtey et al., 1982; Nokleberg et al., 1985, 1994; Savage and Lisowski, 1991; Redfield and Fitzgerald, 1993; Kikuchi and Yamanaka, 2002; Eberhart-Philips et al., 2003; Hreinsdóttir et al., 2003; Lu et al., 2003; Ozacar et al., 2003; Ratchkovski 2003; Ratchovski et al., 2003, 2004; Wright et al., 2003; Doser, 2002, 2004; Dreger et al., 2004; Fisher et al., 2004a, b; Haeussler et al., 2004; Oglesby et al., 2004; Matmon et al., 2006; Haeussler, 2008), along which we observe juxtaposition of significantly different terranes in the central and eastern Alaska Range (Hickman and Craddock, 1976; Richter, 1976; Sherwood and Craddock, 1979; Jones et al., 1987; Brewer, 1982; Sherwood et al., 1984; Nokleberg et al., 1985, 1992b, 1994; Ridgway et al., 1997). The amount, timing and sense of displacement along different segments of the Denali fault continue to be pieced together as new evidence is documented (Forbes et al., 1973a, b; Turner, et al., 1974; Doser, 2002, 2004; Ratchkovski et al., 2004). Seismic data patterns from the 2002 Denali fault events show connection between the Denali fault and the Totschunda fault, which branches from it to the southeast. The Totschunda fault likely connects to the Fairweather fault farther south (Richter and Matson, 1971; Kalbas et al., 2008), creating an arcuate boundary along which northward subduction of the Pacific plate and

collision of the Yakutat terrane could produce counter-clockwise rotation of the southern Alaska block (Lahr and Plafker, 1980; Fletcher, 2002).

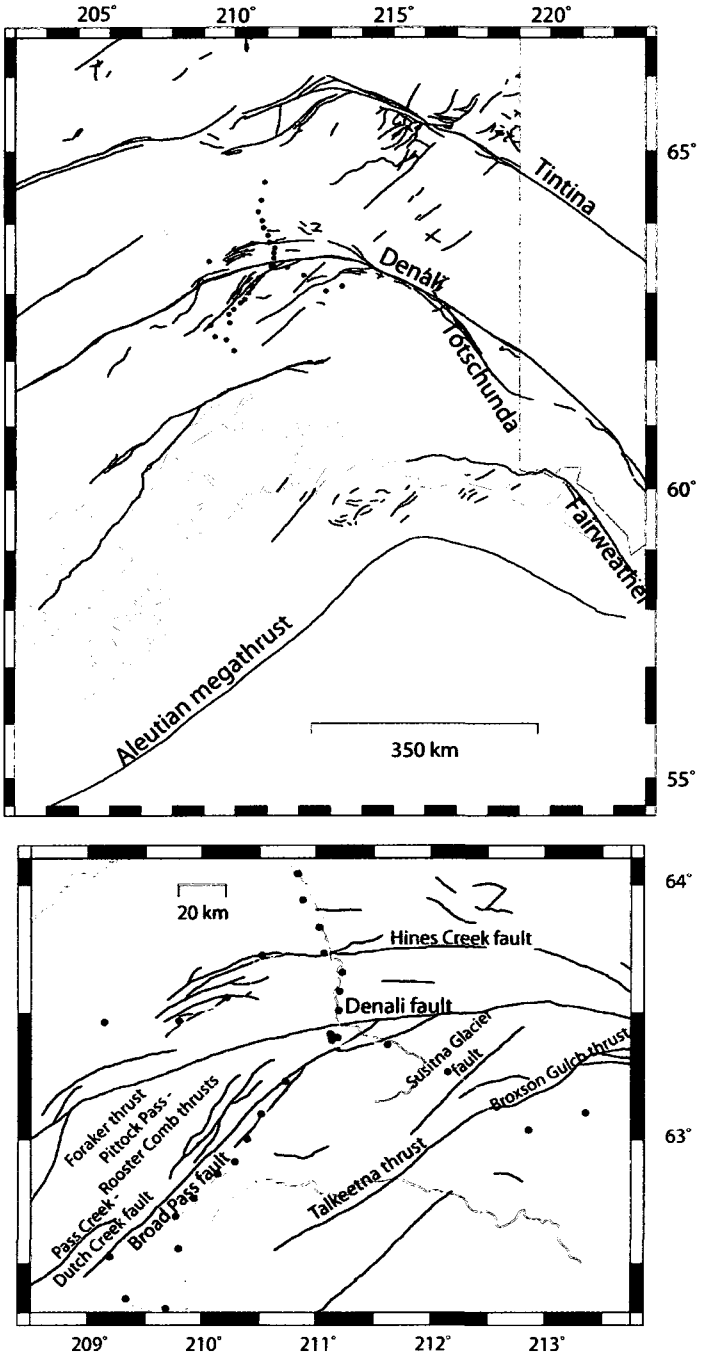

Figure 6: Map of identified faults in south central Alaska. Dots indicate BEAAR station locations. Geometric relationships show dominantly right lateral strike-slip faults such as the Denali fault, arcing around dominantly southwest striking thrust faults, such as the Talkeetna or Broxson Gulch thrust faults.

The Hines Creek fault (Brease, 1995; Ridgway et al., 1997) is a zone of intense shearing and penetrative deformation which may have originated as a major terrane-emplacement fault (Grantz, 1966; Page and Lahr, 1971; Wahrhaftig et al., 1975; Csejtey et al., 1982), or is alternatively interpreted as a structure mostly within the Yukon-Tanana terrane (Nokleberg et al., 1989, 1992b). The Nenana Glacier fault (Brewer, 1982; Nokleberg et al., 1985, 1989, 1992b) is located just north of and subparallel to the Hines Creek fault.

Other faults in our study area may be broadly considered as belonging to groups north and south of the Denali fault. Most faults north of the Denali in our study area are subparallel with the Denali fault, forming an arcuate northern foothills thrust system accommodating north-south contraction (Bemis and Wallace, 2007).

Faults in the group south of the Denali fault in general strike southwest; at an oblique angle to the Denali fault (Figure 6). Thrust displacements of various ages have been documented along the Talkeetna thrust (Csejtey et al., 1978, 1982, 1986; Csejtey and St. Aubin 1981; Nokleberg et al., 1985, 1989; Plafker et al., 1989), Broxson Gulch thrust (Stout, 1976; Nokleberg et al., 1982, 1985, 1989, 1992b, 1994), and Susistna Glacier fault (Eberhart-Philips et al., 2003; Ratchkovski et al., 2003, 2004). Fault identification is incomplete, including many mapped faults that are unnamed. Other named faults south of the Denali fault with southwest strike includes the West Fork fault (Andreasen et al., 1974; Campbell and Nokleberg 1986; Nokleberg et al., 1986), the Foraker and Pittock Pass – Rooster Comb thrusts (Haeussler, 2005), and Pass Creek – Dutch Creek fault (Plafker et al., 1994). Even among identified and named faults documentation of the amount of displacement, timing of displacement and sense of displacement is sparse. Thrust faults with this orientation may accommodate westward displacement of the southern Alaska block south of the Denali fault.

Overview and Motivation

South-central Alaska is a geologically complex and tectonically active region of transition from southeast to northwest from transform to convergent motion between the North American and Pacific plates (Figure 1). The transition from strike-slip to subduction is described as a closed corner transition (Mann and Frohlich, 1999). The Alaska Range forms the corner far inland of the plate boundary, rising to 6,194 m at Mount McKinley, the highest peak in North America. Apatite fission track thermochronology and geologic evidence indicate rapid uplift beginning ca. 5-6 Ma (Fitzgerald et al., 1995); more recent K-spar thermochronologic studies suggest Alaska Range topographic development began more regionally ca. 30 Ma (Benowitz and Layer, 2008). The curvilinear Alaska Range is split by the seismically active Denali fault system, a 1200+ km long dominantly right-lateral strike-slip fault system, responsible for the M_w 7.9 earthquake on 3 November 2002 (Eberhart-Philips et al., 2003). It has been postulated that Alaska Range

thrust faults merge into the Denali fault at depth (Thoms, 2000; Ridgway et al., 2002). This relation between thrust and strike-slip faults in south central Alaska could conceivably produce the topography observed in the Alaska Range, but more information on the subsurface is necessary to identify and evaluate the relative importance of structures and buoyant forces supporting the mountains.

So, while the configuration of mountains, major thrust and strike-slip faults, and tectonic affinities of terranes all reflect the transpressional environment of southern Alaska we must continue to amass different types of high quality data in our attempts to understand this majestic but somewhat mysterious region.

Previous Crustal Studies and Broadband Experiment Across the Alaska Range (BEAAR)

The Fairbanks North profile (65°- 66°N, 148°-150°W) of the Trans-Alaska Crustal Transect (TACT) seismic refraction and reflection project (Page et al., 1986) indicates nearly uniform crustal thickness of 31 to 34 km beneath the northern Yukon-Tanana upland (Beaudoin et al., 1994). The TACT Fairbanks South profile crossed the eastern edge of the Alaska Range along the Richardson Highway, revealing a 30 km deep Moho beneath the southern Yukon-Tanana terrane (Beaudoin et al., 1992), with crust reported to be 50 km thick at the Denali fault and as thin as 28 km north of the range (Brocher et al., 2004). This portion of the BEAAR project examined the crustal structure beneath the central Alaska Range along the Parks and Denali Highways (Figure 7), and crustal thicknesses determined by receiver function analysis are detailed in this manuscript. The BEAAR project also provided data for a number of subcrustal studies of south central Alaska (Ferris et al., 2003; Stachnik et al., 2004; Abers et al., 2006, 2008; Rossi et al., 2006). The crustal thickness data provide an important constraint for hypotheses on tectonic evolution of Alaska, where geological and geophysical differences between allochthonous tectonostratigraphic terranes are incompletely documented.

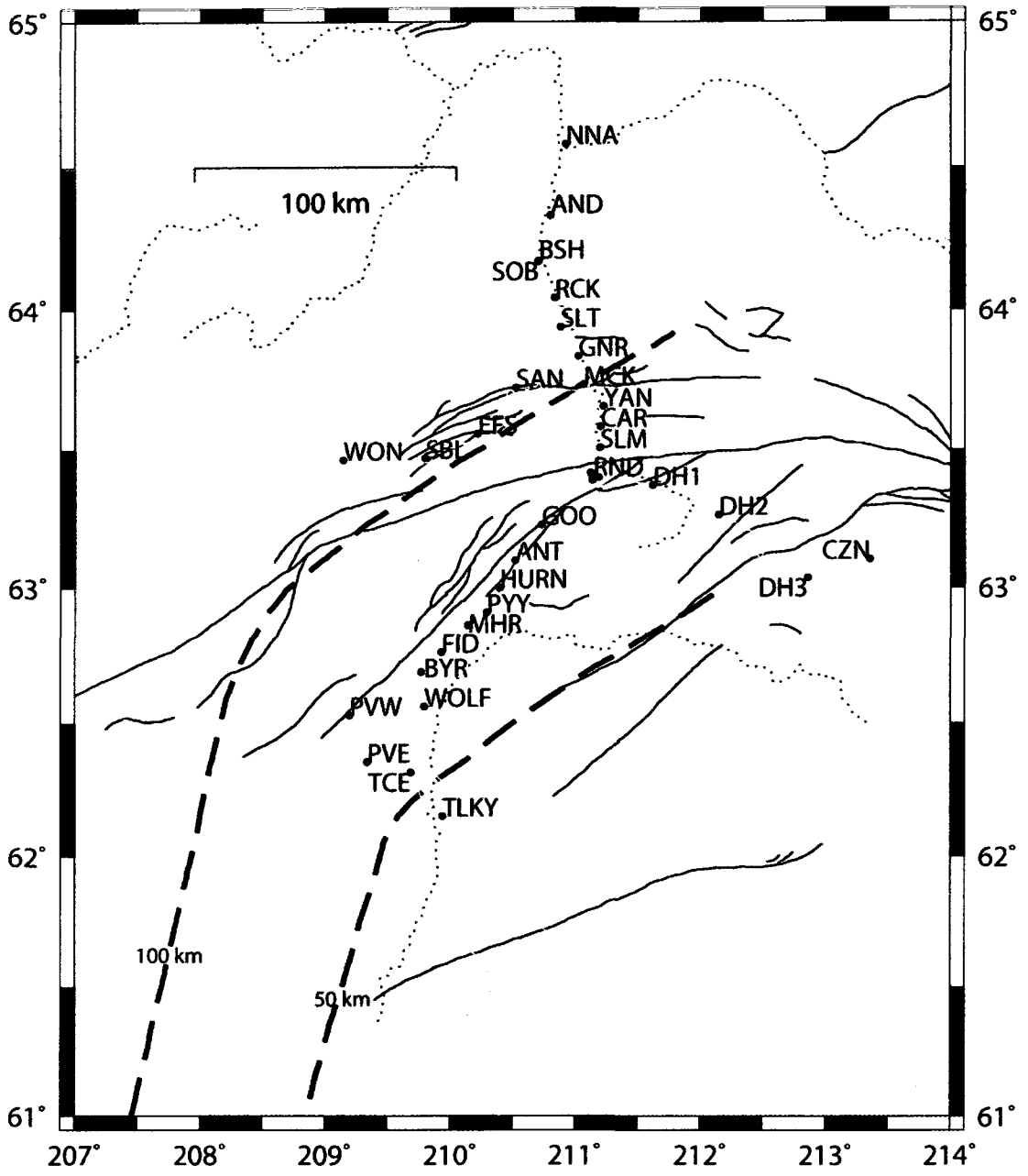

Figure 7: BEAAR station location map. BEAAR station locations labeled with alphanumeric station identifier. Shading indicates topography, Talkeetna Mountains separated from the high peaks of the Alaska Range by the valley along which many stations were deployed. Dashed lines are 50 and 100 km isopleths of Wadati-Benioff zone (south and north respectively) indicating location of the subducting slab. Mapped faults traced in black, roads in white, rivers as dotted lines. The Parks Highway runs roughly north south between TLKY and NNA, the Denali Highway runs roughly east west between RND and CZN, the Denali National Park road runs roughly east west between WON and MCK, and Petersville Road branches off the Parks Highway providing access between TCE and PVW.

This manuscript describes the receiver function analysis portion of the BEAAR project. Chapter 2 provides a description of field methods, including vault preparation and specifications of the instruments deployed. Chapter 3 includes a description of receiver function analysis in general as well as specific variables used in this analysis. Chapter 4 provides a description of modeling receiver functions to determine crustal thickness followed by both graphic and tabular presentation of crustal thickness point values. Discussion of the crustal thickness results is included in Chapter 5. Implications of crustal thickness values are considered in Chapter 6 with comparison between observed and predicted crustal thicknesses.

Chapter 2 - Field Methods

The Broadband Experiment Across the Alaska Range (BEAAR) project was a field based experiment. Instrumentation was provided by Incorporated Research Institutions for Seismology (IRIS) through the Program for the Array Seismic Studies of the Crustal Lithosphere (PASSCAL). Before the initial field deployment, land use permissions were acquired, sites selected, vaults designed and constructed, equipment shipped from New Mexico, and the seismometers and data recorders all tested. Once deployed, sites had to be serviced regularly to retrieve data and repair malfunctioning equipment. Servicing concerns varied depending on season, site type, and location. Following the field experiment, equipment had to be removed, cleaned, inventoried, inspected, and equipment on loan carefully packed for return shipment. Sites had to be reclaimed, and written reports prepared for some landowners.

For logistical reasons, the initial plan for site locations of BEAAR seismic stations included 21 sites located roughly 10 km apart along the Parks Highway, four stations located to the east along the Denali Highway, four stations to the west along the Denali National Park Road, and two stations located west along Petersville Road. Rough locations were identified and located on topographic maps so land owners could be identified and contacted (Table 1). A major consideration for site location was procuring permission from landowners to dig a vault for the seismometer. Site selection involved a number of reconnaissance trips (Figure 8). An ideal site would have roughly a meter of soil over bedrock, located close enough to the road to transport equipment but far enough away from the road to eliminate seismic noise from passing vehicles. The ideal site would be free from trees and other seismic noise sources such as game trails, and located on a gently sloping hill. Additional considerations for site selection included solar panel view or orientation and avoiding detection (theft/vandalism by humans or wildlife).

Table 1: BEAAR site locations with name, standard three to four letter/digit alphanumeric station identification, and station location coordinates. Milepost values are along the Parks Highway with +values indicating mileage along Petersville Road and Denali Highway.

site name	topographic map quadrangle	landowner	milepost	station	latitude (°N)	longitude (°E)
Nenana	Fairbanks C-5	Toghotthele	306.1	**NNA**	64.5797	210.9214
Anderson	Fairbanks B-5	local government	283.4	**AND**	64.3306	210.8004
Browne	Fairbanks A-5	Department of Natural Resources	272.1	**BSH**	64.1713	210.7049
Son of Browne	Fairbanks A-5	Department of Natural Resources		**SOB**	64.1702	210.7007
Rock Creek	Fairbanks A-5	Department of Natural Resources	262.3	**RCK**	64.0412	210.8340
Slate Creek	Healy D-5	Department of Natural Resources	254.5	**SLT**	63.9391	210.8788
Garner	Healy D-4	Alaska Railroad	246.2	**GNR**	63.8345	211.0220
McKinley	Healy C-4	National Park Service	237.3	**MCK**	63.7323	211.0632
Yanert	Healy C-4	Department of Natural Resources	230.0	**YAN**	63.6559	211.2251
Carlo Creek	Healy C-4	Ahtna	225.4	**CAR**	63.5831	211.1984
Slime Creek	Healy C-4	Ahtna	220.0	**SLM**	63.5067	211.1951
Reindeer North	Healy B-4	Ahtna	211.7	**RNDN**	63.4157	211.1222
Reindeer Main	Healy B-4	Ahtna	209.9	**RND**	63.4057	211.1399
Reindeer Tower 5	Healy B-4	Ahtna	209.9	**RND5**	63.4015	211.1449
Reindeer Rock	Healy B-4	Ahtna	209.9	**RNDR**	63.4014	211.1326
Reindeer East	Healy B-4	Ahtna	209.9	**RNDE**	63.4003	211.1850
Reindeer South	Healy B-4	Ahtna	209.9	**RNDS**	63.3896	211.1324
Summit	Healy B-5	Bureau of Land Management	202		63.3333	210.8833
Igloo	Healy A-5	Ahtna	192.7	**GOO**	63.2286	210.7295
Antimony	Healy A-5	Department of Natural Resources	181.2	**ANT**	63.0992	210.5169
Hurricane	Talkeetna Mountains D-6	Department of Natural Resources	173.0	**HURN**	62.9991	210.3936
Parrott Yesteryear	Talkeetna Mountains D-6	State Park	165.5	**PYY**	62.9094	210.2883
Moosehead Rock	Talkeetna Mountains D-6	State Park	159.4	**MHR**	62.8603	210.1352
Byers Creek - Fiddlehead	Talkeetna D-1	State Park	149.8	**FID**	62.7622	209.9309
Byers	Talkeetna C-1	State Park	141.5	**BYR**	62.6893	209.7682
Princess Lodge - Wolf	Talkeetna C-1	private	133.0	**WOLF**	62.5604	209.7961
Trapper Creek Elementary	Talkeetna B-1	local school		**TCE**	62.3147	209.6858
Talkeetna	Talkeetna A-1	private	99.7	**TLKY**	62.1500	209.9391
Denali Highway 1	Healy B-3	Bureau of Land Management	+19.4	**DH1**	63.3734	211.6171
Denali Highway 2	Healy B-2	Department of Natural Resources	+38.0	**DH2**	63.2652	212.1448
Denali Highway 3	Healy A-1	Bureau of Land Management	+71.2	**DH3**	63.0345	212.8562
Crazy Notch	Mount Hayes A-6	Bureau of Land Management	+90.0	**CZN**	63.1033	213.3564
Petersville East	Talkeetna B-2	Department of Natural Resources	+16.1	**PVE**	62.3551	209.3360
Petersville West	Talkeetna C-2	Department of Natural Resources	+32.3	**PVW**	62.5277	209.1961
Sanctuary	Healy C-5	National Park Service		**SAN**	63.7231	210.5225
East Fork / Sable	Healy C-6	National Park Service		**EFS**	63.5581	210.2186
Stony Creek / Bergh Lake	Mount McKinley B-1	National Park Service		**SBL**	63.4686	209.8001
Wonder Lake	Mount McKinley B-1	National Park Service		**WON**	63.4621	209.1457

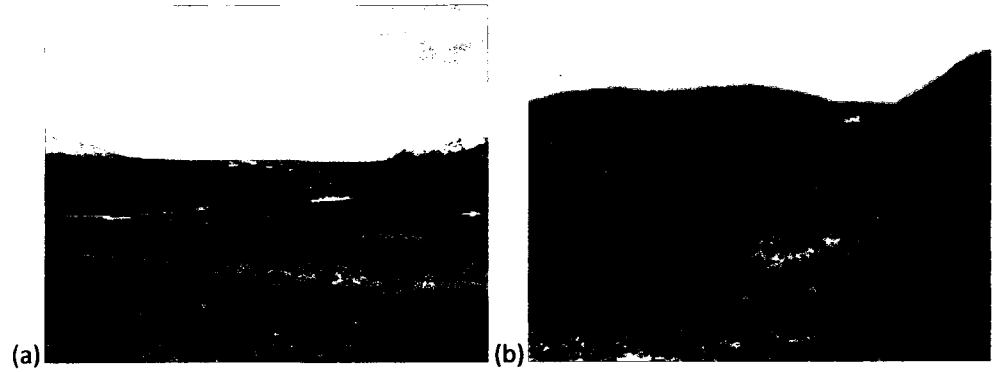

Figure 8: BEAAR reconnaissance site selection. (a) View south from Reindeer Mountain in Cantwell of broad valley between the Talkeetna Mountains on left and the Alaska Range on right. (b) Sites were marked with flag tape like this at CZN.

During major field activity a base camp (Figure 9) was established in Cantwell, near the center of the BEAAR transect. The locked cabin at the University of Alaska Fairbanks Reindeer Research Center provided a relatively secure warehouse for electronic equipment. Huddle tests (Figure 10) were performed in Fairbanks to repair minor defects or damage to seismometers and data recorders incurred during shipment.

Figure 9: Cantwell base camp. (a) UAF Reindeer Research Center cabin, May 2000. (b) Meals generally prepared at the cabin. (c) Summer interns helped load equipment; each vehicle can only hold a couple stations. (d) GPS clocks had to be updated with new electronics, when possible this type of work was done at base camp.

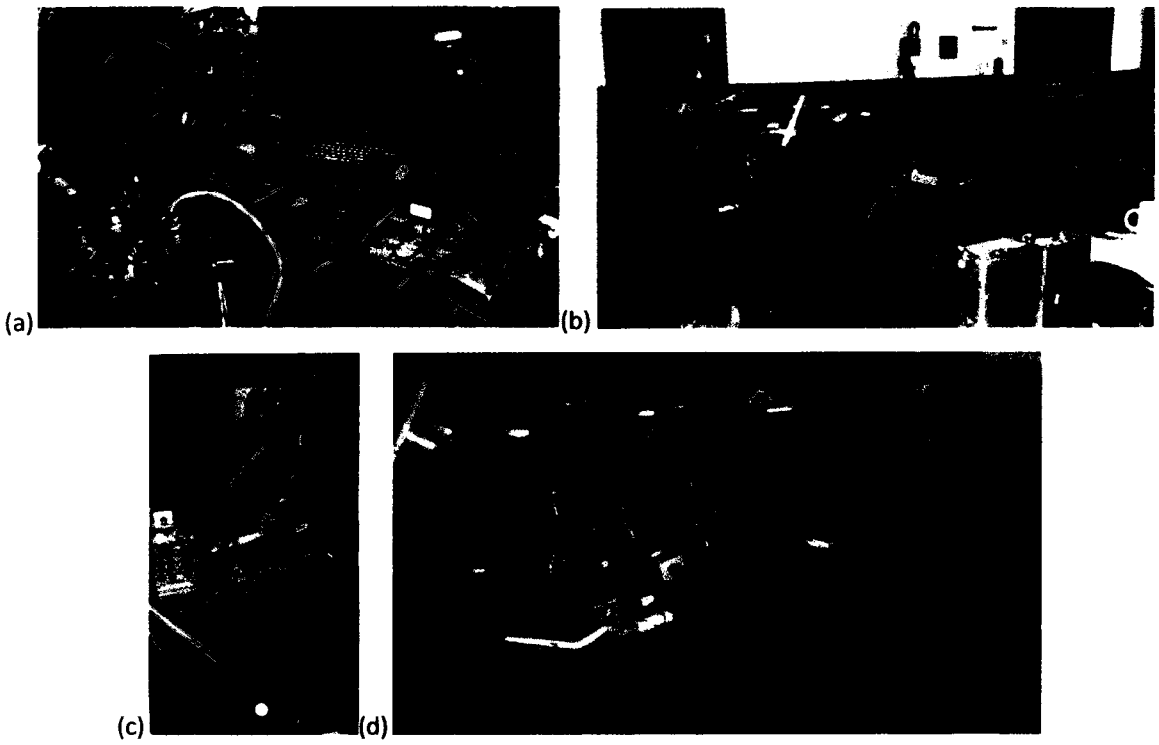

Figure 10: PASSCAL equipment huddle test. Each huddle test provided an opportunity to test equipment and learn about both hardware and software. The main deployment (Phase II) huddle test was performed in the Geophysical Institute garage. (a) Handheld computer is connected to communicate with the Data Acquisition System (DAS). (b) Sensors and batteries seen on floor while DASs, disks, breakout boxes, power boards and GPS clocks stacked on table. (c) Circuitry initially appeared complex, photo illustrates numerous connections. (d) A variety of GPS clocks were supplied, since each required a different type of cable, careful records were necessary for efficient site visits. We performed numerous repairs to sensors and DASs during huddle test.

Once a site was selected and land use approved, vault preparation could begin (Figure 11). Basic equipment for vault construction included a large garbage can or 60 gallon screw-top hazardous waste container (with bottom cut off), two inch diameter PVC pipe, rebar, a bag of cement, and water. Final site selection generally occurred at the time of vault preparation. Holes had to be deep enough to bury the entire garbage can, and trenches had to slope away from the main vault area. For best ground coupling, cement was poured at the base of the vault so it would not touch the sides of the vault, decoupling it from overlying soil movements. Garbage can lids were secured with zip ties, covered with a tarp, buried beneath roughly 10 cm of soil and ideally covered with the preserved vegetative mat. Seismic station maps and flagging made for efficient relocation during later station installation.

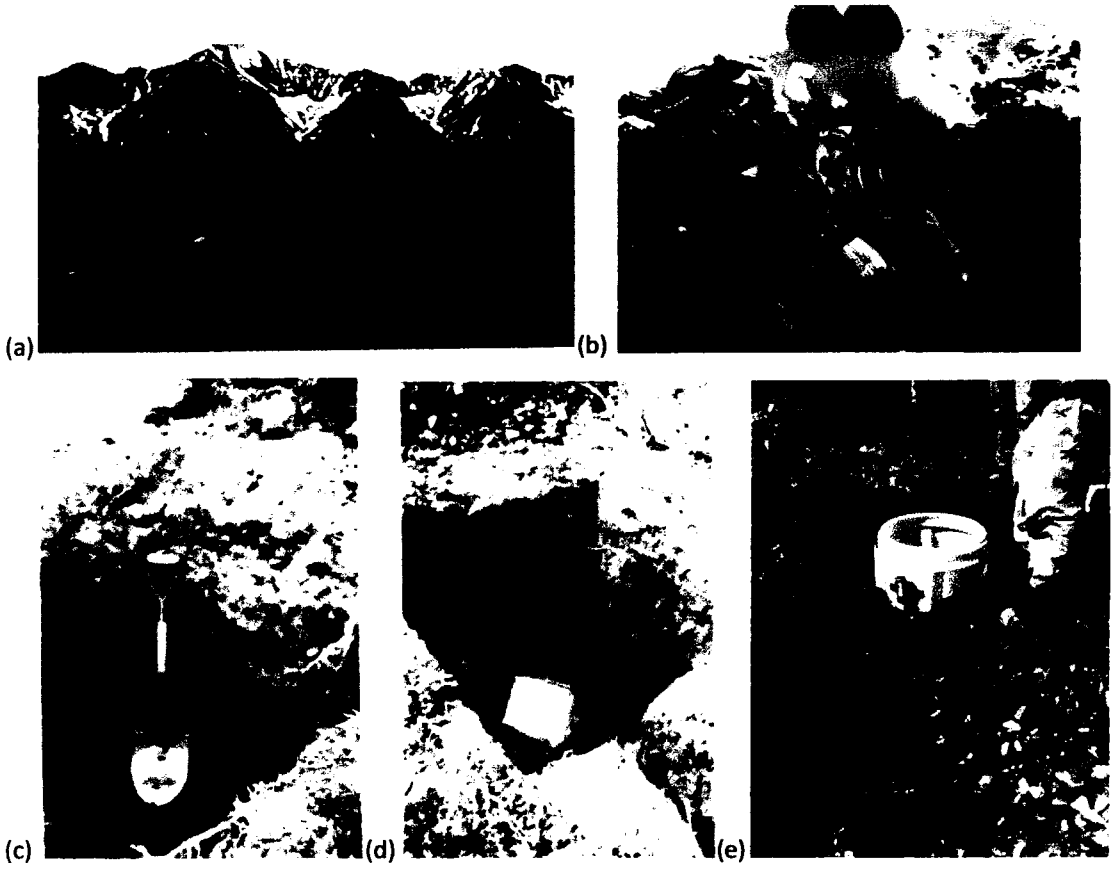

Figure 11: Vault preparation. (a) Yellow drum being carried to RND contrasts with spring vegetation, note Talkeetna Mountains in background across Broad Pass. (b) GOO. (c) DH1. The most useful tools included long handled shovels for near surface digging, short handled shovels for working down in hole, and hatchets, picks and Pulaskis for trench excavation. (d) CZN tile sunk in the wet cement facilitated leveling. The sensor pad had to be within a few degrees of level, and tile marked with North orientation arrow. (e) NNA PVC pipe fit into the base of the can sloping away from the vault was to protect the sensor from water damage.

At the time of station installation (Figure 12), a great deal of heavy equipment was carried to the site. Sensors were aligned north-south with small pointers extending from the base, brass pointer to the north. Seismometers were leveled by adjusting the feet, which must be locked prior to enclosure. Since sensor enclosure is critical to data quality, a five sided box of rigid 2 inch thick foam was built around the 16.8 cm diameter 38 cm high cylindrical seismometer to minimize air currents. Each foam box was custom made with a carefully positioned hole for the sensor cable (a 4 m long cable with PTO6F-16-26S connectors on each end) connecting the seismometer to the Data Acquisition System (DAS). Action Packers sheltered sensitive above ground equipment (Figure 13). The Guralp sensors require 100 mA at 12 VDC with pulses of 400 mA required for centering (and locking the CMG3T sensors – described on p.22). Solar panels and GPS clock towers were supported with rebar.

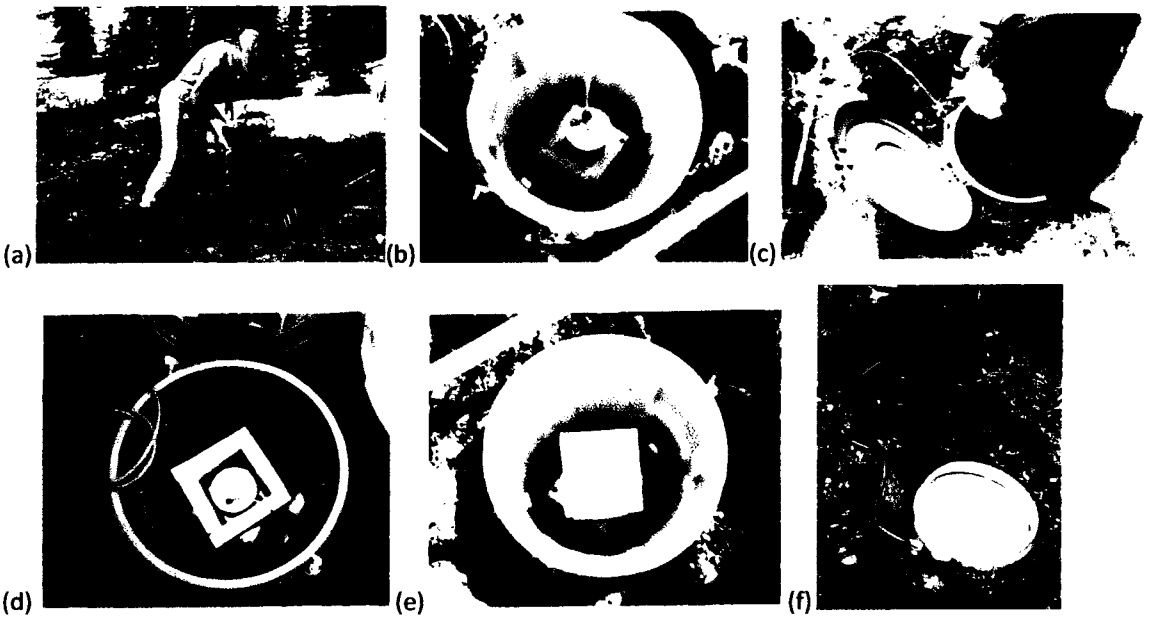

Figure 12: Sensor deployment. (a) ANT. Sensor moved carefully even when masses are locked. (b) YAN semi-permanent AC site vault during deployment shows north-south sensor alignment, and sensor cable conduit, PVC pipe with a 90° elbow at the base. (c) Unlocking CMG3ESP sensor masses at GNR. (d) AND foam box carefully positioned around seismometer; sensor cable cutout customized at each station. Photos documented sensor level and identification prior to sealing vault. (e) YAN June 1999 showing later design foam box and sensor cable. Design modifications included using thicker foam, making the box larger to minimize risk of touching sensor, and making the foam box tall enough to allow sensor cable to exit above sensor but below lid. Ceramic tile was smoother and shape allowed easier positioning of foam box than rectangular stepping stone. (f) NNA two rigid foam disks cut to fit suspended above foam box helped minimize air currents in the vault.

Figure 13: Above ground equipment. (a) WON seismometer cable enters box from right, GPS clock cable leaving box to lower left, wiring to winter power supply to upper left. Action Packers house DAS, disk, power board, breakout box, main battery, and (at some stations) GPS clock. (b) MHR disk swap. (c) HURN. (d) NNA: handheld computer liquid crystal display (LCD) required body heat during transport and hand warmers during use. (e) View south on access trail to YAN: January sunrise-sunset. (f) RND: ARGOS antenna sent a remote DAS status dump at regular intervals, alerting us to problems with data acquisition. Denali was visible in the background.

Eventually 36 three-component broadband seismic stations (Table 1) were deployed, collecting high quality data over a period of 27 months. The deployment occurred in three phases (Figure 14). During phase one, May 1999 to May 2000, we ran seven stations at approximately 50 km spacing. NNA, YAN, RND, BYR, and TLKY station batteries were powered by alternating current from the grid. RCK and HURN station batteries were solar powered. During the main phase of the experiment, phase two, May

2000 to September 2000, we deployed an additional 29 stations to attain approximately 10 km spacing along the main line. During the time limited main phase of the experiment, we had seismic equipment to run 36 stations, so every effort was made to get the seismometers out and running as quickly as possible. Given the travel time to the stations and the amount of equipment to be transported, logistical efficiency was extremely important. During phase three, September 2000 to 2001, half of the instrumentation was arranged in a sparser network: NNA, RCK, GNR, WON, SBL, EFS, SAN, MCK, YAN, RND, DH1, DH3, GOO, HURN, MHR, BYR, PVW, and TLKY. Thanks to a generous donation of batteries from the Alaska Earthquake Information Center (AEIC), stations that would have otherwise been inactive due to lack of solar power during winter months continuously recorded data throughout the third phase of the experiment. PASSCAL provided broadband Guralp sensors and Reftek recorders. We deployed 22 CMG3T and 14 CMG3ESP sensors, slightly different three component broadband seismometers. Guralp CMG3T instruments have a sensitivity of 1500 Volts/meter/second and a natural frequency of 0.0083 Hz (120 seconds) while Guralp CMG3ESP sensors have a sensitivity of 2000 Volts/meter/second and a natural frequency of 0.033 Hz (30 seconds). The CMG3T masses are unlocked electronically via the breakout box, while the CMG3ESP masses are manually unlocked using a 3 mm hex key. Two continuously recording data streams were used: 50 samples per second, and one sample per second.

At each station visit, careful notes were taken, initially in my field books, and later on a standardized station servicing sheet I created for the experiment. Details about site specific concerns such as malfunctioning equipment were documented in these books and binders, but much too lengthy to include here.

Upon return from the field, raw seismic data were downloaded by Doug Christensen.

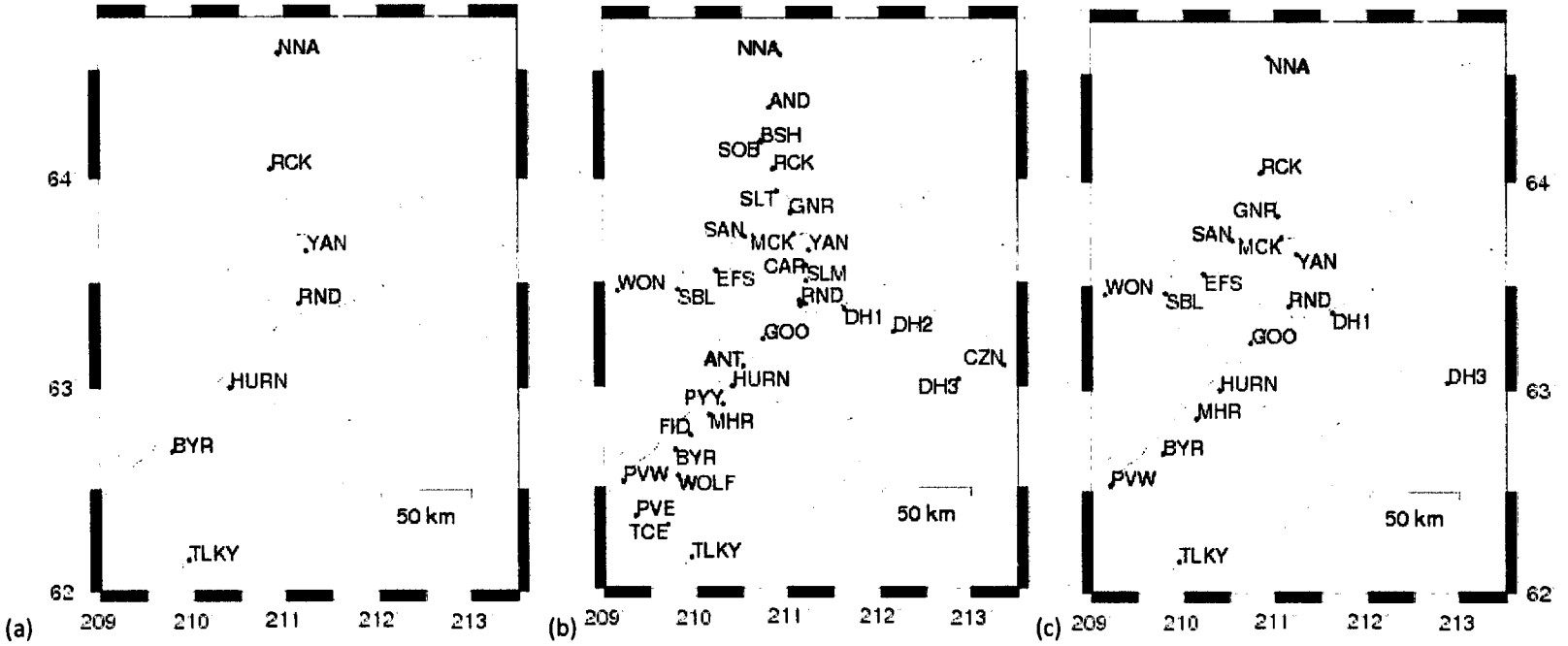

Figure 14: Phase I-II-III station location maps. (a) Phase one, May 1999 to May 2000: seven stations at roughly 50 km spacing. (b) Phase two, May 2000 to September 2000: deployment of an additional 29 stations for approximately 10 km spacing along the main line. (c) Phase three, September 2000 to 2001: half of the instrumentation arranged in a sparser network.

Chapter 3 - Receiver Function Analysis

Teleseismic body waves have been used to infer crustal structure beneath seismic stations, modeled in the frequency domain (Phinney, 1964; Kurita, 1973) or the time domain (Jordan and Frazer, 1975; Burdick and Langston, 1977). Teleseismic P waveforms are used to study lithospheric structure by interpreting the wave train in terms of reflection and transmission of converted waves at discontinuities beneath the recording station (Langston, 1977, 1979, 1981; Owens, 1984; Owens et al., 1984, 1987, 1988; Owens and Zandt, 1985; Ammon, 1991; Sheehan et al., 1995). A receiver function is the contribution to the seismic waveform recorded at a single station due to the response of local crustal structure. The recorded signal may be regarded as a convolution of the source-time function, the receiver function, and the instrument response. For receiver function analysis we consider path effects between the source and the converting discontinuity as part of the seismic source-time function. For steeply incident ray paths, such as those produced by teleseismic events, particle motions are polarized so that most of the P-wave motion is recorded on the vertical component, and most of the S-wave motion is recorded on the horizontal components of the waveform. The Ps conversions occurring beneath the recording station will produce S wave energy immediately following the direct P arrival.

To determine a receiver function, the north-south and east-west components of ground motion are rotated into radial and tangential components. The radial component represents ground motion in the horizontal plane in line with the source-receiver azimuth. The radial component of the waveform is parallel to the direction the ray travels, positive away from the source. The tangential component is horizontal motion perpendicular to the radial component. In an idealized horizontally layered structure, all S wave motion at the point of conversion will be in the direction of the radial component. Deconvolution of the vertical component from the radial and tangential components removes instrument, source, and external path effects.

Rotated into radial and tangential components, the seismogram may be considered a three component trace written in the time domain as radial, tangential, and vertical components, $D_r(t)$, $D_t(t)$, and $D_v(t)$ respectively. These may be written:

$$D_r(t) = I(t)*S(t)*E_r(t), \quad 3.1$$

$$D_t(t)=I(t)*S(t)*E_t(t), \text{ and} \quad 3.2$$

$$D_v(t)=I(t)*S(t)*E_v(t) \quad 3.3$$

where the asterisk (*) represents the convolution operator, I(t) the instrument response, S(t) the seismic source function, and $E_r(t)$, the radial, $E_t(t)$, tangential and $E_v(t)$ vertical components of the receiver function. To remove instrument, source, and external path effects, one deconvolves the vertical

component from the radial and tangential components. The vertical component of the receiver function $E_v(t)$ may be approximated by a Dirac delta function, so

$$D_v(t) \approx I(t) * S(t). \quad 3.4$$

Hence, the vertical component of the seismogram is basically the instrument response and source function that must be deconvolved to isolate the radial and tangential components of the receiver function.

Recognizing that convolution in the time domain is basically multiplication in the frequency domain, the radial and tangential components of the receiver function may be written:

$$E_r(\omega) \approx D_r(\omega)/I(\omega)S(\omega), \quad 3.5$$

$$\text{so } E_r(\omega) \approx D_r(\omega)/D_v(\omega), \quad 3.6$$

$$\text{and similarly } E_t(\omega) \approx D_t(\omega)/I(\omega)S(\omega), \quad 3.7$$

$$\text{so } E_t(\omega) \approx D_t(\omega)/D_v(\omega). \quad 3.8$$

Because noise is present in real seismic data, a Gaussian filter is used in the deconvolution to exclude high frequency noise. If the width of the Gaussian filter is given by a, then the Gaussian filter may be written:

$$G(\omega) = \exp(-\omega/4a^2). \quad 3.9$$

To ensure the stability of the deconvolution we must avoid dividing by zero, so we define a minimum allowable amplitude $\phi(\omega)$ for the vertical seismogram where the minimum spectral amplitude is determined by the water level parameter, c. The water level is a fraction of the maximum spectral amplitude, and so ranges between 0.0 and 1.0, with the optimal value for c such that $c \cdot \max|D_v(\omega)|^2$ is above the noise level (Clayton and Wiggins, 1976). We may then write the minimum allowable spectral amplitude for the vertical seismogram as:

$$\phi(\omega) = \max\{D_v(\omega)\,\overline{D_v(\omega)},\ c \cdot \max[D_v(\omega)\,\overline{D_v(\omega)}]\} \quad 3.10$$

$\overline{D_v(\omega)}$ is the complex conjugate of $D_v(\omega)$. The deconvolution of the radial receiver function is then written:

$$E_r(\omega) \approx \{[D_r(\omega)\,\overline{D_v(\omega)}]/\phi(\omega)\}G(\omega). \quad 3.11$$

Seismic signals may be regarded as a convolution of the source-time function, the receiver function, and the instrument response. Deconvolution of the seismic signal allows inversion for receiver function parameters to elucidate local crustal structure (e.g. Sipkin and Lerner-Lam, 1992; Abers et al., 1995; Sheehan et al., 1995).

Radial and tangential receiver functions were deconvolved from waveforms recorded by BEAAR instruments. The continuously recording data stream with 50 samples per second was decimated to 6.25 samples per second for initial receiver function analysis. A suite of deconvolutions allowed determination

of the filter and water level values that minimized pre-signal noise and provided clear receiver functions. Optimal values varied for each inversion, but after running a suite of deconvolutions (e.g. c=[1.0, 0.1, 0.01, 0.001, 0.0001] and a=[5.0, 2.5]), global parameters were chosen to allow stacking. Initial studies (e.g. Meyers et al., 2000) used older Seismic Analysis Code (SAC) scripts similar to Searcy et al. (1996). Given the sheer volume of BEAAR data, calculations needed to be automated, so new database-communicative scripts were written to streamline the process and reduce the possibility of error. The receiver functions presented in this paper were calculated using *dbrfcn,* a frequency-domain deconvolution routine written by Geoff Abers, incorporated into Antelope database software.

Of the 995 global seismic events with moment magnitudes $M_w \geq 5.5$ between May 31st, 1999 and August 22nd, 2001, 751 were between 29° and 101° from centrally located station RND (63.4057°N 148.8601°W) and thus appropriate for receiver function analysis. Appendix 1 lists the events used to extract teleseismic earthquake signals from the BEAAR database of continuously recorded data. The origin time of each event listed in Appendix 1 was used to predict arrival times for each event at each station. Antelope database software was used extensively, from creating an origin table from the catalog of events, subsetting this master origin table for events matching distance criteria, extracting time-limited waveforms from the master database with *dbwfexerpt*, calculating and associating tables, and picking arrivals. Arrivals were examined using *dbpick*, an interactive graphical program for displaying seismic waveforms, predicted arrivals, and analyst picked phase arrivals. Before calculating the receiver functions, *dbassoc_arrival* was utilized to associate phase arrivals from the database of arrivals with the origins in a separate database, as there must be no extraneous origins or arrivals when automatically calculating receiver functions. These 751 teleseismic events yielded 14,754 three-component seismograms.

I examined raw waveform quality on all three components while picking the direct P-wave arrival at each station for each event. Of 14,754 three-component seismograms, 6,644 were rejected as noisy inferior quality signals. Receiver functions were calculated with the frequency-domain deconvolution subroutine *dbrfcn*. Parameters used in *dbrfcn* included decimation to 8 samples per second (via Fourier series truncation with six-pole two-way [zero phase] Butterworth filter applied at the new Nyquist frequency), a water level of 0.01 (minimum allowed fraction of peak spectral amplitude), a Gaussian frequency of 1.0 Hz (corner frequency for low-pass Gaussian filter), and a high pass frequency filter of 0.01 Hz (corner frequency for high-pass six-pole two-way [zero phase] Butterworth filter). I viewed raw receiver functions in MATLAB, examined with an order five Butterworth filter (passband 0.01 to 0.25), scrutinized individually and in groups. In addition to the rejected 6,644 raw seismograms, another 7,021 receiver functions were rejected mainly due to inferior signal-to-noise ratios. The magnitude threshold of

M_w 5.5 provided a lot of data, and some of the "good" receiver functions were from the lower magnitude events (Appendix 2), but the majority of the lower magnitude teleseismic events produced receiver functions with horrendous signal to noise ratios. Table 2 outlines the number of events and receiver functions at each station. Where the number of events far exceeds the number of receiver functions calculated, this is a pretty good indication that it was a noisy site (e.g. GNR). Final analysis used only the highest quality data, 10% of the receiver functions considered (range 1% @EFS to 32% @TCE). Individual receiver functions at each station were grouped based on similar back-azimuth and distance as well as trace similarity. Regions with strong lateral variations in velocity structure require tighter stacking bounds. However, due to our location, azimuthal sampling is distinctly nonuniform (e.g. a paucity of events in Pacific ocean), which limits resolution. Figure 15 is a sample spoke-plot of back-azimuth vs. ray parameter showing the distribution of seismic events.

Table 2: Quality control. Station column lists the alphanumeric identifier for each BEAAR station. Events column lists the number of teleseismic events extracted from the database of continuously recorded seismicity. The number of receiver functions deconvolved from seismograms at each station is listed in rfcns column. The good column indicates the number of receiver functions accepted for further analysis. The grouped column lists the number of receiver functions that were included in a stacking group (or accepted as the representative trace). The stacks column indicates the number of distinct subdivisions modeled at each station. T_m is the number of crustal thickness estimates accepted. rf is the number of receiver functions at each station that were actually used to determine reported crustal thicknesses. **%** lists the percent of calculated receiver functions used in final analysis.

station	events	rfcns	good	grouped	stacks	Tm	rf	%
NNA	658	543	78	77	15	11	65	12
AND	106	71	15	7	1	1	7	10
BSH	48	31	7	7	1	1	7	23
SOB	112	90	9	8	1	1	8	9
RCK	606	300	36	34	7	7	34	11
SLT	81	47	6	6	1	1	6	13
GNR	449	290	39	32	10	4	23	8
MCK	424	400	56	37	9	3	22	6
SAN	432	347	30	29	5	4	26	7
EFS	600	318	3	3	1	1	3	1
SBL	155	132	8	7	3	1	2	2
WON	405	328	18	18	5	3	16	5
YAN	713	639	76	67	9	6	54	8
CAR	85	56	12	12	3	1	8	14
SLM	112	104	27	26	5	2	20	19
RND	516	490	60	59	13	6	41	8
GOO	417	343	29	29	5	3	26	8
HURN	709	628	99	96	16	14	94	15
PYY	60	52	11	8	2	1	7	13
MHR	303	243	42	42	5	5	42	17
FID	57	41	18	12	2	0	0	0
BYR	767	679	116	112	16	10	90	13
WOLF	91	81	20	19	8	2	11	14
PVW	382	325	42	41	10	4	31	10
PVE	63	37	8	8	1	1	8	22
TCE	123	103	33	33	1	1	33	32
TLKY	773	516	73		11	n/a	n/a	0
CZN	125	123	16	7	3	1	6	5
DH3	357	314	27	26	6	2	11	4
DH2	60	59	9	9	4	2	7	12
DH1	548	380	66	66	10	9	65	17

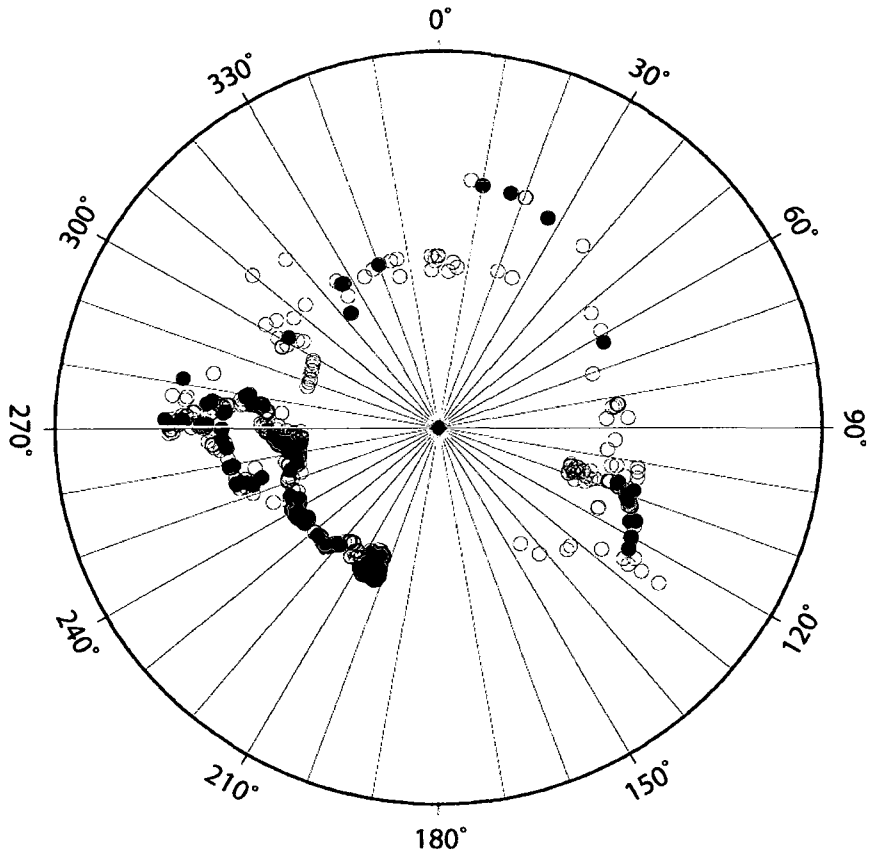

Figure 15: Sample backazimuth versus ray parameter spoke-plot showing distribution of teleseismic events recorded at BYR (diamond at center). Empty circles locate events rejected for inferior quality signals, filled circles locate events accepted for receiver function analysis at BYR. South central Alaska records many events from the west and southwest, earthquakes associated with western Pacific margin tectonic activity. The paucity of events to the south and south-southeast is due to the stability of the central Pacific. Those events originating to the east-southeast are associated with eastern Pacific margin tectonic activity. Events to the north are much less common, so stacks at these station-to-event back-azimuths are typically based on fewer events.

A single high quality receiver function can provide a more accurate crustal thickness than hundreds of noisy low quality receiver functions. Many quantitative quality control methods were tested: calculating cross correlation between each individual trace and (a) a synthetic receiver function or (b) a stack from a preliminary study (Mw > 6.0); calculating semblance (a time domain coherence measure to determine trace similarity) between each individual trace and stack of traces; et cetera. Although significant effort went into developing these automated quality rating routines, they were each eventually abandoned because they rejected high quality receiver functions. Final analysis employed the time consuming, less quantifiable but more reliable, single analyst "by eye" method: examining each trace individually and with neighboring traces and/or with stacked neighboring traces. After many viewing

iterations, I eventually settled on what constituted "good enough" to be considered usable and with which neighbor(s) each trace should be grouped. This binning technique has the advantage of using normalized amplitudes so variation with distance is not so pronounced. Each group was stacked to improve signal-to-noise ratio, and mean distance, mean depth, and mean slowness were calculated. The stack became the representative trace for that station at the mean back-azimuth and distance (Table 3). Appendix 2 is a station specific list of earthquake events that produced receiver functions considered high enough quality to use for stacking and crustal thickness determination. Figure 16 is a sample illustrating how individual traces contribute to a stack. Each stack provides one crustal thickness estimate.

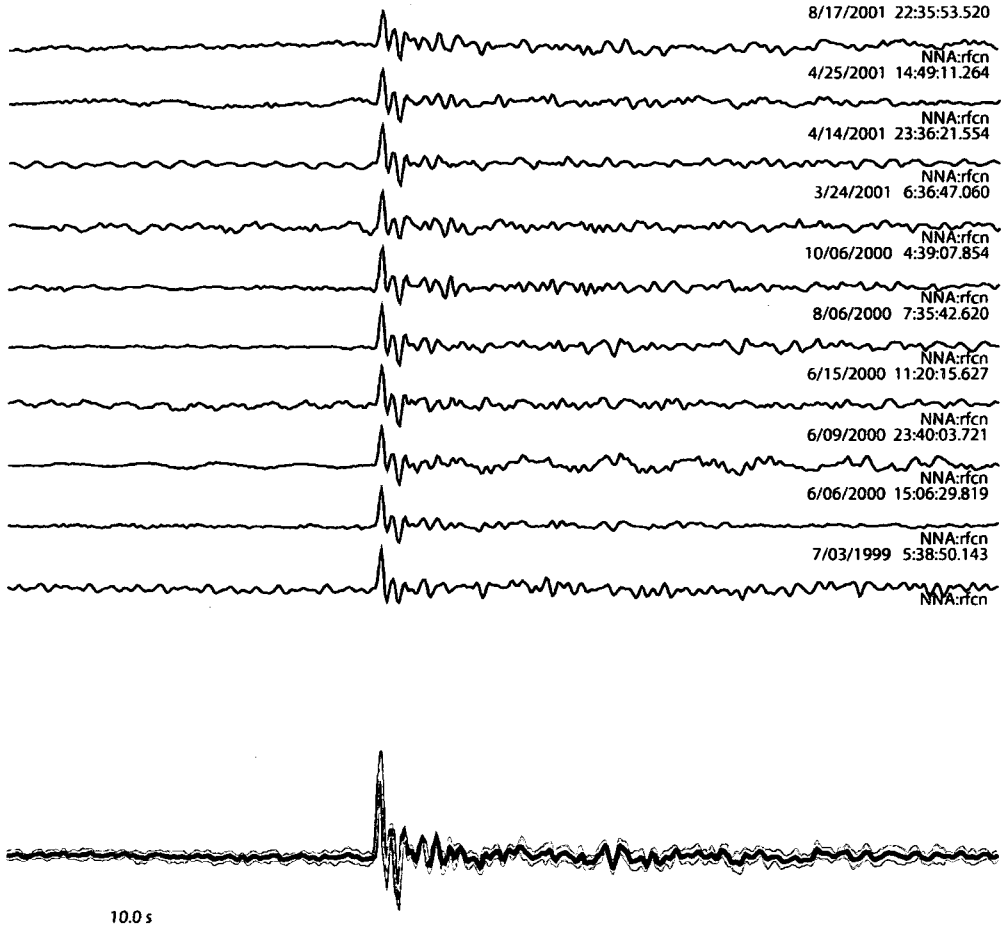

Figure 16: Sample receiver functions and stack. NNA264 (convention: NNA station identifier, 264 backazimuthal group identifier) includes radial receiver functions determined from events recorded at NNA from backazimuths between and including 264° to 278°, at a distance of 52° to 65°. Variance bounds shown on the stack indicate total variance of individual traces in the stack. This stack corresponds to line 8 in table 3.

Table 3: Stack list and crustal thickness results. Stack or representative trace list with station-to-event backazimuth (seaz) range, station-to-event distance (delta) range, mean backazimuth and distance, number of traces (n) in backazimuth and distance range considered high enough quality to use. Additional information for calculation of crustal thickness includes number of seconds fit (t_f) and number of seconds modeled (t_m), and degrees of freedom (N). This table also includes modeled and calculated values such as thickness of basin (T_{basin}), **crustal thickness** (T_m), and upper ($T_{m\,up}$) and lower ($T_{m\,lo}$) limits of crustal thickness at 95% confidence, total error at 95% confidence, and latitude and longitude of Moho piercing point. Crustal thickness values with total error less than 7 km (***T_m***) were considered reliable. Those with ≥7 km total error <u>underlined</u>. Stacks listed in *italics* were eliminated from study as indicated in text.

stack	seaz range (°)		delta range (°)		seaz (°)	delta (°)	n	t_f(s)	t_m(s)	N	T_{basin} (km)	$T_{m\,lo}$ (km)		T_m (km)		$T_{m\,up}$ (km)	T_{mup}-T_{mlo} (km)	latitude (°N)	longitude (°E)
NNA15	15	30	40	50	25	44.5	3	20	60	53.170	x	24.9	*	**25.7**	*	26.8	1.9	64.69014	211.04170
NNA105	105	115	70	90	109	80.7	3	20	60	53.170	x	25.1	*	**26.1**	*	27.6	2.5	64.55498	211.08970
NNA115	115	130	50	60	122	56.7	5	15.5	77.5	68.678	x	23	*	**24.3**	*	25.6	2.6	64.52734	211.11850
NNA200	200	210	80	100	206	83.8	4	20	80	70.893	x	25.2	*	**26.1**	*	27.8	2.6	64.51338	210.84730
NNA220	220	230	80	90	221	86.8	3	20	60	53.170	x	24.7	*	**25.4**	*	26.3	1.6	64.52880	210.81730
NNA235	235	260	70	90	242	81.4	7	20	140	124.063	x	25.1	*	**25.6**	*	26.2	1.1	64.54415	210.76850
NNA261	261	268	85	100	264	88.7	4	20	80	70.893	x	24.7	*	**25.3**	*	26.4	1.7	64.57310	210.76930
NNA264	264	278	52	65	272	57.1	10	20	200	177.232	x	25.3	*	**25.9**	*	26.7	1.4	64.58333	210.67740
NNA265	265	270	75	85	267	82.0	7	20	140	124.063	x	24.9	*	**25.3**	*	25.8	0.9	64.57609	210.75130
NNA268	268	275	29	50	270	39.9	13	20	260	230.402	x	26.5	*	**27.0**	*	27.5	1.0	64.58006	210.60930
NNA269	269	271	50	52	270	51.5	6	20	120	106.339	x	25.9	*	**26.8**	*	29.6	3.7	64.57999	210.64840
AND360	0	360	29	101	260	54.3	7	20	140	124.063	1.5	27	*	**28.6**	*	30.2	3.2	64.30959	210.52660
BSH	0	360	29	101	133	64.0	7	20	140	124.063	1.1	22.8	*	**23.5**	*	24.5	1.7	64.11155	210.84950
SOB	0	360	29	101	224	51.1	8	20	160	141.786	1.1	24.6	*	**25.7**	*	27.2	2.6	64.08933	210.52150
RCK110	110	120	29	101	117	59.5	2	20	40	35.446	1.3	19.3	*	**20.2**	*	21.6	2.3	64.00657	210.99070
RCK200	200	215	29	101	207	83.7	4	20	80	70.893	1.2	21.4	*	**22.1**	*	22.9	1.5	63.98690	210.77220
RCK230	230	240	29	101	238	81.4	3	20	60	53.170	1	21.6	*	**22.7**	*	23.9	2.3	64.00624	210.70540
RCK260	260	280	50	70	272	52.4	12	20	240	212.679	1	22.4	*	**22.7**	*	23.1	0.7	64.04398	210.61160
RCK261	261	281	29	50	273	42.0	4	20	80	70.893	1	21.2	*	**22.5**	*	23.5	2.3	64.04716	210.58420
RCK264	264	280	70	90	270	84.3	3	20	60	53.170	1	21.5	*	**22.6**	*	24	2.5	64.04067	210.68810
RCK300	300	360	29	101	332	75.8	6	20	120	106.339	0.9	21.1	*	**21.8**	*	22.3	1.2	64.10219	210.75890
SLT	0	360	29	101	194	69.7	6	24	144	127.607	1.5	24	*	**24.6**	*	25.3	1.3	63.85536	210.82990

Table 3 Stack list and crustal thickness results continued

Stack	seaz range (°)		delta range (°)		seaz (°)	delta (°)	n	t_f(s)	t_m(s)	N	T_{basin} (km)	$T_{m\,lo}$ (km)		T_m (km)		$T_{m\,up}$ (km)	T_{mup}-T_{mlo} (km)	latitude (°N)	longitude (°E)
GNR90	90	180	29	101	120	68.8	3	20	60	53.170	x	30.4	*	**33.2**	*	36.1	5.7	63.78196	211.22700
GNR200	200	215	29	101	206	86.2	8	20	160	141.786	x	28.1	*	**30.6**	*	34.9	6.8	63.76021	210.94010
GNR220	*220*	*230*	*29*	*101*	*229*	*83.1*	*1*	*18*	*18*	*15.951*	*x*	*21.6*		***29***		*37.3*	*15.7*	*63.78074*	*210.88130*
GNR230	*230*	*240*	*29*	*101*	*237*	*82.0*	*3*	*20*	*60*	*53.170*	*x*	*26.2*		***31***		*34.3*	*8.1*	*63.78490*	*210.85160*
GNR250	250	270	80	101	267	84.0	2	22	44	38.991	x	29.6	*	**30.8**	*	33.2	3.6	63.82981	210.82670
GNR260	260	280	29	52	272	43.8	10	19	190	168.371	x	28.9	*	**29.9**	*	30.8	1.9	63.83816	210.69910
MCK20	20	30	29	101	28.2	46.7	2	20	40	35.446	x	34.1		**37.6**		41.2	7.1	63.88547	211.25010
MCK200	200	216	29	101	207	86.8	8	20	160	141.786	x	36.4	*	**37.0**	*	37.4	1	63.64962	210.96930
MCK220	*220*	*250*	*29*	*101*	*236*	*83.0*		*20*			*x*	*29.5*		***34***		*37.5*	*8*	*63.67855*	*210.88200*
MCK260	260	270	79	101	265	87.6	7	20	140	124.063	x	25.5	*	**26.9**	*	30.2	4.7	63.72616	210.90170
																			210.81010
SAN100	100	112	29	101	108	77.5	6	22	132	116.973	1	28.4	*	**29.3**	*	30.5	2.1	63.69468	210.72060
SAN115	115	130	29	101	122	55.1	4	20	80	70.893	1	28.2	*	**29.4**	*	30.6	2.4	63.65690	210.75610
SAN200	200	250	29	101	223	84.7	7	20	140	124.063	0.9	22.4	*	**22.8**	*	23.4	1	63.67674	210.42380
SAN250	250	290	29	80	271	57.4	9	20	180	159.509	0.9	26.1	*	**27.2**	*	28.1	2	63.72428	210.25390
EFS	0	360	29	101	187	73.2	3	20	60	53.170	x	36.5	*	**39.5**	*	42.4	5.9	63.43090	210.18240
SBL110	110	130	29	101	120	56.2	2	20	40	35.446	x	38.2	*	**42**	*	43.3	5.1	63.38253	210.13600
SBL200	200	270	29	101	237	71.3	4	20	80	70.893	x	37		**40.8**		44	7	63.39334	209.54100

Table 3 Stack list and crustal thickness results continued

Stack	seaz range (°)		delta range (°)		seaz (°)	delta (°)	n	t_f(s)	t_m(s)	N	T_{basin} (km)	$T_{m\,lo}$ (km)		T_m (km)		$T_{m\,up}$ (km)	T_{mup}-T_{mlo} (km)	latitude (°N)	longitude (°E)
WON20	*20*	*30*	*29*	*101*	*27*	*47.3*	*1*	*20*	*20*	*17.723*	*x*	*21.5*		***26.9***		*34.3*	*12.8*	*63.57202*	*209.27240*
WON200	200	240	29	101	218	82.2	8	20	160	141.786	x	28.2	*	**28.4**	*	28.7	0.5	63.39759	209.03460
WON250	250	260	60	61	256	60.6	2	20	40	35.446	x	31.5	*	**34.8**	*	38.2	6.7	63.42927	208.85310
WON265	265	280	35	45	272	40.1	6	20	120	106.339	x	30.2	*	**31.6**	*	33.1	2.9	63.46746	208.79460
YAN105	105	115	65	75	110	69.3	4	20	80	70.893	x	31.3	*	**33**	*	34.7	3.4	63.61640	211.46860
YAN115	*115*	*130*	*49*	*57*	*124*	*53.8*	*4*	*20*	*80*	*70.893*	*x*	*30.1*		***33.8***		*37.6*	*7.5*	*63.57528*	*211.49220*
YAN200	200	230	81	97	211	85.8	14	20	280	248.125	x	37	*	**37.7**	*	38.5	1.5	63.56772	211.10650
YAN230	230	250	29	101	240	82.0	10	20	200	177.232	x	37.8	*	**40.1**	*	42.9	5.1	63.59739	211.00100
YAN250	250	290	29	50	272	39.8	16	20	320	283.572	x	33.2	*	**34.5**	*	36	2.8	63.66197	210.83860
YAN265	265	270	53	60	267	55.0	2	20	40	35.446	x	30.4		**33.9**		37.9	7.5	63.64855	210.91080
YAN269	*269*	*272*	*50*	*53*	*271*	*51.7*	*7*	*20*	*140*	*124.063*	*x*	*32.9*		***36.1***		*40.4*	*7.5*	*63.65920*	*210.87040*
YAN275	275	285	60	80	280	71.8	5	20	100	88.616	x	31.5	*	**33.7**	*	36.1	4.6	63.67462	210.97280
YAN320	320	360	29	101	334	77.7	5	24	120	106.339	x	29.7	*	**30.2**	*	30.8	1.1	63.73953	211.13370
CAR260	260	280	29	101	274	55.4	8	20	160	141.786	x	36.4	*	**38.2**	*	39.9	3.5	63.59436	210.84310
SLM260	260	282	60	96	273	80.1	6	20	120	106.339	x	36.3	*	**38**	*	39.7	3.4	63.51193	210.94060
SLM265	265	285	29	60	273	52.1	14	20	280	248.125	x	35.3	*	**36.3**	*	37.3	2	63.51490	210.84420
SLM300	*300*	*310*	*29*	*101*	*303*	*76.0*	*1*	*20*	*20*	*17.723*	*x*	*29*		***35***		*40.7*	*11.7*	*63.56679*	*210.98530*
RND105	*105*	*115*	*70*	*90*	*108*	*76.8*	*2*	*20*	*40*	*35.446*	*x*	*25.1*		***41.2***		*46.8*	*21.7*	*63.36538*	*211.41190*
RND109	109	114	50	70	110	66.0	3	20	60	53.170	x	40	*	**42.4**	*	44.8	4.8	63.35154	211.46270
RND200	200	210	80	101	207	88.0	7	20	140	124.063	x	27.8	*	**29.4**	*	31.1	3.3	63.33816	211.06350
RND210	*210*	*230*	*80*	*101*	*218*	*84.8*	*3*	*20*	*60*	*53.170*	*x*	*27.7*		***33.1***		*39.3*	*11.6*	*63.33367*	*211.01460*
RND230	*230*	*241*	*80*	*101*	*239*	*81.4*	*6*	*20*	*120*	*106.339*	*x*	*32.1*		***37.8***		*42.2*	*10.1*	*63.34790*	*210.93000*
RND246	246	270	80	101	261	86.0	7	20	140	124.063	x	37.5	*	**39.5**	*	41.6	4.1	63.38921	210.90300
RND250	250	290	60	80	271	67.1	9	20	180	159.509	x	39	*	**40.4**	*	41.8	2.8	63.40874	210.81700
RND265	265	280	50	60	273	53.4	10	20	200	177.232	x	38	*	**39.2**	*	40.4	2.4	63.41260	210.76850
RND270	270	285	29	50	273	40.3	5	20	100	88.616	x	37.7	*	**38.7**	*	39.7	2	63.41551	210.71300

Table 3 Stack list and crustal thickness results continued

Stack	seaz range (°)		delta range (°)		seaz (°)	delta (°)	n	t_f(s)	t_m(s)	N	T_{basin} (km)	$T_{m\,lo}$ (km)		T_m (km)		$T_{m\,up}$ (km)	T_{mup}-T_{mlo} (km)	latitude (°N)	longitude (°E)
RND300	*300*	*310*	*29*	*101*	*303*	*76.0*	*1*	*20*	*20*	*17.723*	*x*	*36.2*		***40.9***		*45.8*	*9.6*	*63.47579*	*210.89550*
RND320	*320*	*325*	29	101	*325*	*87.9*	1	20	*20*	*17.723*	*x*	*23.5*		***40.9***		*53.6*	*30.1*	63.49207	*211.00240*
GOO200	200	270	29	101	230	85.2	14	20	280	248.125	x	36.1	*	**37.9**	*	39.6	3.5	63.16170	210.55350
GOO270	270	290	29	101	279	59.8	7	20	140	124.063	x	37.7	*	**40.4**	*	43.1	5.4	63.25181	210.37940
GOO300	300	360	29	101	328	75.7	5	20	100	88.616	x	44.2	*	**47**	*	49.5	5.3	63.35485	210.55330
HURN10	10	20	29	101	12.7	43.0	3	20	60	53.170	x	31.9	*	**35.3**	*	38.7	6.8	63.16527	210.47640
HURN100	100	130	29	60	121	55.0	4	20	80	70.893	x	32.8	*	**36.3**	*	39.2	6.4	62.92036	210.67830
HURN101	101	120	60	101	110	70.4	5	20	100	88.616	x	35.2	*	**37.9**	*	40.2	5	62.95541	210.66280
HURN200	200	217	29	101	205	84.8	19	26	494	437.764	x		*	**34.3**	*			62.91344	210.30500
HURN220	220	230	29	101	223	83.7	9	20	180	159.509	x	33.5	*	**34.6**	*	35.7	2.2	62.92787	210.24770
HURN230	230	240	29	101	237	81.5	12	20	240	212.679	x	34	*	**35.2**	*	36.3	2.3	62.94372	210.20400
HURN240	240	250	29	101	244	84.1	6	20	120	106.339	x	32.4	*	**34.5**	*	36.5	4.1	62.95682	210.20310
HURN250	250	270	59	70	256	63.3	4	20	80	70.893	x	33.6	*	**36.2**	*	38.6	5	62.96509	210.10270
HURN251	251	270	80	101	264	87.8	10	20	200	177.232	x	36.3	*	**37.5**	*	38.7	2.4	62.98808	210.17640
HURN269	269	280	50	55	274	52.2	7	20	140	124.063	x	35.1	*	**36.5**	*	37.9	2.8	63.00875	210.04560
HURN270	270	285	38	41	277	39.0	3	20	60	53.170	x	35.4	*	**37.3**	*	39.1	3.7	63.02034	209.98650
HURN272	272	280	55	60	275	58.6	3	20	60	53.170	x	36.1	*	**38.1**	*	40.1	4	63.01258	210.05810
HURN278	278	281	60	80	279	69.3	5	20	100	88.616	x	33.6	*	**35.8**	*	37.9	4.3	63.01878	210.12250
HURN300	*300*	*310*	*29*	*101*	*302*	*75.9*	*1*	*20*	*20*	*17.723*	*x*	*30.1*		***35.8***		*41*	*10.9*	*63.05965*	*210.18130*
HURN320	320	330	29	101	326	78.7	4	20	80	70.893	x	33.6	*	**36.2**	*	38.9	5.3	63.09009	210.26000
HURN340	*340*	*344*	*29*	*101*	*341*	*75.6*	*1*	*20*	*20*	*17.723*	*x*	*28.7*		***34.1***		*39.6*	*10.9*	*63.10190*	*210.31450*
PYY270	270	281	29	101	275	58.0	7	20	140	124.063	x	38.4	*	**40.2**	*	41.7	3.3	62.92175	209.93480
PYY302	*302*	*304*	*29*	*101*	*302*	*75.9*	*1*	*20*	*20*	*17.723*	*x*	*34*		***40***		*45.5*	*11.5*	*62.97689*	*210.05160*
MHR100	100	120	29	101	107	71.8	3	20	60	53.170	x	35.6	*	**38.5**	*	41.4	5.8	62.82213	210.40670
MHR200	200	220	29	101	205	84.5	9	20	180	159.509	x	38.8	*	**39.9**	*	41	2.2	62.76011	210.03110
MHR230	230	240	29	101	239	80.2	6	20	120	106.339	x	35.3	*	**37.7**	*	39.9	4.6	62.80179	209.92540
MHR250	250	290	29	101	271	55.1	20	18	360	319.018	x	35.1	*	**36.1**	*	37.1	2	62.86174	209.80590
MHR300	300	360	29	101	323	78.8	4	20	80	70.893	x	34.9	*	**37.1**	*	39.3	4.4	62.95033	209.98800

Table 3 Stack list and crustal thickness results continued

Stack	seaz range (°)		delta range (°)		seaz (°)	delta (°)	n	t_f(s)	t_m(s)	N	T_{basin} (km)	$T_{m\,lo}$ (km)		T_m (km)		$T_{m\,up}$ (km)	T_{mup}-T_{mlo} (km)	latitude (°N)	longitude (°E)
FID217	*217*	*222*	*29*	*101*	*220*	*85.0*	*1*	*20*	*20*	*17.723*	*x*	*23.6*		***37.8***		*45.1*	*21.5*	*62.68279*	*209.78460*
BYR200	200	210	29	101	205	84.0	22	18	396	350.920	x	32.1	*	**33.5**	*	34.7	2.6	62.60479	209.68400
BYR210	210	232	29	101	222	84.0	6	20	120	106.339	x	33.7	*	**35.7**	*	37.5	3.8	62.61521	209.62260
BYR232	232	250	29	101	238	81.2	18	20	360	319.018	x	35.9	*	**36.9**	*	38	2.1	62.63207	209.56880
BYR250	250	260	65	80	254	68.6	4	20	80	70.893	x	36.2	*	**38.4**	*	40.5	4.3	62.65107	209.48620
BYR251	251	270	80	101	262	86.4	10	20	200	177.232	x	36.8	*	**38.6**	*	40.2	3.4	62.67517	209.54330
BYR252	252	280	55	60	269	57.7	7	8	56	49.625	x	37.2	*	**38.9**	*	40.7	3.5	62.68659	209.43000
BYR259	259	260	60	62	260	60.3	1	8	8	7.089	x	35.7	*	**38.5**	*	41.4	5.7	62.66223	209.45030
BYR269	269	289	50	55	272	51.4	9	8	72	63.804	x	39	*	**40.2**	*	41.5	2.5	62.69537	209.38500
BYR270	270	285	29	50	273	38.6	9	20	180	159.509	x	38.2	*	**39.2**	*	40.2	2	62.69744	209.33890
BYR275	275	285	65	80			8	20	160	141.786	x								
BYR320	320	330	29	101	326	78.8	4	20	80	70.893	x	43.4	*	**45.8**	*	48.3	4.9	62.80366	209.59930
WOLF200	*200*	*225*	*29*	*101*	*212*	*85.4*	*3*	*20*	*60*	*53.170*	*x*	*27.9*		***34.3***		*39.6*	*11.7*	*62.48054*	*209.68990*
WOLF250	250	269	60	93	258	81.4	4	20	80	70.893	x	36.5	*	**39.5**	*	42.7	6.2	62.53600	209.55110
WOLF260	*260*	*269*	*93*	*98*	*264*	*94.6*	*1*	*18*	*18*	*15.951*	*x*	*29.7*		***36.7***		*43.8*	*14.1*	*62.55030*	*209.60310*
WOLF269	269	279	50	60	273	53.9	7	18	126	111.656	x	32.3	*	33.5	*	34.8	2.5	62.56653	209.48920
TCE	0	360	29	101	236	63.8	33	20	660	584.867	1.5	26.1	*	**26.5**	*	26.7	0.6	62.25980	209.50910
PVE	260	290	29	101	273	55.3	8	20	160	141.786	1.4	21.8	*	**22.5**	*	23.3	1.5	62.36031	209.13480
PVW105	105	125	50	80	112	63.7	5	20	100	88.616	x	29.9	*	**31.4**	*	33	3.1	62.48279	209.43170
PVW200	200	250	29	101	222	82.4	7	20	140	124.063	x	31.7	*	**34.1**	*	36.6	4.9	62.45425	209.05460
PVW250	250	270	75	101	261	87.1	9	20	180	159.509	x	28.5	*	**29.7**	*	31.1	2.6	62.51541	209.02640
PVW251	*251*	*262*	*50*	*75*	*256*	*62.9*	*4*	*20*	*80*	*70.893*	*x*	*23.7*		***29.2***		*31.7*	*8*	*62.50113*	*208.96500*

Table 3 Stack list and crustal thickness values continued

Stack	seaz range (°)		delta range (°)		seaz (°)	delta (°)	n	t_f(s)	t_m(s)	N	T_{basin} (km)	$T_{m\,lo}$ (km)		T_m (km)		$T_{m\,up}$ (km)	T_{mup}-T_{mlo} (km)	latitude (°N)	longitude (°E)
PVW260	260	275	40	60	270	51.0	10	20	200	177.232	x	25.6	*	**26.1**	*	26.8	1.2	62.52734	208.94790
PVW270	*270*	*280*	*60*	*75*	*277*	*72.6*	*2*	*20*	*40*	*35.446*	*x*	*24.6*		***27.7***		*32*	*7.4*	*62.53893*	*208.99750*
PVW280	*280*	*290*	*38*	*40*	*281*	*38.1*	*1*	*20*	*20*	*17.723*	*x*	*25.1*		***27.5***		*32.9*	*7.8*	*62.55411*	*208.89860*
CZN1	0	1	29	101	0.28	76.2	1	20	20	17.723	x	24.6		**29.7**		38	13.4	63.19736	213.35740
CZN200	200	250	29	101		84.5					x			**36.5**					
CZN250	250	270	29	101	264	89.9	6	20	120	106.339	x	36.7	*	**38.1**	*	39.5	2.8	63.09337	213.14050
DH3 230	*230*	*250*	*80*	*101*	*238*	*83.4*	*3*	*18*	*54*	*47.853*	*x*	*20.1*		***27.2***		*51.2*	*31.1*	*62.99367*	*212.71270*
DH3 250	250	270	80	101	260	89.1	4	20	80	70.893	x	31.5	*	**34.2**	*	36.7	5.2	63.01948	212.66450
DH3 251	251	290	29	80	272	51.8	7	20	140	124.063	x	33.1	*	**34.4**	*	35.7	2.6	63.04047	212.52690
DH3 320	*320*	*350*	*29*	*101*	*333*	*80.2*	*3*	*20*	*60*	*53.170*	*x*	*27.4*		***30.7***		*34.4*	*7*	*63.11520*	*212.76410*
DH2 20	20	30	29	101	28.6	46.9	2	20	40	35.446	x	37.6	*	**41.1**	*	44.5	6.9	63.43170	212.34770
DH2 120	*120*	*130*	*29*	*101*	*124*	*54.6*	*1*	*20*	*20*	*17.723*	*x*	*36.5*		***40.6***		*44.8*	*8.3*	*63.16945*	*212.45850*
DH2 200	*200*	*250*	*29*	*101*	*214*	*85.6*	*1*	*20*	*20*	*17.723*	*x*	*25.6*		***32.6***		*39.9*	*14.3*	*63.19190*	*212.03500*
DH2 260	260	310	29	101	283	63.4	5	20	100	88.616	x	42.8	*	**44.8**	*	46.8	4	63.30300	211.77850
DH1 110	110	126	29	101	117	60.4	6	20	120	106.339	x	40	*	**41.5**	*	43	3	63.29824	211.93820
DH1 200	200	220	29	101	208	86.1	9	20	180	159.509	x	41.5	*	**42.7**	*	43.8	2.3	63.27147	211.49810
DH1 220	220	230	29	101	225	84.1	7	20	140	124.063	x	40.7	*	**42.4**	*	44.2	3.5	63.28934	211.43120
DH1 235	235	245	29	101	239	82.2	13	20	260	230.402	x	41.2	*	**42.3**	*	43.4	2.2	63.30137	211.34840
DH1 250	250	270	70	101	266	86.9	5	20	100	88.616	x	42.3	*	**44.4**	*	46.5	4.2	63.36461	211.35050
DH1 252	252	270	50	70	266	57.6	4	20	80	70.893	x	40.4	*	**42.4**	*	44.3	3.9	63.35982	211.24120
DH1 271	271	280	39	50	273	47.2	2	20	40	35.446	x	39.3	*	**41.9**	*	44.4	5.1	63.38399	211.18830
DH1 270	270	290	50	60	274	53.4	15	20	300	265.849	x	41.8	*	**42.6**	*	43.4	1.6	63.38415	211.21100
DH1 275	275	285	65	75	280	70.9	4	20	80	70.893	x	42.9	*	**45.1**	*	47.3	4.4	63.39960	211.27910
DH1 320	*320*	*326*	*29*	*101*	*325*	*88.1*	*1*	*20*	*20*	*17.723*	*x*	*38.9*		***46.2***		*51.5*	*12.6*	*63.47126*	*211.46400*

Chapter 4 - Determination of Crustal Thickness

A receiver function can be inverted for vertical velocity structure beneath a three-component broadband seismic station. A linearized time domain inversion can be utilized to produce a flat layered velocity model from an observed receiver function. In general, waveform inversion includes selection of an initial velocity model assuming values for thickness and velocity of each layer, calculating the response to this assumed velocity model, comparing the calculated theoretical receiver function to the observed receiver function, evaluating fit, calculating derivatives, and iteratively modifying parameter values to increase correlation (Langston, 1977; Owens et al., 1984; Mellman, 1980; Golub and Kahan, 1965; Wiggins, 1976). The best match between observed receiver function and synthetic receiver function indicates the best estimate of the crustal structure.

While receiver functions can be inverted for a crustal velocity profile beneath a station, the inversion process is nonlinear and the solution nonunique (Ammon et al., 1990). Waveform inversion includes assuming the thickness and velocity of each layer in the initial model prior to calculating the response of the initial model. The arrival times of converted phases are dependent on the velocity and thickness of each layer, producing a trade-off between these two parameters. Accepting there is some tradeoff between thickness and velocity; one may use a priori information on regional velocity and structure to construct a reasonable initial plane layered model.

The phrase "plane layered model" highlights the other important assumption made when inverting receiver functions for vertical velocity structure. The inversions assume horizontal layering, a significant simplification in the Alaska Range given the structural complexities resulting from accretion and transpressional rotation of allochthonous tectonostratigraphic terranes. In areas with structural complexities such as folded and faulted bedding planes, converted energy may be produced at any of the structural boundaries, which in turn can complicate the receiver function. Although we know there are deviations from horizontal layering within the crust, it is reasonable to assume that the Mohorovicic discontinuity is to a first approximation a relatively flat lying discontinuity that marks the base of the crust. Indeed, the strong velocity contrast at the base of the crust produces strong conversions that are clearly visible in the raw receiver functions and remain relatively well behaved over large regions. In an ideal model with a single perfectly horizontal discontinuity, the timing and shape of the Ps conversion along with the timing and shape of the multiple reverberations should allow constraint of both thickness and velocity of the layer. If this discontinuity is dipping, multiple reverberations are either advanced or delayed as the raypath is shortened or lengthened updip or downdip. If a dipping discontinuity were the only complication, there would be some benefit to matching the reverberation, however, the structural complexities in the Alaska Range produced additional arrivals that may overwhelm the multiple

reverberation. One such arrival is the slab conversion explored by Ferris et al. (2003). Given these considerations, the receiver functions in this study are interpreted as a homogeneous crust over mantle, modeling the direct Ps Moho conversion alone, ignoring arrivals caused by structural complexities within the crust and/or mantle.

The timing of the direct Ps Moho conversion depends on two parameters: crustal velocity and depth to Moho. Ideally one could constrain both velocity and depth via a double grid search technique, varying both velocity and depth, and comparing each synthetic receiver function to the observed receiver function to find the best fit. For each stack or representative trace, a homogeneous crust over mantle plane layered model was used to calculate a suite of synthetic receiver functions with crustal compressional velocities between 6.0 and 7.0 km/s as well as a suite of synthetic receiver functions varying interface depth from 20 to 70 km (at 0.5 km intervals). Each synthetic was compared to the representative trace, and minimum root-mean-square misfit calculated to indicate best fit. The depths were generally well constrained but (of course) varied with velocity, which was expected given the nonuniqueness of inverting receiver functions for velocity as introduced above. Figure 17 includes a Moho depth vs. crustal P velocity contour plot which illustrates this relationship between velocity and depth: the linear trend shows that given a conversion arrival time, a higher velocity correlates with a deeper discontinuity. While we hoped to constrain crustal velocity in the 6.0 to 7.0 km/s range with this method, examination of roughly 180 depth vs. velocity contour plots (one for each reasonable stack) revealed no consistent velocity constraint. Figure 17(b) shows that the best fit velocity synthetic (6.1 km/s in this example) and the 6.5 km/s synthetic are very similar.

By assuming an average crustal velocity, the arrival time of the direct Ps conversion constrains depth to Moho. A priori information from the literature guided our choice of the most appropriate crustal velocity. We considered interpretation of data from TACT profiles to the south and north of our study area (Wolf et al., 1991; Beaudoin et al., 1992; Beaudoin et al., 1994), tomographic imaging of the Alaska subduction zone (Zhao and Christensen, 1992; Zhao et al., 1995), and a study of travel times of regional Pn and Sn phases (McNamara and Pasyanos, 2002). In the end, we used 6.5 km/s as the average crustal P velocity. The process was repeated using 6.5 km/s crustal P velocity, i.e. calculating a suite of synthetic receiver functions by varying depth (at 0.1 km intervals), comparing each of these calculated theoretical receiver functions to the observed receiver function, and identifying the best fit model via minimum root-mean-square misfit (sample output in Figure 18). The accuracy of our depth to Moho constraint will be affected by the difference between our assumed velocity and real crustal velocity, so if real crustal velocity is higher than 6.5 km/s the actual depth to Moho will be proportionally deeper. Similarly, if real crustal velocity is lower than 6.5 km/s the actual depth to Moho will be proportionally shallower.

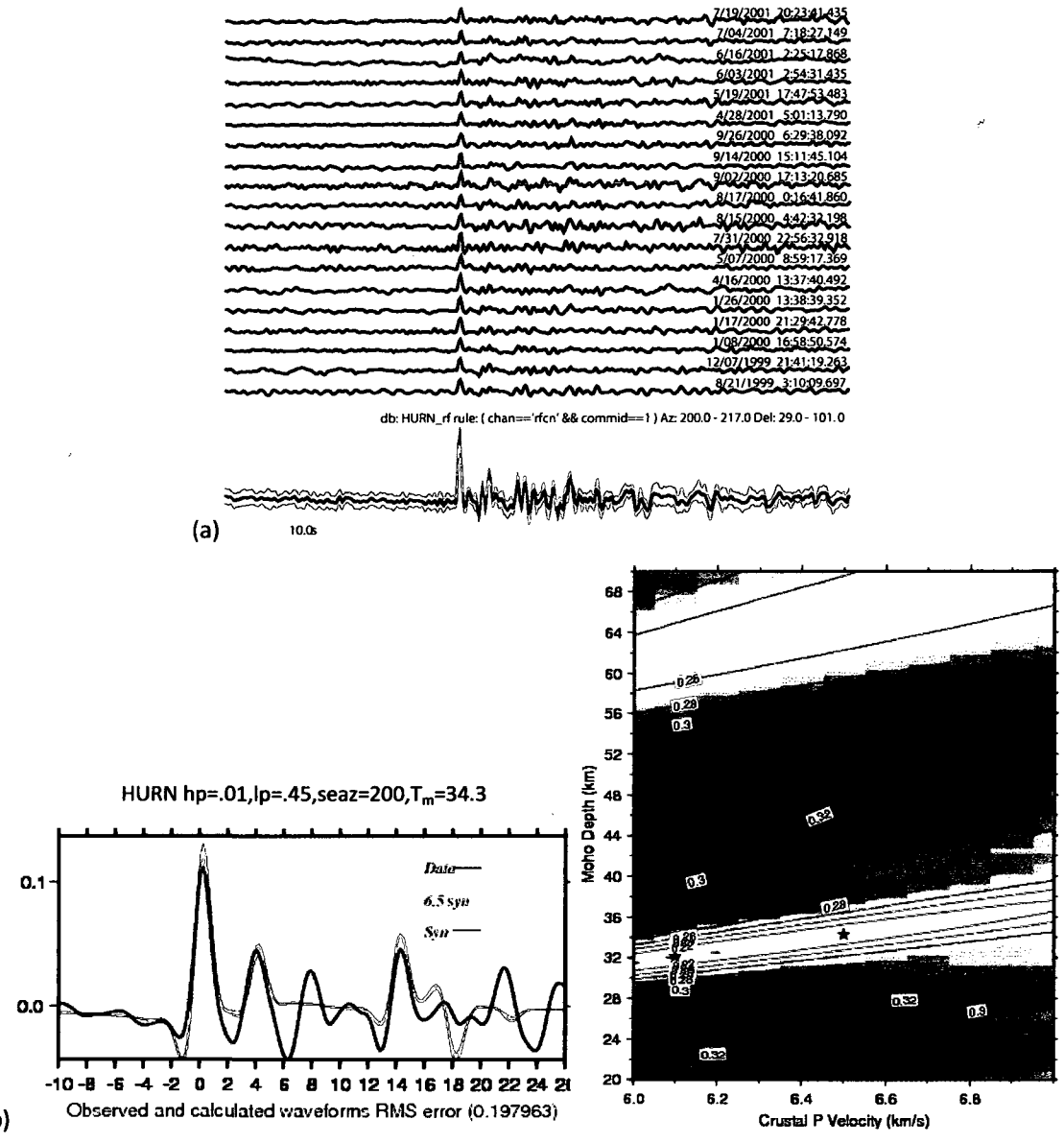

Figure 17: HURN200 -- Sample modeling crustal thickness from a synthetic receiver function by fit between synthetic receiver function and receiver function deconvolved from seismogram. (a) Individual receiver functions from backazimuth range 200° – 217° from HURN, and stack with total variance. (b) Left plot shows time limited receiver function and two synthetics: best fit velocity and 6.5 km/s. These receiver functions display a slab conversion arrival around 8 sec, and a multiple arrival around 14 sec. In this case it was deemed appropriate to vary the time fit from the usual 10 sec beyond direct P wave arrival to 16 sec. The slab arrival causes a second low in the grid search that agrees reasonably well with the slab depth contours determined from seismicity (e.g. Figure 7). The stack was not eliminated because the second low in the root-mean-square misfit was due to a clearly defined slab arrival (vs. an indistinct Ps conversion). Right plot shows Moho depth (star) at minimum root-mean-square misfit (between observed and calculated receiver functions – contours indicate misfit) for crustal P velocity between 6.0 and 7.0 km/s at 0.1 km/s intervals such that 6.5 km/s crust indicates Moho depth at 34.0 km (to nearest 0.5 km). The best fit velocity in the 6.0 to 7.0 km/s range for this stack is 6.1 km/s.

Mohorovicic discontinuity (Moho) depths were determined by fitting 20 seconds of a stacked receiver function to a simple plane layered model with a crustal P velocity (V_P)≈6.5 km/s, a V_p/V_s ratio of 1.73, and a mantle P velocity of 8.2 km/s, minimizing root-mean-square misfit between data and synthetics, similar to Sheehan et al. (1995). The *dep*th *est*imation script written by Geoff Abers is incorporated into the Antelope Software as *depest*. *depest* finds the best fit between observed and synthetic receiver functions. All models presented use identical values for crustal V_p, V_p/V_s, and mantle V_p, but due to waveform complexity the exact number of seconds fit to the observed receiver function (t_f) was allowed to vary where appropriate (Table 3). Figures 17 and 18 are examples of neighboring stacks at HURN that show raw receiver functions deconvolved from seismograms and the resulting stacked receiver functions in (a), and the contour plots comparing Moho depth to crustal P velocity indicating best fit crustal thickness, as well as a time limited plot of observed and synthetic receiver functions in (b).

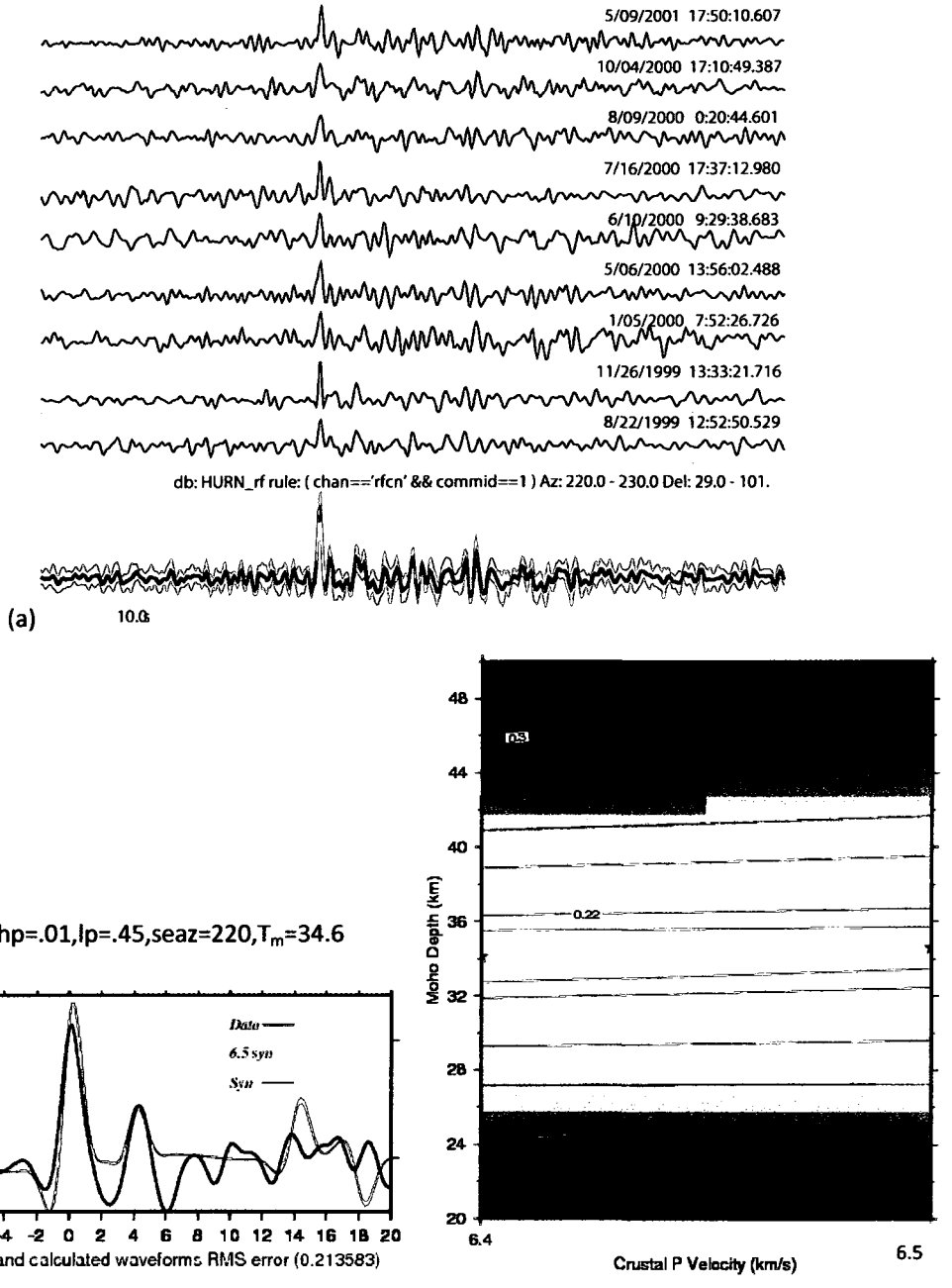

Figure 18: HURN220 -- sample modeling crustal thickness from a synthetic receiver function. (a) Receiver functions in backazimuth range 220°-230° from HURN, variance indicated around stacked receiver function. Background noise to left of P wave arrival was used to evaluate data quality. (b) Left plot shows 30 seconds of observed receiver function and best fit synthetic receiver function. I fit primary arrival and Ps conversion, -10 sec to 10 sec. Synthetic multiple arriving between 14-15 seconds (not fit). Right plot of Moho depth vs. crustal P velocity shows Moho depth at minimum root mean square misfit (between observed and calculated receiver functions – contours indicate misfit) for crustal P velocity 6.4 km/s (left) and 6.5 km/s (right), with 95% confidence interval shown in red, at 33 km and 35 km depth.

Sedimentary basins significantly affect a seismic waveform by delaying and broadening the main pulse (Figure 19). This was observed north of the Alaska Range at stations AND, BSH, SOB, RCK, SLT, and SAN, as well as to the south at PVE, TCE, and TLKY (Figure 7, Table 3). To account for sedimentary basins in receiver function modeling, I employed a double grid search with two interfaces. The uppermost interface was allowed to vary between 0 and 5 km depth (at 0.1 km intervals), representing the base of a sedimentary unit given a compressional velocity of 3.3 km/s and V_p/V_s of 1.97 (Castagna et al., 1985), while the lower interface represented the Moho. The compressional velocity was chosen to be representative of sedimentary units, and the V_p/V_s was determined using Pickett's mudrock trend $V_p=1.16V_s+1.36$ (Ludwig et al., 1970; Castagna et al., 1985), comparable to those determined by Brocher (2005). Modeled basin thicknesses of 0.9 to 1.5 km were in reasonable agreement with available geologic data (Kirschner, 1994a, 1994b; Csejtey et al., 1992).

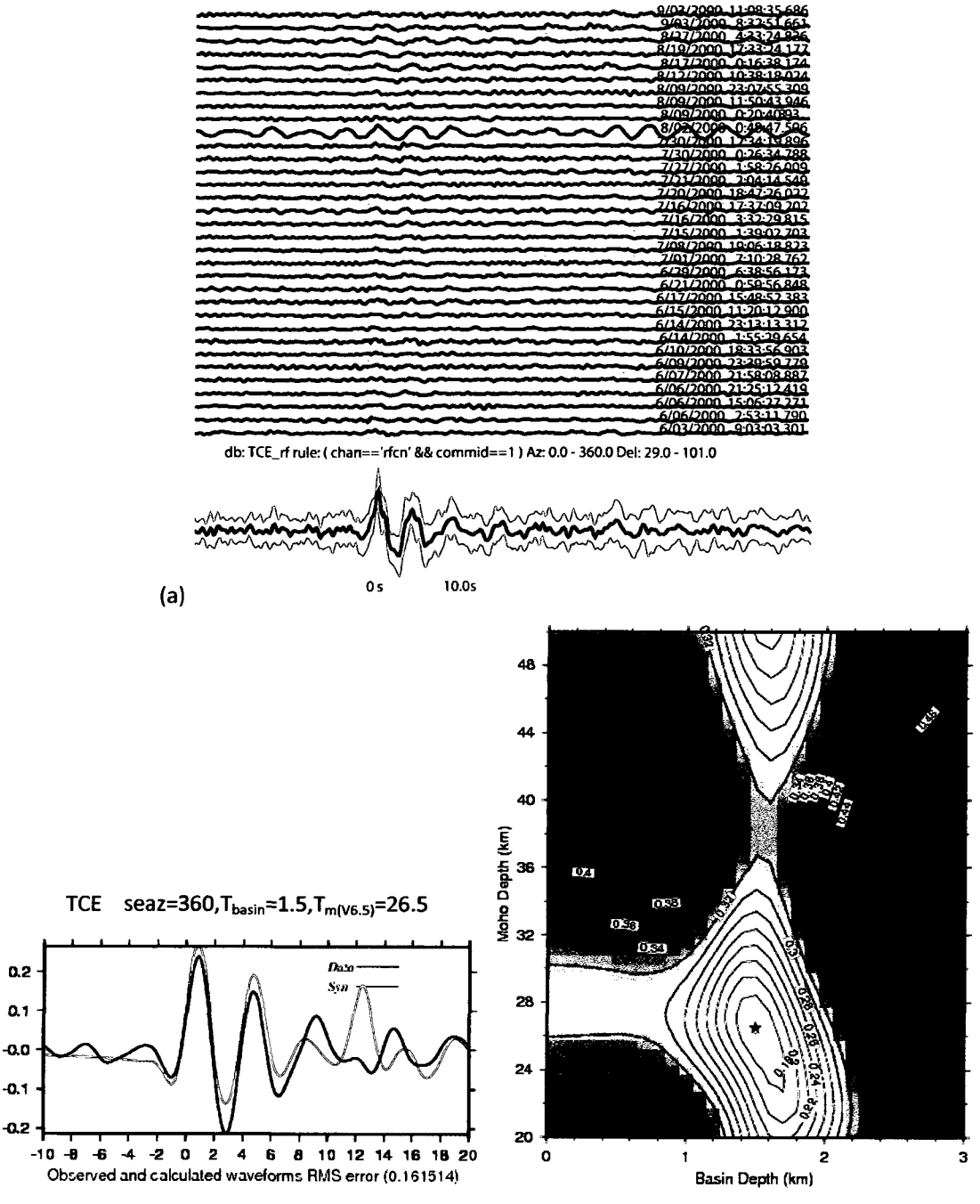

Figure 19: TCE -- Sample simultaneous modeling of both crustal and sedimentary basin thickness. The signal recorded at stations located on sedimentary basins is somewhat ringy with slight broadening of the main pulse and the first converted phase. (a) Receiver functions in 0-360° backazimuth range from TCE, total variance shown around stack. (b) Left plot with 30 seconds of normalized amplitude observed and synthetic receiver functions shows the slab conversion arrives 9-10 seconds after the direct P wave arrival, logically creating a second low in the misfit curve at just over 50 km depth. Right contour plot of Moho depth vs. basin depth shows best fit basin depth of 1.5 km and best fit Moho depth of 26.5 km.

In modeling Moho depths, a standard F test (that uses the ratio of variances to test the null hypothesis that variances are from same population) was used to generate confidence limits on the fully nonlinear grid search (see Ferris et al., 2003). Table 3 lists crustal thickness (T_m), and upper and lower limit crustal thicknesses at 95% confidence ($T_{m(up)}$ and $T_{m(lo)}$ respectively). To determine upper and lower limits of crustal thicknesses at 95% confidence, the total number of seconds modeled (t_m) is the number of traces in the stack (n) times the number of seconds fit for the root-mean-square calculation (t_f). Degrees of freedom (N) = number of seconds modeled /1.128462. (1.128462 seconds per degree of freedom from Geoff Abers' "crude model" for CMG3T filtered 0.01 to 0.45 Hz.) The number of parameters factors into the calculation of confidence limits. In models with one parameter (just crustal thickness), the F test

$$\text{constant} = \text{sqrt}(1+1/(N-1)*\text{finv}(.95,1,N-1)) \quad (4.1)$$

In models with two parameters (basin thickness and crustal thickness), the F test

$$\text{constant} = \text{sqrt}(1+2/(N-2)*\text{finv}(.95,2,N-2)). \quad (4.2)$$

The fit between a stacked waveform and the modeled waveform provided further quality control. I eliminated many crustal thickness estimates because of multiple lows in the root-mean-square misfit curve, indicating an indistinct Ps conversion, including: GNR340, MCK109, MCK280, SLM110, RND120, GOO109, BYR300, BYR330, WOLF20, WOLF100, WOLF270, WOLF300, PVW330, PVW290, and PVW320. The estimates at DH3 110 and DH3 200 were clearly not modeling simple crust, so they were removed from further Moho study.

Complicated waveforms may be produced by geologic structures such as faults and folds, which are common in the Alaska Range. Shallow structure effects (Owens and Crosson, 1988) represent deviations from a simple plane layered model, beyond the scope of this study. Those stacks removed from consideration because they were suspected to be anomalous due to structural anomalies include: NNA280, NNA300, NNA320, NNA340, GNR20, GNR320, GNR350, MCK119, MCK255, CAR200, CAR290, SLM200, RND325, GOO20, FID259, BYR10, BYR106, and BYR108. By referring to Figure 20, one can compare these back-azimuths to mapped faults. The locations of these eliminated stacks suggest that the ray paths may have encountered geologic structures that could have complicated the waveform.

Disappointingly many waveforms recorded at stations in Denali National Park were very poor quality and immediately eliminated. Complex waveforms may have been produced by complex structure associated with accretion and lateral translation of the small terranes in the region. The Neotectonic Map of Alaska (Plafker et al., 1994) shows that the center of the BEAAR transect crosses a zone rife with documented young faults such as the Denali fault system (e.g. Clague, 1979; Denton and Stuvier, 1967; Eberhart-Philips et al., 2003; Hickman, 1971; Hickman et al., 1977; Plafker et al., 1977; Stout et al., 1973),

Healy Fault (Thorson, 1979), Healy Creek Fault (Woodward-Lundgren, 1974; Wahrhaftig, 1970), Wood River Thrust (Csejtey et al., 1986), and Yanert Fork Fault (Csejtey et al., 1986). To the south, suspect back-azimuths cross northeast striking faults that parallel the Broxson Gulch or Pass Creek faults (Nokleberg et al., 1982, 1985; Stout and Chase, 1980). Some waveforms appeared to provide clear arrivals and clean receiver functions, but were excluded from further crustal thickness study as discussed in Chapter 5.

For receiver function stacks with a limited back-azimuth and distance range, lateral offset of the Moho piercing point was determined. The lateral offset is given by:

$$X_s = h\tan(\arcsin(pV_s)), \qquad 4.3$$

h is the crustal thickness (in km), p is the ray parameter (in s/km), and V_s is the S wave velocity (in km/s). For stations that lacked sufficient high quality data for limited back-azimuth and distance range stacking, the Moho depth may be considered to be directly beneath the station, i.e. as if sampling were azimuthally uniform.

Table 3 lists the crustal thickness estimates. Figure 20 shows Moho piercing points, relating data points to the station recording the teleseismic events from which the crustal thickness is determined. For publication (Veenstra et al., 2006) all crustal thickness estimates with total error $\geq$7.0 km were eliminated: GNR220, GNR230, MCK20, YAN115, YAN265, YAN269, SLM300, RND105, RND210, RND230, RND300, RND320, HURN300, HURN340, PYY302, FID217, WOLF200, WOLF260, PVW251, PVW270, PVW280, DH1 320, DH2 120, DH2 200, DH3 320, CZN0.28, SBL200, and WON20. Even with a relatively large confidence interval, these crustal thickness estimates provide potentially interesting data, so they are reported in Table 3 with total error underlined. High quality crustal thickness estimates with 95% confidence interval <7.0 km are highlighted with asterisks in Table 3.

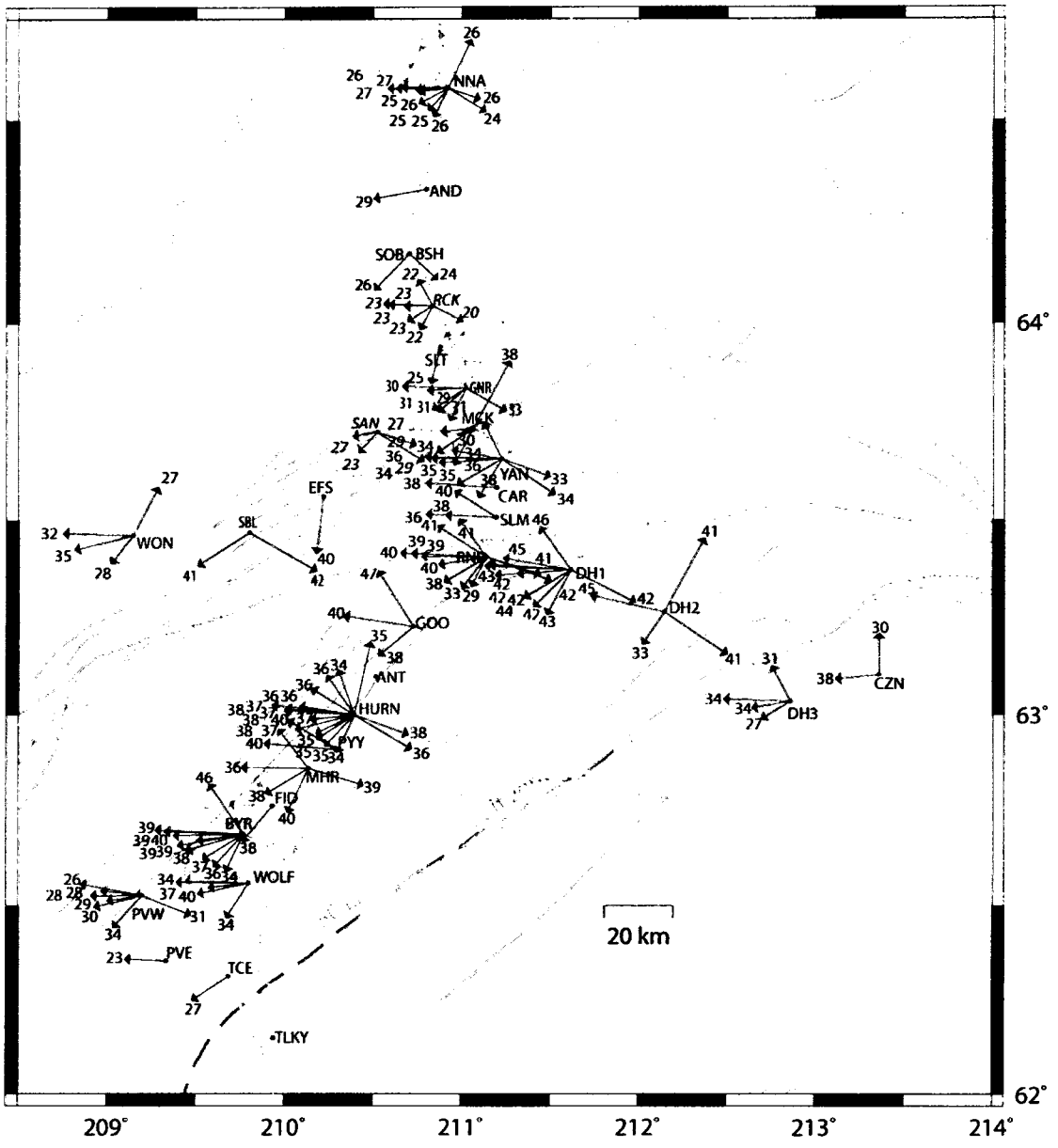

Figure 20: Moho piercing point vector plot. Crustal thicknesses are best plotted in map view above Moho piercing points. This figure illustrates backazimuthal directions of individual stacks, and links crustal thickness data point location (vector endpoint) with the recording station (vector origin). All modeled thicknesses are included in this figure, some of which are later removed as inferior quality or unreliable estimates, as described in more detail in the next chapter. Translucent vectors and crustal thicknesses were among the first to be eliminated. Wadati-Benioff zone 50 km and 100 km isopleth locations are indicated by dashed lines, roads by white lines, and faults by black lines, with background shading indicating topography. Presentation with numerical data plotted with vector at Moho piercing points is difficult to display in a single plot. Details are discussed in Chapter 5.

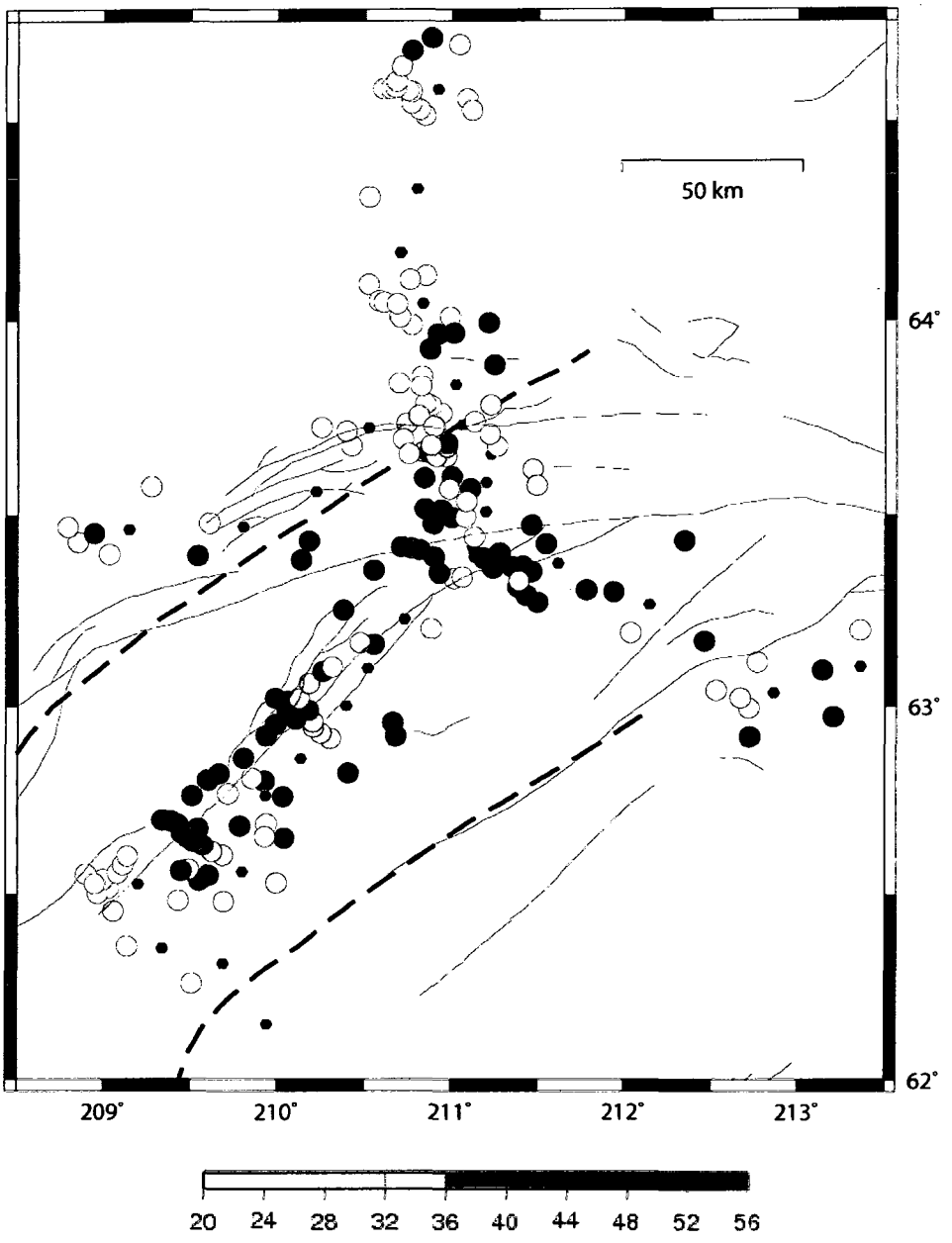

Figure 21: Crustal thicknesses plotted at Moho piercing points. Crustal thicknesses determined by receiver function analysis of BEAAR data are indicated by color scale and plotted at coordinates of the respective Moho piercing points. This color scale presentation provides representation of crustal thickness data better suited to visualization of Moho topography. Station locations indicated by small black dots, mapped faults by thin lines, Wadati-Benioff zone isopleths indicated by dashed lines, and crustal thickness data by colored circles. Dark circles indicate deep Moho and light circles indicate shallow Moho. Light circles, indicating thin crust, are concentrated to north with a few scattered to west and south.

Chapter 5 - Results

The crustal thicknesses determined by modeling receiver functions calculated from BEAAR seismograms indicate a shallow Moho north of the Alaska Range, and a deep irregular Moho in the central Alaska Range. Typical crust north of the range is 26 km thick, while beneath the central Alaska Range it is 35-45 km thick (Figure 21, Table 3). The BEAAR crustal thickness results with total errors <7.0 km at 95% confidence yield an overall average crustal thickness of 33.9 km. The average crustal thickness from data points located north of the Hines Creek fault is 26.5 km. The average crustal thickness from data points located south of the Hines Creek fault is 37.4 km. The average crustal thickness from data points located south of the Denali fault is 37.7 km. In this chapter, I present crustal thickness results station by station with stacks and models for reference. Comments on observed crustal thickness data are followed, in Chapter 6, by a discussion comparing and contrasting these data points with predicted crustal thicknesses. This unique set of crustal thickness data allows consideration of the isostatic compensation of the Alaska Range and brings us one step closer to understanding how such dramatic topography is sustained.

Surface context for BEAAR results

Surface topography in our study area ranges from flat lying sediment filled intermontane basins to extremely rugged mountains. Physiographic divisions indicate areas that differ in topographic appearance from adjacent areas: major divisions are broken into provinces and provinces broken into sections. Major divisions in our study area in south-central Alaska include the Pacific Mountain system and the Intermontane Plateaus. Physiographic sections in our study area include the Yukon-Tanana upland, the Tanana lowland, the northern foothills of the Alaska Range, the central and eastern Alaska Range, Broad Pass depression, Talkeetna mountains, Clearwater mountains, and the Susitna lowland (Figure 22).

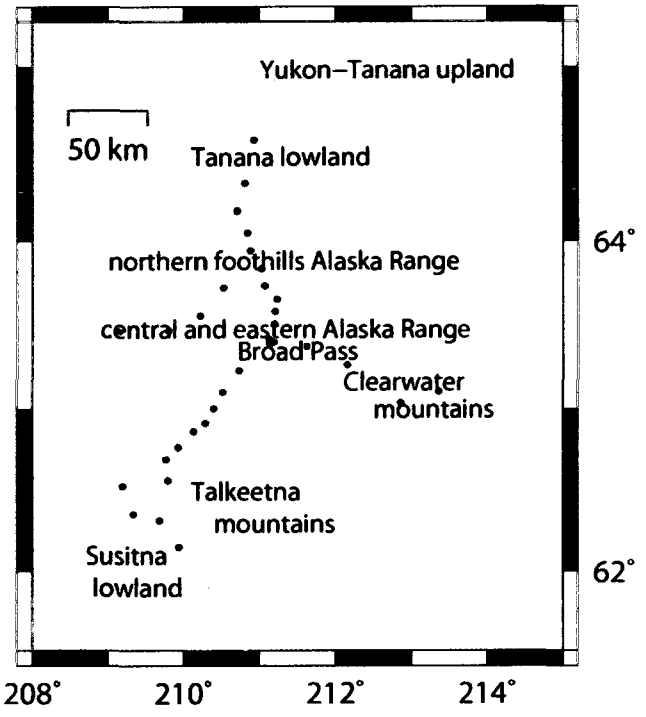

Figure 22: Physiographic section map labels topographic subdivisions in south central Alaska.

The physiographic division, province, and section a station is situated in is straightforward, however, it becomes more complex relating crustal thickness results to geology and tectonostratigraphic terranes. Moho piercing points are offset on the order of 10 km from the seismic station in the direction of the backazimuth, so antipodal backazimuths at a single station may be laterally offset by 20 km (Figure 20). In this region with numerous tectonostratigraphic terranes with a complex structural history, some fault sliced terranes are only 20 km across, so results from a single station may indicate crustal thicknesses of different terranes (Table 4).

For organizational purposes BEAAR stations are subdivided into six subsections: northern stations, national park stations, central Alaska Range stations, south central stations, Denali Highway stations, and southernmost stations.

Northern BEAAR stations

Northern BEAAR stations are those north of the Alaska Range along the Parks Highway: Nenana (NNA), Anderson (AND), Browne (BSH), Son of Browne (SOB), Rock Creek (RCK), Slate (SLT), and Garner (GNR) (Table 4, Figure 23). The northern stations were located in the lowlands and northern foothills of the Alaska Range. These locations are all north of the Hines Creek fault and situated on the Yukon-Tanana composite terrane of metamorphosed continental margin affinity.

Table 4: Northern stations summary table lists physiographic section, geologic setting, terranes, and crustal thickness for northern BEAAR stations. Physiographic section is as described by Wahrahaftig (1992). Geologic setting provides gross lithology as indicated on maps, mainly as described by Wilson et al. (1998) and Beikman (1980).

station	physiographic section(s)	geology	terrane(s)	crustal thickness (km)
NNA	Yukon-Tanana upland meets Tanana lowland	Paleozoic and Late Proterozoic quartz and pelitic schist	southern margin Yukon-Tanana	24-27
AND	Tanana lowland	Quaternary surficial deposits	southern margin Yukon-Tanana	28
BSH	Tanana lowland meets northern foothills of the Alaska Range	Pliocene and late(?) Miocene Nenana gravel	southern margin Yukon-Tanana	24
SOB	Tanana lowland meets northern foothills of the Alaska Range	Pliocene and late(?) Miocene Nenana gravel	southern margin Yukon-Tanana	26
RCK	northern foothills of the Alaska Range	Paleozoic and Late Proterozoic quartz and pelitic schist Pliocene continental deposits	southern margin Yukon-Tanana	20-23
SLT	northern foothills of the Alaska Range	Pliocene-Miocene continental deposits	southern margin Yukon-Tanana	25
GNR	northern foothills of the Alaska Range meets central Alaska Range	Paleozoic and(or) Late(?) Proterozoic pelitic and quartzose schist	southern margin Yukon-Tanana	30-33

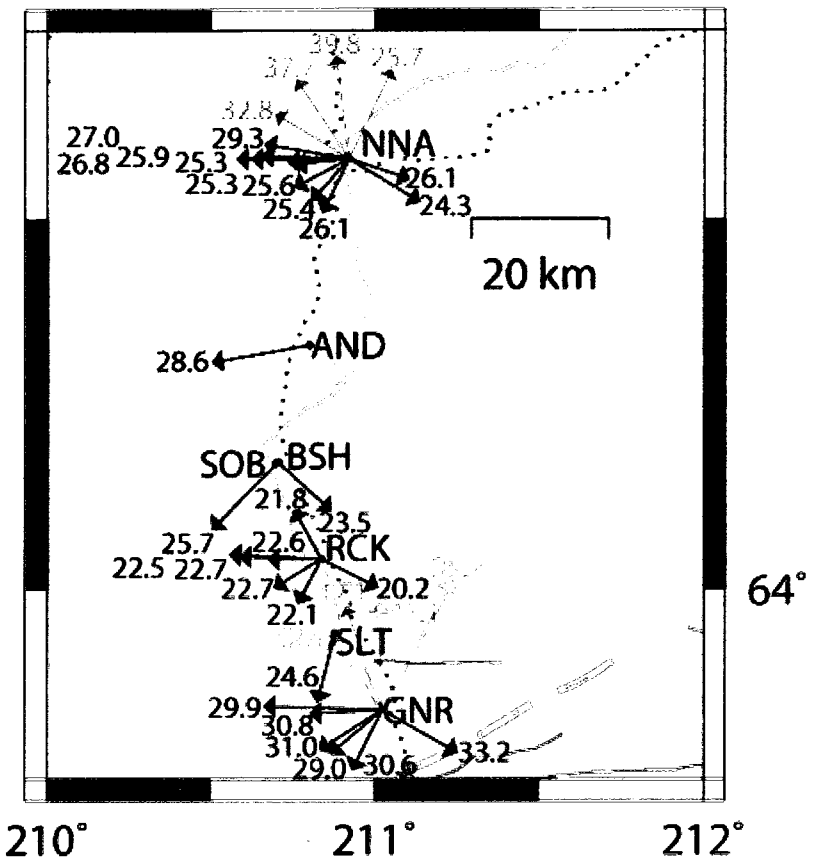

Figure 23: Northern BEAAR stations: NNA, AND, BSH, SOB, RCK, SLT, and GNR. Vector endpoints locate the piercing point of individual crustal thickness estimates. Vector length is determined by lateral offset, calculated as described in Chapter 4, plotted in direction of mean backazimuth of the stack or representative trace modeled. Vectors provide visual connection between a crustal thickness and the station at which the seismic data were recorded. The translucent (lighter) vectors represent receiver functions rejected as inferior quality or as an unreliable estimate of crustal thickness. Some of the opaque vectors are later removed, i.e. those with total error in the crustal thickness estimate $\geq$7.0 km. Recording stations are located by dots, labeled with alphanumeric station identifier. Background shading indicates topographic expression, roads plotted with white lines, mapped faults plotted with black, Wadati-Benioff zone 100 km depth contour plotted with dashed line, and rivers plotted with dotted line.

NNA is the northernmost station in the BEAAR study. The seismometer was well coupled to the schist in the hills just north of the Nenana River (Table 4). The Nenana basin deepens to the northwest to 1-3 km, and is filled with less dense nonmarine coal bearing Cenozoic fill, as indicated by gravity data, outcrop data and measured sections, as well as an exploratory test well (Kirschner, 1994a, b; Boyd and Hiles, 1985; Kirschner et al., 1985; Wahrhaftig et al., 1969; Ridgway et al. 2002). Barnes et al. (1994) showed a roughly -25 mGal Bouguer gravity low in this basin that is only half the -50mGal gravity anomaly indicated by Kirschner (1994), but this may in part be due to the small size of this basin and the relatively

sparse sampling of gravity data used to produce the 1:2,500,00 scale map. Near NNA we should also consider the northeast trending Minto Flats Seismic Zone (Biswas and Tytgat, 1988), with a clear trend in epicentral locations but no known surface faulting. The Minto Flats seismic zone, which may be associated with block rotation between the Denali and Tintina fault systems (Page et al., 1995), cuts through the region northwest of NNA (Figure 3). The receiver functions with back-azimuths to the northwest (NNA280, NNA300, NNA320, and NNA340) are more complicated than those at other backazimuths (Figure 24) with two distinct arrivals. These double pulses produce models with deeper Moho's than the other backazimuths. It is plausible that non-horizontal structures associated with the Nenana basin or Minto Flats Seismic Zone may be responsible for the complications to the receiver functions; the four northwestern backazimuths were not used in the final analysis. Note that at this station all stacks considered usable have crustal thicknesses with a 95% confidence interval <7.0 km. (At many stations that follow there are stacks that are not eliminated in the visual quality control [labeled in italic font and plotted gray], but eliminated due to 95% confidence interval $\geq$ 7.0 km.) The remaining receiver functions have clean arrivals, stacks indicate some backazimuthal variation, with crustal thickness of 24-27 km (Table 3, Figures 21 and 24). These results are in reasonable agreement with studies northeast of NNA, where crustal thickness at COL located in Fairbanks on the Yukon-Tanana terrane, is 27-32 km (Searcy et al., 1996).

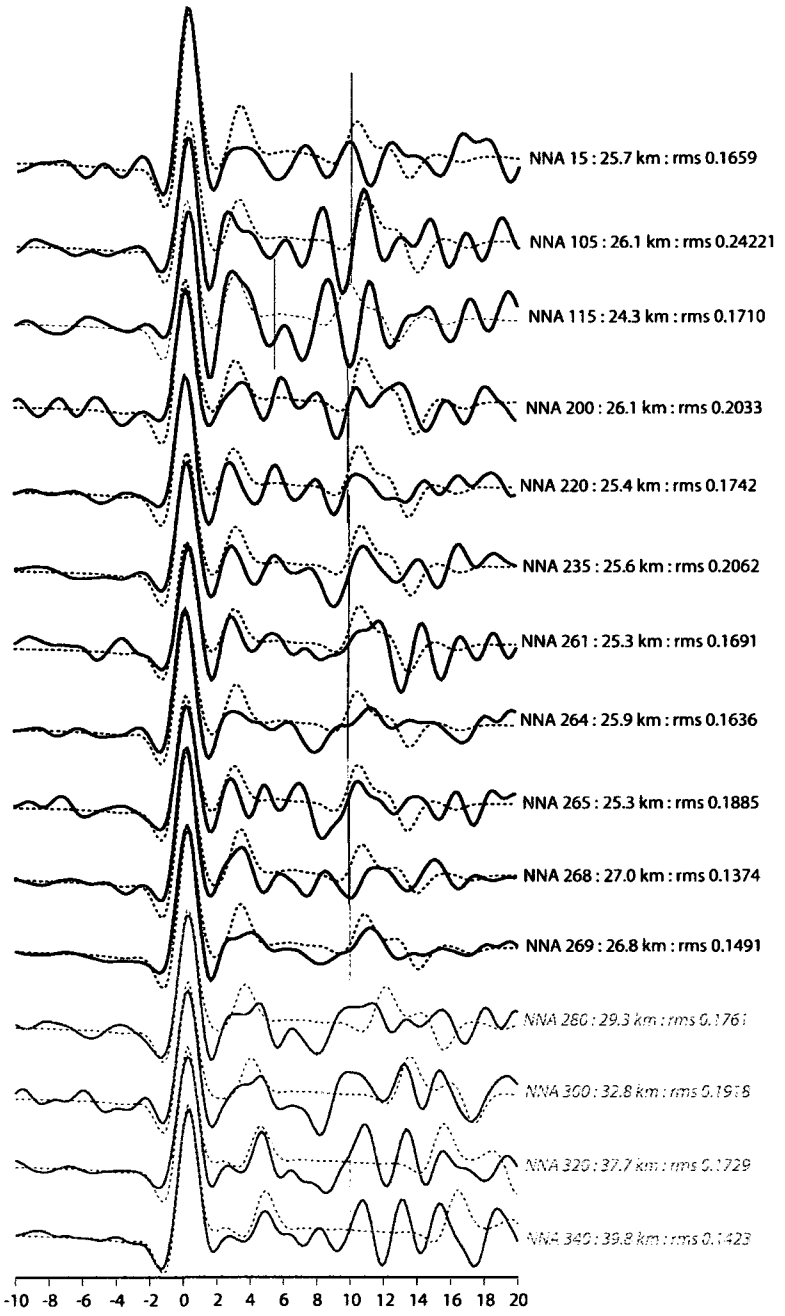

Figure 24: NNA receiver function stacks arranged in station-to-event backazimuthal order, clockwise from north. Horizontal axis is time in seconds from primary arrival, -10 to 20 seconds. Solid trace is observed receiver function, deconvolved from seismogram. Dashed trace is best fit synthetic receiver function, used to determine crustal thickness. Label uses station identifier and backazimuthal group identifier (same convention used throughout figures and tables), crustal thickness, and root-mean-square misfit between the best fit observed and synthetic receiver functions shown. Vertical line through each trace indicates time fit, -10 to 10 s for most. Stacks plotted in gray, labeled in italic font were considered inferior quality and eliminated from further study: NNA280, NNA300, NNA320, and NNA340.

AND was located in the lowlands, situated in sandy soil, part of the aerially extensive Cenozoic fill deposited over the southern margin of the Yukon-Tanana terrane (Table 4). The basin tends to produce noisy, ringy receiver functions (Figure 25). These receiver functions were of insufficient quality to resolve any real azimuthal variation in crustal thickness. Models indicate a 1.5 km thick sedimentary basin with crustal thickness of 28.6 km. AND data suggest slightly deeper Moho beneath AND than beneath NNA (24-27 km).

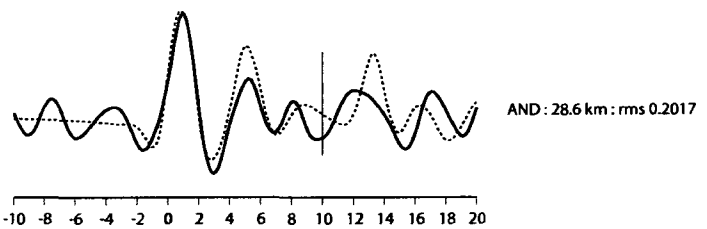

Figure 25: AND receiver function stack includes all receiver functions kept for study at this location, 0-360° backazimuth. Notation and symbols as described in Figure 24 figure caption.

SOB and BSH were installed on a local topographic high, unconsolidated sand and gravel, part of the Cenozoic fill deposited over the southern margin of the Yukon-Tanana terrane where Tanana-Kuskokwim lowland meets the northern foothills of the Alaska Range (Table 4). BSH was beneath power lines. After theft of solar panels and batteries, BSH was removed. SOB was installed nearby, uphill from an AT&T tower. BSH and SOB were both seismically noisy sites with insufficient high quality data to resolve azimuthal variation. The modeled sedimentary basin was 1.1 km thick, crustal thickness 23.5-25.7 km (Table 3, Figures 26 and 27). SOB (25.7 km) and BSH (23.5 km) indicate slightly shallower Moho beneath this region than beneath AND (28.6 km).

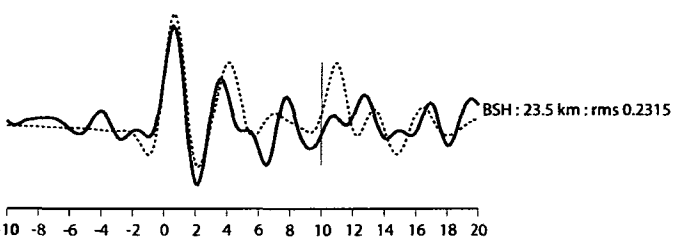

Figure 26: BSH receiver function stack includes all receiver functions kept for study at this location. Notation and symbols as described in Figure 24 caption.

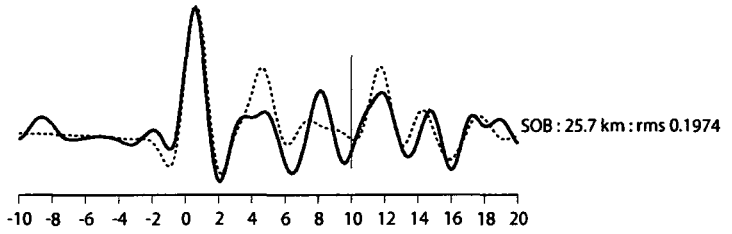

Figure 27: SOB receiver function stack includes all receiver functions kept for study at this location. Notation and symbols as described in Figure 24 caption.

RCK is in the northern foothills of the Alaska Range, to the west of the Parks Highway on a small hill, where a small exposure of the Yukon-Tanana terrane is surrounded by Pliocene continental deposits (Table 4). The vault was installed in unconsolidated sediments, and models indicate 0.9 to 1.3 km thick sedimentary basin. Receiver functions calculated from seismograms recorded at RCK were of sufficient quality to resolve minor azimuthal variation in crustal thickness, 20-23 km thick (Table 3, Figure 28). RCK300 (21.8 km) piercing point plots between piercing points for SOB (25.7 km) and BSH (23.5 km), indicating even thinner crust. Overall the data from NNA (24-27 km), AND (29 km), SOB (26 km), BSH (24 km), and RCK (20-23 km) suggest relatively shallow Moho.

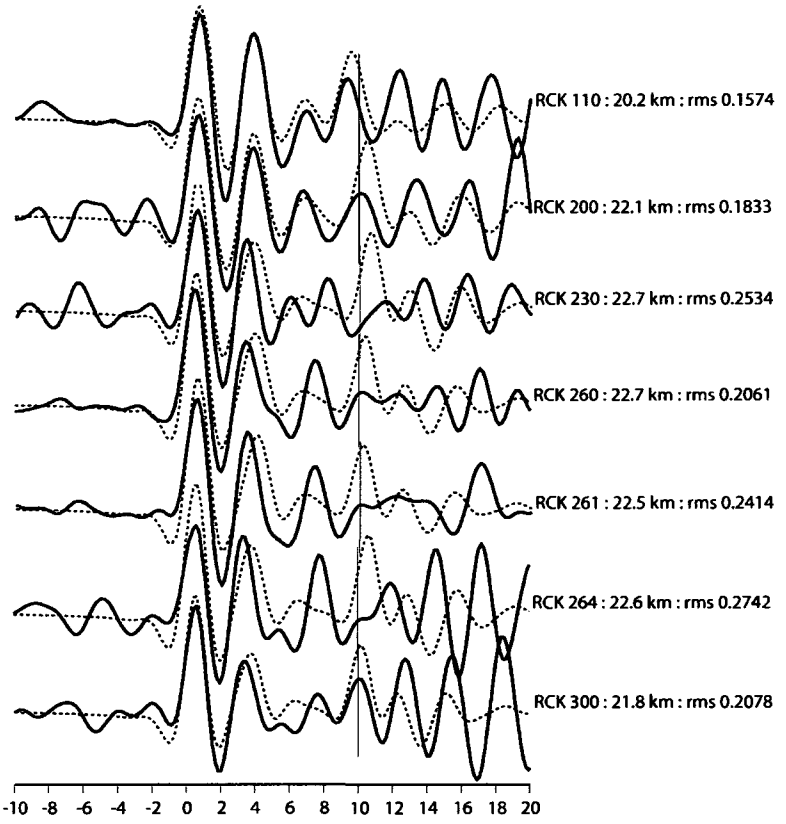

Figure 28: RCK receiver function stacks arranged in backazimuthal order. Notation and symbols as described in Figure 24 caption.

SLT was in the northern foothills of the Alaska Range, just west of the Parks Highway behind a small sand/gravel pit. The geologic maps indicate SLT was located near the boundary between Pliocene and Miocene continental deposits which are part of the Cenozoic fill covering the southern Yukon-Tanana terrane. The vault at SLT was in unsorted sandy conglomeratic soil. Clear receiver functions were not plentiful enough to resolve any azimuthal variation of crustal thickness. Models indicate a 1.5 km thick sedimentary basin and 24.6 km thick crust (Table 3, Figure 29). SLT (25 km) results suggest slightly thicker crust than beneath neighboring station RCK (20-23 km), but within the range of the other northern stations (NNA, AND, SOB, BSH, RCK yield crustal thicknesses 20-29 km).

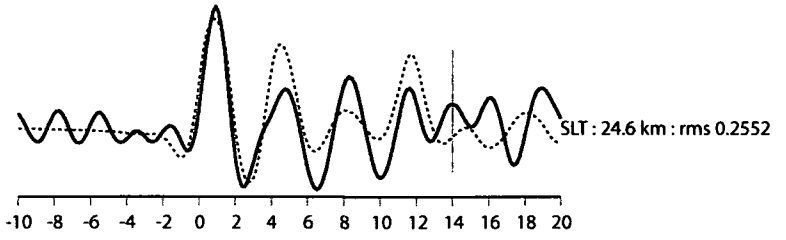

Figure 29: SLT receiver function stack. Notation and symbols as described in Figure 24 caption.

GNR was located at the boundary between the Alaska Range and its northern foothills, just north of the Hines Creek fault. GNR is located near the southernmost edge of the Yukon-Tanana terrane, on a hill east of the Parks Highway. Geologic maps indicate dominantly pelitic and quartzose schist of the Alaska Range (Csejtey et al., 1992; Patton et al., 1989, 1994; Reed and Nelson, 1980; Wilson et al., 1998; Nokleberg et al., 1992a). The wind at GNR was quite intense, and the railway ran at the base of the hill to the east, both of which may have introduced noise to our data, but sufficient high quality data were recorded to resolve some azimuthal variation. Stacks with northern backazimuths (GNR320, GNR340, GNR350, and GNR20) (Figure 30) show multiple pulses where southern backazimuths record a single pulse. These northern stacks model crustal thicknesses of 38-42 km, which if they are real represent significant relief at the base of the crust, a >10 km step between GNR260 (29.9 km) and neighboring stack GNR320 (42.2 km). Given that the piercing points of these northern GNR datapoints (e.g. GNR350 41.1 km) put them very close to RCK southern datapoints (e.g. RCK110 20.0 km), they would indicate a Moho offset on the order of 20 km over a short lateral distance. There is a fault to the north of GNR that strikes east-west (Figure 7), between GNR260 and GNR320 piercing points. While it is possible that these results represent a sliver of thick crust, it is also plausible that non-horizontal structure complicated the receiver function, so the stacks with northern backazimuths were eliminated. The clearest receiver functions at GNR indicate a crustal thickness of 30-33 km (Table 3, Figure 30). Neighboring station SLT (24.6 km) piercing point plots very near GNR250 (30.8 km) and GNR260 (29.9 km), so if all our assumptions were absolutely correct these results should show better agreement. Since piercing point is determined using mean distance and backazimuth, stacks that include all acceptable receiver functions regardless of backazimuth will have less accurate vector endpoint location than those stacks with tight stacking bounds, which could explain why there is not better agreement between SLT and GNR250/GNR260.

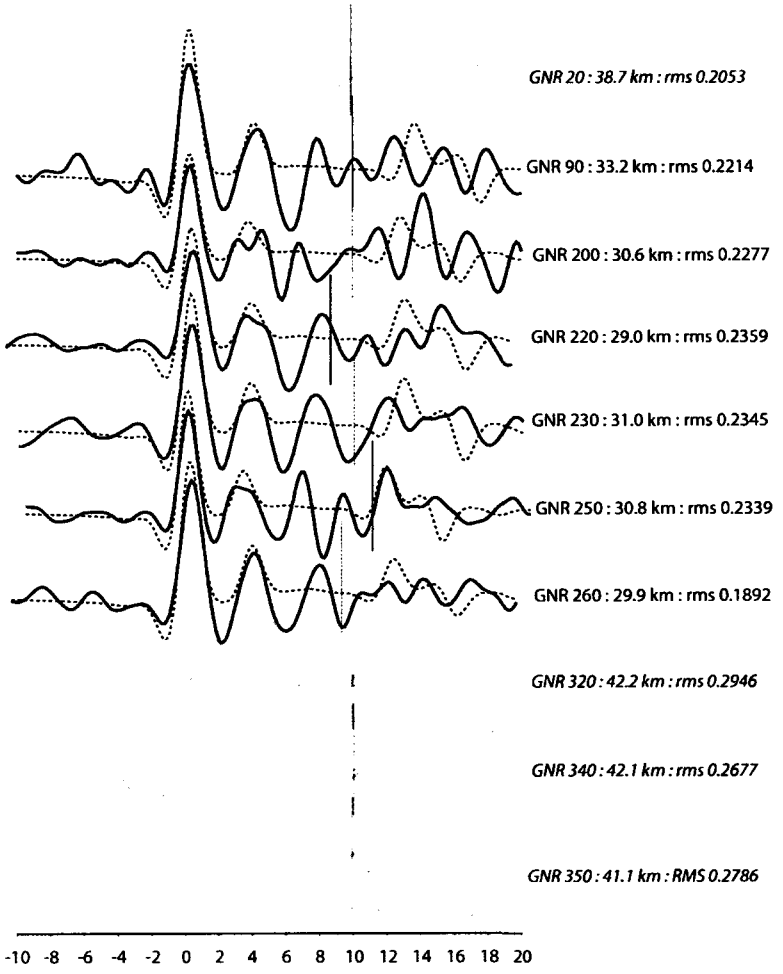

Figure 30: GNR receiver function stacks arranged in backazimuthal order. Notation and symbols as described in Figure 24 caption. GNR20, GNR320, GNR340, and GNR350 were removed. GNR220 and GNR230 eliminated due to large total error (note these are not gray because they were otherwise reasonable looking receiver functions but are eliminated from final analysis).

National Park BEAAR stations

Five stations were located in Denali National Park: McKinley (MCK), Sanctuary (SAN), East Fork / Sable (EFS), Stony Creek / Bergh Lake (SBL), and Wonder Lake (WON) (Table 5, Figure 31). These are all located north of the Denali fault. WON was located in the northern foothills of the Alaska Range near the southern boundary of the Yukon-Tanana terrane, north of the high topography and the projected convergence of the subparallel faults between the western end of Hines Creek fault and Denali fault (Figure 6). MCK, SAN, EFS, and SBL were located in a highly faulted region. There are several narrow terranes adjacent to the Denali fault in the central and eastern Alaska Range, some of which occur in

narrow discontinuous slivers within branches of the Denali fault, such as the Windy terrane. The rocks of the Pingston terrane are strongly folded and faulted. The McKinley terrane is defined as a structural composite.

Table 5: National Park stations summary table lists physiographic section, geologic setting, terranes, and crustal thickness for BEAAR stations deployed in Denali National Park. Physiographic section is as described by Wahrahaftig, (1992). Geologic setting provides gross lithology as indicated on maps, mainly as described by Wilson et al. (1998) and Beikman (1980).

station	physiographic section(s)	geology	terrane(s)	crustal thickness (km)
MCK	central Alaska Range	lower Paleozoic to preCambrian pelitic and quartzose schist	Yukon-Tanana and Pingston	27-38
		Paleocene continental deposits of the Cretaceous Cantwell Formation		
SAN	central Alaska Range	Paleozoic and preCambrian pelitic and quartzose schist of the Alaska Range	Yukon-Tanana and Pingston	23-29
		Tertiary (Miocene? to Paleocene?) coal bearing sedimentary rocks		
		Tertiary (Pliocene and late(?) Miocene) Nenana gravel		
		Paleozoic Spruce Creek metavolcanic sequence		
EFS	central Alaska Range	Cretaceous Cantwell sedimentary rocks subunit	McKinley, Windy, or Dillinger	40
		Tertiary (Paleocene) volcanic rocks of Cantwell formation		
		Tertiary (Miocene? to Paleocene?) coal bearing sedimentary rocks		
		Tertiary (Pliocene and late(?) Miocene) Nenana gravel		
SBL	central Alaska Range	Triassic Nikolai Greenstone and related rocks	McKinley, Windy, or Dillinger	41-42
		Tertiary Nenana gravel		
		Tertiary (Oligocene and Eocene) andesite and basalt		
		Late Triassic to Pennsylvanian flysch-like sedimentary rocks		
WON	northern foothills of the Alaska Range	Paleozoic and preCambrian pelitic and quartzose schist of the Alaska Range	southern margin Yukon-Tanana	28-35

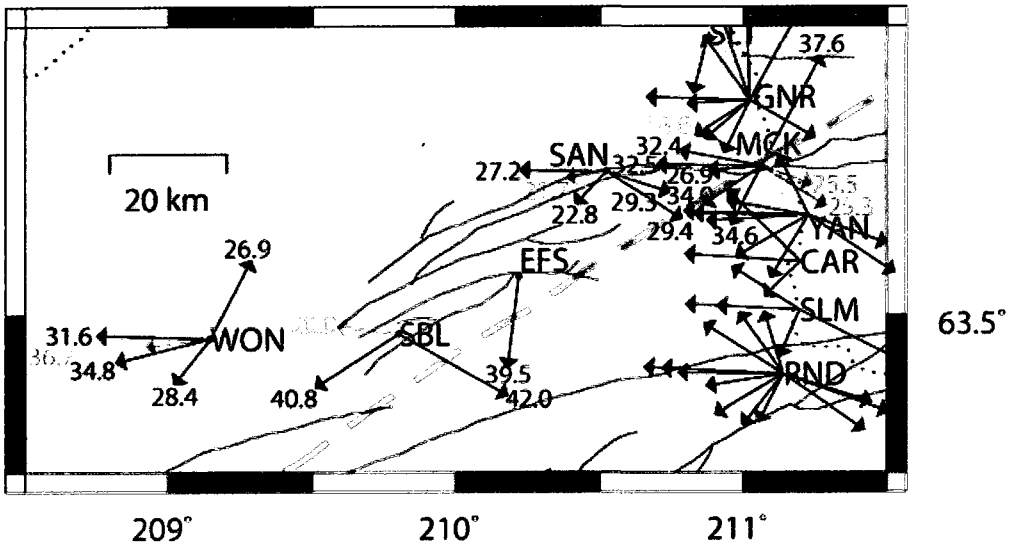

Figure 31: Denali National Park BEAAR stations. Symbols used as in previous figures with translucent vectors indicating inferior quality receiver functions such as those indicated by multiple lows in root-mean-square misfit between observed and modeled receiver functions or estimates deemed unreliable due to structural complexities. Vector endpoint locates the latitude and longitude of Moho piercing point. WON, SBL, EFS, SAN, and MCK labeled with depth (km).

MCK was located in the central Alaska Range physiographic section, along the Hines Creek Fault, on the border between the Yukon-Tanana terrane and the Pingston terrane, on a small hill immediately north of McKinley Park facilities (those that existed in 2000). MCK was at the border between lower Paleozoic to pre-Cambrian schist of the southernmost Yukon-Tanana terrane to the north and Paleocene continental deposits of the Cretaceous Cantwell Formation to the south (Csejtey et al., 1992; Ridgway et al., 1994). The seismometer at MCK was on a huge concrete block in an AEIC shed. Although good results were expected, only three stacks made it though quality control. I suspect the structural complexity in the region contributed to the waveform complexity. As seen in Figure 33, MCK109 and MCK119 have multiple arrivals, contrasted with MCK20 and MCK200 which have a single, clear Ps conversion. MCK109 produced multiple lows in the root-mean-square misfit curve, and was eliminated. Given the similarity to MCK109, and structural complexity in the area, MCK119 was also eliminated. Stacks MCK255, MCK260, MCK270, and MCK280 all have an early arrival that indicates a shallow discontinuity, clearly distinct from MCK200. Of those with an early arrival, receiver functions MCK255, MCK270, and MCK280 are not well behaved. For these stacks, 30 seconds of the trace is fit (Figure 33), but the models varied wildly in experimenting with different time fits, so these were eliminated. MCK260 is the clearest of the stacks with the early arrival, and given that it appears to be modeling something real within our accepted error there is no reason to exclude it. The best fit models suggest a 10 km jump in the Moho discontinuity

beneath MCK200 (37.0 km) and MCK260 (26.9 km), over a short lateral distance. It should be noted that at 95% confidence results actually only indicate a 6 km jump in Moho given the lower limit at 95% confidence of MCK200 is 36.4 km and upper limit at 95% confidence of MCK260 is 30.2 km. If we allow a slightly larger (7.1 km) total error, then crustal thickness results from MCK range from 27 km to 38 km (Table 3, Figure 32). The strict 7.0 km total error provided three crustal thickness estimates around MCK ranging from 27 km to 35 km. While MCK results are intriguing given the potential significance of this Moho relief, given the non-ideal receiver function quality and concerns about structural complexity, these results are best considered within context of neighboring stations that follow.

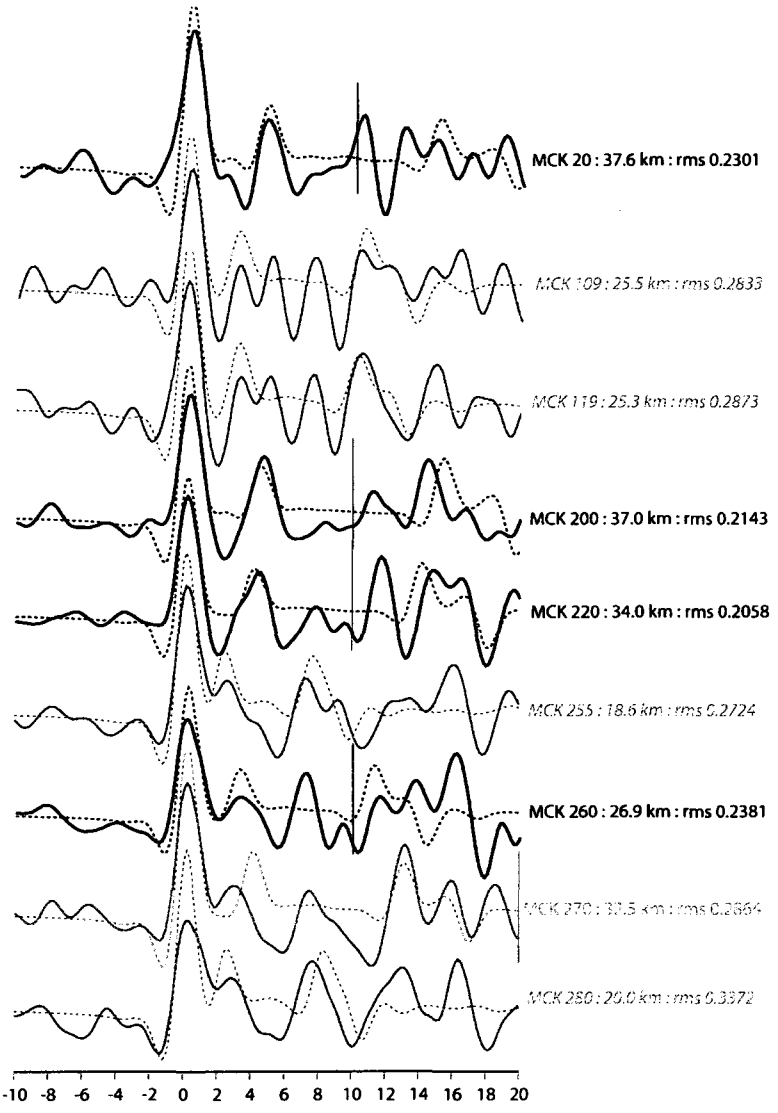

Figure 32: MCK stacks arranged in backazimuthal order. Notation and symbols as described in Figure 24 caption. Receiver functions that would have been immediately removed from consideration at other stations due to noise and waveform complexity were modeled in hopes of pulling some useful data at this station. MCK109, MCK119, MCK255, MCK270, and MCK280 eliminated. MCK20 (37.6 km) had 7.1 km error, removed from further consideration; however, it is interesting to note that the result is similar to MCK200 (37.0 km).

SAN was located in Denali National Park in the central Alaska Range. Part of the Yukon-Tanana and northern Alaska Range metamorphic complex (Table 5), SAN was located near the boundary between the southernmost Yukon-Tanana terrane and the Pingston terrane, near subparallel faults striking west-southwest between Hines Creek and Denali fault systems. Models indicate a 1 km thick sedimentary basin and crustal thicknesses ranging from 23 km to 29 km (Table 3). The modeled basin thickness is in

reasonable agreement with 1.3 km thick moderately deformed Nenana gravel "widely distributed" on the north side of the Alaska Range (Csejtey et al., 1992). There is an early pulse observed in SAN100, SAN115, SAN250, and SAN251 (Figure 33). The models match that early pulse nicely for SAN100, SAN115, and SAN250, giving me confidence that we are indeed modeling Moho. While this early wiggle is not observed in SAN200, it also appears to be a relatively clean, well modeled receiver function (Figure 33). SAN stacks suggest shallow Moho (23-29 km), similar to neighboring stack MCK260 (27 km), as well as stacks from northern stations SLT, RCK, SOB, BSH, AND, and NNA (20-28 km).

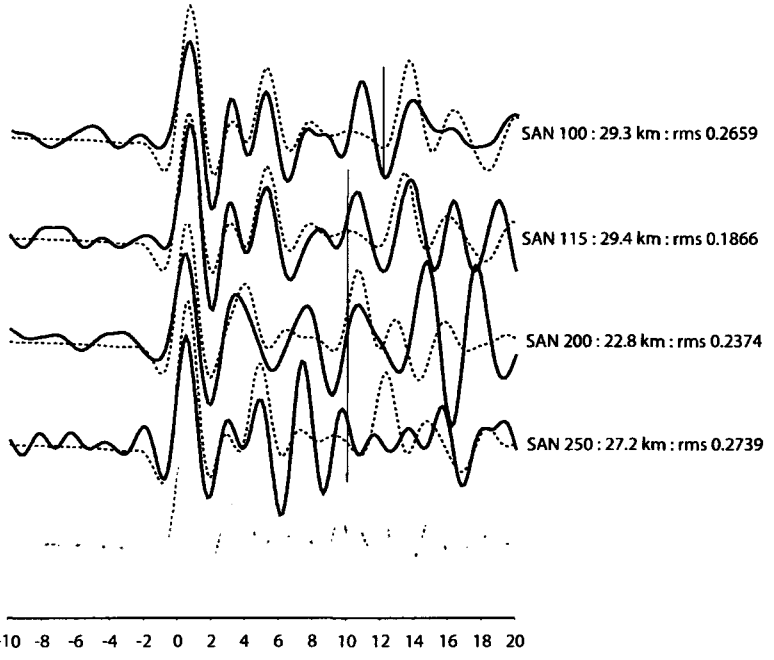

Figure 33: SAN receiver function stacks arranged in backazimuthal order. Notation and symbols as described in Figure 24 caption. SAN 251 eliminated.

EFS was located in Denali National Park in the central Alaska Range, south of the Hines Creek fault and north of the Denali fault where Cantwell Formation and Nenana Gravel may overlie narrow discontinuous slivers of terranes (Table 5). Due to the structural complexity, events recorded at EFS may have been sampling any one of a number of smaller terranes in the central Alaska Range, such as the McKinley, Windy, or Dillinger terranes. Only the three clearest events were used to determine crustal thickness, 39.5 km (Figure 34). The deep discontinuity at EFS (39.5 km) is similar to deep discontinuity at neighboring stack MCK200 (37 km), notably distinct from the shallower northern data.

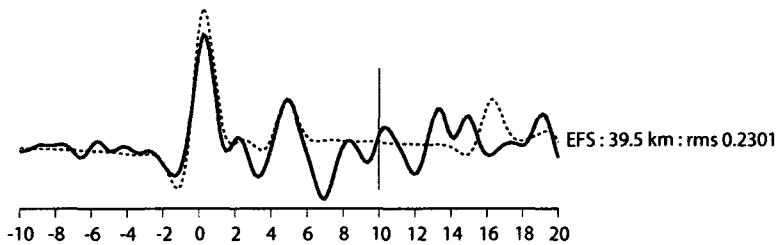

Figure 34: EFS receiver function stack includes the three receiver functions kept for study at this location. Notation and symbols as described in Figure 24 caption.

SBL was located in Denali National Park in the central Alaska Range, south of the Hines Creek fault, north of the McKinley strand of the Denali fault between subparallel faults in a structurally complex region and may have been sampling one of a number of smaller terranes such as the McKinley, Windy, or Dillinger (Table 5). If we allow a 7.0 km total error we have two crustal thickness estimates, 41 km and 42 km thick. The strict <7.0 km total error provided only one crustal thickness estimate, 42 km (Figure 35). Results from SBL (42 km) are in reasonable agreement with results from neighboring station EFS (40 km).

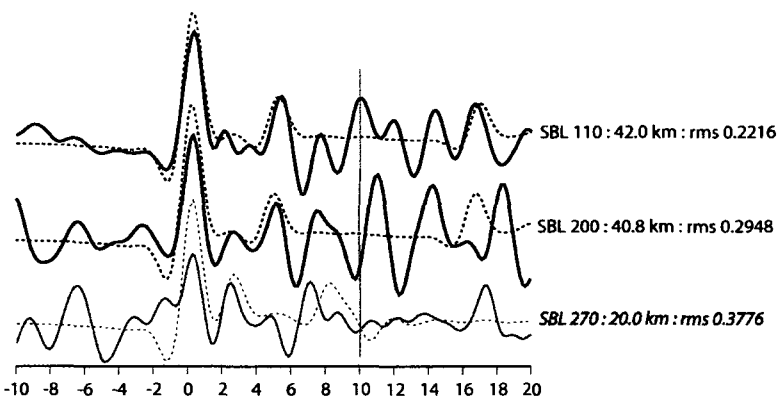

Figure 35: SBL receiver function stacks arranged in backazimuthal order. Notation and symbols as described in Figure 24 caption. Receiver functions that would have been immediately removed from consideration at other stations due to poor signal to noise ratio were modeled in hopes of pulling some useful data at this station. SBL 270 eliminated due to noise level.

WON was located in Denali National Park in the northern foothills of the Alaska Range near the southern boundary of the Yukon-Tanana terrane (Table 5). The series of west-southwest trending faults mapped in the central Alaska Range ends east of WON in the foothills well north of the Denali fault. The Kantishna seismic cluster (Burris, 2007) refers to a cluster of seismic events located near WON, a significant number of relatively small earthquakes with epicenters revealing a NE-SW trend that may (or may not) connect to the Minto Flats seismic zone. Although WON certainly recorded these events, only teleseismic events were used to determine crustal thickness. WON results provided sufficient azimuthal

variation to yield three or four crustal thickness estimates. WON260 shows two distinct pulses, a clean high signal to noise ratio trace (Figure 36), but there exists some uncertainty as to which pulse represents Moho Ps conversion, so the stack was eliminated. WON20 was eliminated because of large error. WON200 is not an ideal receiver function, but Moho arrival is similar to WON20, notably distinct from WON250 and WON265. The strict <7.0 km total error provided crustal thickness estimates of 27 km to 35 km (Table 3). The shallower 27-28 km results are from the northeast (WON20) and south-southwest (WON200); the deeper 32-35 km results are from west-southwest (WON250) and west (WON265 mean backazimuth is 272°). These results, WON 27-35 km, are in reasonable agreement with other stations in the northern foothills of the Alaska Range: RCK 20-23 km, SLT 25 km, and GNR 30-33 km.

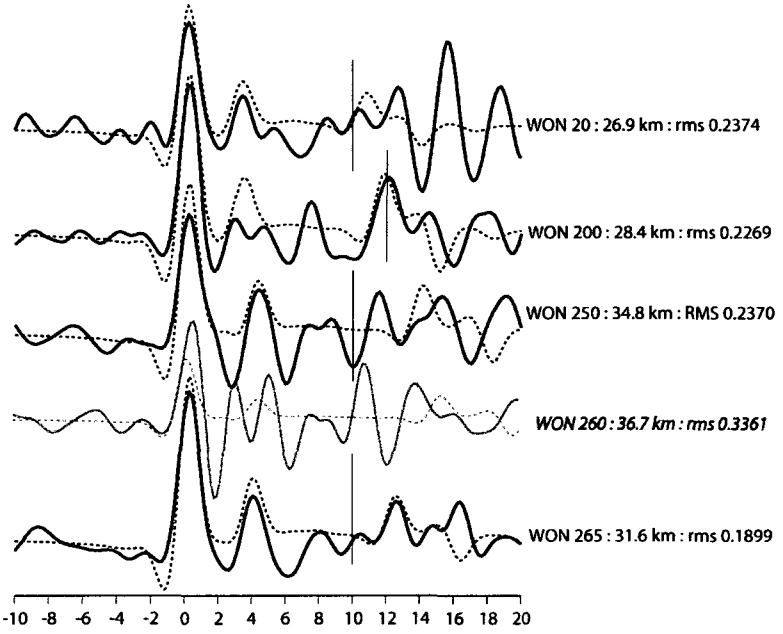

Figure 36: WON stacks arranged in backazimuthal order. Notation and symbols as described in Figure 24 caption. WON260 eliminated: although it is a clear trace with high signal to noise ratio there is some uncertainty about which pulse represents Moho Ps conversion. WON20 had 12.8 km error and eliminated. WON200 kept, despite non-ideal waveform, to represent shallow results.

Central Alaska Range BEAAR stations

The stations located along the Parks Highway in the central Alaska Range include Yanert (YAN), Carlo Creek (CAR), Slime (SLM), and Reindeer (RND) (Table 6, Figure 37). YAN, CAR, and SLM are located south of the Hines Creek fault and north of the Denali fault where mini-terranes Pingston, McKinley, and Windy terranes dominate. RND is located just south of the Denali fault on Reindeer mountain, part of Broad Pass.

Table 6: Central Alaska Range stations summary table lists physiographic section, geologic setting, terranes, and crustal thickness for BEAAR stations located in the heart of the range. Physiographic section is as described by Wahrahaftig, (1992). Geologic setting provides gross lithology as indicated on maps, mainly as described by Wilson et al. (1998) and Beikman (1980).

station	physiographic section(s)	geology	terrane(s)	crustal thickness (km)
YAN	central Alaska Range	Cretaceous Cantwell sedimentary rocks subunit	Pingston or McKinley	30-40
		Tertiary (Paleocene) Cantwell formation volcanic rocks		
CAR	central Alaska Range	Paleocene and Late Cretaceous Cantwell formation sedimentary and volcanic rock subunits	Pingston	38
SLM	central Alaska Range	Late Cretaceous and Late Jurassic portion of flysch	McKinley or Windy	36-38
		Cretaceous Cantwell Formation sedimentary rocks subunit		
		Late and/or Middle Triassic Nikolai Greenstone and related rocks		
RND	central and eastern Alaska Range meets Broad Pass Depression	Cretaceous mélanges of the Alaska Range with Silurian to Cretaceous protoliths	Broad Pass, Windy, McKinley, and Kahiltna	29-42
		earliest Late Cretaceous to Late Jurassic? Kahiltna flysch sequence		
		early Cretaceous and Late Jurassic flysch sequence		
		Miocene to Paleocene, mostly Early Tertiary or Eocene? hypabyssal felsic and intermediate intrusive rocks		
		Tertiary volcanic rocks, undivided		
		Late Triassic, Norian spiculite and sandy limestone		
		Jurassic to Cambrian Mystic and Dillinger stratigraphic sequences		
		Late Triassic to Pennsylvanian flysch-like sedimentary rocks		
		Late and/or Middle Triassic Nikolai greenstone and related rocks		

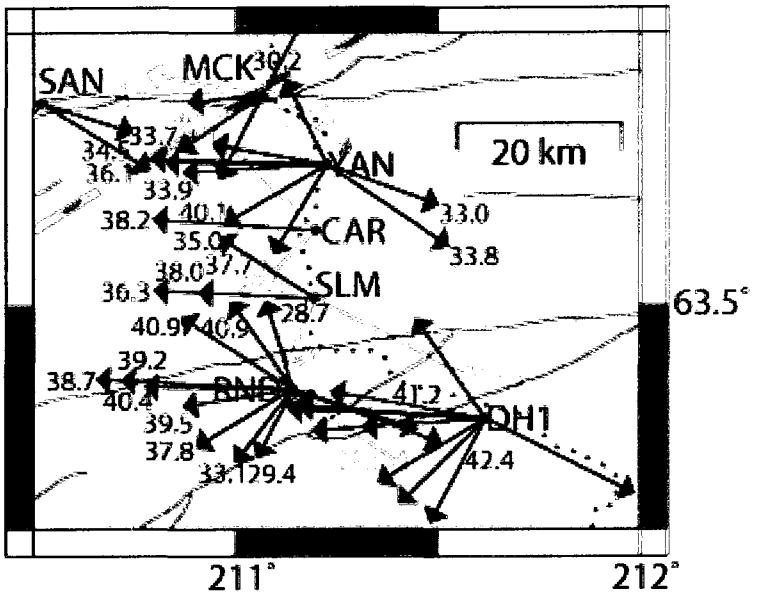

Figure 37: Central Alaska Range BEAAR stations: YAN, CAR, SLM, and RND. Symbols used as in previous figures. Vector endpoints locate the latitude and longitude of the Moho piercing point, labeled with depth (km).

YAN was located south of the Hines Creek fault and north of the Denali fault in the central Alaska Range in an area geologically dominated by Cantwell Formation. As YAN was located in the central Alaska Range these results may have been sampling any one of a number of smaller terranes, most likely Pingston or McKinley. High quality receiver functions provided sufficient data to resolve azimuthal variation, with six crustal thickness estimates ranging from 30 km to 40 km, suggesting significant relief at the base of the crust over short lateral distances. A slightly larger total error of 7.5 km would provide another three crustal thickness estimates, 34 km to 36 km (Table 3, Figure 38). The results are best considered in the context of neighboring stations: MCK 27-38 km, and SAN 23-29 km. For the northern stations, it was sufficient to compare overall station results, but the Central Alaska Range crustal thickness data are complex enough that we must consider the location of each individual piercing point to make meaningful comparisons. SAN was located west of YAN, so I compare YAN's northwest stack with SAN's eastern stack: SAN115 29 km thick crust in reasonable agreement with YAN320 30 km thick crust. MCK was located north of YAN so I compare northern backazimuth from YAN to southern backazimuthal stack from MCK: YAN320 (30 km or between 29.7 km and 30.8 km at 95% confidence) at 63.7395°N has piercing point north of MCK200 (37 km or between 36.4 km and 37.4 km at 95% confidence) at 63.64962°N, with shallow result to north suggesting ~6 km relief at the base of the crust over a short lateral distance.

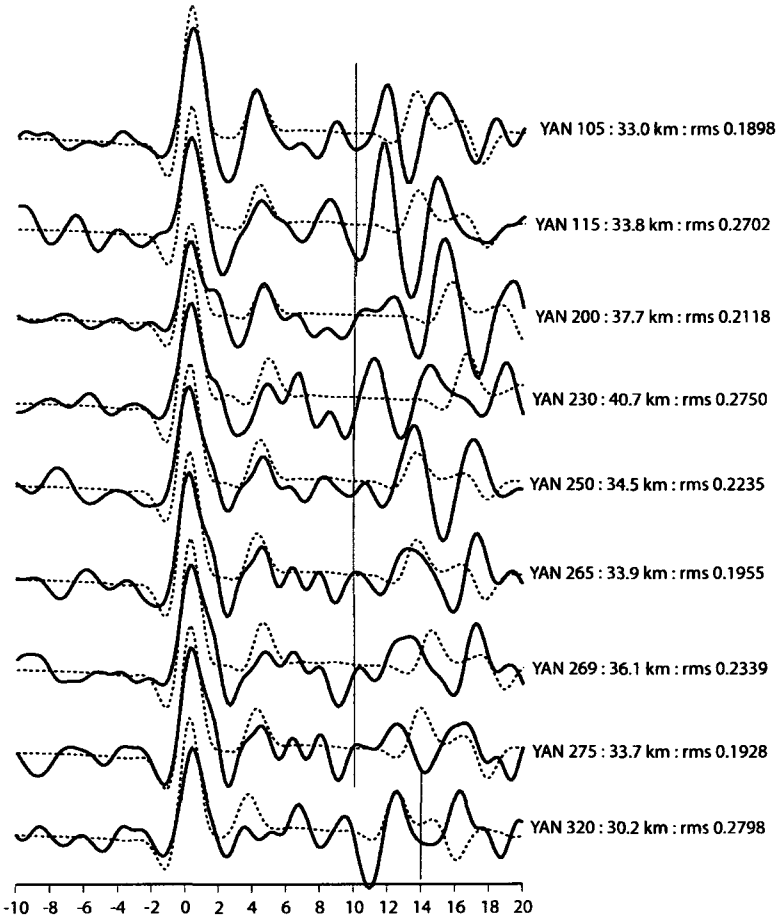

Figure 38: YAN receiver function stacks arranged in backazimuthal order. Notation and symbols as described in Figure 24 caption. YAN115, YAN265, and YAN269 had 7.5 km errors so although eliminated these results (34-36 km) fall within range of high quality "kept" results (30-40 km).

CAR was located south of the Hines Creek fault and north of the active strand of the Denali fault in the central Alaska Range in an area dominated by Cantwell Formation sedimentary and volcanic rock subunits (Wilson et al., 1998, Beikman, 1980). Three distinct backazimuthal groups were identified within the receiver function data, however only one backazimuthal group produced a reliable crustal thickness estimate. The backazimuth of the single crustal thickness estimate suggests that results from CAR represent the Pingston terrane, near the boundary with the McKinley terrane. CAR data indicate a crustal thickness of 38 km (Table 3, Figure 39). Again given the range of results from YAN (30-40 km) it is best to pinpoint the stacks closest to the piercing point of CAR260 (38.3 km). YAN200 (37.7 km) and YAN230 (40.7 km) piercing points are located roughly between CAR260 piercing point and CAR seismometer. Results from YAN200, YAN230, and CAR260 are in good agreement with overlapping 95% confidence intervals (Table 3).

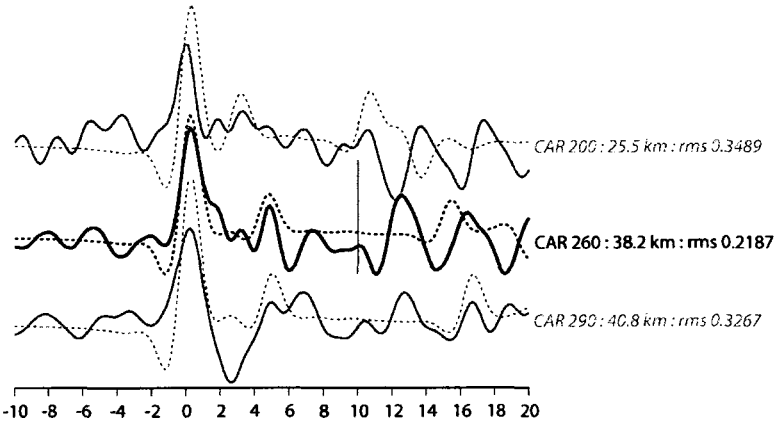

Figure 39: CAR receiver function stacks arranged in backazimuthal order. Notation and symbols as described in Figure 24 caption. Receiver functions that would have been immediately removed from consideration at other stations due to noise and waveform complexity were modeled in hopes of pulling some useful data at this station. CAR200 and CAR290 eliminated.

SLM was located immediately north of the Denali fault, in the central Alaska Range physiographic section. SLM results may represent any one of a number of terranes adjacent to the Denali fault, most likely McKinley, or Windy. SLM results were subdivided into five distinct backazimuthal groups. SLM110 (Figure 41) was not a clean, well-behaved receiver function, and given the backazimuthal direction, the ray paths of SLM110 and SLM200 may have interacted with the Denali fault, so these stacks were both eliminated from further consideration. SLM300 (35.0 km) was eliminated due to lack of reasonable constraint, crustal thickness somewhere between 29.0 km and 40.7 km at 95% confidence. Two reliable crustal thickness estimates were produced, 36 km and 38 km (Table 3, Figure 40). SLM265 36.3 km (35.3 to 37.3 km at 95% confidence) and SLM260 38.0 km (36.3 to 39.7 km at 95% confidence) are best compared with CAR260 38.2 km (36.4 to 39.9 km at 95% confidence), in reasonable agreement with these overlapping errors. CAR and SLM results are showing deeper Moho than the northern stations.

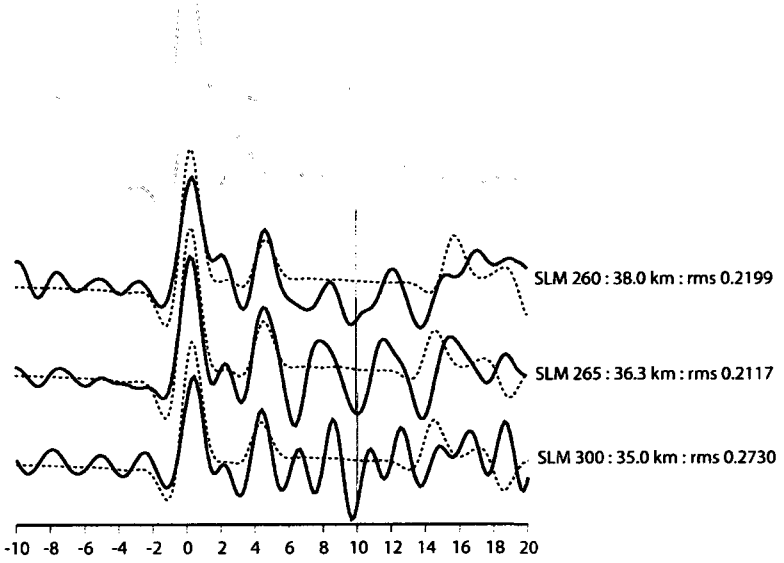

Figure 40: SLM receiver function stacks arranged in backazimuthal order. Notation and symbols as described in Figure 24 caption. SLM110 and SLM200 were eliminated. SLM300 had 11.7 km error, hence eliminated.

RND is located at the border between the Alaska-Aleutian physiographic province and the Coastal Trough physiographic province, where the central and eastern Alaska Range physiographic section meets the Broad Pass Depression between the Alaska Range and the Talkeetna mountains (Wahrhaftig, 1992). RND is located a short distance south of the Denali fault on Reindeer Mountain near Cantwell, Alaska. The results at RND most likely represent a number of terranes, including Broad Pass, Windy, McKinley, and Kahiltna. A temporary array of seismometers was installed on Reindeer Mountain in the summer of 2000, but the reported crustal thicknesses are from the main station which was deployed for the full 27 months. The receiver functions from RND are plentiful enough and of sufficiently high enough quality to resolve some backazimuthal variation (Figure 41). Compared to the other stacks, RND120 and RND325 have poor signal to noise ratios, raising suspicions about the shallow results, so these two stacks were eliminated. The little wiggle between main pulse and Ps conversion, observed from northwest and southeast backazimuths (RND300, RND320, RND105, and RND109), may be indicating some structural complication such as ray paths crossing the Denali fault to the northwest, the mapped fault running along Broad Pass to southeast, or some mid-crustal discontinuity. Such a deviation from the assumed simple plane layered model may be influencing RND200, RND210, and RND230 (e.g., toward modeling somewhat shallower Moho). RND105, RND210, RND230, RND300, and RND320 produce large error and were eliminated. The southwest backazimuth, RND200 displays a reasonable signal to noise ratio, produces a

reasonable model yielding crustal thickness with <7.0 km total error at 95% confidence, and no mapped faults at that backazimuth, so there is no reason to eliminate this shallow 29.4 km crustal thickness. The six crustal thickness estimates that survived quality control range from 29 km to 42 km (Table 3, Figure 41). SLM was located north of RND. Given the piercing point locations RND270 (38.7 km) is best compared to SLM260 (38.0 km), in good agreement. RND results suggest significant relief at the base of the crust. RND200 (29.4 km or between 27.8 km and 31.1 km at 95% confidence) piercing point is not far from RND246 (39.5 km or between 37.5 km and 41.6 km at 95% confidence), indicating ~6 km relief over short lateral distance (Figure 37, 41).

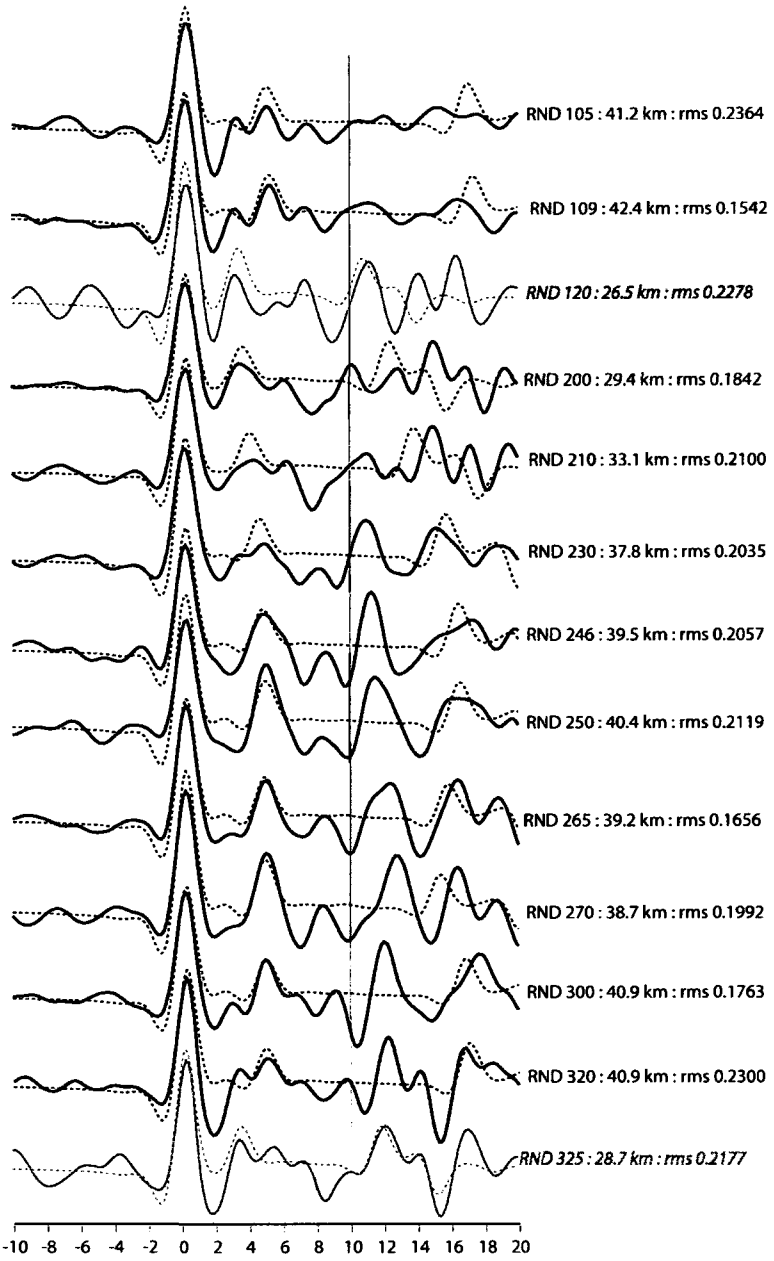

Figure 41: RND receiver function stacks arranged in backazimuthal order. Notation and symbols as described in Figure 24 caption. RND120 and RND325 eliminated. RND105, RND210, RND230, RND300, and RND320 produce large error and are eliminated. Crustal thickness results of the five large error eliminated stacks (33-41 km) are all within the range of crustal thickness results of the six stacks considered acceptable for further analysis (29-42 km).

South central BEAAR stations

South central BEAAR stations are located along the Parks Highway in the Broad Pass Depression between the Talkeetna mountains and the central Alaska Range, including Igloo (GOO), Antimony (ANT),

Hurricane (HURN), Parrot Yesteryear (PYY), Moose Head Rock (MHR), Fiddlehead (FID), Byer (BYR), and Wolf (WOLF) (Table 7, Figure 42). The region is dominated by the Kahiltna terrane, with a number of smaller terranes tectonically intermixed. The Chulitna, West Fork, and Broad Pass terranes have been identified in this region.

Table 7: South central stations summary table lists physiographic section, geologic setting, terranes, and crustal thickness for BEAAR stations deployed south of the Denali fault along the Parks Highway. Physiographic section is as described by Wahrahaftig, (1992). Geologic setting provides gross lithology as indicated on maps, mainly as described by Wilson et al. (1998) and Beikman (1980).

station	physiographic section(s)	geology	terrane(s)	crustal thickness (km)
GOO	Broad Pass Depression between Talkeetna Mountains and central Alaska Range	Cretaceous mélanges of the Alaska Range	Kahiltna, Broad Pass, West Fork, Chulitna, Susitna	38-47
		early Cretaceous and Late Jurassic flysch sequence found in a large folded klippe or thrust sliver		
		Tertiary coal bearing rocks		
		Tertiary (Eocene) granite and granodiorite		
		Early Cretaceous to Late Jurassic argillite, chert, sandstone, and limestone		
HURN	Broad Pass Depression between Talkeetna Mountains and central Alaska Range	Cretaceous mélanges of the Alaska Range	Kahiltna, Broad Pass, West Fork, Chulitna, Susitna	34-38
		Paleocene granitic rocks		
		earliest Late Cretaceous to Late Jurassic (?) Kahiltna flysch sequence of intensely deformed and locally highly metamorphosed turbidites		
		Late Jurassic to Late Triassic? Crystal tuff, argillite, chert, greywacke, and limestone		
		Early Jurassic and Late Triassic red and brown sedimentary rocks and basalt		
		Late Triassic? red beds		
		early Cretaceous and Late Jurassic flysch sequence found in a large folded klippe or thrust sliver		
PYY	Talkeetna Mountains few kilometers east Broad Pass Depression	Paleocene biotite-muscovite granite to quartz monzonite	Broad Pass or West Fork	40
		Cretaceous mélanges of the Alaska Range		
MHR	Talkeetna Mountains near southwestern extent Broad Pass Depression	earliest Late Cretaceous to Late Jurassic (?) Kahiltna flysch sequence of intensely deformed and locally highly metamorphosed turbidites	Kahiltna, Broad Pass, or West Fork	36-40
		Cretaceous mélanges of the Alaska Range		
		Paleocene granitic rocks		
FID	Talkeetna Mountains	Paleocene granitic rocks	Kahiltna	38?
BYR	western boundary Talkeetna Mountains near Susitna lowland	Paleocene granitic rocks	Kahiltna	34-40
		earliest Late Cretaceous to Late Jurassic? Kahiltna flysch sequence		
		Tertiary (Pliocene) Sterling Formation conglomerate		
		Tertiary (Miocene) carbonaceous Tyonek Formation		
WOLF	western boundary Talkeetna Mountains near Susitna lowland	earliest Late Cretaceous to Late Jurassic? Kahiltna flysch sequence	Kahiltna	34-40
		Tertiary (Pliocene) Sterling Formation conglomerate		
		Tertiary (Miocene) carbonaceous Tyonek Formation		

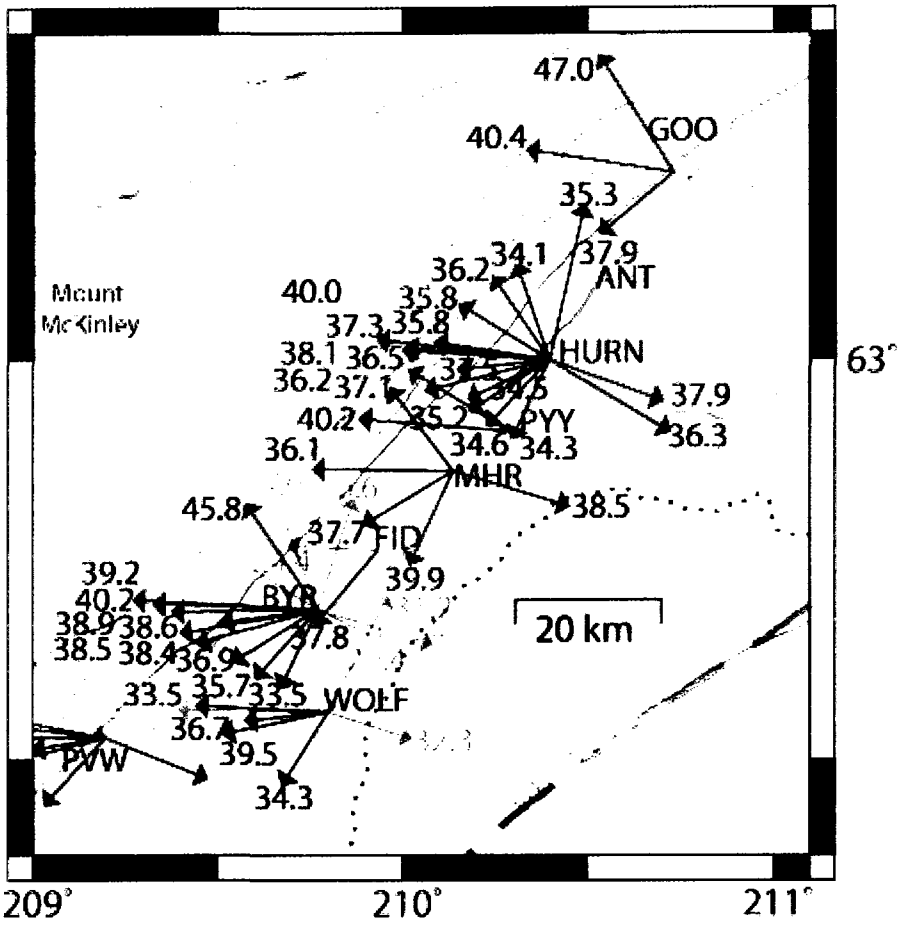

Figure 42: South central BEAAR stations. Symbols used as in previous figures. Vector endpoints locate the latitude and longitude of the Moho piercing point. GOO, HURN, PYY, MHR, FID, BYR, and WOLF depths labeled (km).

GOO was located along the Parks Highway in the Broad Pass Depression between the Talkeetna Mountains and the central Alaska Range. The mountains to the east and west include Kahiltna terrane interrupted by fault slivers and structural mélange including Broad Pass, West Fork, and Chulitna terranes to the west, as well as the Susitna terrane, a rooteless nappé to the east. Receiver functions were subdivided into five groups (Figure 43). GOO20 was eliminated due to inferior signal to noise ratio, and concerns about raypath crossing above mentioned faults. GOO109 was eliminated due to multiple lows in the root-mean-square misfit curve. The remaining groups of receiver functions yielded crustal thickness estimates ranging from 38 km to 47 km (Table 3). These results, from western backazimuths, were sampling beneath the Alaska Range, as opposed to eastern backazimuths which could have sampled beneath the Talkeetna mountains. GOO was southwest of RND and southeast of EFS. GOO200, mean backazimuth of 230° puts the piercing point further south of RND piercing points than GOO300, but the

trend of the faults separating the West Fork terrane from the Chulitna and Broad Pass terranes suggest GOO200 is the stack we should be comparing west-southwest backazimuth RND results with, not the geographically closer GOO300 stack. GOO200 at 37.9 km is in reasonable agreement with southwest RND results: RND246 at 39.5 km, RND250 at 40.4 km, RND265 at 39.2 km, and RND270 at 38.7 km. GOO300 at 47.0 km is just south of the Denali fault. EFS (produced a single stack with a mean backazimuth of 187°, and crustal thickness of 39.5 km) and SBL110 (42.0 km) piercing points are in the neighborhood of GOO300, but both are just north of the Denali fault. There appears to be significant relief at the base of the crust in this region, with GOO crustal thickness results ranging from 38 to 47 km, indicative of a deep Moho.

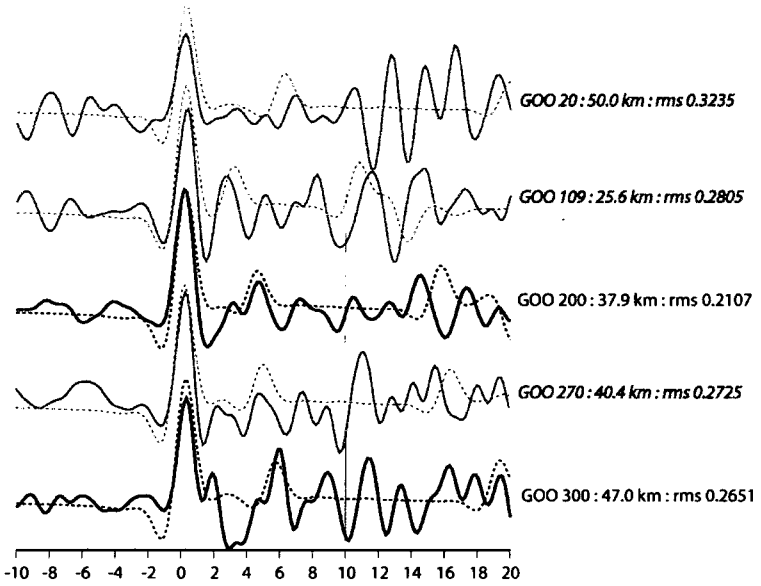

Figure 43: GOO receiver function stacks arranged in backazimuthal order. Notation and symbols as described in Figure 24 caption. Receiver functions that would have been immediately removed from consideration at other stations due to noise and waveform complexity were modeled in hopes of pulling some useful data at this station. GOO20, and GOO109 eliminated.

ANT was located roughly due east of Mount McKinley, along the Parks Highway in the Broad Pass Depression between the northwestern portion of the Talkeetna mountain physiographic section and the southeastern portion of the central Alaska Range (Wahrhaftig, 1992). Due to faulty instrumentation ANT was problematic and did not provide reliable crustal thickness estimates.

HURN was located just south of Hurricane Gulch, east of the Parks Highway in the Broad Pass depression physiographic section. Across Broad Pass, the moderately high rugged mountain area of the Talkeetna mountains physiographic section is only ~20 km east from the extremely high rugged mountain area of the central Alaska Range physiographic section (Wahrhaftig, 1992). The Kahiltna terrane, Broad

Pass terrane, West Fork terrane, Chulitna terrane, and the Susitna terrane surround HURN. The Parks Highway suspension bridge across nearby Hurricane Gulch provided an unexpected noise source. The local bears also provided excitement by gnawing on the Action Packers housing the winter batteries, but the power interruption was quickly identified and remedied. HURN provided a wealth of high quality seismic data, which allowed us to resolve backazimuthal variation surrounding this long term site. The data allowed subdivision by backazimuth and distance into sixteen separate groups (Figure 44). The fourteen stacks that survived quality control yielded crustal thickness estimates ranging from 34 km to 38 km (Table 3), two of which were from easterly backazimuths sampling beneath the Talkeetna mountains. HURN100 piercing point plots beneath the Susitna terrane. HURN was located southwest of GOO. Stacks with northern backazimuths HURN320 and HURN10 yielded crustal thicknesses of 36.2 km and 35.3 km respectively, within a few kilometers of the 37.9 km crustal thickness indicated by nearest piercing point neighbor stack GOO200.

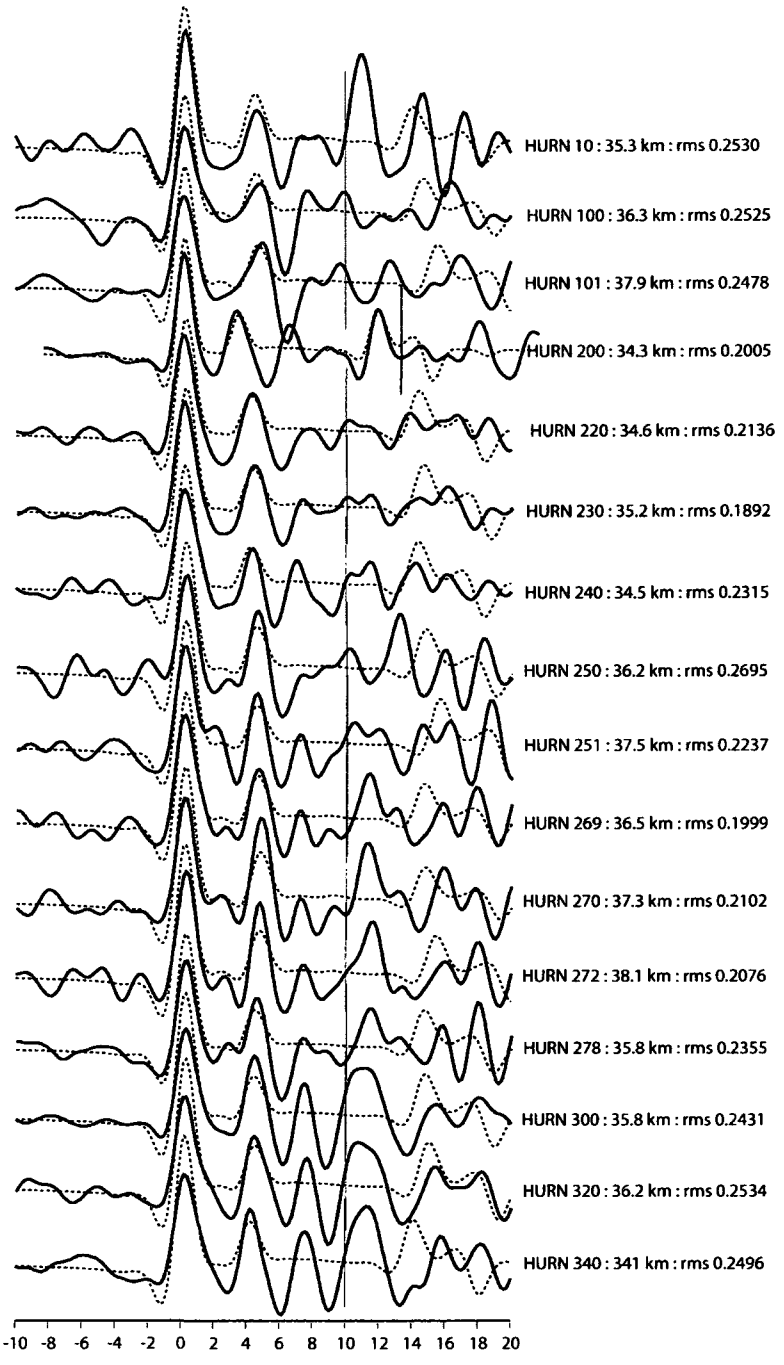

Figure 44: HURN receiver function stacks arranged in backazimuthal order. Notation and symbols as described in Figure 24 caption. HURN300 and HURN340 produced 10.9 km errors so were eliminated, but results, 35.8 km and 34.1 km respectively, were within range of "kept" stacks. Models indicate crustal thickness 34-38 km around HURN.

PYY was located in the Talkeetna mountains physiographic section a few kilometers east of the Broad Pass Depression narrowly separating the Talkeetna Mountains from the central Alaska Range (Wahrhaftig, 1992). A single reliable crustal thickness was determined from PYY, 40 km thick to the west (Table 3, Figure 45), most likely sampling Broad Pass or West Fork terrane. Piercing points indicate PYY is best compared with HURN results at western backazimuth at moderate distance. In this densely sampled region, HURN251 37.5 km, HURN272 38.1 km, HURN270 37.3 km, HURN269 36.5 km, and HURN251 37.5 km all have piercing points in the neighborhood of PYY270. These results suggest deep Moho with a few kilometers relief in this region.

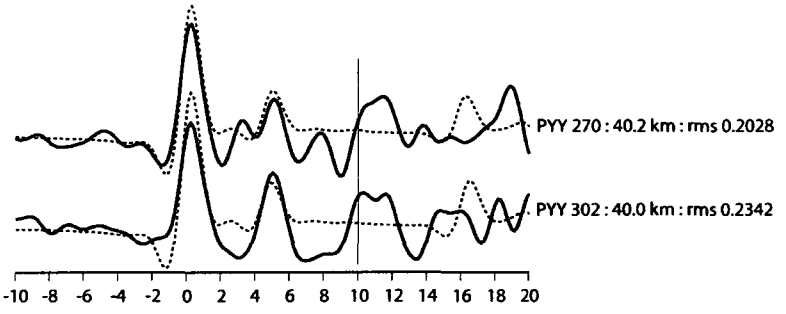

Figure 45: PYY receiver function stacks arranged in backazimuthal order. Notation and symbols as described in Figure 24 caption. PYY302 produced 11.5 km error and eliminated, but result 40.0 km close to "kept" result of 40.2 km.

MHR was located in the Talkeetna mountains physiographic section near the southwestern extent of the Broad Pass Depression (Table 7). MHR produced high quality data, operated over winter with batteries donated from AEIC. Receiver functions from MHR were subdivided into five groups, indicating crustal thicknesses from 36 km to 40 km (Table 3). MHR100 and MHR200 stacks (Figure 46) have an extra pulse between the primary arrival and Moho Ps conversion, perhaps reflecting some mid-crustal discontinuity or structural complexity, but the receiver functions are otherwise well behaved and produce models with reasonable error, so there was no reason to exclude them. MHR is southwest of PYY and HURN, most likely sampling Kahiltna, Broad Pass and/or West Fork terranes. Piercing points put MHR300 (37.1 km) just northeast of PYY270 (40.2 km) and near HURN251 (37.5 km), HURN272 (38.1 km), HURN270 (37.3 km), HURN269 (36.5 km), and HURN251 (37.5 km). MHR100 is in the direction of the Talkeetna mountains, MHR200 is beneath the westernmost edge of the relief associated with the Talkeetna mountains, MHR230 beneath Broad Pass, MHR250 just west of the mapped fault that runs along the western edge of Broad Pass, with MHR300 beneath topography associated with the Alaska Range. Crustal thicknesses beneath MHR (36-40 km) suggest deep Moho with few kilometers relief.

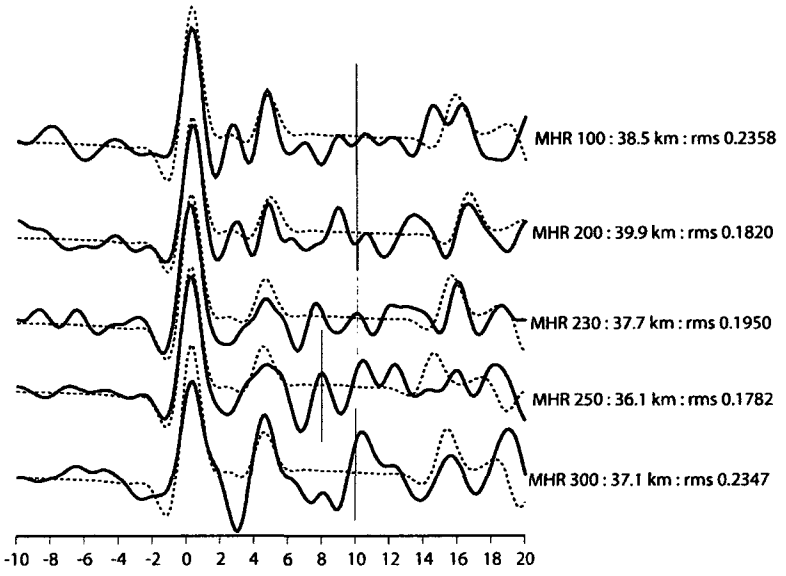

Figure 46: MHR stacks arranged in backazimuthal order. Notation and symbols as described in Figure 24 caption.

FID was located southeast of the highest topography of the Alaska Range, in the low mountains bordering the Susitna River in the Talkeetna mountains physiographic section (Wahrhaftig, 1992). FID was a short term site that recorded plenty of teleseismic events. FID produced two receiver function stacks with reasonable signal to noise ratios (Figure 47), but the results were eliminated from further study. FID259 may be incorrectly modeling the little pulse between the primary arrival and Ps conversion as Moho, so FID259 was eliminated. FID217's crustal thickness of 37.8 km agrees well with neighboring MHR230 (37.7 km), but FID217 error was such that crustal thickness was only constrained between 23.6 and 45.1 km at 95% confidence, so no data from FID survived quality control.

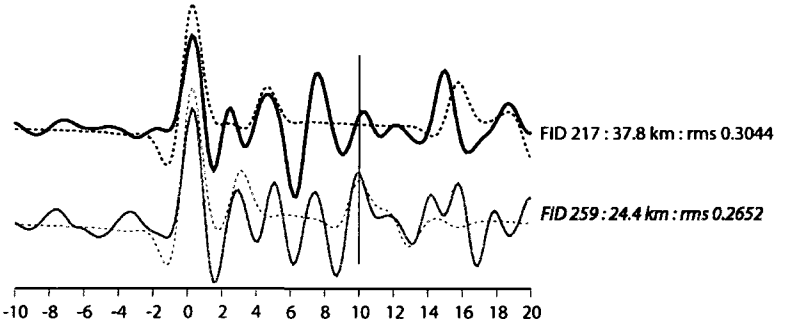

Figure 47: FID stacks arranged in backazimuthal order. Notation and symbols as described in Figure 24 caption. FID 259 eliminated. FID217 produced 21.5 km error, so eliminated.

BYR was located at the western boundary of the Talkeetna mountains physiographic section in the low mountains bordering the Susitna River near the northern edge of the Susitna lowland (Wahrhaftig, 1992). BYR was one of the first few stations deployed and last few taken out, recording high quality data almost continuously for 27 months. Data was subdivided into 16 distance/backazimuth groups (Table 3, Figure 48). BYR10, BYR106, BYR108, BYR300, and BYR330 were eliminated. BYR10 and BYR108 model an early arrival rather than Moho, both were eliminated from further study. (BYR108 and BYR106 are reminiscent of FID259 and FID217 respectively.) BYR106, BYR300, and BYR330 modeled crustal thicknesses were 38.3 km, 43.8 km, and 43.9 km respectively, and although eliminated from further study because they were poorly constrained, the results fall within the range of BYR results deemed worthy of further study (34-46 km). The remaining stacks provided nice resolution in western backazimuths. The stacks to the southwest indicate the crust is 34-39 km thick: BYR200 33.5 km, BYR210 35.7 km, BYR232 36.9 km, BYR250 38.4 km, BYR251 38.6km, and BYR259 38.5 km. Three stacks are just west of the fault on the west side of Broad Pass indicating crustal thickness of 39-40 km: BYR252 38.9 km, BYR269 40.2 km, and BYR270 39.2 km. One stack to the northwest, BYR320 45.8 km, completes the local picture of crust becoming progressively thicker (as the Alaska Range is approached from the south). BYR320 (45.8 km or between 43.4 km and 48.3 km at 95% confidence) piercing point plots near MHR250 (36.1 km or between 35.1 km and 37.1 km at 95% confidence), a jump of ~6 km over a short lateral distance. MHR250 is near the southwestern extent of the West Fork and Broad Pass terranes while BYR results all appear to be sampling Kahiltna terrane.

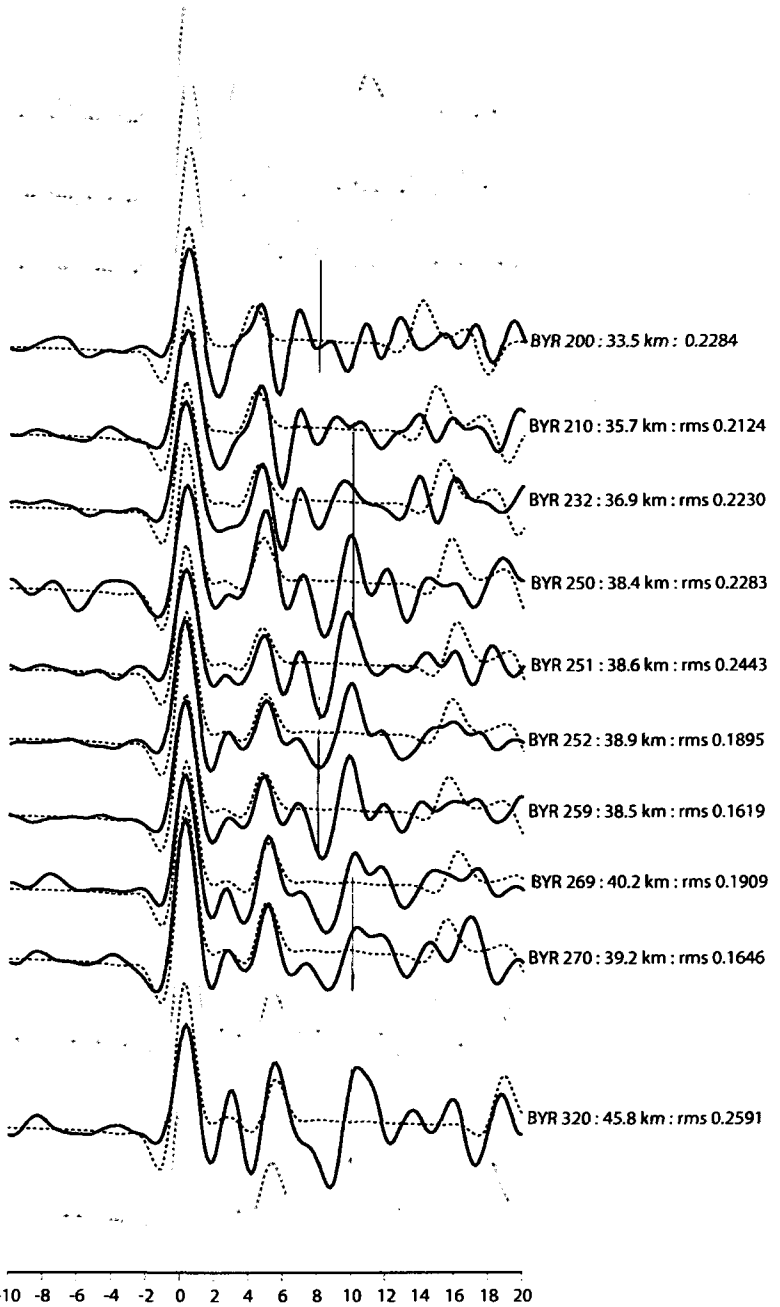

Figure 48: BYR stacks (arranged in backazimuthal order) indicate crustal thicknesses 34-46 km. Notation and symbols as described in Figure 24 caption. BYR10, BYR106, BYR108, BYR300, and BYR330 eliminated from study. BYR320 has strong arrival between direct P and Ps conversion, probably indicating a mid-crustal discontinuity.

WOLF was located in the generally rolling low mountains at the western boundary of the Talkeetna Mountains near the Susitna lowland physiographic section (Wahrhaftig, 1992). WOLF was

located on private property; the station was named for the wolf kept by the owners of the property at the time of installation. Much of the data recorded at WOLF was noisy. WOLF receiver functions were subdivided into eight groups (Table 3, Figure 49). WOLF20 (31.2 km), WOLF100 (32.3 km), WOLF270 (36.2 km), and WOLF300 (47.7 km) produced multiple lows in the root-mean-square misfit curve and were eliminated from study. WOLF200 (34.3 km) had total error of 12 km, and WOLF260 (36.7 km) had total error of 14 km, both were eliminated from further study. The two stacks that produced models with crustal thicknesses deemed reliable at 95% confidence were WOLF250 (39.5 km) and WOLF269 (33.5 km). The piercing points of these two data points are nearest piercing points of BYR southwestern backazimuths: BYR200 at 33.5 km, BYR210 at 35.7 km, BYR232 at 36.9 km, BYR250 at 38.4 km, BYR259 at 38.5 km. These all plot beneath Susitna lowland south of the central Alaska Range topography, probably sampling Kahiltna terrane, suggesting on the order of 6 km relief at the base of the crust in the region.

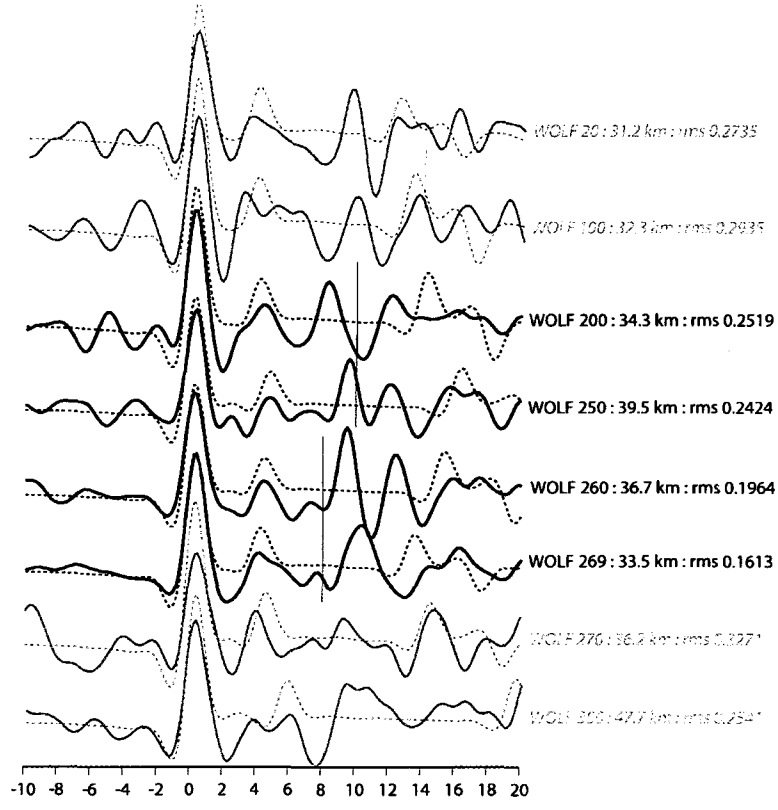

Figure 49: WOLF stacks arranged in backazimuthal order. Notation and symbols as described in Figure 24 caption. Receiver functions that would have been immediately removed from consideration at other stations due to noise and waveform complexity were modeled in hopes of pulling some useful data at this station. WOLF 20, WOLF 100, WOLF270, and WOLF300 eliminated. WOLF200 and WOLF260 had large errors, so were eliminated.

Southernmost BEAAR stations

The stations located furthest south include those out the Petersville Road, Petersville West (PVW), Petersville East (PVE), and Trapper Creek Elementary (TCE), as well as Talkeetna (TLKY) off the Parks Highway (Table 8, Figure 50). The Kahiltna terrane dominates in the region, but is obscured by Quaternary surficial deposits.

Table 8: Southernmost stations summary table lists physiographic section, geologic setting, terranes, and crustal thickness for the BEAAR stations deployed out Petersville Road. Physiographic section is as described by Wahrahaftig, (1992). Geologic setting provides gross lithology as indicated on maps, mainly as described by Wilson et al. (1998) and Beikman (1980).

station	physiographic section(s)	geology	terrane(s)	crustal thickness (km)
TCE	Susitna lowland	Quaternary surficial deposits	Kahiltna or Wrangellia?	27
PVE	Susitna lowland	Quaternary surficial deposits	Kahiltna?	23
		Tertiary (Miocene) Tyonek Formation with carbonaceous sandstone, siltstone, shale and claystone		
PVW	central Alaska Range meets Susitna lowland	earliest Late Cretaceous to Late Jurassic? Kahiltna flysch sequence	Kahiltna	26-34
		Tertiary (Pliocene) Sterling Formation conglomerate		
		Tertiary (Miocene) carbonaceous Tyonek Formation locally divided into sandstone or conglomerate member		

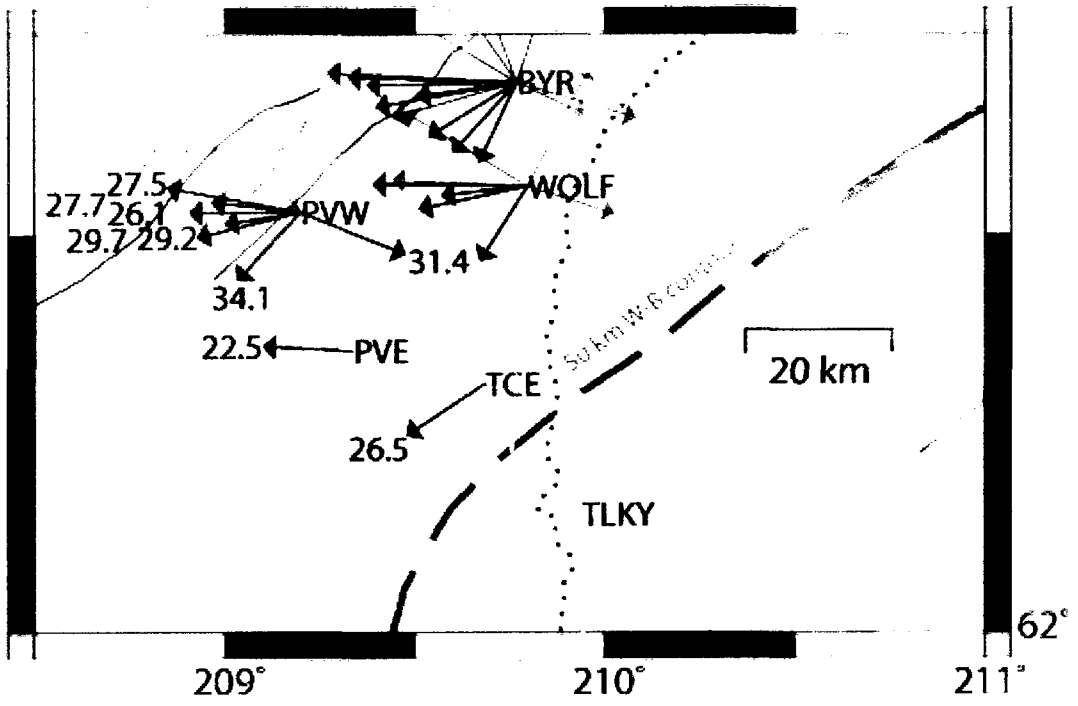

Figure 50: Southernmost BEAAR stations. Symbols used as in previous figures. Vector endpoints locate latitude and longitude of Moho piercing point. PVW, PVE, and TCE depths labeled (km).

PVW was adjacent to the border between the Alaska-Aleutian physiographic province and the Central Trough physiographic province, where the central Alaska Range and the Susitna lowland physiographic sections meet, in an area of rolling topography with altitudes 1000-3000 feet (Wahrhaftig, 1992). The Kahiltna terrane dominates here. Mount McKinley is located just west of a line between PVW and WON. An increasingly rough road south of the national park through Petersville, an abandoned mining village, provided access to sites south of the Alaska Range, west of the Parks Highway, including PVW and PVE. The data from PVW was generally high quality, with sufficient quantity to subdivide into ten groups (Table 3, Figure 51). The piercing points place PVW330 (24.7 km), PVW320 (24.7 km), and PVW290 (23.9 km) data points between southwest trending faults, and although the data is not of sufficient quality to include in our crustal thickness study, the results suggest shallow Moho. PVW280 (27.5 km), PVW 270 (27.7 km), and PVW 251 (29.2 km) have total errors between 7.0 and 8.0 km so although rejected from further study, these crustal thicknesses are within the range of "kept" data from PVW (26-34 km). The PVW105 (31.4 km) piercing point plots nearest the southwest backazimuths of WOLF: WOLF 250 (39.5 km) and WOLF269 (33.5 km). These three data points indicate relief on the order of 8 km at the base of the crust beneath this portion of the Susitna lowland. PVW200 (34.1 km) plots just south of the fault mapped along the western edge of Broad Pass and Susitna lowland, and may be best

considered with PVW105 (31.4 km). Piercing points of the remaining stacks from PVW plot beneath the southernmost topography of the central Alaska Range between the southwest trending faults mentioned above: PVW250 at 29.7 km, and PVW260 at 26.1 km both suggest relatively shallow crust.

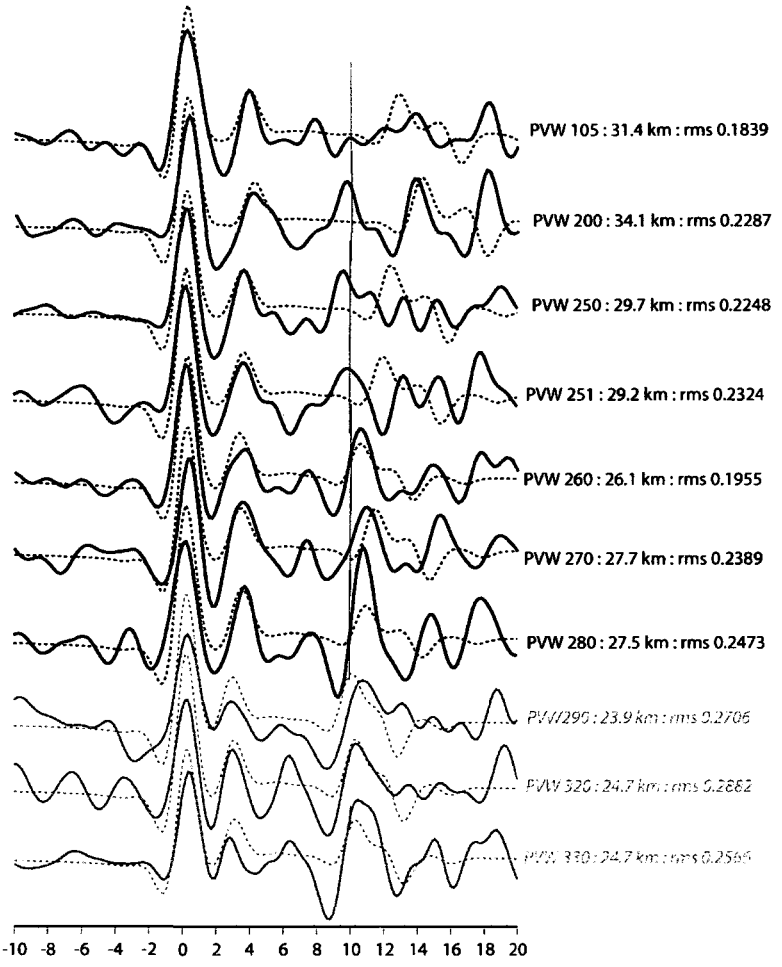

Figure 51: PVW receiver function stacks arranged in backazimuthal order. Notation and symbols as described in Figure 24 caption. PVW330, PVW320, and PVW290 eliminated. PVW280, PVW270, and PVW251 models were poorly constrained so eliminated from further consideration.

PVE was located in the Susitna lowland, situated on the Kahiltna terrane. PVE was on a hill in rolling terrain, well camouflaged by fireweed in midsummer. Fast growing vegetation blocked solar panels, causing depletion of energy reserves and DAS shutdown. Tarps provided an adequate vegetation block once the problem was discovered; however, the quantity of data from this short term station produced only one high quality crustal thickness estimate. Models indicate a basin thickness of 1.4 km, and a crustal thickness of 22.5 km beneath PVE (Table 3, Figure 52). PVE Moho is roughly 10 km shallower than nearest piercing point neighbors: PVW105 (31.4 km) and PVW200 (34.1 km).

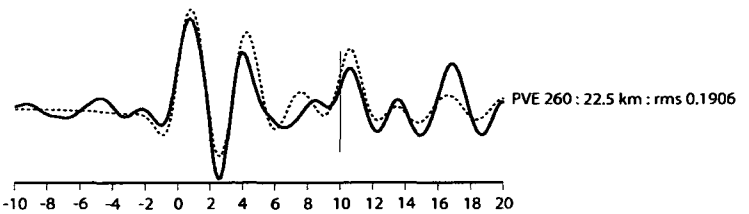

Figure 52: PVE receiver function stack including all acceptable traces in 0-360° backazimuth range. Notation and symbols as described in Figure 24 caption.

TCE was located in the Susitna lowland physiographic section. Installed on the property of Trapper Creek Elementary School, TCE was a sandy site. At the time of installation we deemed a drain unnecessary since the vault was surrounded by well sorted, well drained sandy soil. Models indicate the basin is 1.5 km thick. Although 33 traces were considered usable, the data quality was not sufficient to resolve backazimuthal variation (Table 3, Figure 53). Results indicate crustal thickness of 26.5 km at TCE, located above the roughly 50-55 km depth contour of the subducting slab (Figures 20-21). TCE Moho is 4 km deeper than northern neighbor PVE (22.5 km), both indicating shallow Moho in this region.

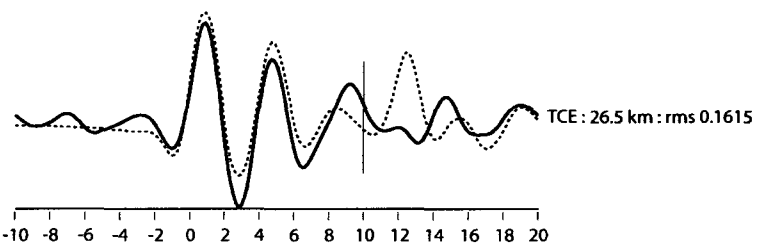

Figure 53: TCE receiver function stack includes all traces in 0-360° station-to-event backazimuth range. Notation and symbols as described in Figure 24 caption.

TLKY was located in the lowland filled with Quaternary surficial deposits, near the border between the Susitna lowland and the Talkeetna mountains physiographic provinces. TLKY was located in the backyard of a schoolteacher who provided AC power for the station. The sedimentary basin and the slab create interesting seismograms and receiver functions but cannot be appropriately modeled by the methods adopted for the other BEAAR stations. With the slab directly under the crust, there is no analogous Moho to be modeled.

Denali Highway BEAAR stations

Four stations were located along the Denali Highway: Crazy Notch (CZN), Denali Highway 3 (DH3), Denali Highway 2 (DH2), and Denali Highway 1 (DH1) (Table 9, Figure 54). The road crosses a number of NE-SW trending faults that, as discussed in the introduction, may accommodate westward rotation of crustal blocks in the region. The varied topography of the different physiographic provinces makes this a beautiful drive, from Broad Pass Depression between the Alaska Range and the Talkeetna

mountains at the western end of the road, through the Clearwater Mountains, to the Gulkana upland in the east.

Table 9: Denali Highway stations summary table lists physiographic section, geologic setting, terranes, and crustal thickness for BEAAR stations deployed along the Denali Highway between Cantwell and Paxson. Physiographic section is as described by Wahrahaftig, (1992). Geologic setting provides gross lithology as indicated on maps, mainly as described by Wilson et al. (1998) and Beikman (1980).

station	physiographic section(s)	geology	terrane(s)	crustal thickness (km)
CZN	Clearwater Mountains meet Gulkana upland	Late and/or Middle Triassic Nikolai greenstone and related rocks	Wrangellia	38
		Early Cretaceous or Jurassic granitic rocks		
DH3	Clearwater Mountains	Pennsylvanian Tetelna volcanics	Wrangellia	34
		Early Permian Eagle Creek formation		
		Late and/or Middle Triassic Nikolai greenstone and related rocks		
		Early Permian and Pennsylvanian Station Creek and Slana Spur formation, and equivalent rocks		
		Late Triassic metavolcanic and associated metasedimentary rocks		
		Jurassic? mafic and ultramafic rocks		
DH2	Broad Pass Depression	earliest Late Cretaceous to Late Jurassic? Kahiltna flysch sequence	MacLaren, Nenana, Kahiltna	41-45
		Late Triassic, middle? Norian and Late Karnian calcareous sedimentary rocks		
		Early Cretaceous and Late Jurassic flysch sequence		
		Mesozoic phyllite, pelitic schist, calc-schist, and amphibolite of the MacLaren metamorphic belt		
DH1	Broad Pass Depression between Talkeetna Mountains and Alaska Range	Late Triassic, middle? Norian and Late Karnian calcareous sedimentary rocks	Nenana, Kahiltna, Broad Pass	41-45
		Cretaceous mélanges of the Alaska Range with Silurian to Cretaceous protoliths		
		earliest Late Cretaceous to Late Jurassic? Kahiltna flysch sequence		
		Early Cretaceous and Late Jurassic flysch sequence		
		Tertiary volcanic rocks, undivided		
		Miocene to Paleocene, mostly Early Tertiary or Eocene? Hypabyssal felsic and intermediate intrusive rocks		
		Eocene granite and granodiorite		

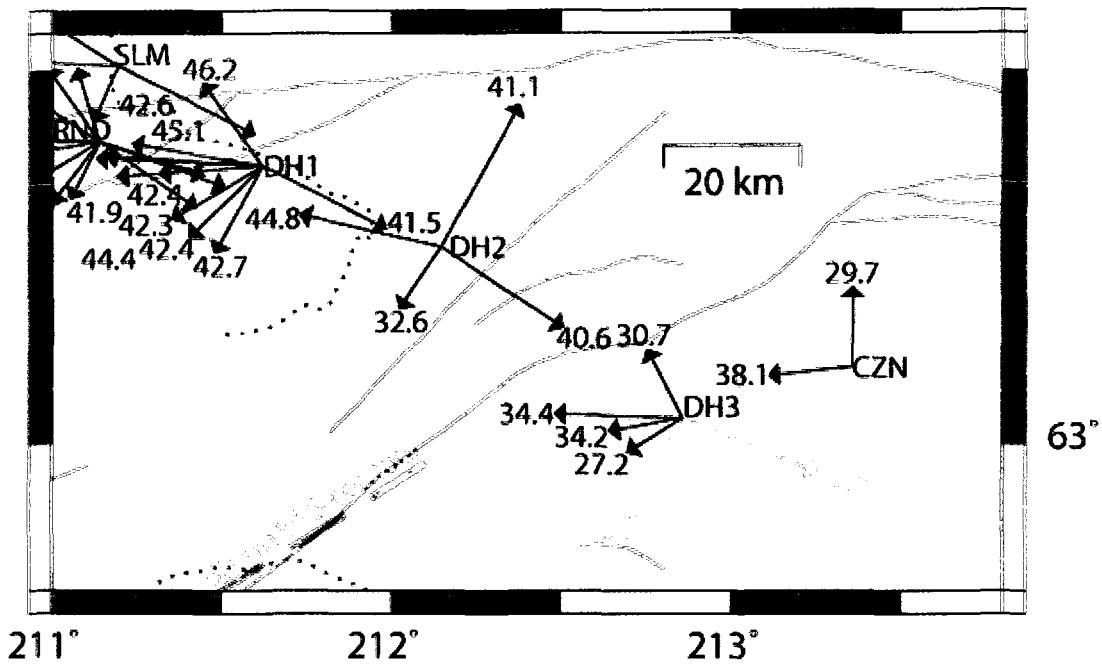

Figure 54: Denali Highway BEAAR stations. Symbols used as in previous figures. Vector endpoints locate the latitude and longitude of the Moho piercing point. DH1, DH2, DH3, and CZN depths labeled (km).

CZN was located just north of the Denali Highway near the boundary between the Clearwater mountain and Gulkana upland physiographic sections. CZN results appear to be sampling Wrangellia terrane. Receiver functions were subdivided into three stacks (Table 3, Figure 55). CZN200 (36.5 km) and CZN250 (38.1 km) both have reasonable signal to noise ratios and show two distinct arrivals of approximately equal amplitude within 5 seconds of the direct P. These multiple arrivals created a second low in the root-mean-square misfit curve of CZN200. The northern stack CZN1 (29.7 km) had 13.4 km total error, so was removed from further consideration. The only stack surviving quality control (CZN250) indicated a crustal thickness of 38 km beneath the easternmost portion of our study area.

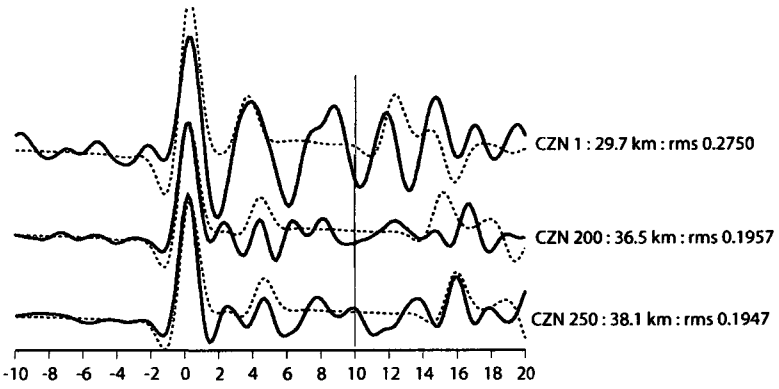

Figure 55: CZN stacks arranged in backazimuthal order. Notation and symbols as described in Figure 24 caption. CZN1 eliminated due to large total error.

DH3 was located just north of the Denali Highway in the Clearwater mountain physiographic section. The waveforms recorded at DH3 are of sufficiently high quality to resolve some backazimuthal variation (Table 3, Figure 56). DH3 110 (52.9 km) piercing point is located near the projection of the 50 km Wadati-Benioff zone depth contour, so it seems reasonable to postulate that the discontinuity being modeled is the top of the subducting slab rather than Moho. DH3 200 (50.2 km) has multiple arrivals, but similar to DH3 100 the best fit model is likely indicating slab rather than Moho. (These piercing points, however, are interestingly located east of the enigmatic eastern "edge" of the Wadati-Benioff zone seismicity.) DH3 230 (27.2 km) receiver function stack looks similar to DH3 200 receiver function stack with three distinct arrivals of approximately equal amplitude, but the signal to noise ratio was poor and total error enormous. DH3 320 (30.7 km) had 7.0 km error and was also eliminated from further analysis. The two stacks that survived quality control include DH3 250 (34.2 km) and DH3 251 (34.4 km). The backazimuths of these stacks suggest these are crustal thicknesses of Wrangellia terrane. The nearest neighbor piercing point is CZN250 (38.1 km), which suggests a slightly deeper Moho at 95% confidence.

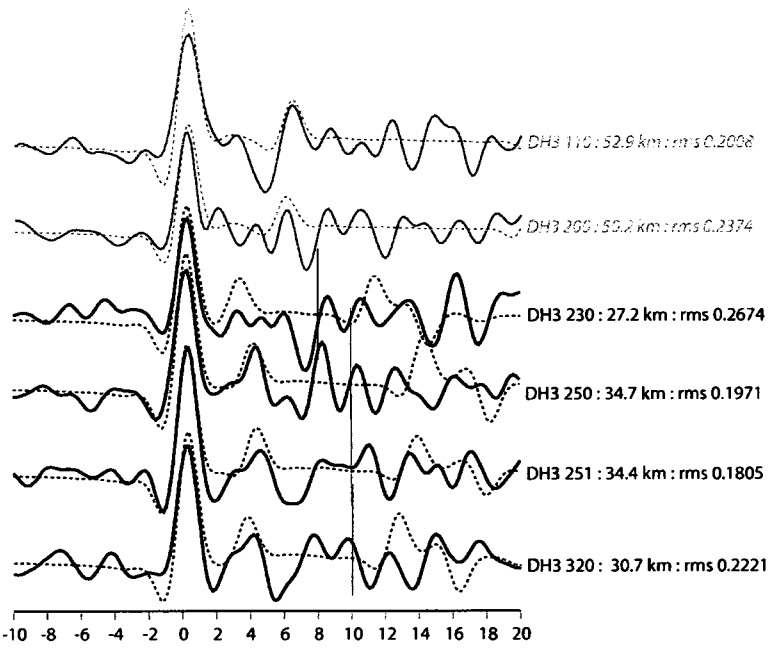

Figure 56: DH3 stacks arranged in backazimuthal order. Notation and symbols as described in Figure 24 caption. DH3 110, and DH3 200 eliminated because depth of discontinuity modeled by these stacks consistent with Wadati-Benioff zone depth contours. DH3 230 had 31 km error, DH3 320 has 7 km error, both eliminated from study.

DH2 was located out the Denali Highway in the Broad Pass depression physiographic section. DH2 had multiple electronic malfunctions, but there was sufficient high quality data to resolve some azimuthal variation (Table 3, Figure 57). DH2 is likely sampling MacLaren, Nenana, Clearwater, and Kahiltna terranes. DH2 20 and DH2 200 have more noise than the other stacks, but a clearly identifiable Ps conversion above the noise. The DH2 20 (41.1 km) piercing point plots just south of the Denali fault beneath the Nenana terrane, indicating a deep Moho beneath this point of the Alaska Range. The DH2 120 (40.6 km) piercing point plots just north of the Broxson Gulch thrust fault, beneath the Clearwater terrane, but total error of 8.3 km caused elimination from further analysis. (The nearest piercing points with which may compare DH2 120 (40.6 km crustal thickness) are DH3 251 (34.4 km) and DH3 250 (34.7 km) which are both south of the Broxson Gulch thrust fault, sampling Wrangellia terrane, and 6 km shallower.) DH2 200 (32.6 km) piercing point plots beneath the Talkeetna Mountains and is likely sampling the Kahiltna terrane, but given 14.3 km total error, this stack and model were eliminated from further study. The DH2 260 (44.8 km) piercing point also plots beneath the topography associated with the Talkeetna Mountains, and appears to be sampling the Kahiltna terrane. DH2 260 (44.8 km) is best compared with DH1 results, presented next.

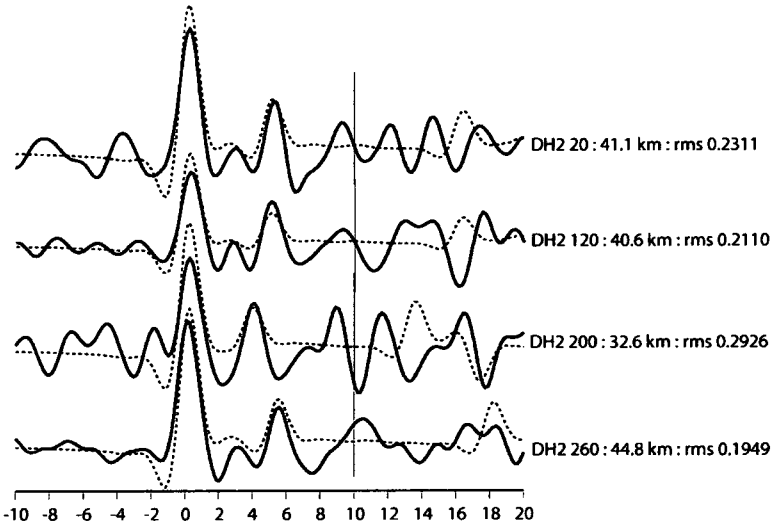

Figure 57: DH2 stacks and corresponding best fit synthetic receiver functions are arranged in backazimuthal order. Notation and symbols as described in Figure 24 caption. DH2 120 had 8 km error, and DH2 200 had 14 km error, both eliminated from crustal thickness study.

DH1 was located just south of the Denali Highway near the northernmost edge of the Talkeetna Mountains where Broad Pass depression barely separates the Talkeetna Mountains from the Alaska Range physiographic province (Wahrhaftig, 1992). DH1 provided lots of high quality data, sufficient to resolve 10 stacks (Table 3, Figure 58). The backazimuths of these stacks suggest that DH1 sampled the Nenana terrane, and Kahiltna terrane. DH1 110 and DH1 200 show a clear pulse between the direct P and the Ps conversion, suggesting the presence of a mid-crustal discontinuity or some structural complexity, reminiscent of some stacks at neighboring station RND. DH1 110 (41.5 km) is best compared with DH2 260 (44.8 km), noting that the piercing point of DH1 110 is closer to DH2 than piercing point of DH2 260 (Figures 20-21). DH1 110 and DH2 260 piercing point locations suggest they are sampling the Nenana terrane near the northern section of the Kahiltna terrane. DH1 320 (46.2 km) piercing point plots immediately north of the Denali fault, mapped as McKinley terrane, but given uncertainties (in fault location at depth, et cetera), DH1 320 could just as easily be argued as sampling Kahiltna terrane. DH1 320, however, produced large error and was removed from further analysis. The remaining eight stacks provide fairly consistent results: DH1 200 at 42.7 km, DH1 220 at 42.4 km, DH1 235 at 42.3 km, DH1 250 at 44.4 km, DH1 252 at 42.4 km, DH1 270 at 42.6 km, DH1 271 at 41.9 km, and DH1 275 at 45.1 km. These eight stacks all appear to be sampling the Kahiltna terrane. Crustal thicknesses modeled from these western backazimuth stacks range from 42 km to 45 km, some of the thickest crust observed. Piercing point locations of the two deepest DH1 values plot over the SE-NW trending faults, not far from their respective convergences with the Denali fault. Piercing point locations suggest the westernmost DH1

results, such as DH1 271 (41.9 km) and DH1 270 (42.6 km), should be comparable to RND109 (42.4 km). The western DH1 results are in reasonable agreement with eastern RND results at 95% confidence.

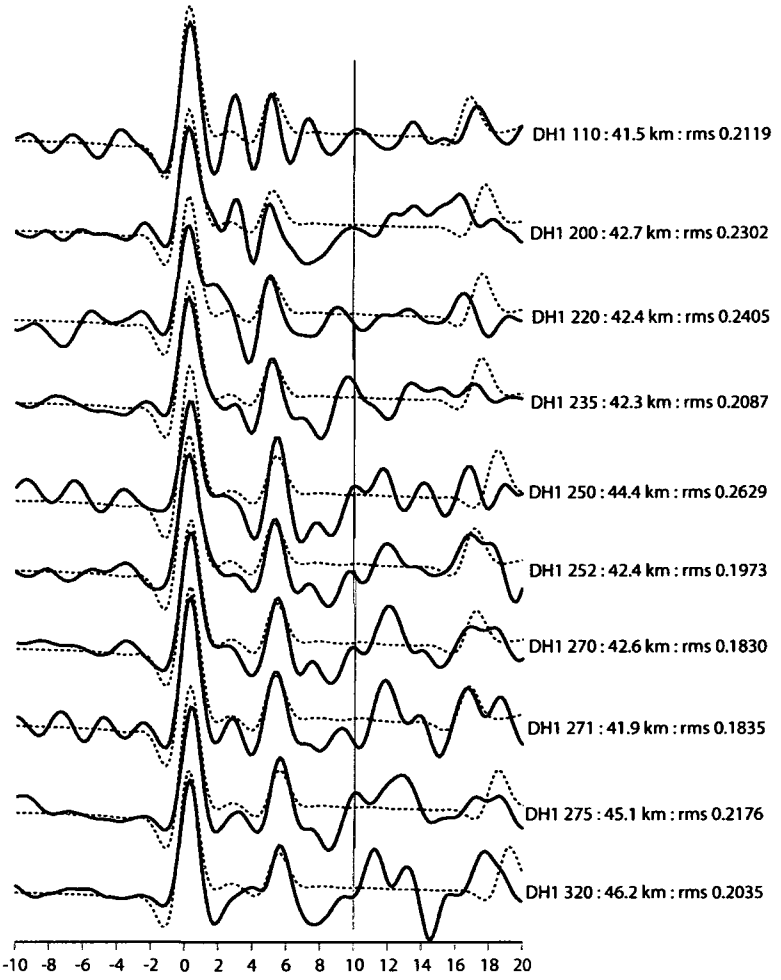

Figure 58: DH1 receiver function stacks and corresponding best fit synthetic receiver functions are arranged in backazimuthal order. Notation and symbols as described in Figure 24 caption. DH1 320 had 12.6 km error and was eliminated.

Results

Each group of receiver functions identified as a line in Table 3 provided new information about the subsurface structure beneath the Alaska Range. The details of each crustal thickness data point, such as stacking bounds, number of receiver functions in each group, piercing point location, as well as upper and lower bounds of crustal thickness at 95% confidence, et cetera, are listed in this lengthy table (Table 3). BEAAR receiver functions reveal a great deal more than can be discussed here (e.g., the slab conversion), so great care was taken to provide a simple graphical presentation of raw receiver functions and models (Figures 24-58), as a reference for those wishing to expand on this study. This BEAAR receiver

function analysis reveals thin crust to the north (typical crust on the order of 26 km thick) and relatively thick crust beneath the mountains (crustal root 35-45 km thick), with significant local relief at the base of the crust. Some relief observed at the base of the crust coincides with the location of major faults, a topic that will be explored further in Chapter 6. In addition to considering the relationship between crustal thickness and surface faults in the Alaska Range, with this plethora of crustal thickness data we can consider whether or not the topography of the Alaska Range is isostatically compensated.

Chapter 6 - Discussion and Implications

Isostatic compensation of the Alaska Range

BEAAR crustal thickness data allow evaluation of the state of isostatic compensation of the Alaska Range. There are three basic models of isostasy: Airy, Pratt, and Vening Meinesz. The Airy model assumes an upper layer of constant density floating on a denser substratum with topography supported by changes in the thickness of the layers. Thus, deep roots sustain high topography and antiroots sustain 'negative' topography. The Pratt model assumes columns with laterally variable density creating an upper layer resting on a flat uniform substratum (i.e. no root zone beneath mountains). Both Airy and Pratt models assume local isostatic compensation, with compensation occurring directly beneath the topographic feature, and complete equilibrium at depth. Airy and Pratt proposed these explanations for anomalous deflections of plumb-lines near mountainous regions in the mid 19th century, before the development of modern seismology. The Vening Meinesz elastic plate model assumes regional compensation through flexure of an elastic sheet distributing the load of a topographic feature over a wider region. In contrast with the local compensation assumed by Airy and Pratt models, the flexural model allows buoyancy of the denser displaced substratum to support the excess load or bent sheet over a broad region. Evidence of crustal thickness distribution amassed since development of modern seismology is in broad agreement with Airy type isostatic compensation. Pure Pratt isostasy requires a flat uniform substratum, contradicting observed Moho depth variations documented by modern seismology, but lateral changes in crustal density are observed (e.g. contrast between oceanic crust and continental crust). The Vening Meinesz flexural model was developed to explain anomalies observed at sea associated with topographic features on oceanic crust, such as deep sea trenches and island arcs, which led him to conclude that compensation is not entirely local.

Assuming perfect Airy isostasy, I compared predicted crustal thicknesses beneath the Alaska Range to those determined by receiver function analysis. Elevation, background crustal thickness (for 0 km elevation), and density contrast between crust and mantle are used to predict crustal thicknesses assuming Airy isostacy. Topography is smoothed to eliminate short wavelength components, averaging elevation around each grid point. Continental crustal thickness is imperfectly known and varies by region, so averages are skewed depending upon studies included in calculation of a reported mean. Tanimoto (1995) reports classical depth to Moho beneath Paleozoic and Mesozoic regions of about 30 km. According to Christensen and Mooney (1995), the global average crustal density is 2830 kg m^{-3}. Parameters used in the calculation of a best fit crustal model were determined by a search of smoothing radius (0-90 km in 10 km intervals), background crustal thickness (24-32 km), and density contrast (470 kg m^{-3} or 500 kg m^{-3} between upper and lower layer) to determine the best fit to the observed data. It

should be noted that parameters used provide the minimum root-mean-square misfit between the observed data and the modeled values. I used a 470 kg m^{-3} density contrast (crustal density of 2830 kg m^{-3}, mantle density of 3300 kg m^{-3}) and an overall background crustal thickness of 31 km to predict the thickness of an isostatically compensated crust. Crustal thicknesses determined by receiver function analysis are shown with crustal thicknesses predicted from topography in Figure 59 and Table 10. These parameters and results seem reasonable given a global average thickness of extended crust of 30.5 km, and an average thickness of crust beneath orogens of 46.3 km (Christensen and Mooney, 1995).

A primary observation is the sharp contrast between Moho depths north and south of the Denali/Hines Creek fault region. Northern Moho depths, considered in isolation, yield a best fit background crustal thickness of 26 km. Southern Moho depths, considered in isolation, yield a best fit background crustal thickness of 33 km. The compensation calculation used the overall average background crustal thickness of 31 km despite the systematic regional difference, an indication of some basic difference between the crust beneath stations in the Alaska Range and the crust beneath stations north of the range. In addition to an Airy model, I also considered a Vening Meinesz flexural model for isostatic compensation with an elastic plate of varying thickness (in which the crust floats buoyantly on a layer that spreads topographic load over a broader region). The flexural model produced results similar to the Airy model with dramatically smoothed topography.

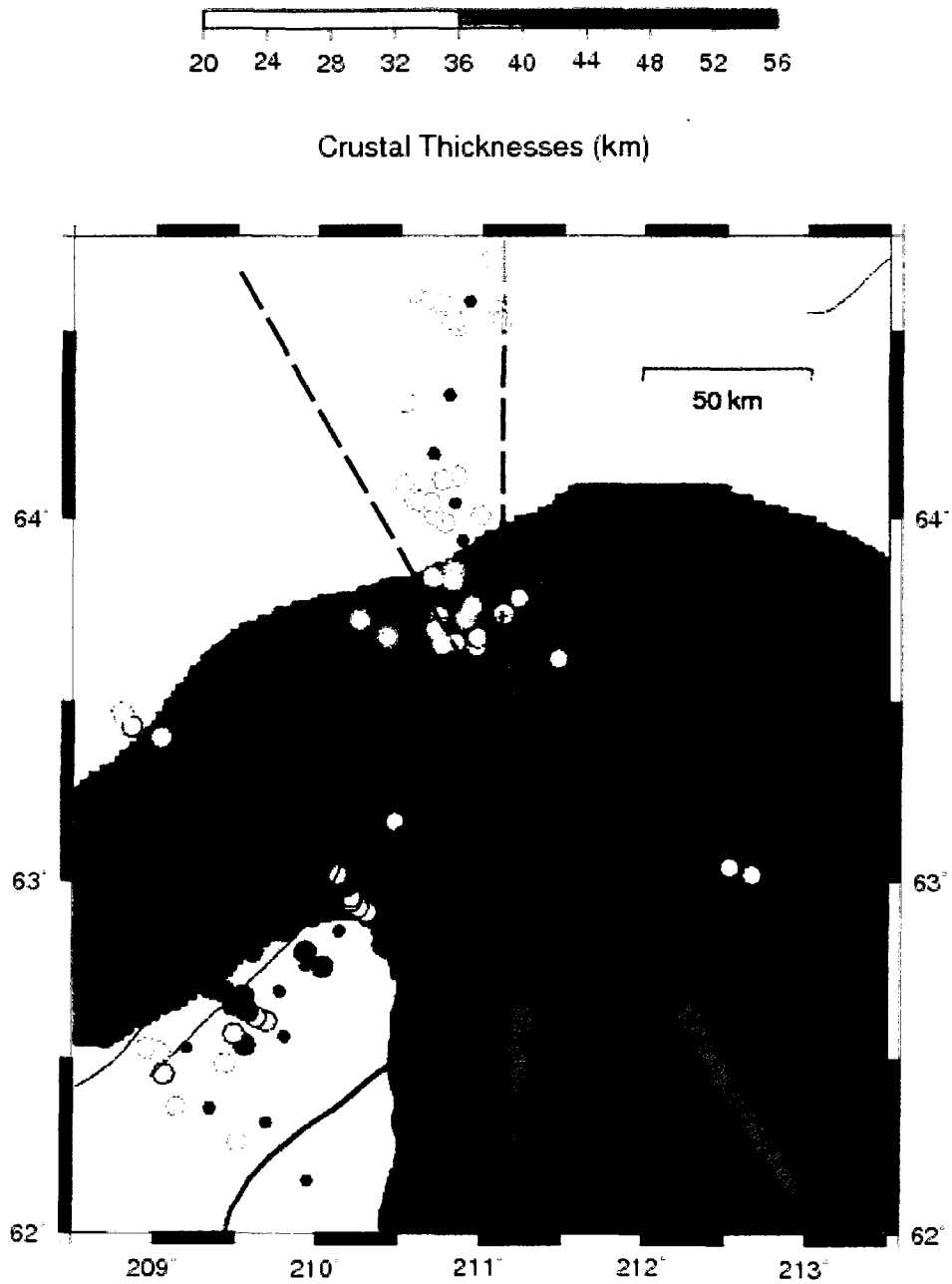

Figure 59: Map view of crustal thickness results plotted with predicted crustal thicknesses. Colored circles are crustal thicknesses determined by modeling receiver functions, plotted on background indicating crustal thickness values predicted from topography by an Airy model. Crustal thicknesses are indicated by shading, lighter shades indicating thinner crust. Notice that the observed crustal thicknesses are consistently shallower than predicted crustal thickness in the north while the observed and predicted crustal thicknesses are fairly consistent in the heart of the Alaska Range.

Table 10: Observed and predicted crustal thickness values at Moho piercing points. Figure 60 is a summary chart of the difference between predicted and observed values of crustal thickness data (plotted in map view in figure 59 and in cross section in figure 61).

Latitude (°N)	Longitude (°E)	observed (km)	predicted (km)
64.690	211.042	25.7	31.8
64.555	211.090	26.1	31.9
64.527	211.119	24.3	31.9
64.513	210.847	26.1	31.9
64.529	210.817	25.4	31.9
64.544	210.768	25.6	31.9
64.573	210.769	25.3	31.9
64.576	210.751	25.3	31.8
64.580	210.609	27.0	31.8
64.580	210.648	26.8	31.8
64.583	210.677	25.9	31.8
64.310	210.527	28.6	32.3
64.112	210.850	23.5	34.4
64.089	210.522	25.7	34.0
64.007	210.991	20.2	35.6
63.987	210.772	22.1	35.3
64.006	210.705	22.7	35.1
64.047	210.584	22.5	34.4
64.044	210.612	22.7	34.4
64.041	210.688	22.6	34.7
64.102	210.759	21.8	34.2
63.855	210.830	24.6	36.4
63.782	211.227	33.2	37.4
63.760	210.940	30.6	37.1
63.781	210.881	29.0	36.9
63.785	210.852	31.0	36.8
63.830	210.827	30.8	36.6
63.838	210.699	29.9	36.4
63.886	211.250	37.6	36.8
63.650	210.969	34.6	37.8
63.726	210.902	26.9	37.3
63.735	210.740	32.5	37.3
63.616	211.469	33.0	38.4
63.575	211.492	33.8	38.4
63.568	211.107	37.7	38.3
63.597	211.001	40.1	38.1
63.662	210.839	34.5	37.8
63.659	210.870	36.1	37.8
63.649	210.911	33.9	37.9
63.675	210.973	33.7	37.7
63.740	211.134	30.2	37.6
63.594	210.843	38.2	38.3
63.515	210.844	36.3	38.3
63.512	210.941	38.0	38.3

Latitude (°N)	Longitude (°E)	observed (km)	predicted (km)
63.567	210.985	35.0	38.3
63.365	211.412	41.2	38.7
63.352	211.463	42.4	38.7
63.334	211.015	33.1	38.9
63.348	210.930	37.8	38.8
63.389	210.903	39.5	38.7
63.416	210.712	38.7	38.8
63.413	210.768	39.2	38.8
63.409	210.817	40.4	38.8
63.476	210.895	40.9	38.4
63.492	211.002	40.9	38.4
63.162	210.554	37.9	38.0
63.252	210.379	40.4	39.1
63.355	210.553	47.0	39.1
63.165	210.476	35.3	38.2
62.920	210.678	36.3	37.2
62.955	210.663	37.9	37.2
62.913	210.305	34.3	36.2
62.928	210.248	34.6	36.2
62.944	210.203	35.2	36.3
62.957	210.203	34.5	36.5
62.988	210.176	37.5	36.7
63.020	209.987	37.3	38.2
63.009	210.046	36.5	37.4
63.013	210.058	38.1	37.4
62.965	210.103	36.2	36.5
63.019	210.123	35.8	37.3
63.060	210.181	35.8	37.7
63.090	210.260	36.2	37.8
63.102	210.315	34.1	37.8
62.922	209.935	40.2	36.5
62.977	210.052	40.0	37.0
62.822	210.407	38.5	36.1
62.760	210.031	39.9	34.9
62.802	209.925	37.7	35.3
62.862	209.806	36.1	36.2
62.950	209.988	37.1	36.7
62.683	209.785	37.8	34.1
62.605	209.684	33.5	33.6
62.615	209.623	35.7	33.7
62.632	209.569	36.9	34.0
62.675	209.543	38.6	34.6
62.697	209.339	39.2	36.1
62.695	209.385	40.2	35.7

Table 10 Observed and predicted crustal thickness values continued

Latitude (°N)	Longitude (°E)	observed (km)	predicted (km)
62.687	209.430	38.9	35.5
62.662	209.450	38.5	34.9
62.651	209.486	38.4	34.6
62.804	209.599	45.8	36.1
62.481	209.690	34.3	32.8
62.536	209.551	39.5	33.3
62.550	209.603	36.7	33.3
62.567	209.489	33.5	33.7
62.260	209.509	26.5	32.3
62.360	209.135	22.5	33.3
62.483	209.432	31.4	33.1
62.454	209.055	34.1	33.9
62.515	209.026	29.7	34.4
62.501	208.965	29.2	34.4
62.539	208.998	27.7	34.8
62.554	208.899	27.5	35.4
62.527	208.948	26.1	34.9
63.298	211.938	41.5	38.4
63.272	211.498	42.7	38.9
63.289	211.431	42.4	38.9
63.310	211.384	42.3	38.8
63.365	211.351	44.4	38.7
63.360	*211.241*	*42.4*	*38.8*
63.384	211.188	41.9	38.8
63.384	211.211	42.6	38.8
63.400	211.279	45.1	38.8
63.471	211.464	46.2	38.3
63.432	212.348	41.1	38.8
63.169	212.458	40.6	38.1
63.192	212.035	32.6	38.2
63.303	211.779	44.8	38.7
63.020	212.665	34.2	37.9
63.041	212.527	34.4	38.0
63.115	212.764	30.7	37.9
63.093	213.141	38.1	38.2
63.197	213.357	29.7	39.2
63.695	210.721	29.3	37.6
63.657	210.756	29.4	37.9
63.677	210.424	22.8	38.0
63.724	210.254	27.2	37.0
63.431	210.182	39.5	39.6
63.383	210.136	42.0	39.8
63.393	209.541	40.8	39.0
63.572	209.272	26.9	36.2
63.398	209.035	28.4	36.6
63.429	208.853	34.8	35.5
63.468	*208.795*	*31.6*	*35.2*

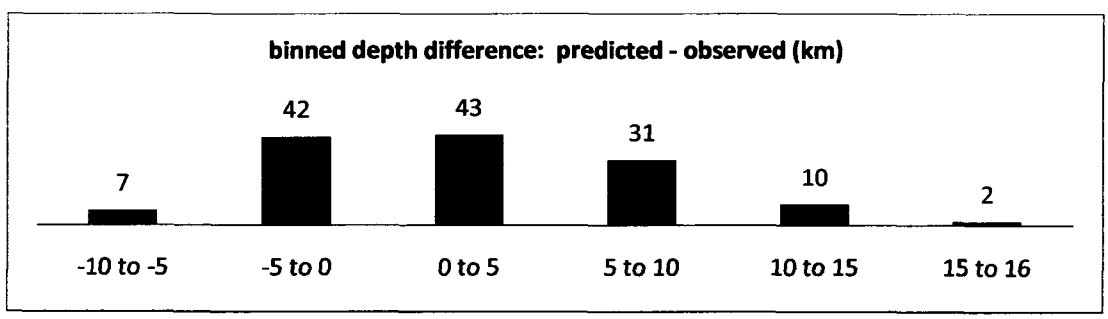

Figure 60: Difference between predicted and observed crustal thickness values. Summary chart of data presented in Table 10, as well as Figures 59 and 61. The number on top of the column indicates the number of modeled points (Table 10) for which the difference between predicted and observed crustal thickness is in the depth range (km) indicated at the base of the column.

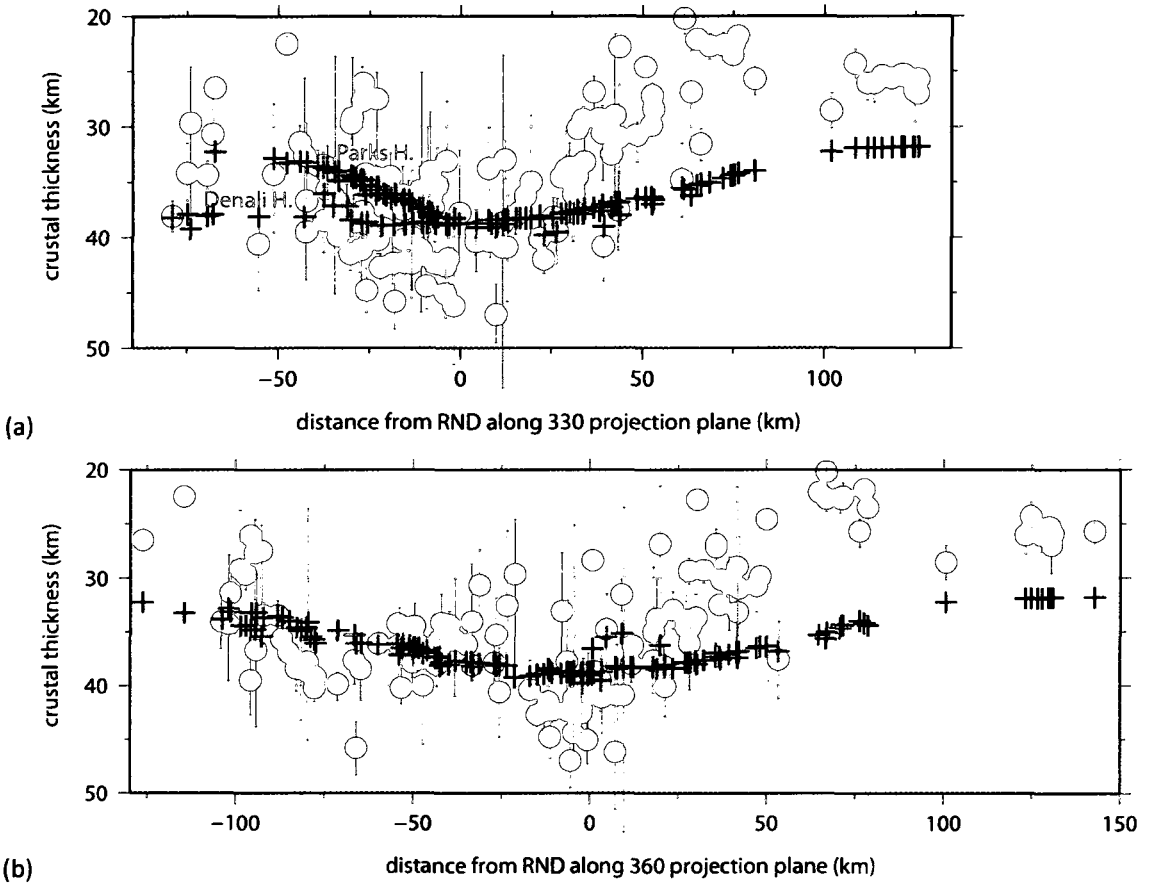

Figure 61: Cross section of observed and predicted crustal thickness values. Dots represent crustal thickness results determined by receiver function analysis; vertical bars indicate 95% confidence interval. Crosses represent crustal thicknesses predicted from topography assuming perfect Airy isostasy with background crustal thickness of 31 km, mean crustal density of 2830 kg m^{-3}, and mantle density of 3300 kg m^{-3}. (a) Predicted and observed crustal thicknesses projected onto vertical plane with azimuth of 330°. The two different trends in the predicted depths are produced due to the projection of "arms" to the south. (Upper arm represents stations along the Parks Highway; lower arm represents stations out the Denali Highway, and a few outliers out Petersville Road.) (b) Crustal thickness results plotted in cross section projected onto N-S plane.

The general similarity between observed crustal thicknesses and those predicted by the isostatic model indicates that the Alaska Range is isostatically compensated by a crustal root (Figure 61 and 62). Although there is scatter and imperfect agreement between observed and predicted crustal thicknesses, the overall picture indicates a crustal root beneath the Alaska Range that is sufficient to support the mountainous topography. In the projection onto a vertical plane oriented with 360° azimuth (Figure 61b) just south of the Denali fault, 0-25 km south of RND, there is a group of observed crustal thicknesses (circles below 40 km) consistently greater than predicted crustal thicknesses (crosses above 40 km). In the same 360° projection, the data farther south, 25-50 km south of RND, are a better match to the

predicted data, with some observed data points slightly shallower than predicted, in contrast to those just mentioned. In the 330° projection (Figure 62a) some of the group greater than 40 km thickness are located farther south along the projection plane, and we see that Parks Highway data diverge from Denali Highway data such that most of the deeper data are associated with the Denali Highway "arm" (c.f. Figure 59). Overall, the central Alaska Range crustal thickness data reveal sufficient crustal root to support the topography as described by Airy type isostasy.

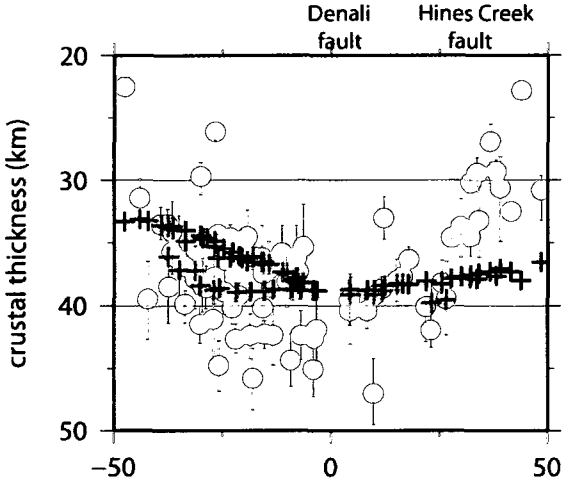

Figure 62: Central Alaska Range crustal thickness data in cross section. Cross sectional plot of central Alaska Range crustal thickness results (95% confidence interval < 7.0 km) projected onto (a) 330° and (b) 360° projection planes. Dots are crustal thickness results determined by receiver function analysis, crosses are crustal thicknesses predicted from topography assuming perfect Airy isostasy with mean crustal density of 2830 kg m^{-3} and background crustal thickness of 31 km.

Anomalously thin crust and the Yukon-Tanana terrane

Crustal thickness estimates vary largely within an overall pattern of thin crust to the north and thick crust beneath the mountains; variations are concentrated at the transitions between lowlands and mountains (Figure 59). Beneath the Alaska Range, observed crustal thicknesses are comparable to those predicted by the isostatic model, while beneath the northern foothills and lowlands the crust is thinner than initially predicted from topography (Figure 61). Observations indicate a transition from thick to thin crust near station MCK, which coincides with the surface location of the Hines Creek fault (Figure 62).

Beneath the northern foothills and lowlands, the crust is thinner than predicted by our simple isostatic model (Figure 61), suggesting that a simple Airy model alone is inadequate. The disparity between thick crust beneath the mountains and thin crust to the north suggests a fundamental change in material properties or mode of compensation. If, as required in a strict Airy model, the real crustal material is uniform across this disparity between thick crust beneath the mountains and thin crust to the north, then the northern lowlands are not in isostatic balance. The average crust in our model had a background crustal thickness of 31 km, a crustal density of 2830 kg m^{-3} and mantle density of 3300 kg m^{-3}. Simple Airy isostasy suggests that, for example, beneath a 3 km high mountain in isostatic equilibrium, a crustal root would form that is 19 km deeper than the 31 km thick average or background crust, and beneath low-lying areas in equilibrium with topography near sea level the crust would be 31 km thick (Figure 63). Observed crustal thicknesses beneath the northern lowlands are less than 31 km, suggesting that the area is undercompensated and should subside to reach isostatic equilibrium. The isostatic gravity map of Alaska (Barnes et al., 1994) suggests that the crust is, however, in isostatic equilibrium, so the crust beneath this area must be compensated by other means. An area in isostatic equilibrium might be compensated by crustal or mantle density variations. If we assume mean crustal density beneath the northern lowlands of 2700 kg m^{-3} (c.f. TACT results e.g. Brocher et al., 1991, 2004), then predicted crustal thicknesses are much closer to our observed values. A 26 km thick section of light 2700 kg m^{-3} crust isostatically balances the 'excess density' of the 3300 kg m^{-3} mantle (Figure 63). Although lateral density variations are not allowed in an ideal Airy model, incorporating Pratt style lateral density variations with an average crustal density of 2700 kg m^{-3} to the north and an average crustal density of 2830 kg m^{-3} to the south would explain the data (Figure 64).

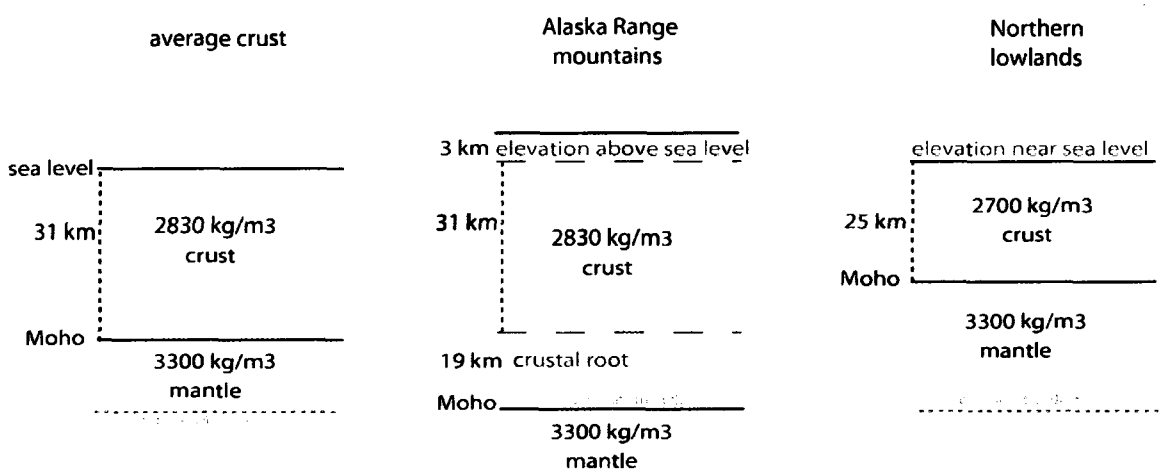

Figure 63: Airy isostatic model. Given background crustal thickness of 31 km, a crustal density of 2830 kg m^{-3} and mantle density of 3300 kg m^{-3}, a topographic feature 3 km above sea level would be isostatically balanced by a 19 km crustal root for 50 km deep Moho, similar to Alaska Range mountains column. Given this same crust (2830 kg m^{-3}) over mantle (3300 kg m^{-3}), a low-lying area at equilibrium would have no crustal root, i.e. a 31 km deep Moho. The northern foothills and lowlands are thought to be in isostatic equilibrium, so the shallow Moho observed with BEAAR receiver functions, similar to Northern lowlands column, is most likely due to less dense crust balancing mantle.

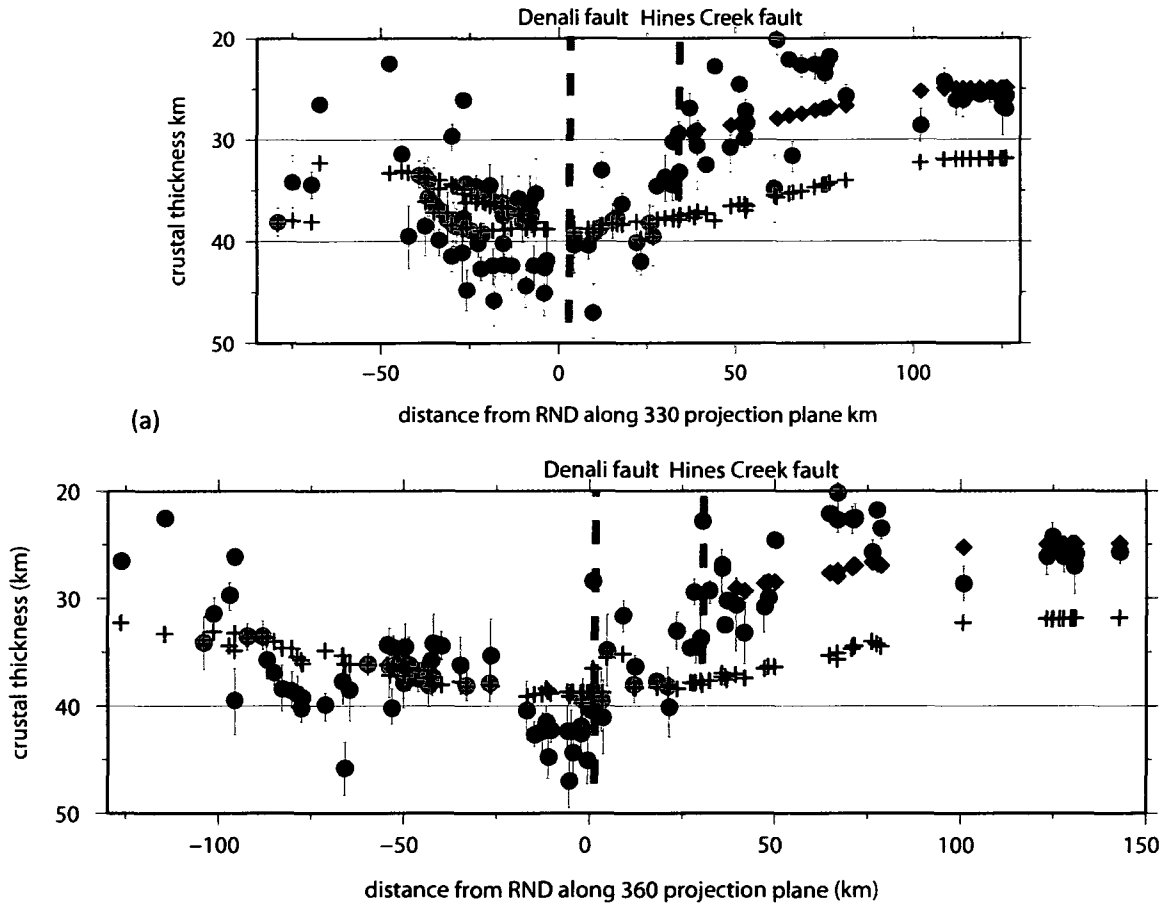

Figure 64: Cross section with crustal thicknesses predicted from different densities. BEAAR crustal thickness results (restricted total error at 95% confidence) plotted in cross section projected onto plane with projection azimuth (a) 330° and (b) 360°. Dots represent crustal thickness results determined by receiver function analysis, crosses are crustal thicknesses predicted from topography assuming perfect Airy isostasy with mean crustal density of 2830 kg m^{-3} and background crustal thickness of 31 km, diamonds are crustal thicknesses of northern data predicted from topography assuming perfect Airy isostasy with mean crustal density of 2700 kg m^{-3}. The crustal thicknesses predicted using mean crustal density of 2700 kg m^{-3} for stations in the north are much closer to observed crustal thicknesses determined from receiver function analysis. To the south predicted (2830 kg m^{-3}) and observed crustal thicknesses are in reasonably good agreement, with some data above and some below predicted. Those differences may be suggestive of minor geophysical differences between accreted terranes.

This Pratt style lateral crustal density contrast seems reasonable given the potential for geophysical disparities between terranes across a major accretionary boundary. Density is a fundamental property that varies for different earth materials, as empirical relationships such as the Nafe-Drake curve (relating density and P wave velocity) describe (Ludwig et al., 1970). Geophysics suggests a lithologic contrast between the rocks north of the Hines Creek fault and rocks to the south (Brocher et al., 1991,

2004). Observed lithologies also suggest differences across this boundary. To the north is the Yukon-Tanana composite terrane, generalized as metamorphosed continental margin (Churkin et al., 1982; Foster et al., 1973, 1987, 1994; Nokleberg and Aleinikoff, 1985; Nokleberg et al., 1989). To the south is dominantly Kahiltna terrane, generalized as a deep marine basinal terrane (Reed and Nelson, 1980; Csejtey et al., 1986; Nokleberg et al., 1982, 1992b; Wallace et al., 1989) and Wrangellia, generalized as a terrane of evolved arc affinity (Jones et al., 1977, 1981, 1987; Nokleberg et al., 1982, 1985, 1992b; Plafker et al., 1989; Richter, 1976; Richter et al., 1977) (Figure 5).

In general, the continental margin affinity terranes north of the Hines Creek fault appear to be composed of more felsic meta-sedimentary and meta-igneous rocks, less dense than the intermediate to mafic volcanic and sedimentary rocks associated with the arc and deep marine affinity terranes south of the Hines Creek fault. The TACT program investigated the structure and composition of the Alaskan crust; Beaudoin et al. (1992, 1994) reported a silicic composition of the majority of the Yukon-Tanana terrane crust. The southern Yukon-Tanana terrane consists of a highly deformed and regionally metamorphosed sequence of largely Devonian metasedimentary and metavolcanic rocks and Mississippian metagranitic rocks (Aleinikoff and Nokleberg, 1985; Nokleberg and Aleinikoff, 1985; Foster et al., 1987; Jones et al., 1987; Nokleberg et al., 1989). The northern Yukon-Tanana terrane consists of two highly deformed and regionally metamorphosed sequences: early Paleozoic(?) and Late Proterozoic and older metasedimentary rocks, and Devonian and older metasedimentary rocks with metavolcanic lenses and abundant Mississippian metagranitic plutons and some Late Cretaceous to early Tertiary granitic plutons (Weber et al., 1978; Foster et al., 1987; Nokleberg et al., 1989). Laboratory measurements of rock samples from a section along the TACT line corresponding to Yukon-Tanana terrane revealed densities in the range 2633-2761 kg m^{-3}, with an average of 2701 kg m^{-3}. Samples taken from an area north of TACT line but corresponding to the Yukon-Tanana terrane revealed densities in the range 2615-2768 kg m^{-3}, with an average of 2651 kg m^{-3} (Brocher et al., 1991, 2004). TACT samples taken from an area dominated by Wrangellia terrane revealed densities in the range 2587-3088 kg m^{-3}, with an average of 2864 kg m^{-3} (Brocher et al., 1991, 2004). Samples taken from an area corresponding to Kahiltna terrane revealed densities in the range 2765-2960 kg m^{-3} with an average of 2834 kg m^{-3} (N. Christensen 2003 unpublished data cited by Brocher et al., 2004). Two groups of TACT data yield average crustal densities of 2651 kg m^{-3} and 2701 kg m^{-3} in the Yukon-Tanana terrane, similar to the 2700 kg m^{-3} required to model crustal thickness of an isostatically compensated crust north of the Hines Creek fault. TACT data reveal an average crustal density of 2864 kg m^{-3} in the rocks to the south, similar to the 2830 kg m^{-3} used to model crustal thickness of an isostatically compensated crust south of the Hines Creek fault.

The similarity between predicted crustal thicknesses and observed crustal thicknesses suggests that compensation occurs in the crust rather than the underlying mantle, an interpretation consistent with subcrustal studies in the region. Seismic attenuation studies use attenuation as a proxy for upper mantle temperature structure, but there is no correlation between our observed compensation boundary and the variation in attenuation (Stachnik et al., 2004) which occurs 30-50 km to the southeast. The subducting slab edge might produce subcrustal density variations, but the slab appears to extend well north of our observed boundary (Ferris et al., 2003; Abers et al., 2006). If the northern lowlands are in isostatic equilibrium, then there must be a change in material properties near the Hines Creek fault. It seems reasonable to expect some difference in material properties across a suture between metamorphosed continental rocks and deep marine and arc affinity rocks. A crustal density contrast across the Hines Creek fault, 2700 kg m^{-3} to the north and 2830 kg m^{-3} to the south, accounts for the difference between the crustal thicknesses predicted by simple Airy isostasy, and the crustal thicknesses determined by receiver function analysis (Figure 65). These data suggest the Alaska Range is held up via Airy type isostasy with Pratt style isostasy describing a lateral density variation across a major fault boundary.

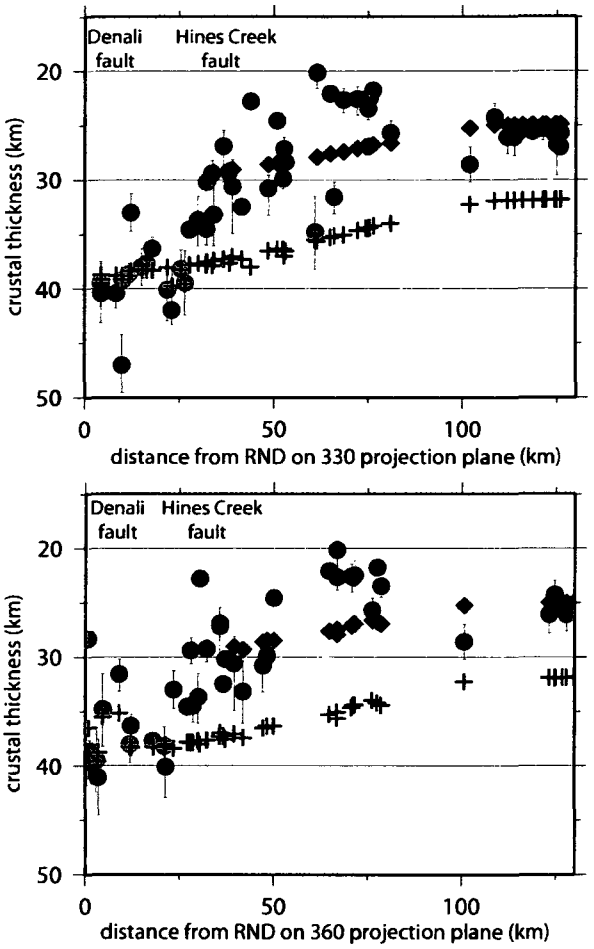

Figure 65: Northern crustal thickness data in cross section. Dots are crustal thickness results from RND north, determined by receiver function analysis, crosses are crustal thicknesses of northern data predicted from topography assuming perfect Airy isostasy with mean crustal density of 2830 kg m^{-3} and background crustal thickness of 31 km, diamonds are crustal thicknesses of northern data predicted from topography assuming perfect Airy isostasy with mean crustal density of 2700 kg m^{-3}. Diamonds fit northern data better than crosses, consistent with density contrast across Hines Creek fault.

Relationship between surface faults and Moho depth

Much of the scatter in Figures 61 and 64 is due to the projection of data points over a large distance (hence across surface faults) to the projection plane. Comparison between the 330° and 360° projections illustrates how changes in the projection angle change the cross sectional distribution. To further investigate the relationship between crustal thicknesses and surface faults, the data are plotted taking into account the curvature of the Alaska Range. Stout and Chase (1980) fit a small circle to the Denali fault with a rotational pole at 59.6°N, 147.4°W (small circle radius 433 km, standard deviation 1.73 km). The curvature of the Alaska Range generally mimics the curvature of the Denali fault, so plotting crustal thickness data with respect to this Euler pole minimizes far field projection problems near the fault

(Figure 66). When plotted using the small circle projection, data scatter in the central Alaska Range is minimized and features that were otherwise obscured become visible. One feature which becomes much clearer is the change from deep Moho in the south to shallower Moho in the north. The linear style projection in Figures 61 and 64 shows that change coincides with the location of the Hines Creek fault, but with a lot of scatter. With the small circle style projection in Figure 66, the change in depth appears better defined with cleaner distribution. First, there appears to be a broadly linear trend in crustal thickness from deepest values south of the Denali fault to shallow values north of the Hines Creek fault. Within that general linear trend there appear to be steps or areas with generally constant depth. Central Alaska Range crustal thickness results plotted in cross section focusing on data from 20 km south of the Denali fault to 50 km north of the Denali fault are shown in Figure 67. The Hines Creek fault has tighter curvature than the Denali fault, so the Hines Creek fault plots between 458 km and 463 km from the Euler pole given the lateral distribution of crustal thickness data points. From the Denali fault twenty kilometers south, average crustal thickness is 42.7 km; between the Denali fault and the Hines Creek fault average crustal thickness is 36.0 km; average crustal thickness from Hines Creek fault twenty kilometers north is 29.6 km. These data are consistent with these major strike-slip faults extending to the base of the crust.

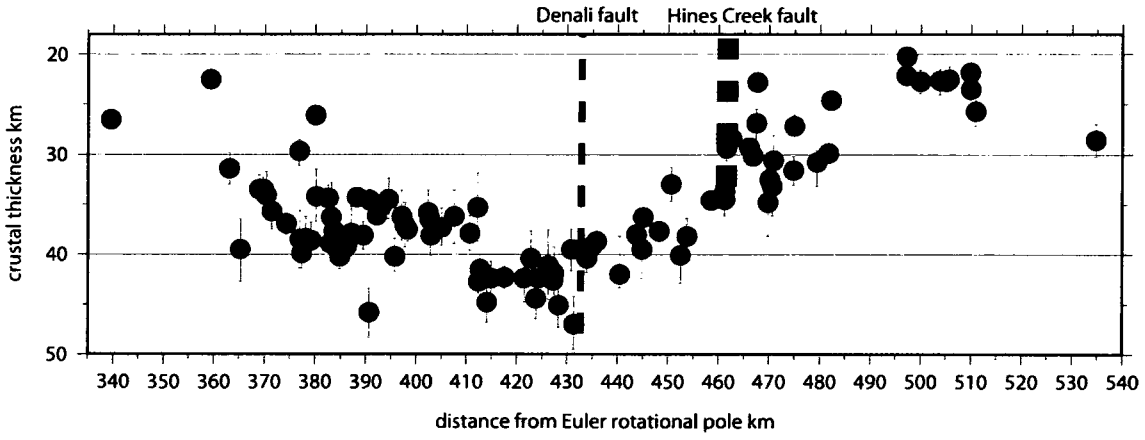

Figure 66: Cross section of crustal thicknesses plotted with respect to Euler rotational pole for Denali fault. BEAAR crustal thickness data plotted in cross section using projection that takes into account the curvature of the Alaska Range by calculating the great circle distance between the Euler rotational pole and crustal thickness data point. In the 360° projections (e.g. Figure 62b or 64b) the shallow WON data is projected east into the heart of the Alaska Range, but in this projection they plot more appropriately with foothills.

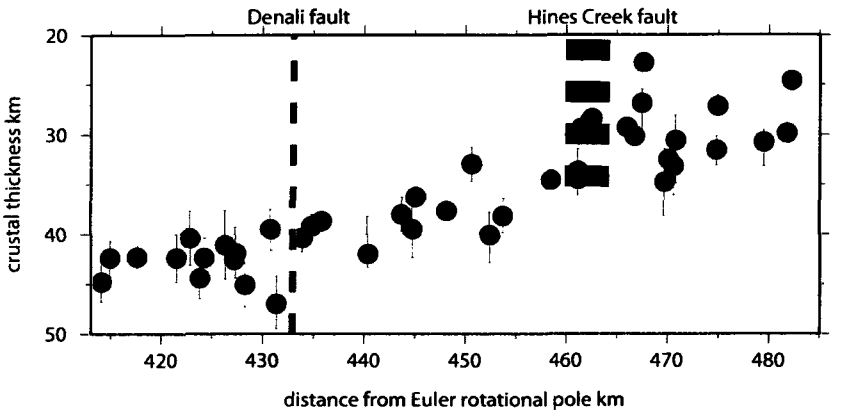

Figure 67: Cross section of crustal thicknesses with focus on faults. BEAAR crustal thickness data plotted using Euler rotational pole defined by curvature of the Denali fault in the central Alaska Range (Stout and Chase, 1990). Since the Euler pole is defined by the shape of Denali fault, the projection is most useful near this structure. The change in crustal thickness might be summarized as a 6 km step in average crustal thickness across both the Denali fault and the Hines Creek fault.

The broadly linear trend in crustal thickness, from deepest values south of the Denali fault to shallow values north of the Hines Creek fault, describes gradual northward decrease in crustal thickness. This trend changes to a more constant thickness beneath the northern stations (Figure 66). The change to a more constant thickness beneath the flatlying lowlands in the north roughly coincides with the northern edge of the northern foothills fold-and-thrust belt (Bemis and Wallace, 2007; Lesh and Ridgway, 2007). The deepest Moho occurs beneath the mountains, with stepwise change in crustal thickness across major structures that traverse the crust, gradually decreasing across the range with this broadly linear trend, including the foothills, approaching an equilibrium or background crustal thickness beneath the Tanana lowland.

Another potentially significant feature worth mention is the change in crustal thickness values roughly 25 km south of RND in the 360° projections (e.g. Figure 64b), near 410 km from Euler rotational pole for Denali fault (Figure 66). The step from deep values near RND and the Denali fault to shallower values farther south coincides with the Broad Pass fault. This step may be an artifact of projecting unevenly (geographically) distributed data onto a plane, or it may represent structural influence on crustal thickness. Figure 59 shows the crustal thickness data in map view; the 360° projection plane is indicated by a dashed line. The step occurs at ~63.22°N. Even if this step results from structural influence in the Alaska Range, not enough is known about the various southwest striking faults south of the Denali fault to asses the reverse vs. strike-slip components of displacement or the extent to which thickness changes across these faults might be inherited from the terranes they cut vs. structural thickening in place.

The Denali fault is one of the most obvious structural features in the Alaska Range. While the presently active strand probably is not the original emplacement fault, a variety of significantly different terranes are juxtaposed across the Denali fault. The Hines Creek fault is a zone of intense shearing interpreted to be a terrane boundary by Wahrhaftig et al. (1975) and Csejtey et al. (1982), but has also been interpreted as a separate younger structure mainly within the southern Yukon-Tanana terrane (Nokleberg et al., 1989, 1992). Our crustal thickness data support the interpretation of both the Denali fault and the Hines Creek fault as major structures that traverse the crust and offset the Moho.

Comparison of Moho depths with other studies of south central Alaska

The crustal thickness results reported here are in accord with other crustal thicknesses reported in the region since the BEAAR deployment. TACT results for the eastern Alaska Range, roughly 150-200 km east, indicate 22 km Moho relief between the northern lowlands and the eastern Alaska Range (Brocher et al., 2004). Brocher et al. (2004) provided evidence for 50 km thick crust near the Denali fault in the eastern Alaska Range. Ai et al. (2005) examined BEAAR waveform data, reporting 24 crustal thicknesses ranging from 26.0 km in the lowlands to 42.6 km in the mountains, results similar to my earlier studies of BEAAR data (Meyers et al., 2000, 2001, 2002). The Moho depths reported by others provide additional evidence for the large (20 km) variation in crustal thickness across the Denali and Hines Creek faults.

A recent tomographic study by Eberhart-Phillips et al. (2006) generally supported these large changes across the Denali and Hines Creek faults. They reported that the accreted terranes south of the Denali fault exhibit differences in velocity among themselves and are different from terranes north of the Denali fault: the accreted terranes exhibit slightly higher crustal V_p than the para-autochthonous terranes of North American continental affinity.

The Eberhart-Phillips et al. (2006) tomography results do not directly constrain Moho depths. However, isovelocity plots of 7.5 km/s and/or 7.8 km/s (presented in their paper) may serve as a proxy for Moho. Many of the features seen in BEAAR data are recognizable in the 7.5 km/s and 7.8 km/s isovelocity plots. The isovelocity contours are deeper under the Alaska Range and shallow significantly north of the range. For comparison, I have superimposed BEAAR crustal thickness data points on Eberhart-Phillips et al. (2006) depth contoured 7.5 km/s and 7.8 km/s isovelocity data (Figures 68 and 69). The dark areas in the southeast corner are not Moho depths, but likely represent velocities in the subducting slab (although the dark area on the 7.5 km/s plot is reminiscent of the enigmatic eastern edge of the Aleutian Wadati-Benioff zone). The difference between BEAAR Moho and 7.5 km/s isovelocity depth was calculated at each data point and results were grouped for comparison. BEAAR results are generally shallower: the difference range in depths is from -6 km to 31.9 km, with median difference of 3.9 km and an average

difference of 5.5 km. The extreme difference between isovelocity depth and BEAAR Moho occurs in the deepest region of the isovelocity plot which is influenced by subducting slab. Similarly, the difference between BEAAR Moho and 7.8 km/s isovelocity depth was calculated at each data point and grouped for comparison. BEAAR results are again generally shallower: the range of differences extends from -1.8 km to 40.7 km, with a median difference of 8.5 km and an average difference of 10.4 km. Again, the extreme differences between isovelocity depth and BEAAR Moho depth occur in the deepest region of the isovelocity plot where isovelocity is influenced by the subducting slab and is not a good proxy for Moho. These comparisons suggests the 7.5 km/s isovelocity depth is in better agreement with BEAAR crustal thickness data than the 7.8 km/s isovelocity depth data.

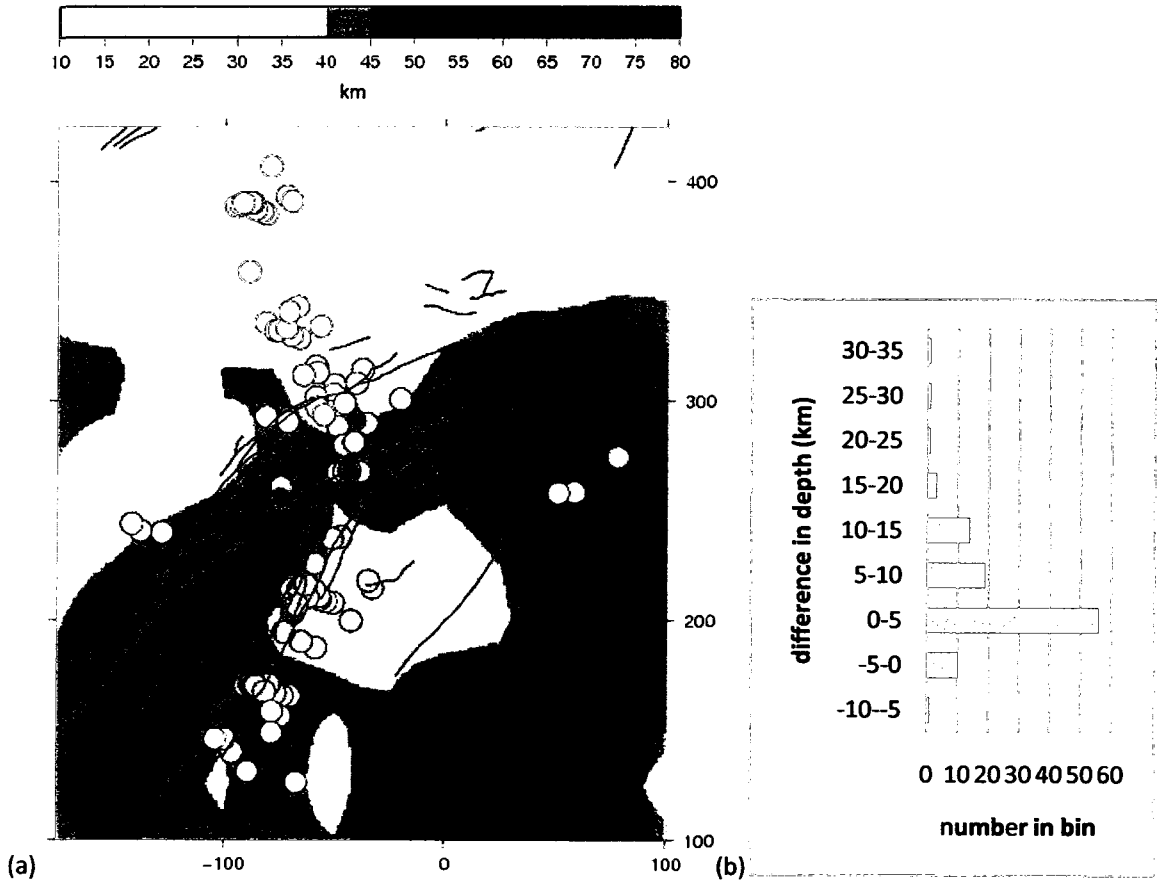

Figure 68: Crustal thickness results plotted with 7.5 km/s isovelocity depth data. Eberhart-Phillips et al. (2006) contoured 7.5 km/s isovelocity depth plot might be considered a proxy for Moho. (a) The isovelocity depth data (km) are plotted with BEAAR crustal thickness data (circles) for a visual comparison. (BEAAR data and fault locations converted from latitude/longitude to xy coordinates.) (b) Comparison between BEAAR Moho depth and 7.5 km/s isovelocity depth points: most are within 5 km.

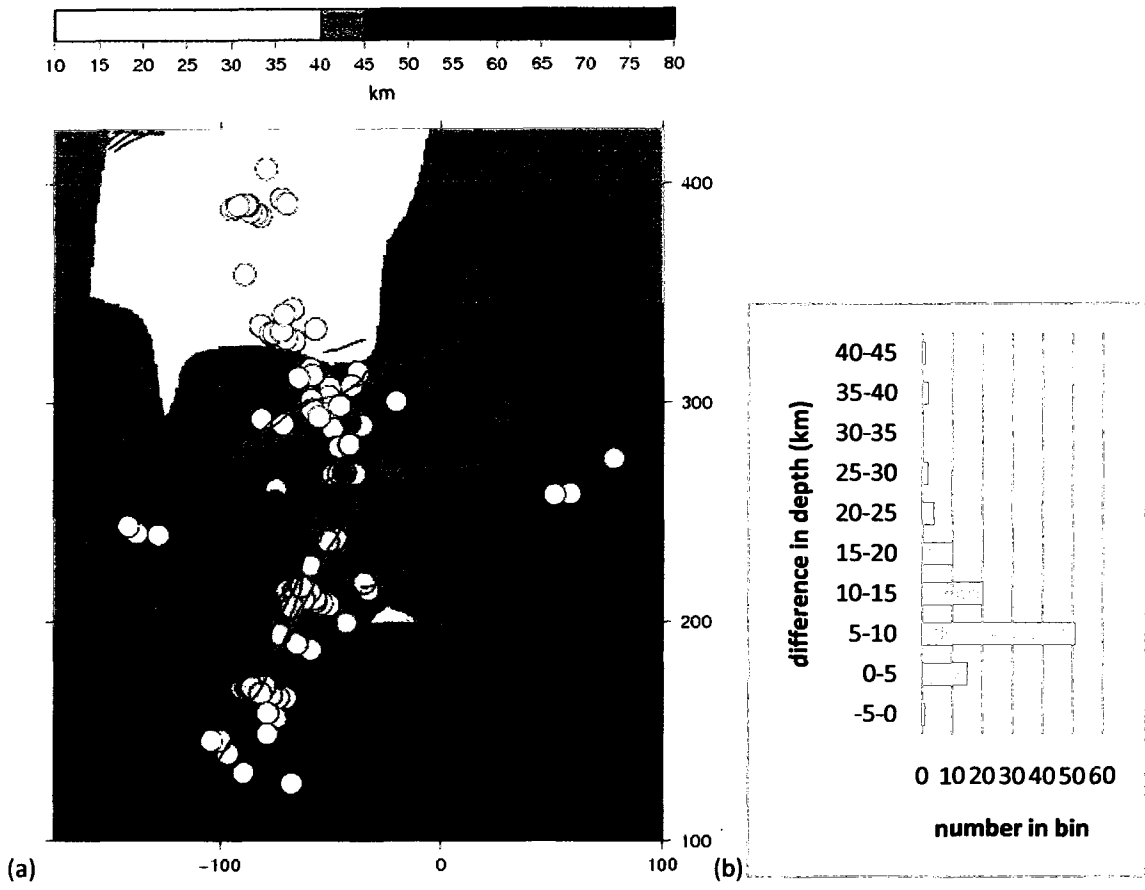

Figure 69: Crustal thickness results plotted with 7.8 km/s isovelocity depth data. Eberhart-Phillips et al. (2006) depth contoured plot of 7.8 km/s isovelocity may be considered a proxy for Moho. (a) The 7.8 km/s isovelocity depth plotted with BEAAR crustal thickness data (circles) for visual comparison. (b) Comparison between BEAAR Moho depth and 7.8 km/s isovelocity depth indicates the 7.5 km/s isovelocity data is in better agreement with BEAAR crustal thickness data.

The Bouguer Gravity Anomaly Map of North America (Committee for the Gravity Anomaly Map of North America, 1987) (Figure 70) provides another useful data set with which to compare our crustal thickness data. Gravity anomalies are associated with inhomogeneities in density distribution such as those produced by significant variations in subsurface structure, like a crustal root zone beneath a mountain range. A strong negative gravity anomaly across a mountain chain would be expected with a crustal root zone representing a large low density mass displacing higher density mantle material. The Bouguer anomaly displays a roughly inverse relationship with crustal thickness and topographic elevation (Robinson and Çoruh, 1988). The gravity map (Figure 70a) shows, in general, little to no anomaly beneath our northern flatland stations and a strong anomaly beneath the mountains of the Alaska Range. This strong anomaly follows the trend of Alaska Range topography. The Bouguer gravity lows correlate with very high topography: Mount McKinley to the west, Deborah, Hess, and Hayes to the east, mountains

that represent significantly higher topography than neighboring parts of the range. To the first order, a stronger gravity anomaly is associated with thicker crust. To visually compare the pattern of gravity data with our crustal thickness data, Figure 70b shows the BEAAR observed and predicted crustal thickness plot next to the gravity anomaly map. Comparison of crustal thickness predicted from topography with the gravity anomaly suggests differences beneath the high mountains (Mount McKinley area, and Deborah – Hayes area), as well as lowlands of the Coastal Trough (including Copper River basin area and the Susitna lowland in the southwest corner of our map immediately west of the 50 km Wadati-Benioff zone contour). The gravity low beneath the Susitna lowland in the southwest corner of the map is the main area of difference between BEAAR crustal thickness and the first order expectation of no anomaly beneath unthickened crust, which may reflect density variations associated with the Susitna Basin. It is also interesting to note that topography does not predict a Moho as deep as we observe in the RND/DH1 area (south of the Denali fault, west of the Susitna Glacier fault); there is a large negative gravity anomaly in the area, consistent with our Moho depth estimate. Visual observation suggest that despite second order, minor differences, there is a first order, general agreement between the pattern of BEAAR crustal thickness data and the gravity anomaly data.

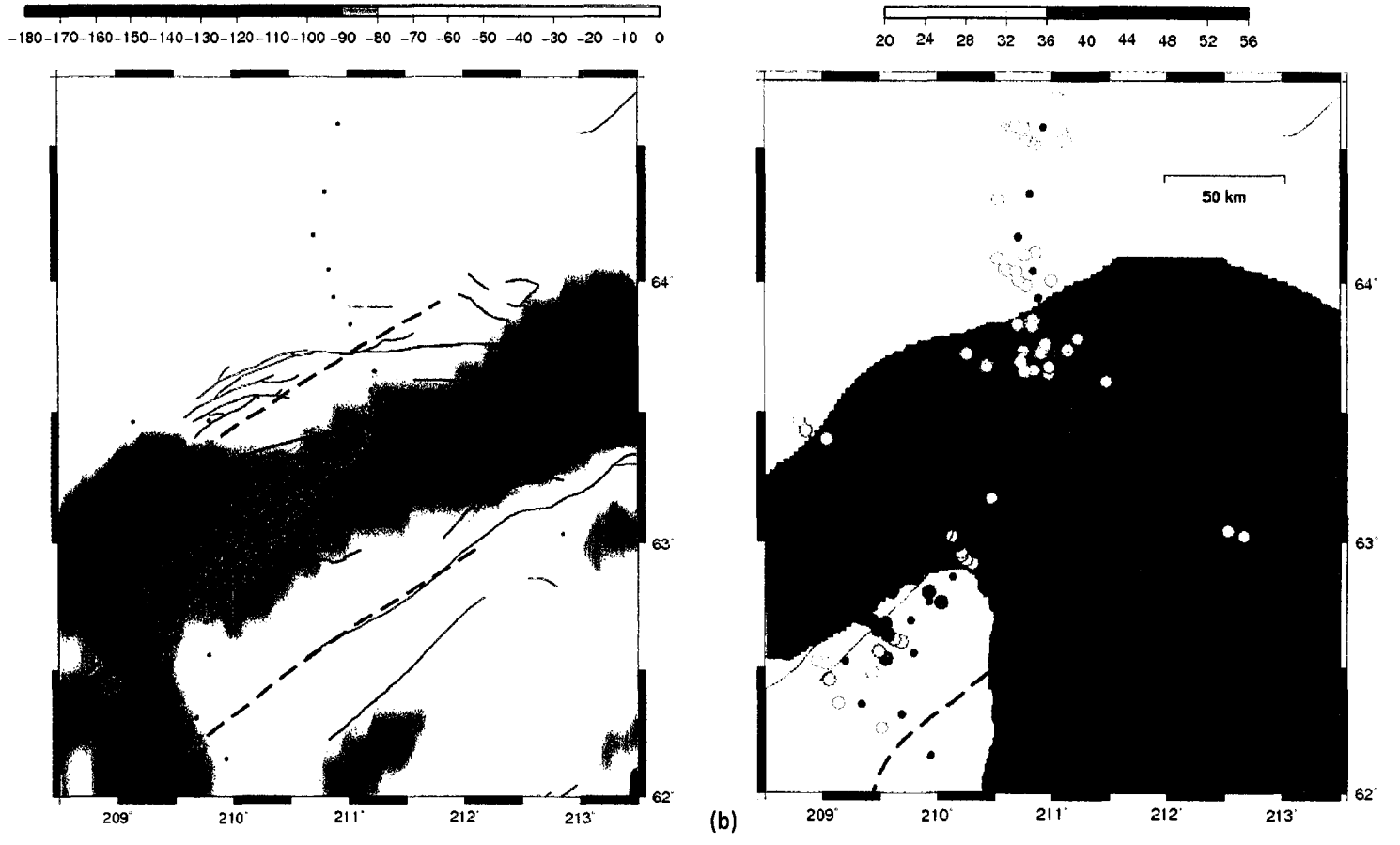

Figure 70: Gravity data from 6 km grid Gravity Anomaly Map. (a) BEAAR stations (dots), Wadati-Benioff zone isopleths (dashed lines), and surface faults plotted with gravity data (in 10 mgal) from 6 km grid file of Gravity Anomaly Map of North America (Committee for the Gravity Anomaly Map of North America, 1987). (b) Observed and predicted BEAAR crustal thickness data (km).

Chapter 7 - Conclusions and Tectonic Implications

The BEAAR project was a massive undertaking: deploying and servicing dozens of widely spaced, often malfunctioning, seismic stations to continuously record seismicity over a period of 27 months, through two interior Alaskan winters. There were many challenges in the field and in the lab. BEAAR receiver function analyses provided insight into crustal scale structure beneath the Alaska Range, which allowed consideration of the relationship between structural geometry and the evolution of the orogen and suggesting how the topography is sustained.

Crustal thicknesses across the central Alaska Range suggest that these mountains are supported by a thickened crustal root, rather than by dynamic forces acting on the base of the crust. Receiver function analysis revealed a thickened crust beneath the central Alaska Range. Calculations indicate this crustal root is sufficient to isostatically support the topography. Sub-crustal studies in the region support the interpretation that compensation occurs in the crust rather than the underlying mantle.

Receiver function analysis of teleseismic waveforms recorded by BEAAR three-component broadband seismometers provided over 100 crustal thickness data points. The data reveal a thin (26 km) crust beneath the southern Yukon-Tanana terrane, and a crustal root beneath the central Alaska Range extending to 47 km (Figure 71). The observed crustal root is sufficient to support the Alaska Range via Airy isostasy and likely formed during orogenesis. Crustal thickness data further suggest differences in terrane thickness: a thin Yukon-Tanana terrane north of the Hines Creek fault and thicker Kahiltna/Wrangellia terranes to the south. Finally, the pattern of thin crust to the north and thicker crust to the south appears to be modified by Late Cenozoic structures such as the Denali fault, with contractional thickening in the Alaska Range, perhaps even including areas north of the Hines Creek fault in the northern foothills fold and thrust belt. BEAAR crustal thickness data suggest that major faults extend to the base of the crust.

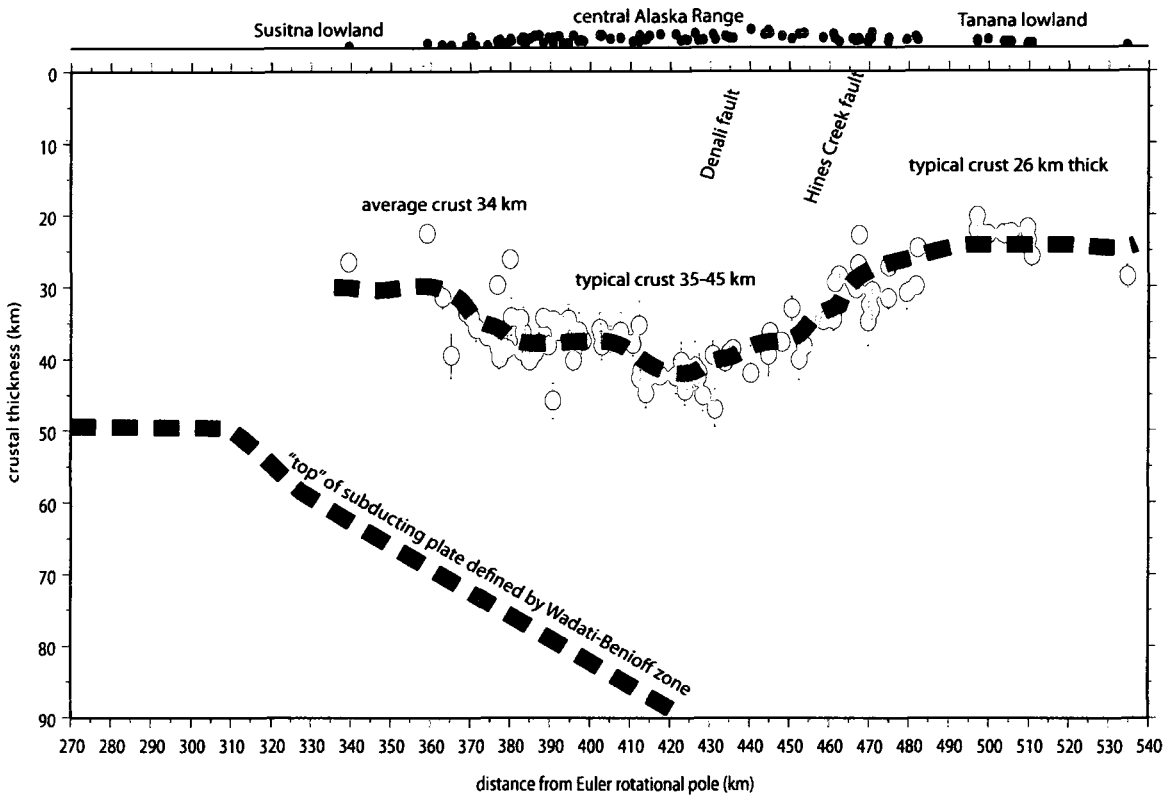

Figure 71: Tectonic cartoon incorporating crustal thickness results. Topographic and crustal thickness data are plotted with respect to the Stout and Chase (1980) Euler pole determined from curvature of the Denali fault in the central Alaska Range. Topography above each piercing point illustrates general increase in elevation across the range. BEAAR instruments were deployed along the road system, generally constructed along river valleys, so with projection taking curvature of the range into account we expect varied elevations at any given distance. The slab, located by the Wadati-Benioff zone seismicity, is portrayed as on a 330° projection plane (roughly parallel plate convergence vector) where slab depth is constant along strike. Yakutat crust may be part of the ~15 km thick slab imaged to 130 km depth beneath the Alaska Range (Ferris et al., 2003; Eberhart-Phillips et al., 2006; Rossi et al., 2006). The overriding plate crustal Moho disappears to the south (e.g. beneath TLKY) where subducting Pacific crust plus mafic Yakutat crust likely underplates Chugach and Prince William terranes.

We observe thin crust beneath the southern Yukon-Tanana composite terrane. The best fit background crustal thickness north of the Denali/Hines Creek fault region is 26 km, while the best fit background crustal thickness to the south is 33 km. Thicker crust is observed south of the Denali/Hines Creek fault region beneath an area dominated by Kahiltna and Wrangellia terranes. Differences in terrane thickness may be original, or thinned crust may have been produced by mid-Cretaceous tectonic extension of the Yukon-Tanana terrane (Pavlis et al., 1993).

An extended region could be undercompensated and subsiding. One might argue that subsiding crust of constant density would be thinner than an isostatically balanced background crust. The isostatic gravity map of Alaska (Barnes et al., 1994) is, however, interpreted to indicate that the northern foothills

and lowlands immediately north of the Alaska Range are in isostatic equilibrium, not subsiding. Accepting that the northern foothills and lowlands are in equilibrium, not subsiding, the similarity between predicted and observed crustal thicknesses support the interpretation that support of the Alaska Range can be approximated by Airy type isostasy with Pratt style isostasy describing a lateral density variation. BEAAR receiver function analysis results indicate that variations in both crustal thickness and density are required to explain the seismic and gravity data in south-central Alaska.

Global comparisons

Deformation hundreds of kilometers inboard of the plate boundary is associated with flat slab subduction (Bird, 1984). The flat slab subduction zone geometry beneath south central Alaska is well defined by Wadati-Benioff zone seismicity (Figure 2). The subducting slab has been imaged 600 km inboard of the Aleutian trench to 130 km depth beneath the Alaska Range (Ferris et al., 2003; Rossi et al., 2006). The distance between the trench and arc volcanoes in southern Alaska illustrates the increase in trench-volcano distance in areas of shallower subduction (Figure 4). Shallow subduction beneath south central Alaska might be compared to shallow subduction beneath portions of the South American Andes. The Andes form along the western margin of South America where oceanic crust subducts beneath continental crust along the Peru-Chile Trench. There is an active volcanic arc beneath more steeply dipping ($\geq 30^{\circ}$) segments of the subduction zone, and an active fold and thrust belt inboard of the mountain chain (e.g. Okaya et al., 1997; Beck and Zandt, 2002; Gilbert et al., 2006).

In Alaska, the subduction dip for the portion of the Pacific plate less than 50 km deep changes gradually from steep in the central Aleutians to shallow beneath south central Alaska (Davies, 1975; Carver and Plafker, 2008). The dip of the subducted plate for the portion deeper than 50 km, and its spatial relationship to the arc front, remain nearly constant along the strike of the arc until about 212°E (Figure 4). Thus the geometry of the sublithospheric subduction system in Alaska remains nearly constant, even though active volcanoes are absent in the gap between Spurr (~208°E) and the "edge" of the Wadati-Benioff zone at ~212°E. This geometry is different than that in the Andes, where the shallowly dipping portions of the slab extend beneath, and eastward of, the projection of the volcanic front from the adjacent "normal geometry" zones. Although geometries differ, the magmatic gaps coincide with gently dipping segments of the subduction zone. Volcano free segments in the Andes may be explained by absence of a fertile asthenospheric wedge between the subducted slab and overriding plate, but it is not yet clear whether that is the case in Alaska. Attenuation studies confirm the presence of an asthenospheric mantle wedge above the slab beneath south central Alaska (Stachnick et al., 2004). Chris Nye (personal communication 2009) has suggested that the compression in the overriding crust may create the Denali volcanic gap by preventing deep magma bodies from rising to the surface. The presence

of a crustal root does not preclude the presence of trapped melt, but our calculations indicate that the mountains of the Alaska Range near BEAAR stations are held up by their own intrinsic buoyancy, not by high heat flow introduced from the mantle.

In the Andes, in central Chile and Argentina, magmatism and deformation nearly 1000 km from the plate boundary has been attributed to shallow dip of the subducting Nazca plate (Gilbert et al., 2006). Shallow subduction is related to subduction of a buoyant feature such as a ridge or oceanic plateau (Nur and Ben-Avraham, 1981; McGeary et al., 1985; Pilger, 1981; Gutscher et al. 1999, 2000; Gutscher, 2002; Yañez et al., 2002). In Alaska the buoyancy is associated with subduction of Yakutat block (Ferris et al., 2003; Eberhart-Phillips et al., 2006; Rondenay et al., 2008; Abers, 2008). Although there are differences between Alaska and the Andes (beneath high elevations in the central Andes, the crust is in excess of 60 km thick in large regions [Beck and Zandt, 2002] and the slab flattens near 100 km depth [Gilbert et al., 2006]), the comparison of subduction zone geometry with crustal thickness and topography in the flat slab regions of the Andes and Alaska could be informative about the processes involved in crustal thickening and the creation of topography. It is clear that subduction of anomalously thick crust is related to gently dipping subduction, but the process or relationship to crustal thickening is poorly understood. More studies are needed to determine the extent to which crustal thickening and the creation of topography in flat slab regions are driven by stronger coupling between the subducting slab and the over-riding crust, support by underlying buoyant subducted crust, and/or the role of pre-existing variations such as juxtaposed terranes in the over-riding plate.

The precise location of the North American – Pacific plate boundary within the collision zone between Yakutat and southern Alaska is somewhat controversial (Bruns, 1983; Plafker et al., 1994; Fletcher and Freymueller, 2003; Gulick et al., 2007). The plate boundary is an evolving zone of distributed deformation within an active collisional fold-and-thrust belt (Wallace, 2008). Neotectonic studies suggest significant spatial and kinematic variations in deformation during Yakutat collision (Carver and Plafker, 2008; Chapman et al., 2008; Freymueller et al., 2008; Haeussler, 2008; Elliott et al., 2009). Uplift of the Alaska Range is asymmetric along and across strike, related to complex strain partitioning along active faults translating and rotating discrete crustal blocks. There is some evidence for topographic development by ~30 Ma with diffuse orogenic pulses at ~20 Ma and ~11 Ma (Reinink-Smith and Leopold, 2005; Ridgway et al., 2007; Benowitz and Layer, 2008; Haeussler et al., 2008), with a strong signal at 6 Ma in the central Alaska Range (Fitzgerald et al., 1995). The Yakutat crust has likely been subducting since at least ~12 Ma based on the geophysically visible extent of thickened subducted crust. Abers (2008) quantitatively evaluated the change in buoyancy expected for subduction of thickened crust, concluding that large decreases in slab pull can produce high topography. The curvature of the Alaska Range appears

to be associated with the closed corner type transition between the contractional margin to the west in the Aleutians and the translational margin to the east in the Alaskan Panhandle. The curvature of structures in the Alaska Range long predates Yakutat arrival, although gently dipping subduction of the "Yakutat indenter" has probably accentuated that curvature and had a major influence on topographic development in south central Alaska for at least 6 My. The Late Cenozoic orogenesis in southern Alaska may well be driven largely by subduction and accretion of the thick Yakutat crust (Pavlis et al., 2004; Abers, 2008; Chapman et al., 2008; Wallace, 2008).

References Cited

Abers, G.A., Hu, X., and Sykes, L.R., 1995, Source scaling of earthquakes in the Shumagin region, Alaska; time domain inversions of regional waveforms: *Geophysical Journal International*, v. 123, p. 41-58.

Abers, G.A., van Keken, P.E., Kneller, E.A., Ferris, A., Stachnik, J.C., 2006, The thermal structure of subduction zones constrained by seismic imaging: Implications for slab dehydration and wedge flow: *Earth and Planetary Science Letters*, v. 241, p. 387-397.

Abers, G.A., 2008, Orogenesis from subducting thick crust and evidence from Alaska, *in* Freymueller, J.T., Haeussler, P.J., Wesson, R.L., and Ekstrom, G., eds., Active Tectonics and Seismic Potential of Alaska, Geophysical Monograph 179, American Geophysical Union, p.337-349.

Agnew, J.D., 1980, Seismicity of the central Alaska Range, Alaska, 1904-1978: University of Alaska Fairbanks M.S. thesis, 88p.

Ai, Y., Zhao, D., Gao, X., and Xu, W., 2005, The crust and upper mantle discontinuity structure beneath Alaska inferred from receiver functions: *Physics of the Earth and Planetary Interiors*, v. 150, p. 339-350.

Aleinikoff, J.N., 1984, Age and origin of metaigneous rocks from terranes north and south of the Denali fault, Mt. Hayes quadrangle, east-central Alaska: *Geological Society of America Abstracts with Programs*, v. 16, p. 266.

Aleinikoff, J.N., Dusel-Bacon, C., Foster, H.L., and Nokleberg, W.J., 1987, Pb-isotope fingerprinting of tectonostratigraphic terranes, east-central Alaska: *Canadian Journal of Earth Sciences*, v. 24, p. 2089-2098.

Aleinikoff, J.N., and Nokleberg, W.J., 1985, Age of Devonian igneous-arc terranes in the northern Mount Hayes quadrangle, eastern Alaska Range, *in* Bartsch-Winkler, S., ed., The United States Geological Survey in Alaska—Accomplishments during 1984: U.S. Geological Survey Circular 967, p. 44-49.

Ammon, C.J., 1991, The isolation of receiver effects from teleseismic P waveforms: *Bulletin of the Seismological Society of America*, v. 81, p. 2504-2510.

Ammon, C.J., Randal, G.E., and Zandt, G., 1990, On the Nonuniqueness of Receiver Function Inversions: *Journal of Geophysical Research*, v. 95, no. B.10, p. 15,303-15,318.

Andreasen, G.E., Grantz, A., Zeitz, I., and Barnes, D.G., 1974, Geologic interpretation of magnetic and gravity data in the Copper River Basin, Alaska: U.S. Geological Survey Professional Paper 316-H, p. 135-153.

Barnes, D.F, Mariano, J., Morin, R.L., Roberts, C.W., and Jachens, R.C., 1994, Incomplete isostatic gravity map of Alaska, *in* Plafker, G., and Berg, H.D., eds., The geology of Alaska: Boulder, Colorado, Geological Society of America, Geology of North America, v. G-1, plate 9, scale 1:2,500,000.

Beaudoin, B.C., Fuis, G.S., Lutter, W.J., Mooney, W.D., and Moore, T.E., 1994, Crustal velocity structure of the northern Yukon-Tanana upland, central Alaska: Results from TACT refraction/wide-angle reflection data: *Geological Society of America Bulletin*, v. 106, p. 981-1001.

Beaudoin, B.C., Fuis, G.S., Mooney, W.D., Nokleberg, W.J., and Christensen, N.I., 1992, Thin, low-velocity crust beneath the southern Yukon-Tanana terrane, east central Alaska: Results from Trans-Alaska Crustal Transect refraction/wide-angle reflection data: *Journal of Geophysical Research*, v. 97, no. B2, p. 1921-1942.

Beck, W.L., and Zandt, G., 2002, The nature of orogenic crust in the central Andes: *Journal of Geophysical Research*, v. 107, no. B10, 2230, doi:10.1029/2000JB000124.

Beikman, H.M., 1980, Geologic map of Alaska: U.S. Geological Survey Special Map, 2 sheets, scale 1:2,500,000.

Bemis, S., and Wallace, W., 2007, Neotectonic framework of the north-central Alaska Range foothills, *in* Ridgway K.D., et al., eds., Tectonic Growth of a Collisional Continental Margin: Crustal evolution of Southern Alaska, Geological Society of America Special Paper v. 431, Geological Society of America, Boulder, Colorado, pp. 549-572.

Benowitz, J.A, and Layer, P., 2008, K-Spar Thermochronological constraints on the correlation between "Modern" East to West Variations in Slip-rates Along the Denali Fault with Long Term Exhumation Patterns: *EOS Transactions American Geophysical Union*, v. 89, no 53, Fall Meeting Supplement, Abstract T53B-1948.

Bird, P., 1984, Laramide crustal thickening event in the Rocky Mountain foreland and Great Plains, *Tectonics*, v. 3, p. 741-758.

Biswas, N.N., 1973, P-wave travel time anomalies: Aleutian-Alaska region: *Tectonophysics*, v. 19, p. 361-367.

Biswas, N.N., and Tytgat, G., 1988, Intraplate seismicity in Alaska: *Seismological Research Letters*, v. 59, p. 227-233.

Boyd, K.A., and Hiles, R.M., 1985, Oil and gas developments in Alaska in 1984: *American Association of Petroleum Geologists Bulletin*, v. 69, no. 10, p. 1486.

Brease, P., 1995, The Hines Creek fault in the Denali Park area, *in* Brease, P., and Til, A., eds., The Geology and glacial history of Denali National Park and vicinity: Geological Society of America Cordilleran Section, Field Trip 9 Guidebook and Road log, p. 17-21.

Brewer, W.M., 1982, Stratigraphy, structure, and metamorphism of the Mount Deborah area, central Alaska Range, Alaska [Ph.D. thesis]: Madison, University of Wisconsin, 318p.

Brocher, T.M., 2005, Empirical relations between elastic wave speeds and density in the Earth's crust: *Seismological Society of America Bulletin*, v. 95, p 2081-2092.

Brocher, T.M., Fuis, G.S., Lutter, W.J., Christensen, N.I., and Ratchovski, N.A., 2004, Seismic velocity models for the Denali fault zone along the Richardson Highway, Alaska: *Bulletin of the Seismological Society of America*, v. 94, no. 6B, p. S85-S106.

Brocher, T.M., Nokleberg, W.J., Christensen, N.I., Lutter, W.J., Geist, E.L., and Fisher, M.A., 1991, Seismic reflection/refraction mapping of faulting and regional dips in the Eastern Alaska Range: *Journal of Geophysical Research*, v. 96, no. B6, p. 10,233-10,249.

Brogan, G.E., Cluff, L.S., Korringa, M.K., and Slemmons, D.B., 1975, Active faults of Alaska: *Tectonophysics*, v. 29, p. 73-85.

Bruns, T.R., 1983, Model for the origin of the Yakutat block, an accreting terrane in the northern Gulf of Alaska: *Geology*, v. 11, p. 718-721.

Burdick, L.J., and Langston, C.A., 1977, Modeling crustal structure through the use of converted phases in teleseismic body waveforms: *Bulletin of the Seismological Society of America*, v. 67, p. 677-691.

Burris, L., 2007, Seismicity and stresses in the Kantishna Seismic Cluster: central Alaska: University of Alaska Fairbanks, M.S. thesis, 80pp.

Campbell, D.L., and Nokleberg, W.J., 1986, Magnetic profile and model across northern Copper River Basin, northwestern Gulkana quadrangle, Alaska, *in* Bartsch-Winkler, s., and Reed, K., eds., Geologic studies in Alaska by the U.S. Geological Survey during 1985: U.S. Geological Survey Circular 978, p. 35-38.

Carver, G., and Plafker, G., 2008, Paleoseismicity and Neotectonics of the Aleutian Subduction Zone—An Overview, *in* Freymueller, J.T., Haeussler, P.J., Wesson, R.L., and Ekstrom, G., eds., Active Tectonics and Seismic Potential of Alaska, Geophysical Monograph 179, American Geophysical Union, p. 43-63.

Castanga, J.P., Batzle, M.L., and Eastwood, R.L., 1985, Relationships between compressional-wave and shear-wave velocities in clastic silicate rocks: *Geophysics*, v. 50, p. 571-581.

Chapman, J.B., Pavlis, T.L., Gulick, S., Berger, A., Lowe, L., Spotila, J., Bruhn, R., Vorkink, M., Koons, P., Barker, A., Picornell, C., Ridgway, K., Hallet, B., Jaeger, J., and McCalpin, J., 2008, Neotectonics of the Yakutat Collision: Changes in Deformation Driven by Mass Redistribution, *in* Freymueller, J.T., Haeussler, P.J., Wesson, R.L., and Ekstrom, G., eds., Active Tectonics and Seismic Potential of Alaska, Geophysical Monograph 179, American Geophysical Union, p. 65-81.

Christensen, N.K., and Mooney, W.D., 1995, Seismic velocity structure and composition of the continental crust: A global view: *Journal of Geophysical Research*, v. 100, no. B7, p. 9761-9788.

Churkin, M., Jr., Foster, H.L., Chapman, R.M., and Weber, F.R., 1982, Terranes and suture zones in east central Alaska: *Journal of Geophysical Research*, v. 87, no. B5, p. 3718-3730.

Clague, J.J., 1979, The Denali Fault System in southwest Yukon Territory – A geologic hazard? *In* Current Research, Part 1: Geological Survey Canada Paper 79-1A, p. 169-178.

Clayton, R.W., and Wiggins, R.A., 1976, Source shape estimation and deconvolution of teleseismic body waves: *Geophysical Journal of the Royal Astronomical Society*, v. 47, p. 151-177.

Coats, R.R., 1962, Magma type and crustal structure in the Aleutian arc, *in* The crust of the Pacific Basin, American Geophysical Union Geophysical Monograph 6, p. 92-109.

Committee for the Gravity Anomaly Map of North America, 1987, Gravity Anomaly Map of North America: Geological Society of America, Continental-Scale Map-002, scale 1:5,000,000.

Coney, P.J., Jones, D.L., and Monger, J.W.H., 1980, Cordilleran suspect terranes: *Nature*, v. 228, p. 329-333.

Csejtey, B., Jr., and St. Aubin, D.R., 1981, Evidence for northwestward thrusting of the Talkeetna superterrane and it regional significance, *in* Albert, N.R.D., and Hudson, T., eds., 1981, The U.S. Geological Survey in Alaska: Accomplishments during 1979: U.S. Geological Survey Circular 823-B, p. B49-B51.

Csejtey, B., Jr., Cox, D.P., Evarts, R.C., Stricker, G.D., and Foster, H.L., 1982, The Cenozoic Denali fault system and the Cretaceous accretionary development of southern Alaska: *Journal of Geophysical Research*, v. 87, p. 3741-3754.

Csejtey, B., Jr., Mullen, M.W., Cox, D.P., and Sticker, G.D., 1992, Geology and geochronology of the Healy quadrangle, south-central Alaska: U.S. Geological Survey Miscellaneous Investigations Series, Map I-1961, scale 1:250,000, 63p.

Csejtey, B., Jr., Mullen, M.W., Cox, D.P., Gilbert, W.G., Yeend, W.E., Smith, T.E., Wahrhaftig, C., Craddock, C., Brewer, W.M., Sherwood, K.M., Hickman, R.G., Stricker, G.D., Aubin, D.R., and Goerz, D.J., III, 1986, Geology and geochronology of the Healy quadrangle, Alaska: *U.S. Geological Survey Open-File Report 86-396*, scale 1:250,000, 92p.

Csejtey, B., Jr., Nelson, W.H., Jones, D.L., Silberling, N.J., Dean, R.M., Morris, M.S., Lanphere, M.A., Smith, J.G., an Silberman, M.L., 1978, Reconnaissance geologic map and geochronology, Talkeetna Mountains quadrangle, northern par of Anchorage quadrangle, and southwest corner of Healy quadrangle, Alaska: *U.S. Geological Survey Open-File Report 78-558A*, scale 1:250,000, 62p.

Davies, J.N., 1975, Seismoiogical interpretation of plate tectonics in south central Alaska: University of Alaska Fairbanks Ph.D. thesis, 193p.

Davies, J.N., and House, L., 1979, Aleutian subduction zone seismicity, volcano-trench separation, and their relation to great thrust-type earthquakes: *Journal of Geophysical Research*, v. 84, p. 4583-4591.

Delong, S.E., Fox, P.J., and McDowell, 1978, Subduction of the Kula Ridge at the Aleutian trench: *Geological Society of America Bulletin,* v. 89, p. 83-95.

DeMets, G., Gordon, R.G., Argus, D.F., and Stein, S., 1990, Current plate motions: *Geophysical Journal International*, v. 101, p. 425-478.

Denton, G.H., and Stuiver, M., 1967, Late Pleistocene glacial stratigraphy and chronology, northeastern St. Elias Mountains, Yukon Territory, Canada: *Geological Society of America Bulletin*, v. 78, p. 485-510.

Detterman, R.L., 1988, Mesozoic biogeography of southern Alaska with implications for the paleogeography: U.S. Geological Survey Open-File Report 88-662, 27p.

Doser, D., 2002, Historical seismicity of the Denali Fault system: *EOS Transactions* American Geophysical Union, v. 83, S72f-1338.

Doser, D.I., 2004, Seismicity of the Denali fault zone (1912-1988): *Bulletin of the Seismoiogical Society of America*, v. 94, no. 6B, p. S132-S144.

Dreger, D., Oglesby, D.D., Harris, R.A., Ratchkovski, N., and Hansen, R., 2004, Kinematic and dynamic rupture models of the November 3, 2002 Mw 7.9 Denali, Alaska, earthquake, *Geophysical Research Letters*, v. 31, L04605, doi 10.1020/2003GL018333.

Dusel-Bacon, C. 1994, Metamorphic history of Alaska, *in* Plafker, G., and Berg, H.C., eds., The Geology of Alaska: Boulder, Colorado, Geological Society of America, The Geology of North America, v. G-1, p. 495-533.

Dusel-Bacon, C., 1991, Metamorphic history of Alaska: U.S. Geological Survey Open-File Report 91-556, 48p.

Dusel-Bacon, C., Csejtey, B., Foster, H.L., Doyle, E.O., Nokleberg, W.J., and Plafker, G., 1994, Distribution, facies, age, and proposed tectonic associations of regionally metamorphosed rocks in east and south-central Alaska: U.S. Geological Survey Professional Paper 1497-C, 59p.

Eberhart-Phillips, D., Christensen, D.H., Brocher, T.M., Hansen, R., Ruppert, N.A., Haeussler, P.J., and Abers, G.A., 2006, Imagine the transition from Aleutian subduction to Yakutat collision in central Alaska, with local earthquakes and active source data: *Journal of Geophysical Research*, v. 111, B11303, doi:10.1029/2005JB004240.

Eberhart-Phillips, D., Haeussler, P.J., Freymueller, J.T., Frankel, A.D., Rubin, C.M., Craw, P., Ratchkovski, N.A., Anderson, G., Carver, G.A., Crone, A.J., Dawson, T.E., Fletcher, H., Hansen, R., Harp, E.L., Harris, R.A., Hill, D.P., Hreinsdóttir, S., Jibson, R.W., Jones, L.M., Kayen, R., Keefer, D.K., Larsen, C.F., Moran, S.C., Personius, S.F., Plafker, G., Sherrod, B., Sieh, K., Sitar, N., Wallace, W., 2003, The 2002 Denali fault earthquake, Alaska: A large magnitude, slip-partitioned event: *Science*, v. 300, p. 1113-1118.

Eisbacher, G.H., 1976, Sedimentology of the Dezadeash flysch and its implications for strike-slip faulting along the Denali fault, Yukon Territory and Alaska: *Canadian Journal of Earth Sciences*, v. 13, p. 1495-1513.

Elliott, J., Freymueller, J., and Larsen, C., 2009, Accretionary Tectonics of Southern Alaska constrained by GPS: *Alaska Geological Society*, 2009 Technical Conference, Fairbanks, Alaska, abstract volume p. 20.

Engdahl, E.R., and Scholz, C.H., 1977, A double Benioff zone beneath the central Aleutians: an unbending of the lithosphere: *Geophysical Research Letters*, v. 4, p. 473-476.

Engebretson, D.C., Cox, A., and Gordon, R.G., 1985, Relative motions between oceanic and continental plates in the Pacific basin: Geological Society of America Special Paper 206, 59p.

England, P., and McKenzie, D., 1982, A thin viscous sheet model for continental deformation: *Royal Astronomical Society Geophysical Journal*, v. 70, p. 295-321.

Ferris, A., Abers, G.A., Christensen, D.H., and Veenstra, E., 2003, High resolution of the subducted Pacific (?) plate beneath central Alaska, 50-150 km depth: *Earth and Planetary Science Letters*, v. 214, p. 575-588.

Fisher, M.A., Nokleberg, W.J., Ratchkovski, N.A., Pellerin, L., Glen, J.M., Brocher, T.M., Booker, J., 2004a, Geophysical investigation of the Denali fault and Alaska Range orogen within the aftershock zone of the October-November 2002, M=7.9 Denali fault earthquake, *Geology*, v. 32, no. 3, p. 269-272.

Fisher, M.A., Ratchkovski, N.A., Nokleberg, W.J., Pellerin, L., and Glen, J.M., 2004b, Geophysical data reveal the crustal structure of the Alaska Range orogen within the aftershock zone of the M 7.9 Denali fault earthquake, *Bulletin of the Seismological Society of America*, v. 94, no. 6B, S107-S131.

Fitzgerald, P.G., Sorkhabi, R.B., Redfield, T.F., and Stump, E., 1995, Uplift and denudation of the central Alaska Range: A case study in the use of apatite fission track thermochronology to determine absolute uplift parameters: *Journal of Geophysical Research*, v. 100, no. B10, p. 20,175-20,191.

Fletcher, H., 2002, Crustal Deformation in Alaska measured using the Global Positioning System, Ph.D. thesis, University of Alaska Fairbanks.

Fletcher, H., and Freymueller, J.T., 1999, New GPS Constraints on the Motion of the Yakutat Block, *Geophysical Research Letters*, v. 26, p. 3029-3032.

Fletcher, H., and Freymueller, J.T., 2003, New constraints on the motion of theFairweather Fault, Alaska, from GPS observations: *Geophysical Research Letters*, v. 30, no. 3, p. 1139.

Forbes, R.B., Turner, D.L., Smith, T.E., Stout, J.H., and Weber, F.R., 1973a, The Denali fault offset problem, U.S. Geological Survey Alaska Program, U.S. Geological Survey Circular 683, 46.

Forbes, R.B., Turner, D.L., Stout, J.H., and Smith, T.E., 1973b, Cenozoic offset along the Denali fault, Alaska [abs.]: *Eos Transactions,* American Geophysical Union, v. 54, p. 495.

Foster, H.L., Keith, T.E.C., and Menzie, W.D., 1987, Geology of east-central Alaska: U.S. Geological Survey Open-File Report 87-188, 59p.

Foster, H.L., Keith, T.E.C., and Menzie, W.D., 1994, Geology of the Yukon-Tanana area of east-central Alaska, *in* Plafker, G., and Berg, H.D., eds., The geology of Alaska: Boulder, Colorado, Geological Society of America, Geology of North America, v. G-1, p. 205-240.

Foster, H.L., Weber, F.R., Forbes, R.B., and Brabb, E.E., 1973, Regional geology of the Yukon-Tanana Upland, Alaska, *in* Pitcher, M.G., ed., Arctic geology: American Association of Petroleum Geologists Memoir 19, p. 388-395.

Freymueller, J.T., Woodard, H., Cohen, S.C., Cross, R., Elliott, J., Larsen, C.F., Hreinsdóttir, S., and Zweck, C., 2008, Active Deformation Processes in Alaska, Based on 15 years of GPS measurements, *in* Freymueller, J.T., Haeussler, P.J., Wesson, R.L., and Ekstrom, G., eds., Active Tectonics and Seismic Potential of Alaska, Geophysical Monograph 179: American Geophysical Union, p. 1-42.

Fuis, G.S., Moore, T.E., Plafker, G., Brocher, T.M., Fisher, M.A., Mooney, W.D., Nokleberg, W.J., Page, R.A., Beaudoin, B.C., Christensen, N.I., Levander, A.R., Lutter, W.J., Saltus, R.W., Ruppert, N.A., 2008, Trans-Alaska Crustal Transect and continental evolution involving subduction underplating and synchronous foreland thrusting, *Geology*, v. 36, no.3, p. 267-270.

Gardner, MC., Bergman, S.C., MacKevett, E.M., Jr., Plafker, G., Campbell, R.C., Cushing, G.W., Dodds, C.J., and McClelland, W.D., 1988, Middle Pennsylvanian pluton stitching of Wrangellia and the Alexander terrane, Wrangell Mountains, Alaska: *Geology*, v. 16, p. 967-971.

Gedney, L., 1970, Tectonic stresses in southern Alaska in relationship to regional seismicity and the new global tectonics: *Bulletin of the Seismological Society of America*, v. 60, p. 1789-1802.

Gedney, L., and Davies, J.N., 1986, Additional evidence for down-dip tension in the Pacific plate beneath central Alaska, *Bulletin of the Seismological Society of America*, v. 76, p. 1207-1214.

Gilbert, H., Beck, S., and Zandt, G., 2006, Lithospheric and upper mantle structure of central Chile and Argentina: *Geophysical Journal International*, v. 165, p. 383-398.

Gilbert, W.G., and Bundtzen, T.K., 1984, Stratigraphic relationships between Dillinger and Mystic terranes, western Alaska Range, Alaska: *Geological Society of America Abstracts with Programs*, v. 16, p. 286.

Gilbert, W.G., Nye, C.J., and Sherwood, K.W., 1984, Stratigraphy, petrology, and geochemistry of Upper Triassic rocks from the Pingston and McKinley terranes, central Alaska Range: Alaska Division of Geological and Geophysical Surveys Report of Investigations 84-30, 14p.

Golub, G.H., and Kahan, W., 1965, Calculating the singular values and pseudoinverse of a matrix: *SIAM Journal of Numerical Analysis*, v. 2, p. 205-224.

Grantz, A., 1966, Strike-slip faults in Alaska: U.S. Geological Survey Open-File Report, 82p.

Gulick, S.P.S., Lowe, L.A., Pavlis, T.L., Gardner, J.V., and Mayer, L.A., 2007, Geophysical insights into the Transition fault debate: Propagating strike slip in response to stalling Yakutat subduction in the Gulf of Alaska: *Geology*, v. 35, p. 763-766.

Gutscher, M.-A., Malavieille, J., Lallemand, S., Collot, J.-Y., 1999, Tectonic segmentation of the North Andean margin: impact of the Carnegie Ridge collision: *Earth and Planetary Science Letters,* v. 168, p. 255-270.

Gutscher, M., Spakman, W., Bijwaard, H., and Engdahl, E., 2000, Geodynamics of flat subduction: Seismicity and tomographic constraints from the Andean margin, *Tectonics*, v. 19, p. 814-833.

Gutscher, M., 2002, Andean subduction styles and their effect on thermal structure and interplate coupling: *Journal of South American Earth Sciences*, v. 15, p. 3-10.

Haeussler, P.J., 2005, What Made Denali so tall? Structural geology of the high peaks of the Alaska Range: *Alaska Geology*, v. 35, no. 8, p. 1.

Haeussler, P.J., 2008, An Overview of the Neotectonics of Interior Alaska: Far-Field Deformation from the Yakutat microplate collision, *in* Freymueller, J.T., Haeussler, P.J., Wesson, R.L., and Ekstrom, G., eds., Active Tectonics and Seismic Potential of Alaska, Geophysical Monograph 179, American Geophysical Union, p. 83-108.

Haeussler, P.J., Coe, R.S., Onstott, T.C., and Renne, P., 1989, A second look at the paleomagnetism of the Late Triassic Hound Island Volcanics of the Alexander terrane [abs.]: *EOS Transactions*, American Geophysical Union, v. 70, p. 1068.

Haeussler, P.J., O'Sullivan, P., Berger, A.L., and Spotila, J.A., 2008, Neogene exhumation of the Tordrillo Mountains, Alaska, and correlations with Denali (Mount McKinley), *in* Freymueller, J.T., Haeussler, P.J., Wesson, R.L., and Ekstrom, G., eds., Active Tectonics and Seismic Potential of Alaska, Geophysical Monograph 179, American Geophysical Union, p.269-285.

Haeussler, P.J., Schwartz, D.P., Dawson, T.E., Stenner, H.D., Lienkaemper, J.J., Sherrod, B., Cinti, F.R., Montone, P., Craw, P.A., Crone, A.J., and Personius, S.F., 2004, Surface rupture and slip distribution of the Denali and Totschunda faults in the 3 November 2002 M 7.9 earthquake, Alaska: *Bulletin of the Seismological Society of America*, v. 94, no. 6B, p. S23-S52.

Hickman, R.G., 1971, The Denali Fault near Cantwell, Alaska: Madison, Wisconsin, University of Wisconsin M.S. thesis, 76p.

Hickman, R.G., and Craddock, C., 1976, Geologic map of central Healy quadrangle, Alaska: Alaska Division of Geological and Geophysical Surveys Open-File Report AOF-95, scale 1:63,360.

Hickman, R.G., Craddock, C., and Sherwood, K.W., 1977, Structural geology of the Nenana River segment of the Denali fault system, central Alaska Range: *Geological Society of America Bulletin*, v. 88, no. 9, p. 1217-1230.

Hillhouse, J.W., and Gromme, C.S., 1984, Northward displacement and accretion of Wrangellia: New paleomagnetic evidence from Alaska: *Journal of Geophysical Research*, v. 89, p. 4461-4467.

Howell, D.G., 1985, Tectonostratigraphic terranes of the Circum-pacific region: Circum-Pacific Council for Energy and Mineral Resources, Earth Sciences Series no. 1, p. 3-30.

Hreinsdóttir, S., Freymueller, J.T., Fletcher, H.J., Larsen, C.F., and Burgmann, R., 2003, Coseismic slip distribution of the 2002 Mw 7.9 Denali Fault earthquake, Alaska, determined from GPS measurements, *Geophysical Research Letters*, v. 30, p. 1670.

Jacob, K.H., Nakamura, K., and Davies, J.N., 1977, Trench-volcano gap along the Alaska-Aleutian Arc: Facts and speculations on the role of terrigenous sediments for subduction, *in* Talwani, M., and Pitman, W.C., eds., Island Arcs, Deep Sea Trenches, and Back-Arc Basins, Maurice Ewing Series, AGU, Washington, D.C., v. 1, p. 243-258.

Jones, D.L., Irwin, W.P., and Ovenshine, A.T., 1972, Southeastern Alaska – a displaced continental fragment?: U.S. Geological Survey Professional Paper 800-B, p. B211-217.

Jones, D.L., Silberling, N.J., Berg, H.C., and Plafker, G., 1981, Map showing tectonostratigraphic terranes of Alaska, columnar sections, and summary description of terranes: U.S. Geological Survey Open-File Report 81-792, 20p., 2 sheets, scale 1:2,500,000.

Jones, D.L., Silberling, N.J., and Coney, P.J., 1983, Tectono-stratigraphic map and interpretative bedrock geologic map of the Mount McKinley region, Alaska: U.S. Geological Survey Open-File Report 83-11, 2 sheets, scale 1:250,000.

Jones, D.L., Silberling, N.J., Coney, P.J., and Plafker, G., 1984, Lithotectonic terrane map of Alaska (west of the 141st meridian), in Silberling, N.J., and Jones, D.L., eds., Lithotectonic terrane maps of North American Cordillera: U.S. Geological Survey Open-File Report 84-523, scale 1:2,500,000.

Jones, D.L., Silberling, N.J., Coney, P.J., and Plafker, G., 1987, Lithotectonic terrane map of Alaska (west of the 141st meridian): U.S. Geological Survey Miscellaneous Field Studies Map MF-1874, scale 1:2,500,000.

Jones, D.L., Silberling, N.J., Csejtey, B., Jr., Nelson, W.H., and Blome, C.D., 1980, Age and structural significance of ophiolite and adjoining rocks in the Upper Chulitna district, south-central Alaska: U.S. Geological Survey Professional Paper 1121-A, 21p.

Jones, D.L., Silberling, N.J., Gilbert, W., and Coney, P., 1982, Character, distribution, and tectonic significance of accretionary terranes in the central Alaska Range: *Journal of Geophysical Research*, v. 87, p. 3709-3717.

Jones, D.L., Silberling, N.J., Hilhouse, J., 1977, Wrangellia—A displaced terrane in northwestern North America: *Canadian Journal of Earth Sciences*, v. 14, p. 2565-2577.

Jones, D.L., Silberling, N.J., 1979, Mesozoic stratigraphy—The key to tectonic analysis of southern and central Alaska: U.S. Geological Survey Open-File Report 79-1200, 37p.

Jordan, T.H., and Frazer, L.N., 1975, Crustal and upper mantle structure from Sp phases: *Journal of Geophysical Research,* v. 80, p. 1504-1518.

Kalbas, J.L., Freed, A.M., and Ridgway, K.D., 2008, Contemporary Fault Mechanics in Southern Alaska, *in* Freymueller, J.T., Haeussler, P.J., Wesson, R.L., and Ekstrom, G., eds., Active Tectonics and Seismic Potential of Alaska, Geophysical Monograph 179, American Geophysical Union, p. 321-336.

Kienle, J., Swanson, S.E., and Pulpan, H., 1983, Magmatism and Subduction in the Eastern Aleutian Arc, *in* Shimozuru, D., and Yokoyama, I., eds., Arc Volcanism: Physics and Tectonics, Terra Scientific Publishing Company, Tokyo, p. 191-224.

Kikuchi, M., and Yamanaka, Y., 2002, Source rupture processes of the central Alaska earthquake of Nov. 3, 2002, inferred from teleseismic body waves (+the 10.23 M6.7event), EIC seismological note 129, Earthquake Research Institute, University of Tokyo, Tokyo.

Kirschner, C.E., 1994a, Interior basins of Alaska, *in* Plafker, G., and Berg, H.D., eds., The geology of Alaska: Boulder, Colorado, Geological Society of America, Geology of North America, v. G-1, p. 469-493.

Kirschner, C.E., 1994b, Map Showing Sedimentary Basins in Alaska, *in* Plafker, G., and Berg, H.D., eds., The geology of Alaska: Boulder, Colorado, Geological Society of America, Geology of North America, v. G-1, plate 7, scale 1:2,500,000.

Kirschner, C.E., Fisher, M.A., Bruns, T.R., and Stanley, R.G., 1985, Interior provinces in Alaska [abs.]: *American Association of Petroleum Geologists Bulletin*, v. 69, no. 4, p. 667.

Kissling, E., and Lahr, J.C., 1991, Tomographic image of the Pacific Slab under southern Alaska: *Eclogue Geol. Helv.*, v. 84, p. 297-315.

Kurita, T., 1973, A procedure of elucidating fine structure of the crust and upper mantle from seismological data: *Bulletin of the Seismological Society of America*, v. 63, p. 189-204.

Lahr, J.C., 1975, Detailed seismic investigation of Pacific-North American plate interaction in southern Alaska, Ph.D. thesis, Columbia University, New York, 88p.

Lahr, J.C., and Plafker, G., 1980, Holocene Pacific-North American interaction in southern Alaska: Implications for the Yakutaga seismic gap: *Geology*, v. 8, 483-486.

Lahr, J.C., Page, R.A., Stephens, C.D., and Christensen, D.H., 1988, Unusual earthquakes in the Gulf of Alaska and fragmentation of the Pacific plate: *Geophysical Research Letters*, v. 15, p. 1483-1486.

Langston, C.A., 1977, The effect of planar dipping structure on source and receiver responses for constant ray parameter: *Bulletin of the Seismological Society of America*, v. 67, p. 1029-1050.

Langston, C.A., 1979, Structure under Mount Rainier, Washington, inferred from teleseismic body waves: *Journal of Geophysical Research*, v. 84, no. B9, p. 4749-4762.

Langston, C.A., 1981, Evidence for subducting lithosphere under southern Vancouver Island and western Oregon from teleseismic P wave conversions: *Journal of Geophysical Research*, v. 86, p. 3857-3866.

Lanphere, M.A., 1978, Displacement history of the Denali fault system, Alaska and Canada: *Canadian Journal of Earth Sciences*, v. 15, p. 817-822.

Lesh, M.E., and Ridgway, K.D., 2007, Geomorphic evidence of active transpressional deformation in the Tanana foreland basin, south-central Alaska, *in* Ridgway K.D., et al., eds., Tectonic Growth of a Collisional Continental Margin: Crustal evolution of Southern Alaska, Geological Society of America Special Paper v. 431, Geological Society of America, Boulder, Colorado, doi:10.1130/2007.2431(22).

Lu, Z., and Wyss, M., 1996, Segmentation of the Aleutian plate boundary derived from stress direction estimates based on fault plane solutions: *Journal of Geophysical Research*, v. 101, p. 803-816.

Lu, Z., Wright, T.J., and Wicks, C., 2003, Deformation of the 2002 Denali fault earthquakes, Alaska, mapped by Radarsat-1 interferometry: *EOS Transactions* American Geophysical Union, v. 84, p.. 425-431.

Ludwig, W.J., Nafe, J.E., and Drake, C.L., 1970, Seismic refraction, *in* Maxwell, A.E., ed., The sea, Volume 4: New York, Wiley-Interscience, p. 53-84.

Mann, P., and Frohlich, C., 1999, Classification and tectonic comparison of subduction to strike-slip transitions on active plate boundaries: Penrose Conference abstract, p. 60-62: http://people.uncw.edu/grindlayn/revabstra_vol.pdf.

Matmon, A., Schwartz, D.P., Haeussler, P.J., Finkel, R., Llenkaemper, J.J., Stenner, H.D., and Dawson, T.E., 2006, Denali fault slip rates and Holocene-late Pleistocene kinematics of central Alaska: *Geology*, v. 34, p. 645-648.

McGeary, S., Nur, A., Ben-Avraham, Z., 1985, Spatial gaps in arc volcanism: the effect of collision or subduction of oceanic plateaus: *Tectonophysics*, v. 119, p. 195-221.

McNamara, D.E., and Pasyanos, M.E., 2002, Seismological evidence for a sub-volcanic arc mantle wedge beneath the Denali volcanic gap, Alaska: *Geophysical Research Letters*, v. 29.

Mellman, G.R., 1980, A method of body-wave waveform inversion for determination of earth structure: *Geophysical Journal of the Royal Astronomical Society,* v. 62, p. 481-504.

Melosh, H.J., and Raefsky, A., 1980, The dynamical origin of subduction zone topography: *Royal Astronomical Society Geophysical Journal*, v. 60, p. 333-354.

Meyers, E. Veenstra, Christensen, D.H., Abers, G.A., 2002, Moho topography beneath the Alaska Range: *Eos Transactions,* American Geophysical Union, v. 83, no. 47, abs S52A-1073, p. F968.

Meyers, E. Veenstra, Christensen, D.H., Abers, G.A., Stachnik, J.C., Holland, A.R., and Beebe, K.B., 2000, Broadband (seismic) Experiment Across the Alaska Range (BEAAR) to determine the crustal and upper mantle structure beneath central Alaska: *Eos Transactions,* American Geophysical Union, v. 81, no. 48, abs. S72A-11, p. F877.

Meyers, E. Veenstra, Christensen, D.H., Ferris, A., Abers, G.A., and Lucier, A.M., 2001, Crustal thickness across the Alaska Range: *Eos Transactions,* American Geophysical Union, v. 82, no. 47, abs. T41C-0907, p. F1204.

Miller, T.P. and Richter, D.H., 1994, Quaternary volcanism in the Alaska Peninsula and Wrangell Mountains, Alaska, *in* Plafker, G., and Berg, H.C., eds., The Geology of Alaska: Boulder, Colorado, Geological Society of America, The Geology of North America, v. G-1, p. 759-779.

Monger, J.W.H., and Berg, H.C., 1987, Lithotectonic terrane map of western Canada and southeastern Alaska: U.S. Geological Survey Map, MF-1874-B.

Newton, C.R., 1983, Paleozoogeographic affinities of Norian bivalves from the Wrangellian, Peninsular, and Alexander terranes, western North America, *in* Stevens, C.H., ed., Pre-Jurassic rocks in western North America suspect terranes: Los Angeles, California, Pacific Section, Society of Economic Paleontologists and Mineralogists, p. 37-48.

Nichols, K.M., and Silberling, N.J., 1979, Early Triassic (Smithian) ammonites of paleoequatorial affinity from the Chulitna terrane, south-central Alaska: U.S. Geological Survey Professional Paper 1121-B, 5p.

Nokleberg, W.J., Albert, N.R.D., Bond, G.C., Herzon, P.L., Miyaoka, N.W.H., Richter, D.H., Smith, T.P., Stout, J.H., Yeend, W., Zehrner, R.E., 1982, Geologic map of the southern part of the Mt. Hayes quadrangle, Alaska: U.S. Geological Survey Open-File Report, OF82-52, scale 1:250,000, 26 p.

Nokleberg, W.J., and Aleinikoff, J.N., 1985, Summary of stratigraphy, structure, and metamorphism of Devonian igneous-arc terranes, north-eastern Mount Hayes quadrangle, eastern Alaska Range, *in* Bartsch-Winkler, S., ed., The United States Geological Survey in Alaska—Accomplishments during 1984: U.S. Geological Survey Circular 967, p. 66-71.

Nokleberg, W.J., Aleinikoff, J.N., Dutro, J.T., Jr., Lanphere, M.A., Silberling, N.J., Silva, S.R., Smith, T.E., and Turner, D.L., 1992a, Map, tables, and summary of fossil and isotopic age data, Mount Hayes quadrangle, eastern Alaska Range, Alaska: U.S. Geological Survey Miscellaneous Field Studies Map 1996-D, 86p., 1 sheet, scale 1:250,000.

Nokleberg, W.J., Aleinikoff, J.N., Lange, I.M., Silva, S.R., Miyaoka, R.T., Schwab, C.E., and Zehner, R.E., 1992b, Preliminary geologic map of the Mount Hayes quadrangle, eastern Alaska Range, Alaska: U.S. Geological Survey Open-File Report 92-594, 39p., 1 sheet, scale 1:250,000.

Nokleberg, W.J., Foster, H.L., and Aleinikoff, J.N., 1989, Geology of the northern Copper River Basin, eastern Alaska Range, and southern Yukon-Tanana Basin, southern and east-central Alaska, *in* Nokleberg, W.J., and Fisher, M.A., eds., Alaskan geological and geophysical transect: International Geological Congress, 27th, Guidebook T104, p. 34-64.

Nokleberg, W.J., Jones, D.L., and Silberling, N.J., 1985, Origin and tectonic evolution of the Maclaren and Wrangellia terranes, eastern Alaska Range, Alaska: *Geological Society of America Bulletin*, v.96, p. 1251-1270.

Nokleberg, W.J., Plafker, G., and Wilson, F.H., 1994, Geology of south-central Alaska, *in* Plafker, G., and Berg, H.D., eds., The geology of Alaska: Boulder, Colorado, Geological Society of America, Geology of North America, v. G-1, p. 311-366.

Nokleberg, W.J., and Richter, D.H., 2007, Origin of narrow terranes and adjacent major terranes occurring along the Denali fault in the eastern and central Alaska range, Alaska, *in* Ridgway, K.D., Trop, J.M., Glen, J.M.G., and O'Neill, J.M., editors, Tectonic growth of a collisional continental margin: Crustal evolution of southern Alaska: Geological Society of America Special Paper 431, p. 129-154.

Nokleberg, W.J., Wade, W.M., Lange, I.M., and Plafker, G. 1986, Summary of geology of the Peninsular terrane, metamorphic complex of Gulkana River, and Wrangellia terrane, north-central and northwestern Gulkana quadrangle, *in* Bartsch-Winkler, S., and Reed, K., eds., Geologic studies in Alaska by the U.S. Geological Survey during 1985: U.S. Geological Survey Circular 978, p. 69-74.

Nur, A., and Ben-Avraham, Z., 1981, Volcanic gaps and the consumption of aseismic ridges in South America, *in* Kulm, L., ed., Nazca Plate: Crustal Formation and Andean convergence, Geological Society of America, Boulder, pp. 729-740.

Nye, C.J., 1983, Petrology and geochemistry of Okmok and Wrangell Volcanoes, Alaska, Ph.D. thesis, University of California, Santa Cruz, 208p.

Nye, C.J., 1999, The Denali volcanic gap – Magmatism at the eastern end of the Aleutian Arc, *Eos Transactions* American Geophysical Union, v. 80, no. 46, Fall Meeting Supplement, F1202.

Nye, C., Wyss, M., Ratchkovski, N., Fletcher, H., 2002, Magmatism in the Denali Volcanic Gap, Southern Alaska, *Eos Transactions* American Geophysical Union, v. 83, no. 47, Fall Meeting Supplement, V12C-06.

Oglesby, D.D., Dreger, D.S., Harris, R.A., Ratchkovski, N.A., and Hansen, R., 2004, Inverse kinematic and forward dynamic models of the 2002 Denali, Alaska, earthquake: *Bulletin of the Seismological Society of America*, v. 94, no. 6B, p. S214-S233.

Okaya, N., Tawackoli, S., Giese, P., 1997, Area-balanced model of late Cenozoic tectonic evolution of the central Andean arc and back arc (lat 20°-22°S): *Geology*, v. 25, no. 4, p. 367-370.

Owens, T.J., 1984, Determination of crustal and upper mantle structure from analysis of broadband teleseismic P-waveforms, Ph.D. thesis, University of Utah, 145p.

Owens, T.J., and Crosson, R.S., 1988, Shallow structure effects on broad-band teleseismic P-waveforms: *Bulletin of the Seismological Society of America*, v. 77, p. 631-662.

Owens, T.J., Crosson, R.S., and Hendrickson, M.A., 1988, Constraints on the subduction geometry beneath western Washington from broadband teleseismic waveform modeling: *Bulletin of the Seismological Society of America*, v. 78, p. 1319-1334.

Owens, T.J., Taylor, S.R., and Zandt, G., 1987, Crustal structure at regional seismic test network stations determined from inversion of broadband teleseismic P waveforms: *Bulletin of the Seismological Society of America*, v. 77, p. 631-662.

Owens, T.J., and Zandt, G., 1985, The response of the continental crust-mantle boundary observed on broadband teleseismic receiver functions: *Geophysical Research Letters*, v. 12, no. 10, p. 705-708.

Owens, T.J., Zandt, G., and Taylor, S.R., 1984, Seismic evidence for an ancient rift beneath the Cumberland Plateau, Tennessee: A detailed analysis of broadband teleseismic P waveforms: *Journal of Geophysical Research*, v. 89, no. B9, p. 7783-7795.

Ozacar, A.A, Beck, S.L., and Christensen, D.H., 2003, Source process of the 3 November 2002 Denali fault earthquake (central Alaska) from teleseismic observations, *Geophysical Research Letters*, v. 30, p. 1638.

Packer, D.R., and Stone, D.B., 1972, An Alaskan Jurassic paleomagnetic pole and the Alaskan orocline: *Nature*, v. 237, p. 25-26.

Packer, D.R., and Stone, D.B., 1974, Paleomagnetism of Jurassic rocks from southern Alaska, and their tectonic implications: *Canadian Journal of Earth Science*, v. 11, no. 7, p. 976-997.

Packer, D.R., Brogan, G.E., and Stone, D.B., 1975, New data on plate tectonics of Alaska: *Tectonophysics*, v. 29, p. 87-102.

Page, R.A., and Lahr, J., 1971, Measurements for fault slip on the Denali, Fairweather, and Castle Mountain faults: *Journal of Geophysical Research*, v. 76, p. 8534-8543.

Page, R.A., Biswas, N.N., Lahr, J.C., and Pulpan, H., 1991, Seismicity of continental Alaska, *in* Slemmons, D.B., Engdahl, E.R., Zoback, M.D., Zoback, M.L., and Blackwell, D., eds., Neotectonics of North America: Boulder, Colorado, The Geological Society of America, CSM V-1.

Page, R.A., Plafker, G., Fuis, G.S., Nokleberg, W.J., Ambos, E.L, Mooney, W.D., and Campbell, D.L., 1986, Accretion and subduction tectonics in the Chugach Mountains and Copper River Basin, Alaska: Initial results of the Trans-Alaskan Crustal Transect: *Geology*, v. 14, p. 501-505.

Page, R.A., Plafker, G., Pulpan, H., 1995, Block rotation in east-central Alaska: A framework for evaluating earthquake potential? *Geology*, v. 23, no. 7, p. 629-632.

Page, R.A., Stephens, C.D., and Lahr, J.C., 1989, Seismicity of the Wrangell and Aleutian Wadati-Benioff zones and the North American plate along the Trans-Alaska crustal Transect, Chugach mountains and Copper River basin, southern Alaska: *Journal of Geophysical Research*, v. 94, p. 16,059-16,082.

Panuska, B.C., 1985, Paleomagnetic evidence for a post-Cretaceous accretion of Wrangellia: *Geology*, v. 13, no. 2, p. 880-883.

Panuska, B.C., and Stone, D.B., 1981, Late Paleozoic paleomagnetic data from Wrangellia: Resolution of the polarity ambiguity: *Nature*, v. 293, p. 561-563.

Panuska, B.C., and Stone, D.B., 1985, Latitudinal Motion of the Wrangellia and Alexander Terranes and the Southern Alaska Superterrane, *in* Howell, D.G., ed., Tectonostratigraphic Terranes of the CircumPacific Region, Circum-Pacific Council for Energy and Mineral Resources, Houston, TX, p. 109-120.

Patton, W.W., Jr., Box, S.E., Moll-Stalcup, E.J., and Miller, T.P., 1989, Geology of west-central Alaska: U.S. Geological Survey Open-File Report 89-554, 53p.

Patton, W.W., Jr., Box, S.E., Moll-Stalcup, E.J., and Miller, T.P., 1994, Geology of west-central Alaska, *in* Plafker, G., and Berg, H.D., eds., The geology of Alaska: Boulder, Colorado, Geological Society of America, Geology of North America, v. G-1, p. 241-269.

Pavlis, T.L., Picornell, C., Serpa, L., Bruhn, R.L., and Plafker, G., 2004, Tectonic processes during oblique collision: Insights from the St. Elias orogen, northern North American Cordillera: *Tectonics*, v. 23, TC3001, doi:10.1029/2003TC001557.

Pavlis, T.L., and Roeske, S.M., 2007, The Border Ranges fault system, southern Alaska, *in* Ridgway, K.D., Trop, J.M., Glen, J.M.G., and O'Neill, J.M., editors, Tectonic growth of a collisional continental margin: Crustal evolution of southern Alaska: Geological Society of America Special Paper 431, p. 95-127.

Pavlis, T.L., Sisson, V.B., Foster, H.L., Nokleberg, W.J., and Plafker, G., 1993, Mid-Cretaceous extensional tectonics of the Yukon-Tanana terrane, Trans-Alaska Crustal Transect (TACT), east-central Alaska: *Tectonics*, v. 12, p. 103-122.

Perez, O.J., and Jacob, K.H., 1980, Tectonic model and seismic potential of the eastern Gulf of Alaska and Yakataga seismic gap: *Journal of Geophysical Research*, v. 85, p. 7132-7150.

Phinney, R.A., 1964, Structure of the earth's crust from spectral behavior of long-period body waves: *Journal of Geophysical Research*, v. 69, p. 2997-3017.

Pilger, R.H., 1981, Plate reconstructions, aseismic ridges, and low-angle subduction beneath the Andes: *Geological Society of America Bulletin*, v. 92, p. 448-456.

Plafker, G., and Berg, H.C., 1994, Overview of the geology and tectonic evolution of Alaska, *in* Plafker, G., and Berg, H.D., eds., The geology of Alaska: Boulder, Colorado, Geological Society of America, Geology of North America, v. G-1, p. 989-1021.

Plafker, G., Gilpin, L.M., and Lahr, J.C., 1994, Neotectonic Map of Alaska, *in* Plafker, G., and Berg, H.D., eds., The geology of Alaska: Boulder, Colorado, Geological Society of America, Geology of North America, v. G-1, plate 12, scale 1:2,500,000.

Plafker, G., Hudson, T., and Richter, D.H., 1977, Preliminary observations on late Cenozoic displacements along the Totschunda and Denali fault systems, *in* Blean, K.M. ed., Geologic studies of Alaska by the U.S. Geological Survey during 1976: U.S. Geological Survey Circular 751-B, p. B67-B69.

Plafker, G., Nokleberg, W.J., and Lull, J.S., 1989, Bedrock geology and tectonic evolution of the Wrangellia, Peninsular, and Chugach terranes along the Trans-Alaskan Crustal Transect in northern Chugach Mountains and southern Copper River basin, Alaska: *Journal of Geophysical Research*, v. 94, p. 4255-4295.

Pulpan, H., and Frohlich, C., 1985, Geometry of the subducted plate near Kodiak Island and lower Cook Inlet, Alaska, determined from relocated earthquake hypocenters: *Bulletin of the Seismological Society of America*, v. 75, p. 791-810.

Ratchkovski, N.A., 2001, Seismological constraints on tectonics of southern and central Alaska: Earthquake Locations and Source Mechanisms, Ph.D. thesis, 149p.

Ratchkovski, N.A., 2003, Change in stress direction along the central Denali fault, Alaska, after the 2002 earthquake sequence: *Geophysical Research Letters*, v. 30, 2017, doi 10.1029/2003GL017905.

Ratchkovski, N.A., and Hansen, R.A., 2002a, New constraints on tectonics of interior Alaska: Earthquake locations, source mechanisms, and stress regime: *Bulletin of the Seismological Society of America*, v. 92, p. 998-1014.

Ratchkovski, N.A., and Hansen, R.,A., 2002b, New evidence for segmentation of the Alaska subduction zone: *Bulletin of the Seismological Society of America*, v. 92, p. 1754-1765.

Ratchkovski, N.A., Hansen, R., Stachnik, J.C., Cox, T., Fox, O., Rao, L., Clark, E., Lafevers, M., Estes, S., MacCormack, J.B., and Wlliams, T., 2003, Aftershock sequence of the Mw 7.9 Denali, Alaska, earthquake of 3 November 2002 from regional seismic network data: *Seismological Research Letters*, 74, 743-752.

Ratchkovski, N.A., Wiemer, S., and Hansen, R.A., 2004, Seismotectonics of the Central Denali fault, Alaska, and the 2002 Denali fault earthquake sequence: *Bulletin of the Seismological Society of America*, v. 94, no., 6B, p. S156-174.

Redfield, T.F., and Fitzgerald, P.G., 1993, Denali fault system of southern Alaska: An interior strike-slip structure responding to dextral and sinistral shear coupling: *Tectonics*, v. 12, 1195-1208.

Reed, B.L., and Nelson, S.W., 1980, Geologic map of the Talkeetna quadrangle, Alaska: U.S. Geological Survey Miscellaneous Investigations Map I-1174A, 15 p., scale 1:250,000.

Reed, G.L., and Lanphere, M.A., 1974, Offset plutons and history of movement along the McKinley segment of the Denali fault system, Alaska: *Geological Society of America Bulletin*, v. 85, p. 1883-1892.

Reinink-Smith, L.M., and Leopold, E.B., 2005, Warm climate in the late Miocene of the south coast of Alaska and the occurrence of Podocarpaceae pollen: *Palynology*, v. 29, p. 205-262.

Richter, D.H., 1976, Geologic map of the Nabesna quadrangle, Alaska: U.S. Geological Survey Miscellaneous Geological Investigations Series Map I-932, scale 1:250,000.

Richter, D.H., and Matson, N.A., Jr., 1971, Quaternary faulting in the eastern Alaska Range: *Geological Society of America Bulletin*, v. 82, p. 1529-1540.

Richter, D.H., Sharp, W.N., Dutro, J.T., Jr., and Hamilton, W.B., 1977, Geologic map of parts of the Mount Hayes A-1 and A-2 quadrangles, Alaska: U.S. Geological Survey Miscellaneous Investigations Series Map I-1031, 1 sheet, scale 1:63,360.

Ridgway, K.D., Trop, J.M., Nokleberg, W.J., Davidson, C.M., Eastham, K.R., 2002, Mesozoic and Cenozoic tectonics of the eastern and central Alaska Range: progressive basin development and deformation in a suture zone: *Geological Society of America Bulletin*, v. 114, p. 1480-1504.

Ridgway, K.D., Trop, J.M., and Sweet, A.R., 1994, Depositional systems, age, and provenance of the Cantwell Formation, Cantwell Basin, Alaska Range: *Geological Society of America Abstracts with Programs*, v. 26, no. 7, p. A-492.

Ridgway, K.D., Trop, J.M., and Sweet, A.R., 1997, Thrust-top basin formation along a suture zone, Cantwell basin, Alaska Range: Implications for development of the Denali fault system: *Geological Society of America Bulletin*, v. 109, no. 5, p. 505-523.

Robinson, E.S., and Çoruh, C., 1988, *Basic Exploration Geophysics*: John Wiley & Sons, New York.

Rondenay, S., Abers, G.A., and van Keken, P., 2008, Seismic imaging of subduction zone metamorphism: *Geology*, v. 36, no. 4, p. 275-278.

Rossi, G., Abers, G.A., Rondenay, S., and Christensen, D.H., 2006, Unusual mantle Poisson's ratio, subduction, and crustal structure in central Alaska: *Journal of Geophysical Research, v.* 111, B09311, doi: 10.1029/2005JB003956.

Sainsbury, C.L., and Twenhofel, W.S., 1954, Fault patterns in southeastern Alaska: *Geological Society of America Bulletin*, v. 65, p. 1300.

Savage, J.C., and Lisowski, M., 1991, Strain accumulation along the Denali fault at the Nenana river and Delta river crossings: *Journal of Geophysical Research*, v. 96, p. 14,481-14,492.

Savage, J.C., Lisowski, M., and Prescott, W., 1981, Strain accumulation across the Denali fault system in the Delta River Canyon, Alaska: *Journal of Geophysical Research*, v. 86, p. 1005-1014.

Searcy, C., Christensen, D., and Zandt, G., 1996, Velocity Structure beneath College Station Alaska from Receiver Functions: *Bulletin of the Seismological Society of America*, v. 86, p. 232-241.

Sheehan, A.F., Abers, G.A., Jones, C.H., and Lerner-Lam, A.L., 1995, Crustal thickness variations across the Colorado Rocky Mountains from teleseismic receiver functions: *Journal of Geophysical Research*, v. 100, p. 20,391-20,404.

Sherwood, K.W., and Craddock, C., 1979, General geology of the central Alaska Range between the Nenana River and Mount Deborah: Alaska Division of Geological and Geophysical Surveys Open-File Report 116, 22p., 2 plates, scale 1:63,360.

Sherwood, K.W., Brewer, W.M., Craddock, C., Umhoefer, P.J., and Hickman, R.G., 1984, The Denali fault system and terranes of the central Alaska Range region, Alaska: *Geological Society of America Abstracts with Programs*, v. 16, p. 332.

Silberling, N.J., 1985, Paleogeographic significance of the Upper Triassic bivalve Monotis in Circum-Pacific accreted terranes, *in* Howell, D.G., ed., Tectonostratigraphic terranes of the circum-Pacific region: American Association of Petroleum Geologist Circum-Pacific Earth Science Series, no. 1, p. 63-70.

Silberling, N.J., Jones, D.L., Monger, J.W.H., Coney, P.J., Berg, H.C., and Plafker, G., 1994, Lithotectonic terrane map of Alaska and adjacent parts of Canada, *in* Plafker, G., and Berg, H.D., eds., The geology of Alaska: Boulder, Colorado, Geological Society of America, Geology of North America, v. G-1, plate 3, scale 1:2,500,000.

Sipkin, S.C., and Lerner-Lam, A.L., 1992, Pulse-shape distortion introduced by broadband deconvolution: *Bulletin of the Seismological Society of America*, v. 82, p. 238-258.

Smith, T.E., 1981, Geology of the Clearwater Mountains, south-central Alaska: Alaska Division of Geological and Geophysical Surveys Geologic Report 60, 72p.

Smith, T.E., Forbes, R.B., and Turner, D.L., 1974, A solution to the Denali fault offset problem: Alaska Division of Geological and Geophysical Surveys Annual Report, 1973, p. 25-27.

Smith, T.E., and Lanphere, M.A., 1971, Age of the sedimentation, plutonism and regional metamorphism in the Clearwater Mountains region, central Alaska: *Isochron/West*, no. 2, p. 17-20.

St. Amand, P., 1954, Tectonics of Alaska as deduced from seismic data: *Geological Society of America Bulletin*, v. 65, 1350.

St. Amand, P., 1957, Geological and geophysical synthesis of the tectonics of portions of British Columbia, the Yukon Territory, and Alaska: *Geological Society of America Bulletin*, v. 68, p. 1343-1370.

Stachnik, J.C., Abers, G.A., and Christensen, D.H., 2004, Seismic attenuation and mantle wedge temperatures in the Alaska subduction zone: *Journal of Geophysical Research*, v. 109, no. B10, p. B10304.

Stamatakos, J.A., Trop, J.M., and Ridgway, K.D., 2001, Late Cretaceous paleogeography of Wrangellia: Paleomagnetism of the MacColl Ridge Formation, southern Alaska, revisited: *Geology*, v. 29, p. 947-950.

Stanley, W.D., Labson, V.F., Nokleberg, W.J., Csejtey, B., Jr., and Fisher, M.A., 1990, The Denali fault system and Alaska Range of Alaska: Evidence for suturing and thin-skinned tectonics from magnetotellurics: *Geological Society of America Bulletin*, v. 102, p. 160-173.

Stephens, C.S., Fogelman, K.A., Lahr, J.C., and Page, R.A., 1984, Wrangell Benioff Zone, southern Alaska: *Geology*, v. 12, p. 373-376.

Stone, D.B., 1977, Paleomagnetism, plate tectonics, and the northeast Pacific: *Geophysical Surveys*, v. 3, p. 3-37.

Stone, D.B., 1983, Present Day Plate Boundaries in Alaska and the Arctic: *Journal of the Alaska Geological Society*, v. 3, p. 1-14.

Stone, D.B., and Wallace, W.K., 1987, A geological framework of Alaska: *Episodes*, v. 10, no. 4, p. 283-289.

Stone, D.B., Panuska, B.C., and Packer, D.R., 1982, Paleolatitudes versus time for southern Alaska: *Journal of Geophysical Research*, v. 87, no. B5, p. 3697-3707.

Stout, J.H., 1976, Geology of the Eureka Creek area, east-central Alaska Range: Alaska Division of Geological and Geophysical Surveys Geologic Report 46, 32p.

Stout, J.H., and Chase, C.G., 1980, Plate kinematics of the Denali fault system: *Canadian Journal of Earth Sciences*, v. 171, p. 1527-1537.

Stout, J.H., Brady, J.B., Weber, F.R., and Page, R.A., 1973, Evidence of Quaternary movement on the McKinley strand of the Denali in the Delta River area, Alaska: *Geological Society of America Bulletin*, v. 84, no. 3, p. 939-948.

Taber, J.J., Billington, S., and Engdahl, E.R., 1991, Seismicity of the Aleutian arc, *in* Slemmons, D.B., Engdahl, E.R., Zoback, M.D., Zoback, M.L., and Blackwell, D., eds., Neotectonics of North America: Boulder, Colorado, The Geological Society of America, CSM V-1.

Tanimoto, T., 1995, Crustal structure of the earth, *in* Ahrens, T.J., ed., Global earth physics: a handbook of physical constants: Washington, D.C., American Geophysical Union, AGU Reference Shelf 1, 1-14, p. 214-224.

Thoms, E.E., 2000, Late Cenozoic unroofing sequence and foreland basin development of the central Alaska Range: Implications from the Nenana Gravel: University of Alaska Fairbanks, thesis, 221p.

Thorson, R.M., 1979, Recurrent late Quaternary faulting near Healy Alaska: Division of Geological and Geophysical Surveys, Geologic Report, no. 61, p. 10-14.

Turner, D.L., and Smith, T.E., 1974, Geochronology and generalized geology of the central Alaska Range, Clearwater Mountains and northern Talkeetna Mountains: *Alaska Division of Geological and Geophysical Surveys Open-File Report* AOF-72, 10p.

Turner, D.L., Smith, T.E., and Forbes, R.B., 1974, Geochronology of offset along the Denali fault system in Alaska: *Geological Society of America Abstracts with Programs*, v. 6, p. 268-269.

Twenhofel, W.S., and Sainsbury, C.S., 1958, Fault patterns in southeastern Alaska: *Geological Society of America Bulletin*, v. 69, p. 1431-1442.

van der Voo, R., Jones, M., Gromme, D.S., Eberein, G.D., and Churkin, M., Jr., 1980, Paleozoic paleomagnetism and northward drift of the Alexander terrane, southeastern Alaska: *Journal of Geophysical Research*, v. 85, p. 5281-5296.

van Wormer, J.D., Davies, J., and Gedney, L., 1974, Seismicity and plate tectonics in south central Alaska: *Bulletin of the Seismological Society of America*, v. 64, p. 1467-1475.

Veenstra, E., Christensen, D., Abers, G.A., and Ferris, A., 2006, Crustal thickness variation in south-central Alaska: *Geology*, v. 34, no. 9, p. 781-784.

Von Huene, R., 1972, Structure of the continental margin and tectonism at the eastern Aleutian trench: *Geological Society of America Bulletin*, v. 83, p. 3613-3626.

Wahrahaftig, C. Turner, D.L., Weber, F.R., and Smith, T.E., 1975, Nature and timing of movement on the Hines Creek strand of the Denali fault system, Alaska: *Geology*, v. 3, p. 463-466.

Wahrahaftig, C., 1992, Maps of Physiographic Divisions of Alaska, *in* Plafker, G., and Berg, H.D., eds., The geology of Alaska: Boulder, Colorado, Geological Society of America, Geology of North America, v. G-1, plate 2, scale 1:2,500,000.

Wahrhaftig, C., 1970, Geologic map of the Healy D-4 quadrangle, Alaska: *U.S. Geological Survey Geologic Quadrangle Map* GQ-806, scale 1:63,360.

Wahrhaftig, C., Wolfe, J.A., Leopold, E.B., and Lanphere, M.A., 1969, The Coal-bearing Group in the Nenana Coal Field, Alaska: *U.S. Geological Survey Bulletin* 1274-D.

Wallace, W.K., 2008, Yakataga Fold and Thrust Belt: Structural Geometry and Tectonic Implications of a Small Continental Collision Zone, *in* Freymueller, J.T., Haeussler, P.J., Wesson, R.L., and Ekstrom, G., eds., Active Tectonics and Seismic Potential of Alaska, Geophysical Monograph 179, American Geophysical Union, p. 237-256.

Wallace, W.K., and Engebretson, D.C., 1984, Relationships between plate motions and Late Cretaceous to Paleogene magmatism in Southwestern Alaska: *Tectonics*, v. 3, no. 2, p. 295-315.

Wallace, W.K., Hanks, C.L., and Rogers, J.F., 1989, The southern Kahiltna terrane: Implications for the tectonic evolution of southwestern Alaska: *Geological Society of America Bulletin*, v. 101, p. 1389-1407.

Weber, F.R., Foster, H.L., Keith, T.E.C., and Dusel-Bacon, C., 1978, Preliminary geologic map of the Big Delta Quadrangle: *U.S. Geological Survey Open-File Report 78-529A*, scale 1:250,000.

Wessel, P., and Smith, W.H.F., 1995, New version of the generic mapping tools released: *Eos Transactions*, American Geophysical Union, v. 76, p. 329.

Wiggins, R., 1976, A fast, new computational algorithm for free oscillations and surface waves: *Geophysical Journal of the Royal Astronomical Society*, v. 47, p. 135-150.

Wilson, F.H., Dover, J.H., Bradley, D.C., Weber, F.R., Bundtzen, T.K., and Haeussler, P.J., 1998, Geologic Map of Central (Interior) Alaska: *U.S. Geological Survey Open File Report and Map 98-133*, scale 1:500,000, 76 p.

Wolf, L.W., Stone, D.B., and Davies, J.N., 1991, Crustal structure of the active margin, south central Alaska: An interpretation of seismic refraction data from the Trans-Alaska Crustal Transect: *Journal of Geophysical Research*, v. 96, no. B10, p. 16455-16,469.

Woodward-Lundgren and Associates, 1974, Summary report basis for pipeline design for active-fault crossings for the Trans-Alaska pipeline system: unpublished report prepared for Alyeska Pipeline service Company, Houston, Texas, 115 p., appendices.

Wright, T.J., Lu, Z., and Wicks, C., 2003, Source model for the Mw 6.7, 23 October 2002, Nenana Mountain Earthquake (Alaska) from InSAR: *Geophysical Research Letters*, v. 30, 1974, doi 100.1029/2003GL018014.

Yañez, G., Cembrano, J., Pardo, M., Ranero, C., and Selles, D., 2002, The Challenger-Juan Fernandez-Maipo major tectonic transition of the Nazca-Andean subduction system at 33-34°S: Geodynamic evidence and implications: *Journal of South American Earth Science*, v. 15, p. 23-28.

Yole. R.W., and Irving, E., 1980, Displacement of Vancouver Island: Paleomagnetic evidence from the Karmutsen Formation: *Canadian Journal of Earth Sciences*, v. 17, p. 1210-1288.

Zhao, D., and Christensen, D.H., 1992, Tomographic imaging of the crust and upper mantle beneath central and southern Alaska: *Seismological Research Letters*, v. 63, p. 64.

Zhao, D., Christensen, D.H., and Pulpan, H., 1995, Tomographic imaging of the Alaska subduction zone: *Journal of Geophysical Research*, v. 100, no. B4, p. 6478-6504.

Appendix 1: Teleseismic event list

As described in the text, I used events with moment magnitudes $M_w \geq 5.5$. Earthquakes at distances between 29° and 101° from centrally located BEAAR station RND (63.4057°N 211.1399°E) were considered teleseismic events for the purpose of receiver function analysis. The locations and origin times below were used to predict arrival times for each event at each station. The number of stations recording an individual event is listed (n). The list is arranged chronologically by origin time.

latitude (°N)	longitude (°E)	depth (km)	date	(ordinal day)	time	n	Mw
0.053	123.484	161	6/2/1999	(153)	23:19.0	4	5.7
40.802	47.448	33	6/4/1999	(155)	12:50.0	4	5.5
13.897	269.232	33	6/6/1999	(157)	08:05.0	6	6.3
8.586	125.854	33	6/7/1999	(158)	45:49.0	4	5.7
73.017	5.187	10	6/7/1999	(158)	10:33.0	5	5.5
73.077	5.453	10	6/7/1999	(158)	35:46.0	5	5.5
15.040	299.579	54.6	6/8/1999	(159)	04:00.0	5	5.8
-19.281	186.443	33	6/9/1999	(160)	02:04.0	4	5.6
8.592	125.868	33	6/9/1999	(160)	05:32.0	5	5.5
18.386	262.564	70	6/15/1999	(166)	42:05.0	4	7.0
-17.037	186.638	75.3	6/16/1999	(167)	35:59.0	4	5.8
-14.965	184.146	33	6/16/1999	(167)	32:32.0	4	5.9
5.514	126.639	33	6/18/1999	(169)	55:25.0	4	6.4
-5.414	146.879	208.5	6/19/1999	(170)	03:09.0	4	5.7
8.228	141.301	33	6/21/1999	(172)	35:46.0	4	5.6
36.388	70.707	230.2	6/21/1999	(172)	37:27.0	4	5.5
18.324	258.461	68.7	6/21/1999	(172)	43:04.0	4	6.3
-4.508	133.947	33	6/22/1999	(173)	47:42.0	4	5.7
19.279	145.575	103	6/23/1999	(174)	37:22.0	3	5.6
3.802	126.347	33	6/25/1999	(176)	12:29.0	4	5.6
30.098	69.444	33	6/26/1999	(177)	54:10.0	5	5.6
-17.956	181.813	590.4	6/26/1999	(177)	05:28.0	5	6.0
36.622	71.353	189.3	6/29/1999	(180)	18:05.0	6	5.7
70.386	344.848	10	7/1/1999	(182)	06:58.0	1	5.5
70.280	344.649	10	7/1/1999	(182)	08:02.0	1	5.7
26.323	140.482	430.6	7/3/1999	(184)	30:10.0	5	6.1
49.233	155.559	33	7/7/1999	(188)	52:57.0	4	6.1
-30.247	181.869	116.5	7/8/1999	(189)	04:49.0	1	5.7
-6.514	154.944	29	7/9/1999	(190)	04:42.0	4	6.3
-20.095	181.840	567	7/9/1999	(190)	16:20.0	4	5.6
15.782	271.670	10	7/11/1999	(192)	14:16.0	5	6.7
30.069	69.419	51.5	7/12/1999	(193)	42:16.0	5	5.7
5.513	126.709	33	7/12/1999	(193)	57:59.0	5	5.7
13.749	269.580	70	7/13/1999	(194)	02:30.0	5	5.6
-18.230	168.178	33	7/15/1999	(196)	26:25.0	4	5.5
-22.546	179.412	590.9	7/18/1999	(199)	34:03.0	4	6.0
-28.629	182.392	39	7/19/1999	(200)	17:03.0	4	6.5
26.904	141.455	89.5	7/20/1999	(201)	53:24.0	3	5.6
-18.289	182.094	560.8	7/21/1999	(202)	10:44.0	4	5.7
4.567	97.211	175	7/21/1999	(202)	46:29.0	4	5.6
-5.151	151.942	69.4	7/26/1999	(207)	33:20.0	4	6.2
40.780	141.675	104.1	7/26/1999	(207)	45:47.0	3	5.7
-2.979	150.494	33	7/26/1999	(207)	48:34.0	3	5.6

latitude (°N)	longitude (°E)	depth (km)	date	(ordinal day)	time	n	Mw
-3.046	150.572	33	7/26/1999	(207)	18:34.0	2	5.5
-15.201	186.676	33	7/27/1999	(208)	30:20.0	5	5.5
-28.690	182.477	33	7/28/1999	(209)	16:57.0	6	6.1
-30.285	181.986	25	7/28/1999	(209)	08:20.0	7	6.3
29.999	69.397	33	7/28/1999	(209)	17:12.0	7	5.5
5.201	277.421	10	7/31/1999	(212)	11:35.0	7	5.5
-30.367	182.168	10	8/1/1999	(213)	39:04.0	6	6.5
37.390	242.920	7.6	8/1/1999	(213)	06:22.0	7	5.7
-12.550	167.175	251.2	8/2/1999	(214)	47:12.0	7	5.7
-3.453	280.838	88.1	8/3/1999	(215)	58:57.0	7	5.9
49.933	156.261	57.8	8/6/1999	(218)	32:41.0	6	5.9
-21.086	183.941	33	8/7/1999	(219)	17:28.0	7	5.6
9.346	276.033	33	8/10/1999	(222)	55:42.0	5	5.6
34.791	32.939	33	8/11/1999	(223)	27:55.0	6	5.6
-18.721	183.118	33	8/12/1999	(224)	25:06.0	5	5.5
-1.716	122.456	33	8/12/1999	(224)	44:59.0	6	6.2
-0.688	127.273	79.7	8/12/1999	(224)	43:46.0	3	5.6
-1.776	122.492	33	8/13/1999	(225)	12:20.0	6	5.6
-5.396	152.529	33	8/15/1999	(227)	50:12.0	5	5.9
9.044	275.841	20	8/20/1999	(232)	02:21.0	6	6.9
34.024	135.405	65.5	8/20/1999	(232)	33:10.0	6	5.7
-20.389	186.243	33	8/21/1999	(233)	58:05.0	6	5.7
8.918	276.062	24.2	8/21/1999	(233)	49:51.0	6	5.8
-16.117	168.039	33	8/22/1999	(234)	40:45.0	6	6.6
-19.059	169.612	263.4	8/25/1999	(237)	06:22.0	5	5.7
10.376	126.006	62.6	8/26/1999	(238)	24:42.0	7	5.9
-3.522	145.657	33	8/26/1999	(238)	39:28.0	7	6.2
-3.472	145.611	33	8/26/1999	(238)	02:17.0	5	5.8
19.119	121.152	33	8/26/1999	(238)	38:11.0	7	5.7
-1.287	282.451	196.4	8/28/1999	(240)	40:06.0	7	6.3
38.119	23.605	10	9/7/1999	(250)	56:49.0	7	6.0
7.138	123.678	117.9	9/8/1999	(251)	29:00.0	4	5.5
47.506	154.334	33	9/9/1999	(252)	02:01.0	6	5.5
46.024	150.260	91.2	9/10/1999	(253)	45:23.0	7	5.7
28.970	142.053	33	9/12/1999	(255)	03:18.0	6	5.9
-3.636	149.515	56.7	9/13/1999	(256)	43:19.0	2	5.6
40.709	30.045	13	9/13/1999	(256)	55:28.0	7	5.9
15.090	146.223	91.5	9/14/1999	(257)	17:24.0	7	5.5
-13.790	167.238	196.8	9/17/1999	(260)	54:48.0	6	6.3
-14.408	181.790	33	9/17/1999	(260)	48:11.0	6	5.5
-4.422	255.556	10	9/18/1999	(261)	01:04.0	1	5.6
-6.443	147.799	48.8	9/18/1999	(261)	50:58.0	6	5.6
51.207	157.556	60	9/18/1999	(261)	28:33.0	6	6.0
-19.713	169.205	102.8	9/18/1999	(261)	51:30.0	6	5.9
46.419	153.377	45.6	9/19/1999	(262)	27:23.0	1	5.8
-3.624	150.875	430.5	9/19/1999	(262)	18:54.0	6	5.9
46.334	153.463	33	9/20/1999	(263)	32:42.0	5	5.5
23.772	120.982	33	9/20/1999	(263)	47:18.0	2	7.7
23.390	120.964	33	9/20/1999	(263)	46:42.0	6	6.4
23.729	121.167	26	9/22/1999	(265)	14:39.0	6	6.4
23.642	121.136	33	9/22/1999	(265)	49:42.0	6	5.8
23.738	121.158	17	9/25/1999	(268)	52:48.0	6	6.5
2.667	127.914	33	9/27/1999	(270)	42:49.0	5	5.7

latitude (°N)	longitude (°E)	depth (km)	date	(ordinal day)	time	n	Mw
16.059	263.069	60.6	9/30/1999	(273)	31:15.0	6	7.5
-0.279	122.702	64.4	10/1/1999	(274)	24:00.0	5	5.8
40.186	143.040	33	10/2/1999	(275)	08:41.0	5	5.6
-13.357	248.686	10	10/3/1999	(276)	10:14.0	6	5.7
-10.685	284.365	33	10/4/1999	(277)	57:38.0	6	5.6
36.730	28.240	33	10/5/1999	(278)	53:28.0	3	5.6
51.207	157.610	76.7	10/5/1999	(278)	01:35.0	6	5.6
-6.158	149.287	57.7	10/7/1999	(280)	27:07.0	5	5.7
-21.054	185.505	33	10/8/1999	(281)	09:48.0	6	5.7
-21.890	183.283	183.8	10/8/1999	(281)	13:16.0	6	5.6
-1.990	134.279	33	10/10/1999	(283)	03:04.0	5	6.1
-21.116	185.511	33	10/12/1999	(285)	27:45.0	5	5.7
-3.407	150.948	33	10/12/1999	(285)	46:01.0	5	5.5
-14.281	289.516	202.2	10/14/1999	(287)	00:49.0	6	5.5
-6.940	129.336	189	10/20/1999	(293)	28:52.0	5	5.8
13.726	125.197	42.7	10/21/1999	(294)	15:22.0	5	5.6
23.445	120.506	33	10/22/1999	(295)	18:58.0	6	5.9
23.433	120.508	33	10/22/1999	(295)	10:19.0	5	5.6
-4.808	153.414	83.3	10/23/1999	(296)	12:05.0	6	6.3
44.612	149.440	33	10/24/1999	(297)	21:41.0	6	6.4
-19.442	186.120	33	10/25/1999	(298)	01:20.0	6	5.9
-2.119	134.192	33	10/25/1999	(298)	43:06.0	6	5.5
31.971	142.251	33	10/25/1999	(298)	29:55.0	5	5.8
-23.681	248.385	10	10/27/1999	(300)	09:30.0	3	5.6
39.463	144.682	33	10/28/1999	(301)	58:40.0	6	5.5
-15.838	186.272	33	10/30/1999	(303)	43:21.0	5	5.7
-33.057	180.460	33	10/30/1999	(303)	16:40.0	3	5.5
23.378	121.520	33	11/1/1999	(305)	53:00.0	6	6.3
-15.761	187.462	33	11/3/1999	(307)	50:24.0	5	5.6
36.522	71.240	228.4	11/8/1999	(312)	45:43.0	7	6.5
35.726	61.205	25.9	11/8/1999	(312)	37:23.0	6	5.5
-6.410	252.767	10	11/10/1999	(314)	25:38.0	4	5.6
49.315	155.633	33	11/11/1999	(315)	41:05.0	6	6.4
40.744	30.266	22	11/11/1999	(315)	41:25.0	7	5.7
1.276	100.322	211	11/11/1999	(315)	05:43.0	7	6.2
40.758	31.161	10	11/12/1999	(316)	57:19.0	7	7.3
38.304	142.309	50.6	11/15/1999	(319)	34:35.0	6	5.6
-5.978	148.820	47.5	11/17/1999	(321)	27:42.0	7	6.9
-6.004	148.803	45.3	11/17/1999	(321)	36:34.0	7	6.3
-6.576	148.672	54.8	11/18/1999	(322)	20:22.0	5	5.7
0.523	126.066	33	11/18/1999	(322)	27:42.0	7	5.9
-6.429	148.533	33	11/19/1999	(323)	21:28.0	1	5.9
-6.351	148.763	33	11/19/1999	(323)	56:46.0	7	7.0
18.544	252.832	33	11/21/1999	(325)	46:19.0	1	6.1
-16.152	186.943	33	11/22/1999	(326)	45:20.0	7	5.5
-0.944	121.487	33	11/25/1999	(329)	00:09.0	5	5.7
-30.234	182.322	33	11/26/1999	(330)	56:07.0	6	5.8
-16.423	168.214	33	11/26/1999	(330)	21:15.0	7	7.5
-15.576	167.918	33	11/26/1999	(330)	03:20.0	7	5.9
-14.529	288.709	126.4	11/27/1999	(331)	31:49.0	7	5.9
-4.692	153.016	89.4	11/27/1999	(331)	41:11.0	7	5.9
0.581	126.205	33	11/28/1999	(332)	53:42.0	1	5.6
0.565	126.110	33	11/29/1999	(333)	07:02.0	1	5.6

latitude (°N)	longitude (°E)	depth (km)	date	(ordinal day)	time	n	Mw
-21.284	169.105	33	11/30/1999	(334)	23:34.0	7	5.8
-21.325	181.338	547.9	11/30/1999	(334)	10:22.0	7	5.8
17.647	277.644	10	12/1/1999	(335)	23:06.0	7	6.3
-22.031	169.977	33	12/1/1999	(335)	45:22.0	1	5.6
10.961	289.659	10	12/2/1999	(336)	33:00.0	7	5.5
-10.961	164.235	33	12/2/1999	(336)	54:42.0	1	5.5
40.358	42.346	19.3	12/3/1999	(337)	06:54.0	2	5.7
57.667	327.420	10	12/4/1999	(338)	01:34.0	1	5.6
3.282	128.088	33	12/4/1999	(338)	45:01.0	7	5.7
57.812	327.272	10	12/5/1999	(339)	21:51.0	6	5.5
29.920	138.689	448.9	12/5/1999	(339)	00:34.0	7	5.7
-15.911	186.016	137.7	12/7/1999	(341)	29:49.0	7	6.4
-9.843	159.965	33	12/8/1999	(342)	34:44.0	6	6.0
-6.028	148.144	58.3	12/9/1999	(343)	18:17.0	7	6.4
-22.303	179.613	599.9	12/10/1999	(344)	34:45.0	7	5.6
-13.912	167.188	202.8	12/11/1999	(345)	18:41.0	6	5.7
-17.715	181.207	558.2	12/11/1999	(345)	38:06.0	7	5.7
15.766	119.740	33	12/11/1999	(345)	03:36.0	7	7.3
14.765	268.814	157.5	12/12/1999	(346)	57:28.0	7	5.8
-2.889	128.155	33	12/12/1999	(346)	24:18.0	2	5.6
2.077	127.115	84.6	12/13/1999	(347)	30:39.0	7	5.8
-0.138	125.119	66.3	12/13/1999	(347)	40:13.0	6	5.8
17.189	274.866	10	12/15/1999	(349)	00:44.0	7	5.7
-5.786	150.974	33	12/15/1999	(349)	41:12.0	7	6.3
7.982	322.032	10	12/17/1999	(351)	00:25.0	1	5.5
8.069	321.974	10	12/17/1999	(351)	03:27.0	1	5.6
-2.425	139.675	16.2	12/18/1999	(352)	44:55.0	7	6.2
12.870	144.571	50.9	12/19/1999	(353)	48:36.0	7	6.0
-3.986	131.331	33	12/19/1999	(353)	38:32.0	2	5.8
-4.579	151.234	33	12/19/1999	(353)	19:25.0	2	5.7
55.830	110.029	10	12/21/1999	(355)	00:48.0	7	5.5
-10.885	165.457	33	12/22/1999	(356)	32:37.0	1	6.0
35.321	358.719	10	12/22/1999	(356)	36:56.0	7	5.6
-0.625	268.118	10	12/22/1999	(356)	08:07.0	4	5.7
-6.130	284.729	26.6	12/25/1999	(359)	19:30.0	7	5.5
-27.992	183.208	33	12/25/1999	(359)	38:50.0	7	5.7
5.609	277.355	10	12/28/1999	(362)	46:58.0	6	6.2
1.674	128.288	65.5	12/28/1999	(362)	51:24.0	6	5.7
-11.150	165.543	33	12/28/1999	(362)	56:06.0	6	5.8
18.244	258.568	69.9	12/29/1999	(363)	19:46.0	6	5.9
-10.860	165.354	33	12/29/1999	(363)	29:19.0	6	6.9
-10.980	165.251	33	12/29/1999	(363)	15:51.0	2	5.9
-11.210	165.321	33	12/29/1999	(363)	59:31.0	5	5.7
-10.938	165.258	33	12/29/1999	(363)	36:37.0	5	5.7
-11.165	165.330	33	12/29/1999	(363)	53:57.0	6	6.2
47.579	154.508	33	12/30/1999	(364)	21:36.0	5	5.6
37.269	134.664	371.4	12/31/1999	(365)	09:11.0	6	5.6
-17.943	181.524	582.3	1/2/2000	(2)	14:39.0	5	5.5
-20.771	185.764	33	1/2/2000	(2)	16:32.0	6	5.8
-20.964	185.903	33	1/5/2000	(5)	32:19.0	6	5.6
-11.371	165.378	33	1/5/2000	(5)	40:40.0	6	6.1
-11.462	165.413	33	1/5/2000	(5)	41:40.0	5	5.5
32.222	92.700	33	1/5/2000	(5)	45:18.0	5	5.5

latitude (°N)	longitude (°E)	depth (km)	date	(ordinal day)	time	n	Mw
16.095	119.484	33	1/6/2000	(6)	31:06.0	6	6.2
-9.805	159.811	33	1/8/2000	(8)	19:46.0	5	6.4
-16.925	185.752	183.4	1/8/2000	(8)	47:20.0	6	7.2
-2.476	140.350	10	1/9/2000	(9)	48:30.0	6	5.5
-18.823	174.370	33	1/9/2000	(9)	54:40.0	4	6.5
27.350	139.979	453.2	1/10/2000	(10)	40:42.0	6	5.7
-17.610	181.258	535	1/13/2000	(13)	07:14.0	6	6.2
-15.285	186.475	33	1/14/2000	(14)	44:44.0	5	5.5
25.591	101.164	33	1/14/2000	(14)	09:04.0	5	5.5
25.607	101.063	33	1/14/2000	(14)	37:07.0	4	5.9
-6.345	148.430	72.4	1/15/2000	(15)	04:00.0	5	5.8
-21.216	180.745	632.8	1/15/2000	(15)	49:45.0	6	6.0
-30.238	181.867	33	1/16/2000	(16)	00:40.0	5	5.8
-11.656	166.317	39.5	1/16/2000	(16)	19:42.0	6	5.7
-11.593	166.301	33	1/17/2000	(17)	04:00.0	6	5.7
6.785	288.029	33	1/17/2000	(17)	20:05.0	7	5.6
-14.512	182.404	33	1/17/2000	(17)	18:04.0	7	5.8
-14.319	182.325	33	1/18/2000	(18)	31:36.0	5	5.5
36.372	70.379	206.9	1/19/2000	(19)	09:33.0	7	6.0
-28.227	183.437	33	1/20/2000	(20)	59:23.0	4	5.8
-6.261	147.555	33	1/20/2000	(20)	54:34.0	4	5.5
13.147	125.755	33	1/21/2000	(21)	12:00.0	7	5.5
-7.967	120.613	46.8	1/23/2000	(23)	08:24.0	5	5.8
30.239	130.768	42.9	1/23/2000	(23)	40:04.0	6	5.5
-7.973	120.646	46.3	1/23/2000	(23)	03:01.0	6	5.6
-17.513	183.269	33	1/23/2000	(23)	57:02.0	5	5.8
-17.207	182.774	33	1/23/2000	(23)	14:46.0	4	5.5
-17.272	185.998	33	1/26/2000	(26)	26:50.0	7	6.3
-7.485	122.678	574.9	1/28/2000	(28)	17:52.0	4	5.5
43.046	146.837	61.1	1/28/2000	(28)	21:07.0	7	6.8
26.076	124.496	193.9	1/28/2000	(28)	39:24.0	7	6.0
-9.691	118.764	83.4	1/28/2000	(28)	57:51.0	4	5.6
13.572	121.546	33	2/3/2000	(34)	42:25.0	6	5.5
75.271	10.195	10	2/3/2000	(34)	53:12.0	5	5.5
1.295	126.272	33	2/6/2000	(37)	08:07.0	5	5.5
-5.844	150.876	33	2/6/2000	(37)	33:52.0	7	6.6
0.931	126.242	50.3	2/10/2000	(41)	03:35.0	5	5.5
-15.893	185.197	226.6	2/12/2000	(43)	39:54.0	7	5.9
-6.573	155.009	33	2/12/2000	(43)	29:20.0	7	5.9
42.853	131.572	513.6	2/13/2000	(44)	57:08.0	7	6.0
5.694	127.068	141.4	2/13/2000	(44)	19:42.0	7	5.7
17.675	145.401	521.5	2/15/2000	(46)	05:00.0	7	5.9
-10.806	166.570	33	2/16/2000	(47)	35:21.0	6	5.6
-10.905	166.687	33	2/17/2000	(48)	54:26.0	5	5.9
16.569	313.416	10	2/18/2000	(49)	06:15.0	6	5.6
8.854	275.874	20	2/20/2000	(51)	27:22.0	6	5.7
-6.279	154.758	54.7	2/21/2000	(52)	36:21.0	5	5.7
18.562	252.926	33	2/21/2000	(52)	29:40.0	7	5.7
21.611	143.631	33	2/22/2000	(53)	37:55.0	5	5.5
-5.322	154.160	99.4	2/23/2000	(54)	57:58.0	5	5.6
17.387	299.237	33	2/23/2000	(54)	20:26.0	5	5.5
-19.528	173.818	33	2/25/2000	(56)	43:58.0	7	7.1
-20.053	174.363	33	2/25/2000	(56)	54:12.0	7	5.6

latitude (°N)	longitude (°E)	depth (km)	date	(ordinal day)	time	n	Mw
-19.826	174.195	33	2/25/2000	(56)	16:01.0	6	5.5
13.795	144.782	132.2	2/26/2000	(57)	11:48.0	7	6.2
9.406	281.468	65	2/26/2000	(57)	24:39.0	7	6.1
-21.762	184.710	33	2/28/2000	(59)	45:08.0	5	5.7
-17.588	181.016	538	2/28/2000	(59)	15:20.0	5	6.0
-18.158	169.014	33	2/29/2000	(60)	44:58.0	1	6.0
-19.005	180.639	675	3/1/2000	(61)	21:01.0	6	5.8
-19.103	180.639	671.9	3/1/2000	(61)	46:29.0	7	5.6
-7.321	128.491	141.9	3/3/2000	(63)	09:13.0	7	6.4
-6.817	143.807	10	3/3/2000	(63)	22:40.0	7	6.6
-3.876	151.359	33	3/9/2000	(69)	14:59.0	5	5.5
4.738	96.007	33	3/10/2000	(70)	32:12.0	1	5.5
14.975	267.556	62	3/12/2000	(72)	21:30.0	7	6.3
-24.362	178.983	551.9	3/18/2000	(78)	22:52.0	6	5.5
-6.212	147.587	95.5	3/20/2000	(80)	02:30.0	1	5.5
3.155	128.034	102.7	3/21/2000	(81)	26:07.0	7	5.9
-14.558	167.273	168.7	3/22/2000	(82)	32:26.0	6	5.5
27.551	248.697	10	3/24/2000	(84)	23:45.0	5	5.6
-16.193	187.088	33	3/27/2000	(87)	35:00.0	4	5.6
22.338	143.730	126.5	3/28/2000	(88)	00:22.0	6	7.6
-28.127	183.691	10	3/29/2000	(89)	13:53.0	1	5.7
-17.899	181.355	608.1	4/1/2000	(92)	10:49.0	6	5.6
-17.756	181.246	555.8	4/1/2000	(92)	13:24.0	5	5.7
-15.861	185.863	104.9	4/2/2000	(93)	57:24.0	5	5.6
0.267	122.051	187	4/3/2000	(94)	55:00.0	6	5.5
4.082	125.610	150	4/3/2000	(94)	20:01.0	7	6.2
34.220	25.690	38	4/5/2000	(96)	36:58.0	5	5.6
-7.206	129.193	153.2	4/7/2000	(98)	55:46.0	3	5.5
-18.271	184.728	207.6	4/7/2000	(98)	42:23.0	6	5.7
1.091	120.151	33	4/8/2000	(99)	28:23.0	1	5.6
-27.944	181.614	201.2	4/11/2000	(102)	41:26.0	5	5.8
-15.568	186.667	54.5	4/11/2000	(102)	56:59.0	6	5.7
10.301	126.523	33	4/13/2000	(104)	54:14.0	6	5.9
-18.702	186.314	65.4	4/16/2000	(107)	25:48.0	6	5.6
-22.169	180.647	539.3	4/17/2000	(108)	25:20.0	6	5.6
3.959	128.269	56.6	4/17/2000	(108)	08:17.0	6	5.5
3.913	128.215	86.3	4/17/2000	(108)	07:22.0	5	5.5
4.022	128.455	33	4/18/2000	(109)	23:15.0	5	5.6
-20.664	183.531	220.7	4/18/2000	(109)	28:12.0	6	6.0
35.667	135.486	346.5	4/21/2000	(112)	06:16.0	6	5.5
37.842	29.328	33	4/21/2000	(112)	23:10.0	1	5.5
40.178	143.236	33	4/26/2000	(117)	55:04.0	1	5.6
-33.619	180.988	33	4/26/2000	(117)	54:07.0	1	5.5
-6.407	282.943	124.6	4/29/2000	(120)	52:21.0	6	5.7
-3.986	146.556	10	4/30/2000	(121)	08:35.0	4	5.9
38.176	73.053	140.5	5/1/2000	(122)	41:41.0	6	5.6
-15.540	182.479	400.6	5/2/2000	(123)	58:34.0	6	5.5
17.439	147.516	55	5/2/2000	(123)	03:36.0	6	6.0
-1.105	123.573	26	5/4/2000	(125)	21:16.0	6	7.6
-17.914	181.478	515.8	5/4/2000	(125)	36:32.0	6	6.5
17.513	147.629	33	5/4/2000	(125)	24:37.0	5	5.5
-1.215	123.359	33	5/5/2000	(126)	24:26.0	1	5.7
-11.295	165.432	12	5/6/2000	(127)	44:13.0	6	6.3

latitude (°N)	longitude (°E)	depth (km)	date	(ordinal day)	time	n	Mw
-15.227	186.386	33	5/7/2000	(128)	47:39.0	6	5.7
-2.540	122.551	31.3	5/7/2000	(128)	21:12.0	3	5.6
11.045	124.733	11.5	5/8/2000	(129)	25:23.0	3	5.6
-4.457	150.004	502	5/8/2000	(129)	28:25.0	6	6.1
11.045	124.771	10	5/8/2000	(129)	54:57.0	5	5.5
-31.319	179.839	383.1	5/8/2000	(129)	35:42.0	4	5.6
35.975	70.657	107.7	5/12/2000	(133)	10:29.0	6	6.3
-1.420	123.354	33	5/14/2000	(135)	47:43.0	6	5.6
-4.296	123.164	33	5/14/2000	(135)	08:34.0	6	6.3
-23.775	179.956	547.6	5/20/2000	(141)	59:35.0	5	5.6
71.190	351.737	10	5/21/2000	(142)	58:47.0	9	5.9
-4.096	278.904	33	5/22/2000	(143)	15:08.0	10	5.8
36.042	22.012	33	5/24/2000	(145)	40:37.0	8	5.7
11.359	139.245	33	5/26/2000	(147)	30:04.0	11	6.0
38.922	20.640	0	5/26/2000	(147)	28:22.0	4	5.6
35.552	140.464	62.3	6/3/2000	(155)	54:49.0	23	6.1
40.693	32.992	10	6/6/2000	(158)	41:49.0	26	6.0
37.012	103.791	10	6/6/2000	(158)	59:09.0	23	5.6
29.424	131.421	33	6/6/2000	(158)	57:02.0	26	6.4
36.829	135.464	10	6/6/2000	(158)	16:42.0	26	5.9
4.943	126.820	86.1	6/7/2000	(159)	45:37.0	18	5.5
26.856	97.238	33	6/7/2000	(159)	46:55.0	25	6.3
14.207	267.944	58.8	6/8/2000	(160)	08:11.0	23	5.5
-5.071	152.495	33	6/9/2000	(161)	27:15.0	24	6.3
-11.301	162.062	33	6/9/2000	(161)	41:59.0	12	6.0
30.472	137.682	472.6	6/9/2000	(161)	35:13.0	24	5.8
30.491	137.730	485.3	6/9/2000	(161)	31:45.0	25	6.3
-17.565	187.385	33	6/10/2000	(162)	49:47.0	26	5.5
-11.448	166.239	33	6/10/2000	(162)	17:53.0	27	5.9
-4.695	153.134	76.8	6/10/2000	(162)	11:59.0	21	5.5
23.843	121.225	33	6/10/2000	(162)	23:29.0	27	6.4
17.315	120.200	63	6/14/2000	(166)	44:28.0	31	5.7
-25.516	178.046	604.6	6/14/2000	(166)	15:25.0	32	6.4
46.640	152.587	33	6/14/2000	(166)	11:07.0	31	5.5
4.542	127.722	89.5	6/14/2000	(166)	00:48.0	32	6.3
-17.902	176.212	33	6/14/2000	(166)	01:14.0	30	5.9
29.368	132.082	10	6/15/2000	(167)	10:46.0	29	6.1
-28.876	181.536	222.6	6/16/2000	(168)	23:33.0	19	5.6
63.966	339.513	10	6/17/2000	(169)	40:41.0	35	6.8
16.967	120.408	33	6/19/2000	(171)	59:34.0	36	5.7
14.011	120.532	115	6/19/2000	(171)	34:57.0	36	5.6
63.980	339.242	10	6/21/2000	(173)	51:46.0	37	6.5
14.112	144.962	112.2	6/21/2000	(173)	25:06.0	36	5.9
-27.882	183.617	33	6/21/2000	(173)	28:04.0	18	5.5
1.279	126.266	65.3	6/23/2000	(175)	01:54.0	36	5.8
31.183	131.206	10	6/25/2000	(177)	34:42.0	35	6.0
-7.096	125.906	496.1	6/27/2000	(179)	37:05.0	29	5.8
34.056	139.561	10	6/29/2000	(181)	02:36.0	27	5.5
34.027	139.359	10	6/29/2000	(181)	30:22.0	35	5.6
13.031	144.538	52.4	6/29/2000	(181)	59:06.0	35	5.9
34.221	139.131	10	7/1/2000	(183)	01:55.0	35	6.1
34.076	139.226	10	7/2/2000	(184)	03:34.0	30	5.7
20.240	122.163	33	7/4/2000	(186)	19:44.0	21	5.6

latitude (°N)	longitude (°E)	depth (km)	date	(ordinal day)	time	n	Mw
34.053	139.126	10	7/8/2000	(190)	57:44.0	33	5.9
-16.209	182.318	33	7/9/2000	(191)	42:27.0	30	5.9
46.828	145.422	359.6	7/10/2000	(192)	58:18.0	32	5.8
-18.343	184.417	251.9	7/13/2000	(195)	41:54.0	31	5.6
34.319	139.260	10	7/15/2000	(197)	30:30.0	29	6.0
-7.027	128.931	217.9	7/15/2000	(197)	13:44.0	31	5.9
20.253	122.043	33	7/16/2000	(198)	21:45.0	29	6.4
-4.193	138.912	33	7/16/2000	(198)	38:18.0	29	5.7
-12.404	166.509	33	7/16/2000	(198)	25:23.0	28	6.1
36.283	70.924	141.4	7/17/2000	(199)	53:47.0	28	6.3
17.905	120.782	33	7/18/2000	(200)	59:16.0	29	5.7
36.510	140.983	47.1	7/20/2000	(202)	39:18.0	25	6.0
9.416	274.671	33	7/21/2000	(203)	53:35.0	28	6.4
35.181	141.066	52.4	7/21/2000	(203)	16:37.0	27	5.7
9.287	274.820	33	7/21/2000	(203)	46:27.0	28	5.5
18.414	261.084	80.1	7/21/2000	(203)	13:41.0	27	5.9
35.229	323.955	10	7/22/2000	(204)	50:00.0	2	5.5
34.126	139.116	10	7/23/2000	(205)	52:44.0	27	5.6
34.208	139.370	10	7/27/2000	(209)	49:53.0	28	5.6
34.204	139.248	10	7/27/2000	(209)	12:50.0	27	5.5
-12.360	166.490	37.3	7/28/2000	(210)	38:33.0	29	5.8
23.359	120.915	33	7/28/2000	(210)	28:12.0	24	5.6
33.933	139.350	10	7/30/2000	(212)	18:00.0	25	5.7
-10.935	165.934	45.6	7/30/2000	(212)	03:32.0	25	5.6
33.901	139.376	10	7/30/2000	(212)	25:45.0	26	6.5
-16.697	174.542	10	7/31/2000	(213)	44:30.0	26	6.2
-29.279	183.650	10	7/31/2000	(213)	01:49.0	21	6.2
-16.817	174.361	33	8/1/2000	(214)	21:37.0	22	5.8
-17.945	185.180	191.2	8/2/2000	(215)	37:16.0	24	5.6
-12.037	166.448	33	8/3/2000	(216)	09:38.0	25	6.6
31.078	131.308	35	8/3/2000	(216)	30:12.0	21	5.6
0.482	121.286	101.3	8/3/2000	(216)	53:19.0	15	5.6
0.152	126.438	114.8	8/4/2000	(217)	47:44.0	15	5.6
48.786	142.246	10	8/4/2000	(217)	13:02.0	27	6.8
-6.377	130.209	140.5	8/5/2000	(218)	30:10.0	18	5.5
-5.845	130.309	171.2	8/5/2000	(218)	43:07.0	19	5.5
28.856	139.556	394.8	8/6/2000	(219)	27:12.0	25	7.4
29.025	131.207	33	8/7/2000	(220)	23:40.0	18	5.7
-7.018	123.357	648.5	8/7/2000	(220)	33:55.0	27	6.5
-11.864	166.135	33	8/7/2000	(220)	29:49.0	14	5.7
-15.693	167.986	33	8/9/2000	(222)	08:41.0	31	6.3
18.198	257.520	45.8	8/9/2000	(222)	41:47.0	30	6.5
-16.797	174.332	33	8/9/2000	(222)	55:59.0	28	6.4
-3.072	136.112	33	8/12/2000	(225)	26:15.0	31	6.0
8.369	256.043	10	8/12/2000	(225)	13:09.0	30	5.6
12.078	277.081	10	8/13/2000	(226)	04:06.0	27	5.5
-9.377	153.854	10	8/14/2000	(227)	11:16.0	30	6.0
-31.511	179.725	357.7	8/15/2000	(228)	30:08.0	31	6.6
43.046	146.759	33	8/15/2000	(228)	20:43.0	25	5.8
-21.901	185.229	33	8/17/2000	(230)	04:29.0	28	5.8
-16.887	187.341	33	8/17/2000	(230)	59:59.0	28	5.6
5.772	94.753	68.3	8/17/2000	(230)	40:09.0	18	5.7
34.127	139.180	10	8/18/2000	(231)	52:20.0	28	5.7

latitude (°N)	longitude (°E)	depth (km)	date	(ordinal day)	time	n	Mw
36.244	141.420	33	8/19/2000	(232)	41:28.0	23	5.5
43.816	147.167	62.4	8/19/2000	(232)	26:27.0	24	5.7
7.427	126.549	174.3	8/20/2000	(233)	55:49.0	29	5.6
-1.397	123.134	33	8/20/2000	(233)	38:30.0	20	5.5
-6.274	154.664	70.4	8/22/2000	(235)	51:29.0	28	5.7
38.117	57.376	10	8/22/2000	(235)	55:13.0	17	5.9
21.335	251.186	10	8/23/2000	(236)	46:11.0	23	5.5
-17.517	180.936	548.9	8/27/2000	(240)	22:27.0	29	5.5
22.219	143.760	99.6	8/27/2000	(240)	19:06.0	27	5.6
4.352	126.579	88.1	8/28/2000	(241)	37:02.0	26	5.6
-4.110	127.394	16	8/28/2000	(241)	05:47.0	26	6.8
-3.986	127.325	10	8/28/2000	(241)	38:06.0	26	6.1
-4.124	127.027	33	8/28/2000	(241)	29:32.0	27	6.3
5.069	123.212	588.3	8/31/2000	(244)	24:11.0	27	5.7
1.438	96.591	33	9/1/2000	(245)	56:51.0	28	6.0
-5.053	133.611	33	9/2/2000	(246)	25:48.0	27	5.5
-17.917	181.675	587.5	9/2/2000	(246)	19:13.0	25	5.7
-20.073	180.865	687.6	9/2/2000	(246)	02:19.0	25	6.0
-20.547	182.179	363.8	9/3/2000	(247)	21:23.0	28	5.8
43.024	146.773	52.7	9/3/2000	(247)	01:31.0	28	5.5
7.183	122.094	32.9	9/8/2000	(252)	41:25.0	29	5.5
6.422	95.456	229.3	9/9/2000	(253)	01:53.0	4	5.7
-22.763	184.655	33	9/9/2000	(253)	00:33.0	26	5.6
13.690	120.174	65.6	9/10/2000	(254)	16:15.0	25	5.5
24.008	121.526	34.8	9/10/2000	(254)	54:45.0	27	5.8
-1.179	129.348	33	9/10/2000	(254)	11:55.0	21	5.5
-1.112	129.332	33	9/10/2000	(254)	06:15.0	30	6.1
-15.877	186.309	115.4	9/11/2000	(255)	17:53.0	30	6.3
35.389	99.343	10	9/12/2000	(256)	27:58.0	29	6.1
-15.742	179.801	33	9/14/2000	(258)	59:57.0	30	6.2
-22.468	183.668	109.5	9/14/2000	(258)	33:28.0	29	5.5
0.253	122.073	211.2	9/16/2000	(260)	03:20.0	31	5.5
-30.256	181.858	62.9	9/16/2000	(260)	26:24.0	28	5.6
-5.361	146.765	228	9/17/2000	(261)	29:56.0	33	5.9
-1.885	279.539	33	9/20/2000	(264)	37:16.0	31	5.5
-29.847	181.619	156.5	9/22/2000	(266)	21:31.0	9	5.5
4.367	327.407	10	9/23/2000	(267)	13:32.0	9	5.5
4.276	327.393	10	9/23/2000	(267)	17:43.0	9	5.5
-11.674	166.405	125	9/23/2000	(267)	42:08.0	23	5.5
-17.178	186.073	56	9/26/2000	(270)	17:52.0	33	6.4
1.123	127.442	142	9/26/2000	(270)	49:33.0	34	5.9
-0.215	279.418	22.9	9/28/2000	(272)	23:43.0	34	6.4
12.073	122.381	33	9/29/2000	(273)	48:11.0	30	5.6
-4.046	127.334	33	10/1/2000	(275)	03:28.0	33	5.7
29.443	129.388	33	10/2/2000	(276)	29:42.0	35	5.8
29.520	129.396	33	10/2/2000	(276)	44:10.0	35	5.5
40.282	143.124	33	10/3/2000	(277)	13:30.0	36	6.3
11.124	297.441	110.3	10/4/2000	(278)	37:44.0	35	6.2
-15.421	166.910	23	10/4/2000	(278)	58:44.0	35	7.0
-15.636	166.995	33	10/4/2000	(278)	48:27.0	31	5.8
31.732	319.042	10	10/5/2000	(279)	39:11.0	34	6.1
6.853	126.822	87.3	10/5/2000	(279)	06:14.0	34	6.0
35.456	133.134	10	10/6/2000	(280)	30:19.0	34	6.7

latitude (°N)	longitude (°E)	depth (km)	date	(ordinal day)	time	n	Mw
-9.974	119.378	33	10/7/2000	(281)	57:40.0	34	5.9
9.845	125.557	10	10/8/2000	(282)	36:32.0	29	5.7
10.002	92.952	33	10/9/2000	(283)	30:00.0	32	5.9
-6.276	154.627	100	10/10/2000	(284)	23:09.0	36	5.6
-20.645	182.015	488.6	10/11/2000	(285)	13:35.0	33	5.8
-1.577	123.305	33	10/11/2000	(285)	34:32.0	27	5.6
23.866	94.863	116.5	10/11/2000	(285)	42:09.0	32	5.6
12.452	124.967	28.8	10/12/2000	(286)	25:51.0	33	5.5
23.556	141.833	137.5	10/14/2000	(288)	02:52.0	34	5.5
-6.859	129.300	186.4	10/15/2000	(289)	07:30.0	31	5.6
15.521	267.929	180.5	10/17/2000	(291)	00:36.0	32	5.8
-4.623	253.956	10	10/20/2000	(294)	47:24.0	30	5.5
-17.286	184.824	291.8	10/21/2000	(295)	25:14.0	33	6.3
1.671	269.089	10	10/21/2000	(295)	24:09.0	31	5.6
1.832	269.415	10	10/21/2000	(295)	52:47.0	32	5.9
13.679	120.729	151.8	10/21/2000	(295)	30:32.0	33	5.8
7.106	126.752	82.4	10/22/2000	(296)	21:44.0	34	5.6
-15.229	167.701	142.7	10/22/2000	(296)	26:39.0	33	5.7
-4.054	127.388	33	10/23/2000	(297)	04:11.0	27	5.7
-6.943	129.004	158.2	10/26/2000	(300)	44:05.0	18	5.5
54.707	94.983	33	10/27/2000	(301)	08:53.0	33	5.5
26.266	140.460	388	10/27/2000	(301)	21:51.0	34	6.1
17.598	298.806	37.9	10/27/2000	(301)	02:52.0	34	5.6
18.298	146.483	51.1	10/28/2000	(302)	12:35.0	34	5.7
-4.766	153.945	50	10/29/2000	(303)	37:08.0	34	7.0
-15.138	186.583	33	10/29/2000	(303)	30:50.0	33	5.8
47.782	155.651	49.6	10/29/2000	(303)	03:56.0	33	5.5
17.637	298.807	33	10/30/2000	(304)	07:10.0	34	5.8
-9.708	119.075	33	10/30/2000	(304)	01:30.0	32	5.9
34.300	136.214	34.9	10/30/2000	(304)	42:51.0	33	5.5
-10.513	165.764	108.4	10/30/2000	(304)	28:46.0	31	5.6
-2.449	140.073	33	10/30/2000	(304)	12:19.0	28	5.5
-17.964	184.741	33	10/31/2000	(305)	09:36.0	32	5.7
-17.867	184.688	33	10/31/2000	(305)	43:20.0	34	6.1
-7.950	285.578	150.9	11/1/2000	(306)	27:45.0	34	5.9
5.762	125.773	133.8	11/4/2000	(309)	38:41.0	34	5.8
9.938	92.978	33	11/5/2000	(310)	47:04.0	33	5.6
-5.432	154.016	90.5	11/7/2000	(312)	50:09.0	33	6.2
7.042	282.171	17	11/8/2000	(313)	59:58.0	34	6.5
23.251	124.150	14.4	11/8/2000	(313)	36:21.0	34	5.7
-2.458	139.996	33	11/9/2000	(314)	32:44.0	31	5.5
5.737	127.174	63	11/9/2000	(314)	46:42.0	29	5.7
-15.425	186.580	53.1	11/9/2000	(314)	45:54.0	33	5.8
36.601	4.773	10	11/10/2000	(315)	10:53.0	33	5.7
-5.391	154.181	84	11/13/2000	(318)	03:03.0	31	5.7
-8.175	280.071	33	11/13/2000	(318)	46:11.0	32	5.8
21.692	92.908	33	11/13/2000	(318)	56:49.0	26	5.5
42.489	144.765	33	11/13/2000	(318)	57:21.0	33	6.0
-21.263	180.766	628.2	11/13/2000	(318)	17:28.0	34	5.6
42.521	144.785	33	11/14/2000	(319)	52:59.0	33	5.5
17.342	119.787	54.5	11/15/2000	(320)	23:40.0	29	5.5
-21.664	170.439	200	11/15/2000	(320)	36:21.0	26	5.9
38.397	42.922	65.3	11/15/2000	(320)	05:38.0	18	5.6

latitude (°N)	longitude (°E)	depth (km)	date	(ordinal day)	time	n	Mw
-14.605	166.656	33	11/15/2000	(320)	27:14.0	33	5.6
-3.980	152.169	33	11/16/2000	(321)	54:56.0	34	8.0
-5.233	153.102	30	11/16/2000	(321)	42:16.0	34	7.8
-4.264	152.649	33	11/16/2000	(321)	03:44.0	32	5.7
-5.120	152.897	33	11/17/2000	(322)	37:04.0	33	5.8
-6.268	153.366	33	11/17/2000	(322)	22:55.0	33	5.7
-5.496	151.781	33	11/17/2000	(322)	01:56.0	34	7.8
-5.097	153.181	33	11/18/2000	(323)	05:48.0	33	6.6
-5.589	152.883	33	11/18/2000	(323)	22:35.0	30	5.7
-5.228	151.771	33	11/18/2000	(323)	54:58.0	34	6.8
-4.632	153.129	33	11/18/2000	(323)	51:38.0	33	5.6
-5.384	153.452	33	11/18/2000	(323)	05:39.0	32	6.1
-4.682	153.100	33	11/19/2000	(324)	38:36.0	33	5.7
-5.133	151.655	57.8	11/19/2000	(324)	45:27.0	33	6.0
-4.858	153.015	63.8	11/19/2000	(324)	29:25.0	33	5.5
-5.588	151.867	33	11/19/2000	(324)	35:19.0	34	6.1
-4.801	153.112	33	11/19/2000	(324)	22:14.0	34	5.8
-4.484	152.785	33	11/21/2000	(326)	44:18.0	32	5.7
-5.486	152.153	33	11/21/2000	(326)	33:34.0	34	6.2
-3.617	150.823	33	11/21/2000	(326)	03:48.0	32	5.8
-5.430	152.688	33	11/21/2000	(326)	21:05.0	33	6.0
-6.378	153.340	33	11/22/2000	(327)	27:13.0	33	5.5
-15.015	166.768	33	11/22/2000	(327)	35:04.0	34	5.7
-5.589	152.567	33	11/23/2000	(328)	13:00.0	32	5.7
-5.076	152.559	33	11/23/2000	(328)	56:38.0	34	5.5
12.866	144.070	10	11/23/2000	(328)	11:45.0	31	5.6
-4.585	153.058	33	11/23/2000	(328)	43:15.0	33	6.3
-4.655	152.998	33	11/23/2000	(328)	10:35.0	33	5.8
-5.425	153.605	33	11/25/2000	(330)	46:58.0	34	5.6
40.245	49.946	50.4	11/25/2000	(330)	09:11.0	34	6.8
40.167	49.954	33	11/25/2000	(330)	10:47.0	34	6.5
13.775	120.657	117.5	11/29/2000	(334)	48:44.0	33	5.5
35.255	324.672	10	12/1/2000	(336)	27:33.0	30	5.8
14.876	266.056	33	12/4/2000	(339)	43:09.0	18	6.1
35.748	140.948	59.8	12/4/2000	(339)	47:37.0	31	5.7
4.222	126.439	101.4	12/5/2000	(340)	08:25.0	31	5.7
39.566	54.799	30	12/6/2000	(341)	11:06.0	35	7.0
-4.218	152.725	31	12/6/2000	(341)	57:40.0	35	6.5
-4.274	152.786	33	12/7/2000	(342)	31:19.0	34	5.8
-4.599	153.255	33	12/8/2000	(343)	24:14.0	33	5.5
22.706	252.448	10	12/8/2000	(343)	56:18.0	34	5.5
-0.847	121.554	33	12/10/2000	(345)	05:49.0	22	5.5
19.083	121.187	33	12/10/2000	(345)	30:34.0	35	5.5
0.050	127.380	150	12/10/2000	(345)	58:36.0	30	5.7
19.091	292.907	52.6	12/11/2000	(346)	54:07.0	30	5.5
6.015	277.321	10	12/12/2000	(347)	26:45.0	35	6.1
-3.095	148.331	33	12/13/2000	(348)	10:22.0	30	5.7
38.457	31.351	10	12/15/2000	(350)	44:47.0	35	6.0
-15.669	182.669	33	12/15/2000	(350)	43:11.0	31	5.6
-26.820	246.658	10	12/16/2000	(351)	05:28.0	24	5.5
-3.966	151.484	33	12/16/2000	(351)	57:59.0	35	5.6
-21.178	180.876	628.2	12/18/2000	(353)	19:21.0	35	6.6
-21.182	180.903	648.7	12/18/2000	(353)	15:30.0	35	5.7

latitude (°N)	longitude (°E)	depth (km)	date	(ordinal day)	time	n	Mw
-17.571	167.721	33	12/19/2000	(354)	50:19.0	18	5.7
11.765	144.760	33	12/19/2000	(354)	11:47.0	35	6.1
9.418	274.548	33	12/20/2000	(355)	17:19.0	32	5.5
-24.123	183.198	68.8	12/20/2000	(355)	39:26.0	35	5.7
-9.231	*154.353*	*33*	*12/20/2000*	*(355)*	*49:43.0*	*35*	*6.6*
-5.706	151.122	33	12/21/2000	(356)	01:27.0	35	6.4
-5.354	154.133	386.7	12/21/2000	(356)	41:23.0	33	5.9
-3.263	150.445	33	12/21/2000	(356)	14:33.0	34	5.7
-3.109	150.743	33	12/21/2000	(356)	53:11.0	33	5.5
-10.560	164.220	33	12/22/2000	(357)	30:39.0	35	5.8
44.790	147.196	140.4	12/22/2000	(357)	13:01.0	35	6.2
-7.873	135.816	61.7	12/23/2000	(358)	13:24.0	34	6.0
-4.196	123.247	33	12/24/2000	(359)	11:07.0	24	5.6
-21.264	180.876	644.8	12/25/2000	(360)	11:58.0	35	5.6
-9.330	154.593	33	12/27/2000	(362)	03:47.0	34	5.9
-4.228	152.730	33	12/27/2000	(362)	26:31.0	35	5.8
-4.050	152.307	33	12/28/2000	(363)	34:28.0	34	6.2
-12.472	166.934	220.7	12/30/2000	(365)	42:46.0	34	5.5
6.898	126.579	33	1/1/2001	(1)	57:04.0	35	7.4
6.631	126.899	33	1/1/2001	(1)	54:31.0	35	6.8
6.749	126.809	33	1/2/2001	(2)	30:03.0	35	6.3
-11.160	162.440	33	1/2/2001	(2)	17:41.0	29	6.0
43.932	147.813	33	1/3/2001	(3)	47:49.0	35	5.9
16.113	298.966	33	1/5/2001	(5)	06:46.0	33	5.7
6.917	126.842	83.6	1/5/2001	(5)	51:53.0	32	5.5
6.772	126.867	33	1/6/2001	(6)	45:29.0	35	5.6
5.846	127.349	53.4	1/6/2001	(6)	55:31.0	31	5.7
15.550	267.101	91.9	1/9/2001	(9)	46:13.0	34	5.6
-18.491	176.054	33	1/9/2001	(9)	52:03.0	35	5.5
-14.928	167.170	103	1/9/2001	(9)	49:28.0	35	7.1
-18.785	183.266	10	1/11/2001	(11)	59:39.0	31	5.9
-15.578	285.191	39.1	1/12/2001	(12)	47:40.0	18	5.7
-16.950	185.005	258	1/12/2001	(12)	07:57.0	34	5.5
17.333	120.908	33	1/12/2001	(12)	18:25.0	33	5.5
13.049	271.340	60	1/13/2001	(13)	33:32.0	35	7.6
22.094	143.751	87.3	1/14/2001	(14)	58:25.0	35	5.9
13.118	271.406	48.8	1/14/2001	(14)	41:28.0	35	5.7
13.181	271.208	67.7	1/15/2001	(15)	09:11.0	30	5.6
13.076	271.420	74.6	1/15/2001	(15)	20:10.0	34	5.8
13.017	271.404	44	1/16/2001	(16)	22:09.0	32	5.7
12.985	271.303	62.6	1/16/2001	(16)	58:17.0	35	5.6
2.490	126.344	38.2	1/18/2001	(18)	32:32.0	32	5.6
15.402	267.282	93.2	1/19/2001	(19)	12:52.0	35	6.0
-11.662	166.380	50	1/19/2001	(19)	10:14.0	31	6.3
2.874	126.529	74.7	1/20/2001	(20)	59:10.0	35	5.5
10.172	126.223	33	1/21/2001	(21)	44:01.0	35	5.6
14.017	269.093	64.4	1/23/2001	(23)	23:32.0	35	5.9
29.992	142.036	54.6	1/23/2001	(23)	24:03.0	31	5.6
-0.198	99.245	77.8	1/23/2001	(23)	38:12.0	18	5.6
12.907	271.121	33	1/25/2001	(25)	28:51.0	34	5.6
23.419	70.232	16	1/26/2001	(26)	16:40.0	35	7.6
-10.846	161.578	77.4	1/26/2001	(26)	59:39.0	34	5.6
-4.352	283.128	117.2	1/27/2001	(27)	57:01.0	35	5.5

latitude (°N)	longitude (°E)	depth (km)	date	(ordinal day)	time	n	Mw
23.507	70.517	10	1/28/2001	(28)	02:10.0	34	5.8
-0.677	133.334	33	1/29/2001	(29)	21:25.0	35	6.0
-5.900	147.048	99.9	2/1/2001	(32)	02:17.0	35	5.6
12.819	271.031	54.4	2/2/2001	(33)	10:40.0	34	5.7
-19.273	183.889	33	2/2/2001	(33)	52:06.0	33	5.5
13.211	271.059	63.6	2/7/2001	(38)	23:09.0	35	5.8
52.751	153.848	426.6	2/7/2001	(38)	16:15.0	35	5.7
24.269	125.112	15.7	2/8/2001	(39)	41:39.0	35	5.8
-19.078	183.926	33	2/9/2001	(40)	26:15.0	29	5.8
-6.150	147.758	43.6	2/9/2001	(40)	07:42.0	31	5.5
13.671	271.062	10	2/13/2001	(44)	22:05.0	35	6.5
48.544	153.297	147.8	2/14/2001	(45)	36:39.0	35	5.6
-19.494	177.330	10	2/14/2001	(45)	04:25.0	34	6.1
-19.691	177.390	10	2/14/2001	(45)	16:59.0	35	6.2
-5.560	148.304	168.6	2/15/2001	(46)	46:59.0	35	5.6
-7.161	117.488	521	2/16/2001	(47)	59:09.0	35	6.1
-15.345	289.525	210.1	2/16/2001	(47)	19:45.0	34	5.5
13.062	271.091	33	2/17/2001	(48)	17:31.0	33	5.5
20.247	122.428	33	2/17/2001	(48)	49:26.0	31	5.5
-11.276	285.486	33	2/21/2001	(52)	20:21.0	33	5.6
6.622	126.923	75.3	2/21/2001	(52)	50:29.0	33	5.5
17.448	276.412	10	2/22/2001	(53)	02:55.0	35	5.5
29.513	101.129	33	2/23/2001	(54)	09:23.0	33	5.6
-30.715	181.737	59.9	2/23/2001	(54)	52:24.0	31	5.5
1.271	126.249	35	2/24/2001	(55)	23:48.0	35	7.1
1.559	126.354	33	2/24/2001	(55)	07:47.0	33	5.8
1.555	126.431	33	2/24/2001	(55)	33:44.0	35	6.0
37.217	142.146	33	2/24/2001	(55)	53:54.0	35	5.8
36.424	70.881	202.5	2/25/2001	(56)	21:59.0	35	6.2
46.815	144.525	392	2/26/2001	(57)	58:22.0	34	6.1
6.582	126.852	60.5	2/28/2001	(59)	35:16.0	31	5.8
-6.944	155.833	33	2/28/2001	(59)	31:04.0	34	5.6
-21.986	170.207	10	2/28/2001	(59)	30:14.0	32	6.5
-22.002	170.108	10	2/28/2001	(59)	05:31.0	29	6.3
13.283	271.173	65.3	2/28/2001	(59)	50:13.0	18	6.1
-22.293	170.324	10	3/1/2001	(60)	59:54.0	28	5.8
28.564	129.002	79.8	3/5/2001	(64)	08:34.0	33	5.5
34.369	86.902	33	3/5/2001	(64)	50:06.0	31	5.7
-10.430	161.298	89.5	3/7/2001	(66)	09:24.0	33	5.7
-25.373	182.034	231	3/11/2001	(70)	50:40.0	31	5.8
18.772	121.218	33	3/13/2001	(72)	04:57.0	31	5.7
0.451	121.892	109.4	3/14/2001	(73)	56:18.0	33	6.0
8.656	94.013	33	3/15/2001	(74)	22:43.0	31	6.0
13.144	271.301	48.9	3/16/2001	(75)	01:18.0	33	5.8
46.691	151.298	103.1	3/17/2001	(76)	24:24.0	31	5.5
12.540	272.601	95.5	3/18/2001	(77)	43:21.0	32	5.7
-4.029	128.020	33	3/19/2001	(78)	52:15.0	32	6.5
-4.527	153.114	33	3/21/2001	(80)	47:34.0	32	5.9
32.951	46.625	33	3/23/2001	(82)	24:11.0	30	5.5
44.071	148.054	33	3/23/2001	(82)	30:10.0	31	6.0
34.083	132.526	50	3/24/2001	(83)	27:53.0	30	6.7
13.082	271.061	33	3/29/2001	(88)	54:28.0	31	5.8
-2.747	138.899	33	3/30/2001	(89)	25:28.0	31	5.5

latitude (°N)	longitude (°E)	depth (km)	date	(ordinal day)	time	n	Mw
11.848	147.325	56.5	4/2/2001	(92)	50:06.0	28	5.7
40.589	141.772	63.8	4/2/2001	(92)	54:18.0	28	5.6
-5.176	132.369	33	4/4/2001	(94)	44:11.0	31	6.4
21.705	143.325	33	4/7/2001	(97)	13:27.0	30	5.9
-27.554	183.664	33	4/7/2001	(97)	17:37.0	31	6.0
24.768	99.061	10	4/12/2001	(102)	47:00.0	28	5.5
12.910	144.580	33	4/14/2001	(104)	16:14.0	30	5.5
30.092	141.768	10	4/14/2001	(104)	27:26.0	30	6.0
-7.414	155.964	10	4/19/2001	(109)	40:36.0	31	5.8
-7.455	155.893	12	4/19/2001	(109)	13:25.0	30	6.0
-7.306	155.965	20	4/19/2001	(109)	58:26.0	30	6.2
-7.410	155.865	17	4/19/2001	(109)	43:42.0	31	6.7
32.824	132.023	33	4/25/2001	(115)	40:06.0	30	5.7
43.097	145.923	86	4/26/2001	(116)	48:57.0	30	6.0
-18.064	183.063	351.8	4/28/2001	(118)	49:53.0	31	6.8
18.736	255.455	10	4/29/2001	(119)	26:54.0	30	6.1
43.881	147.392	47.9	4/30/2001	(120)	02:02.0	30	5.5
3.577	148.489	33	5/2/2001	(122)	57:14.0	30	5.5
0.462	126.299	33	5/3/2001	(123)	31:57.0	30	5.5
-23.523	248.122	10	5/5/2001	(125)	21:15.0	25	5.7
-10.318	161.232	67.9	5/9/2001	(129)	38:26.0	29	6.3
-4.236	143.422	133	5/16/2001	(136)	26:21.0	26	5.5
0.414	97.784	33	5/18/2001	(138)	05:33.0	24	5.9
-19.903	182.485	368.7	5/19/2001	(139)	36:25.0	29	6.0
18.816	255.554	33	5/20/2001	(140)	21:43.0	27	6.3
-17.708	181.297	567.2	5/23/2001	(143)	35:23.0	31	5.7
44.268	148.393	33	5/25/2001	(145)	40:50.0	31	6.6
-20.292	182.158	406.5	5/26/2001	(146)	57:26.0	32	6.4
-6.609	132.346	33	5/28/2001	(148)	37:05.0	31	6.1
-7.022	155.037	14	5/29/2001	(149)	37:19.0	30	6.4
-7.199	154.923	33	6/1/2001	(152)	36:56.0	33	5.8
-29.666	181.367	178.1	6/3/2001	(154)	41:57.0	33	7.1
17.096	145.830	83	6/4/2001	(155)	41:01.0	34	5.8
-6.884	146.388	10	6/5/2001	(156)	00:05.0	34	6.1
-6.815	146.410	10	6/5/2001	(156)	13:58.0	34	5.8
24.463	122.397	77.5	6/13/2001	(164)	17:55.0	34	5.6
24.513	122.033	32.1	6/14/2001	(165)	35:25.0	33	5.9
-22.053	180.539	604	6/14/2001	(165)	27:04.0	34	5.7
-20.709	181.679	537	6/14/2001	(165)	08:10.0	34	5.6
18.852	146.810	33	6/14/2001	(165)	31:28.0	34	5.8
18.833	146.983	33	6/15/2001	(166)	17:45.0	34	6.0
-14.889	186.661	10	6/16/2001	(167)	13:38.0	32	6.0
1.443	125.691	70.3	6/23/2001	(174)	34:19.0	33	5.7
-16.265	286.359	33	6/23/2001	(174)	33:14.0	34	8.4
44.189	148.510	33	6/24/2001	(175)	18:51.0	35	6.0
-4.070	255.531	10	6/26/2001	(177)	33:52.0	36	6.0
-6.406	146.761	103.5	6/30/2001	(181)	34:36.0	36	6.0
-4.312	152.956	28	7/1/2001	(182)	46:06.0	37	6.1
-6.033	154.806	210.7	7/3/2001	(184)	18:07.0	21	5.8
-16.623	286.029	33	7/3/2001	(184)	57:42.0	23	5.6
21.641	142.984	290	7/3/2001	(184)	10:42.0	35	6.5
-21.725	183.295	184.6	7/4/2001	(185)	06:31.0	35	6.5
32.156	139.545	33	7/4/2001	(185)	47:45.0	34	5.7

latitude (°N)	longitude (°E)	depth (km)	date	(ordinal day)	time	n	Mw
-16.086	286.013	62	7/5/2001	(186)	53:48.0	33	6.6
-17.543	287.923	33	7/7/2001	(188)	38:43.0	35	7.6
-6.663	152.108	10	7/8/2001	(189)	54:18.0	35	6.2
28.750	316.563	10	7/13/2001	(194)	48:19.0	37	5.6
-16.971	185.324	226.6	7/19/2001	(200)	12:15.0	36	5.9
-5.147	132.338	33	7/22/2001	(203)	15:09.0	30	6.0
13.878	120.716	108.4	7/23/2001	(204)	46:58.0	37	5.5
-17.692	181.174	564	7/31/2001	(212)	57:40.0	37	5.6
1.557	126.399	33	7/31/2001	(212)	11:18.0	36	5.5
8.023	117.466	33	7/31/2001	(212)	41:30.0	30	5.5
2.809	126.995	33	8/4/2001	(216)	44:53.0	36	5.8
12.224	93.352	96.4	8/5/2001	(217)	16:16.0	37	6.0
-8.535	284.991	136.7	8/6/2001	(218)	08:46.0	37	5.5
-14.258	287.317	33	8/9/2001	(221)	06:59.0	24	5.6
-5.506	149.597	145.3	8/9/2001	(221)	57:49.0	36	5.5
-14.700	167.106	82	8/10/2001	(222)	24:35.0	37	5.8
41.046	142.308	38	8/13/2001	(225)	11:23.0	37	6.4
-22.664	179.317	586.8	8/15/2001	(227)	08:19.0	37	5.6
25.748	126.190	33	8/17/2001	(229)	25:49.0	37	5.9

Appendix 2: Station specific event list

After picking the precise arrival time (for each event for each station deployed at the time of the earthquake, i.e. ~15,000 picks), the seismic signal was deconvolved to isolate the receiver function. Many receiver functions were eliminated due to poor signal to noise ratios. Table 3 gives the backazimuth range and distance range for each stack. This list provides the station-to-event distance and backazimuth for each event that produced a "usable" receiver function, grouped by station and arranged azimuthally within each station group.

sta	date	ordinal day	time	delta	seaz
NNA	5/21/2000	(142)	06:05.0	41.61	17.9
NNA	6/17/2000	(169)	48:34.7	46.05	28.5
NNA	6/21/2000	(173)	59:39.2	45.98	28.6
NNA	8/28/1999	(240)	51:41.0	83.36	107.3
NNA	4/29/2000	(120)	04:28.0	88.23	109.0
NNA	7/21/2000	(203)	04:15.9	70.42	110.1
NNA	9/30/1999	(273)	40:43.9	59.80	118.6
NNA	7/21/2000	(203)	22:47.5	56.89	119.6
NNA	12/29/1999	(363)	28:48.1	56.12	122.3
NNA	6/21/1999	(172)	52:05.4	56.01	122.4
NNA	4/29/2001	(119)	35:52.2	54.56	125.4
NNA	1/2/2000	(002)	28:46.5	87.54	203.4
NNA	5/7/2000	(128)	59:25.5	81.98	203.9
NNA	7/9/2000	(191)	54:22.5	83.70	207.6
NNA	1/17/2000	(017)	29:50.8	82.02	207.8
NNA	8/22/1999	(234)	52:57.2	87.05	220.9
NNA	8/9/2000	(222)	20:51.3	86.66	221.1
NNA	10/4/2000	(278)	10:56.0	86.71	222.1
NNA	4/19/2001	(109)	55:34.6	82.69	235.0
NNA	8/14/2000	(227)	23:22.8	85.23	236.2
NNA	7/9/1999	(190)	16:30.2	82.17	236.2
NNA	7/26/1999	(207)	45:02.4	82.00	239.5
NNA	2/6/2000	(037)	45:44.1	83.04	240.3
NNA	8/26/1999	(238)	51:19.3	82.89	246.0
NNA	5/26/2000	(147)	40:54.0	71.93	258.2
NNA	9/10/2000	(254)	18:28.9	87.41	261.9
NNA	8/28/2000	(241)	18:20.1	90.94	262.4
NNA	7/3/1999	(184)	38:50.1	58.04	264.5
NNA	4/14/2001	(104)	36:21.6	54.20	265.6
NNA	8/4/2001	(216)	56:54.3	84.86	265.7
NNA	2/24/2001	(055)	35:57.5	86.57	265.7
NNA	6/14/2000	(166)	12:33.2	82.98	265.8
NNA	8/6/2000	(219)	35:42.6	56.22	266.9
NNA	5/4/2000	(125)	33:42.5	89.86	267.1
NNA	7/12/1999	(193)	09:48.5	82.54	267.1
NNA	6/18/1999	(169)	07:14.6	82.57	267.2
NNA	1/2/2001	(002)	41:46.4	81.38	267.6
NNA	1/1/2001	(001)	08:47.2	81.35	267.9
NNA	7/7/1999	(188)	58:54.5	32.50	268.9
NNA	8/6/1999	(218)	38:28.8	31.68	269.2
NNA	4/13/2000	(104)	05:40.8	78.30	269.4
NNA	7/21/2000	(203)	24:56.7	50.12	269.5
NNA	10/24/1999	(297)	28:31.8	38.72	269.5
NNA	6/9/2000	(161)	40:03.7	55.58	269.5
NNA	9/18/1999	(261)	34:07.5	30.18	269.7
NNA	2/24/2001	(055)	01:59.1	47.93	269.9
NNA	7/30/2000	(212)	34:23.9	51.94	270.2
NNA	3/23/2001	(082)	37:09.4	39.75	270.2
NNA	1/3/2001	(003)	54:50.1	39.96	270.3
NNA	7/27/2000	(209)	58:29.9	51.68	270.4
NNA	1/28/2000	(028)	28:14.6	41.10	270.4
NNA	8/15/2000	(228)	27:53.8	41.13	270.5
NNA	7/8/2000	(190)	06:22.7	51.91	270.5
NNA	7/20/2000	(202)	47:30.0	49.03	270.5
NNA	7/15/2000	(197)	39:06.6	51.63	270.5
NNA	7/1/2000	(183)	10:32.6	51.77	270.6
NNA	8/19/2000	(232)	33:28.2	40.33	270.8
NNA	4/26/2001	(116)	56:05.0	41.45	271.3
NNA	8/13/2001	(225)	19:01.9	44.67	272.7
NNA	6/15/2000	(167)	20:15.6	58.98	273.9
NNA	6/6/2000	(158)	06:29.8	59.21	274.5
NNA	4/25/2001	(115)	49:11.3	56.01	276.0
NNA	3/24/2001	(083)	36:47.1	54.71	276.3
NNA	10/6/2000	(280)	39:07.9	53.28	276.7
NNA	8/17/2001	(229)	35:53.5	64.67	277.1
NNA	11/1/1999	(305)	03:30.5	68.75	280.0
NNA	9/22/1999	(265)	25:09.5	68.58	280.5
NNA	9/26/1999	(269)	03:19.9	68.58	280.5
NNA	9/20/1999	(263)	57:13.9	68.97	280.5
NNA	6/10/2000	(162)	33:57.7	68.46	280.5
NNA	6/7/2000	(159)	58:04.7	75.28	302.4
NNA	1/26/2001	(026)	28:54.0	86.89	324.4
NNA	11/8/1999	(312)	56:24.0	74.07	327.3
NNA	7/17/2000	(199)	04:39.2	74.37	327.5
NNA	5/12/2000	(133)	21:27.0	74.73	327.6
NNA	12/6/2000	(341)	22:09.7	74.17	341.1
NNA	6/6/2000	(158)	52:59.0	74.72	358.4
NNA	11/12/1999	(316)	08:28.7	74.66	359.8
AND	8/9/2000	(222)	50:48.6	55.70	123.2
AND	6/9/2000	(161)	38:59.3	81.55	239.0
AND	8/6/2000	(219)	35:42.2	56.15	266.9
AND	7/21/2000	(203)	24:56.3	50.06	269.6
AND	7/30/2000	(212)	34:23.5	51.89	270.2
AND	7/30/2000	(212)	26:38.4	51.87	270.3
AND	6/3/2000	(155)	03:06.9	50.01	270.4
AND	7/2/2000	(184)	12:11.9	51.80	270.5
AND	7/20/2000	(202)	47:29.6	48.98	270.6
AND	7/1/2000	(183)	10:32.3	51.72	270.7
AND	6/15/2000	(167)	20:15.4	58.94	273.9
AND	6/6/2000	(158)	06:29.6	59.18	274.6
AND	6/6/2000	(158)	25:14.6	51.09	275.7
AND	6/25/2000	(177)	44:03.0	57.75	275.8

sta	date	ordinal day	time	delta	seaz	sta	date	ordinal day	time	delta	seaz
AND	8/4/2000	(217)	19:54.4	38.52	280.1	GNR	5/24/2000	(145)	52:12.3	79.87	7.4
BSH	6/8/1999	(159)	15:11.4	76.01	84.3	GNR	6/17/2000	(169)	48:39.7	46.69	28.2
BSH	8/28/1999	(240)	51:40.8	83.33	107.1	GNR	6/21/2000	(173)	59:44.2	46.62	28.3
BSH	8/3/1999	(215)	10:50.8	84.63	109.5	GNR	6/23/2001	(174)	46:17.9	98.29	110.2
BSH	6/15/1999	(166)	51:15.9	57.37	117.6	GNR	5/20/2001	(140)	30:34.1	54.05	124.9
BSH	6/21/1999	(172)	52:04.4	55.87	121.9	GNR	4/29/2001	(119)	35:48.8	54.09	125.1
BSH	8/1/1999	(213)	12:26.8	32.92	128.8	GNR	6/10/2000	(162)	01:41.1	83.44	202.6
BSH	7/3/1999	(184)	38:49.2	57.91	264.6	GNR	6/16/2001	(167)	25:22.6	80.93	203.8
SOB	6/21/2000	(173)	59:42.4	46.39	28.3	GNR	9/26/2000	(270)	29:42.6	83.29	203.9
SOB	7/21/2000	(203)	22:46.6	56.78	119.1	GNR	7/4/2001	(185)	18:31.3	88.26	205.6
SOB	8/14/2000	(227)	23:21.2	84.93	236.0	GNR	6/3/2001	(154)	54:35.4	96.39	205.6
SOB	6/29/2000	(181)	38:59.4	51.74	270.4	GNR	4/28/2001	(118)	01:18.1	84.72	206.6
SOB	7/20/2000	(202)	47:29.3	48.94	270.6	GNR	5/19/2001	(139)	47:57.7	86.63	206.7
SOB	7/23/2000	(205)	01:21.6	51.76	270.7	GNR	6/14/2000	(166)	13:21.3	86.06	213.0
SOB	8/15/2000	(228)	27:53.0	41.04	270.7	GNR	5/9/2001	(129)	50:14.5	83.15	229.2
SOB	8/19/2000	(232)	33:27.5	40.25	271.1	GNR	4/19/2001	(109)	55:32.6	82.30	235.2
SOB	8/4/2000	(217)	19:54.3	38.51	280.2	GNR	6/1/2001	(152)	48:45.0	82.44	236.2
RCK	7/21/2000	(203)	04:15.0	70.28	109.8	GNR	11/16/2000	(321)	53:59.4	81.29	238.6
RCK	3/12/2000	(072)	31:15.8	62.33	114.2	GNR	6/14/2001	(165)	41:13.9	61.86	255.1
RCK	7/21/2000	(203)	22:45.8	56.66	119.2	GNR	7/3/2001	(184)	19:55.3	61.03	260.2
RCK	9/26/2000	(270)	29:43.4	83.44	203.8	GNR	2/24/2001	(055)	35:57.5	86.56	265.9
RCK	9/11/2000	(255)	29:30.8	82.12	203.8	GNR	4/14/2001	(104)	36:21.5	54.19	266.2
RCK	1/26/2000	(026)	38:44.7	83.55	203.8	GNR	1/1/2001	(001)	08:47.3	81.36	268.1
RCK	8/9/2000	(222)	08:03.9	85.58	214.8	GNR	7/4/2001	(185)	56:31.3	53.40	269.5
RCK	5/29/2001	(149)	49:10.0	82.28	235.9	GNR	6/9/2000	(161)	40:04.0	55.62	270.1
RCK	6/9/2000	(161)	38:58.6	81.41	239.0	GNR	6/24/2001	(175)	25:48.4	39.51	270.9
RCK	11/16/2000	(321)	06:34.8	80.52	239.8	GNR	6/29/2000	(181)	39:00.5	51.89	270.9
RCK	2/6/2000	(037)	45:42.5	82.74	240.2	GNR	6/3/2000	(155)	03:07.7	50.11	271.0
RCK	8/7/2000	(220)	45:40.9	95.21	264.7	GNR	5/25/2001	(145)	47:47.3	39.50	271.1
RCK	6/14/2000	(166)	12:32.8	82.90	265.8	GNR	3/23/2001	(082)	37:09.8	39.80	271.2
RCK	8/6/2000	(219)	35:42.2	56.15	267.1	GNR	7/1/2000	(183)	10:33.0	51.82	271.3
RCK	7/21/2000	(203)	24:56.4	50.08	269.9	GNR	1/3/2001	(003)	54:50.6	40.02	271.3
RCK	7/30/2000	(212)	34:23.6	51.90	270.5	GNR	4/26/2001	(116)	56:05.6	41.51	272.2
RCK	7/30/2000	(212)	26:38.5	51.89	270.5	GNR	12/22/2000	(357)	19:48.6	39.61	272.7
RCK	6/29/2000	(181)	38:59.9	51.80	270.6	GNR	8/13/2001	(225)	19:02.6	44.76	273.6
RCK	6/3/2000	(155)	03:07.0	50.03	270.7	GNR	6/6/2000	(158)	06:30.5	59.32	275.0
RCK	5/25/2001	(145)	47:46.6	39.41	270.7	GNR	1/26/2001	(026)	28:57.0	87.52	324.5
RCK	7/8/2000	(190)	06:22.5	51.88	270.8	GNR	12/6/2000	(341)	22:13.9	74.89	341.2
RCK	7/20/2000	(202)	47:29.7	49.00	270.9	GNR	6/6/2000	(158)	53:03.3	75.46	358.5
RCK	7/15/2000	(197)	39:06.3	51.60	270.9	MCK	6/17/2000	(169)	48:40.4	46.77	28.2
RCK	7/1/2000	(183)	10:32.4	51.74	270.9	MCK	6/21/2000	(173)	59:44.8	46.70	28.3
RCK	1/28/2000	(028)	28:14.4	41.07	270.9	MCK	7/21/2000	(203)	04:13.8	70.08	110.0
RCK	6/6/2000	(158)	25:14.9	51.14	275.9	MCK	6/23/2001	(174)	46:17.7	98.24	110.2
RCK	6/25/2000	(177)	44:03.3	57.80	276.0	MCK	6/6/1999	(157)	18:03.6	63.77	113.2
RCK	10/6/2000	(280)	39:08.0	53.31	277.0	MCK	7/21/2000	(203)	22:44.1	56.42	119.2
RCK	6/14/2000	(166)	55:31.2	74.75	278.3	MCK	8/9/2000	(222)	50:45.5	55.27	123.1
RCK	8/4/2000	(217)	19:55.0	38.59	280.4	MCK	5/20/2001	(140)	30:33.6	53.98	124.9
RCK	6/7/2000	(159)	58:06.2	75.53	302.4	MCK	4/29/2001	(119)	35:48.3	54.02	125.1
RCK	9/12/2000	(256)	38:21.3	67.05	304.5	MCK	6/10/2000	(162)	01:40.7	83.35	202.7
RCK	1/26/2001	(026)	28:56.0	87.31	324.3	MCK	8/17/2000	(230)	16:45.6	87.99	203.9
RCK	12/6/2000	(341)	22:12.6	74.67	341.1	MCK	9/26/2000	(270)	29:42.2	83.20	204.0
RCK	6/6/2000	(158)	53:02.1	75.25	358.3	MCK	6/3/2001	(154)	54:35.0	96.30	205.7
RCK	11/12/1999	(316)	08:31.8	75.20	359.7	MCK	7/4/2001	(185)	18:30.9	88.17	205.7
SLT	6/21/2000	(173)	59:43.7	46.56	28.3	MCK	5/26/2001	(146)	08:56.5	87.00	207.0
SLT	6/23/2001	(174)	46:18.3	98.39	110.1	MCK	9/14/2000	(258)	11:49.2	83.06	210.2
SLT	8/9/2000	(222)	20:48.8	86.17	221.1	MCK	8/9/2000	(222)	08:03.0	85.39	215.1
SLT	8/7/2000	(220)	45:40.9	95.22	264.7	MCK	1/9/2001	(009)	01:24.7	85.58	222.2
SLT	7/1/2000	(183)	10:32.6	51.76	271.1	MCK	10/4/2000	(278)	10:53.1	86.12	222.3
SLT	8/19/2000	(232)	33:28.2	40.33	271.5	MCK	5/9/2001	(129)	50:14.3	83.09	229.2

sta	date	ordinal day	time	delta	seaz	sta	date	ordinal day	time	delta	seaz
MCK	4/19/2001	(109)	10:15.2	82.12	235.2	YAN	4/19/2001	(109)	55:32.5	82.27	235.4
MCK	4/19/2001	(109)	25:16.4	82.28	235.2	YAN	6/1/2001	(152)	48:44.8	82.42	236.4
MCK	4/19/2001	(109)	55:32.4	82.25	235.3	YAN	10/29/2000	(303)	48:44.8	80.53	238.2
MCK	6/1/2001	(152)	48:44.8	82.40	236.2	YAN	11/16/2000	(321)	53:59.3	81.28	238.8
MCK	8/14/2000	(227)	23:20.7	84.82	236.4	YAN	12/6/2000	(341)	09:18.9	80.48	239.6
MCK	10/29/2000	(303)	48:44.7	80.51	238.1	YAN	11/17/2000	(322)	13:42.8	82.03	239.9
MCK	11/16/2000	(321)	53:59.2	81.26	238.7	YAN	11/18/2000	(323)	06:43.5	81.78	240.1
MCK	12/6/2000	(341)	09:18.8	80.46	239.4	YAN	2/6/2000	(037)	45:42.3	82.70	240.7
MCK	11/17/2000	(322)	13:42.7	82.00	239.8	YAN	2/15/2001	(046)	58:37.5	83.44	243.1
MCK	11/16/2000	(321)	06:34.5	80.45	240.0	YAN	6/5/2001	(156)	26:05.3	85.35	244.4
MCK	6/30/2001	(181)	46:28.8	84.80	244.1	YAN	3/28/2000	(088)	09:46.2	60.15	260.1
MCK	6/5/2001	(156)	12:12.5	85.39	244.2	YAN	9/10/2000	(254)	18:28.9	87.41	262.2
MCK	6/5/2001	(156)	26:05.2	85.31	244.2	YAN	8/7/2000	(220)	45:41.5	95.34	265.0
MCK	6/15/2001	(166)	27:30.5	61.80	255.0	YAN	6/23/2000	(175)	14:00.2	86.62	266.1
MCK	6/14/2001	(165)	41:13.9	61.86	255.2	YAN	2/24/2001	(055)	35:57.8	86.63	266.1
MCK	7/3/2001	(184)	19:55.3	61.04	260.3	YAN	4/14/2001	(104)	36:22.1	54.26	266.5
MCK	8/28/2000	(241)	18:19.8	90.89	262.5	YAN	5/4/2000	(125)	33:42.9	89.95	267.4
MCK	8/28/2000	(241)	42:03.0	91.07	262.8	YAN	8/6/2000	(219)	35:43.2	56.31	267.8
MCK	8/7/2000	(220)	45:41.2	95.28	264.8	YAN	1/1/2001	(001)	08:47.7	81.45	268.3
MCK	10/27/2000	(301)	30:35.1	58.09	265.2	YAN	8/20/2000	(233)	07:14.1	80.99	268.5
MCK	2/24/2001	(055)	35:57.5	86.57	265.9	YAN	9/20/1999	(263)	39:07.5	35.74	269.1
MCK	8/4/2001	(216)	56:54.3	84.86	265.9	YAN	9/9/1999	(252)	08:15.5	34.46	269.7
MCK	6/14/2000	(166)	12:33.2	82.98	266.0	YAN	11/11/1999	(315)	47:02.8	32.54	270.7
MCK	8/6/2000	(219)	35:42.8	56.24	267.6	YAN	8/6/1999	(218)	38:30.0	31.81	270.9
MCK	1/1/2001	(001)	08:47.4	81.38	268.1	YAN	10/24/1999	(297)	28:32.9	38.86	270.9
MCK	6/9/2000	(161)	40:04.1	55.64	270.2	YAN	7/30/2000	(212)	34:24.9	52.08	271.2
MCK	7/21/2000	(203)	24:57.2	50.18	270.3	YAN	7/30/2000	(212)	26:39.8	52.06	271.2
MCK	7/30/2000	(212)	34:24.4	52.01	270.9	YAN	6/29/2000	(181)	39:01.2	51.98	271.3
MCK	6/3/2000	(155)	03:07.8	50.13	271.1	YAN	6/3/2000	(155)	03:08.4	50.21	271.3
MCK	7/8/2000	(190)	06:23.3	51.99	271.3	YAN	6/24/2001	(175)	25:49.1	39.60	271.3
MCK	7/15/2000	(197)	39:07.1	51.70	271.3	YAN	7/8/2000	(190)	06:23.8	52.06	271.5
MCK	7/20/2000	(202)	47:30.6	49.10	271.4	YAN	5/25/2001	(145)	47:48.0	39.59	271.5
MCK	7/1/2000	(183)	10:33.2	51.84	271.4	YAN	7/15/2000	(197)	39:07.7	51.78	271.5
MCK	6/15/2000	(167)	20:16.5	59.10	274.5	YAN	7/20/2000	(202)	47:31.1	49.18	271.6
MCK	6/6/2000	(158)	06:30.7	59.35	275.1	YAN	7/1/2000	(183)	10:33.7	51.92	271.6
MCK	6/10/2000	(162)	33:59.1	68.68	280.9	YAN	1/28/2000	(028)	28:15.9	41.25	271.7
YAN	11/12/1999	(316)	08:34.0	75.59	0.1	YAN	8/15/2000	(228)	27:55.0	41.28	271.8
YAN	8/21/1999	(233)	00:36.8	71.02	109.0	YAN	8/19/2000	(232)	33:29.5	40.49	272.2
YAN	8/20/1999	(232)	13:06.1	70.81	109.1	YAN	10/3/2000	(277)	21:13.0	45.12	272.6
YAN	7/21/2000	(203)	04:13.2	69.98	110.1	YAN	11/13/2000	(318)	04:43.9	42.61	273.0
YAN	1/13/2001	(013)	43:37.7	65.31	111.6	YAN	12/22/2000	(357)	19:49.4	39.71	273.1
YAN	7/21/2000	(203)	22:43.4	56.32	119.4	YAN	4/2/2001	(092)	02:00.6	45.47	274.0
YAN	8/9/2000	(222)	50:44.8	55.17	123.2	YAN	12/11/1999	(345)	14:53.0	76.56	278.5
YAN	5/20/2001	(140)	30:32.8	53.88	125.0	YAN	7/16/2000	(198)	32:32.9	71.57	278.6
YAN	8/23/2000	(236)	54:35.3	49.99	128.7	YAN	8/26/1999	(238)	49:07.2	72.96	278.8
YAN	8/17/2000	(230)	16:45.4	87.95	204.0	YAN	9/20/1999	(263)	57:15.8	69.27	281.1
YAN	9/26/2000	(270)	29:42.0	83.16	204.1	YAN	9/26/1999	(269)	03:21.7	68.88	281.1
YAN	9/11/2000	(255)	29:29.3	81.84	204.2	YAN	8/4/2000	(217)	19:57.0	38.83	281.2
YAN	5/7/2000	(128)	59:21.4	81.19	204.2	YAN	1/26/2001	(026)	28:58.0	87.72	324.7
YAN	7/19/2001	(200)	23:45.3	83.10	204.9	YAN	7/17/2000	(199)	04:44.1	75.22	327.8
YAN	6/3/2001	(154)	54:34.8	96.27	205.8	YAN	5/12/2000	(133)	21:31.9	75.58	327.9
YAN	7/4/2001	(185)	18:30.7	88.14	205.8	YAN	11/25/2000	(330)	21:55.8	75.12	345.3
YAN	9/2/2000	(246)	13:24.2	87.02	208.4	YAN	11/25/2000	(330)	20:17.3	75.04	345.3
YAN	9/14/2000	(258)	11:49.0	83.03	210.4	CAR	7/31/2000	(213)	56:36.4	85.15	215.0
YAN	8/9/2000	(222)	08:02.9	85.37	215.2	CAR	8/14/2000	(227)	23:20.5	84.78	236.5
YAN	11/26/1999	(330)	33:25.4	86.68	221.0	CAR	6/14/2000	(166)	17:33.7	35.88	270.3
YAN	8/22/1999	(234)	52:54.2	86.44	221.2	CAR	6/9/2000	(161)	40:04.6	55.70	270.4
YAN	8/9/2000	(222)	20:48.3	86.05	221.4	CAR	6/29/2000	(181)	39:01.1	51.97	271.3
YAN	1/9/2001	(009)	01:24.7	85.57	222.4	CAR	6/15/2000	(167)	20:17.0	59.18	274.7

sta	date	ordinal day	time	delta	seaz	sta	date	ordinal day	time	delta	seaz
CAR	6/6/2000	(158)	06:31.2	59.42	275.3	RND	7/3/2001	(184)	19:55.2	61.01	260.5
CAR	6/25/2000	(177)	44:04.8	58.01	276.6	RND	9/10/2000	(254)	18:28.5	87.34	262.2
CAR	6/6/2000	(158)	25:16.5	51.35	276.6	RND	8/7/2000	(220)	45:41.2	95.28	264.9
CAR	7/16/2000	(198)	32:32.8	71.57	278.6	RND	2/24/2001	(055)	35:57.6	86.58	266.0
CAR	6/6/2000	(158)	09:14.9	64.35	302.3	RND	6/14/2000	(166)	12:33.3	82.99	266.2
CAR	7/17/2000	(199)	04:44.4	75.28	327.8	RND	8/6/2000	(219)	35:42.9	56.26	267.8
SLM	7/21/2000	(203)	04:13.0	69.94	110.0	RND	1/1/2001	(001)	08:47.5	81.40	268.2
SLM	7/21/2000	(203)	22:43.0	56.26	119.2	RND	6/9/2000	(161)	40:04.4	55.68	270.5
SLM	8/9/2000	(222)	50:44.3	55.10	123.1	RND	7/7/1999	(188)	58:55.3	32.60	271.0
SLM	6/10/2000	(162)	01:39.7	83.17	202.8	RND	7/30/2000	(212)	34:24.7	52.05	271.3
SLM	8/17/2000	(230)	16:44.8	87.81	204.0	RND	6/29/2000	(181)	39:01.0	51.95	271.4
SLM	8/7/2000	(220)	45:41.4	95.32	264.9	RND	6/3/2000	(155)	03:08.2	50.18	271.5
SLM	6/14/2000	(166)	12:33.4	83.03	266.2	RND	6/24/2001	(175)	25:48.9	39.57	271.6
SLM	8/6/2000	(219)	35:43.1	56.29	267.8	RND	7/8/2000	(190)	06:23.6	52.03	271.6
SLM	8/20/2000	(233)	07:14.1	80.97	268.5	RND	7/20/2000	(202)	47:30.9	49.15	271.7
SLM	6/9/2000	(161)	40:04.6	55.70	270.5	RND	7/1/2000	(183)	10:33.5	51.89	271.7
SLM	7/30/2000	(212)	34:24.9	52.07	271.2	RND	5/25/2001	(145)	47:47.8	39.56	271.7
SLM	7/30/2000	(212)	26:39.8	52.05	271.3	RND	3/23/2001	(082)	37:10.3	39.87	271.8
SLM	6/3/2000	(155)	03:08.3	50.20	271.4	RND	8/19/2000	(232)	33:29.3	40.46	272.4
SLM	7/8/2000	(190)	06:23.7	52.05	271.6	RND	11/13/2000	(318)	04:43.7	42.59	273.2
SLM	8/18/2000	(231)	00:59.1	51.97	271.6	RND	12/22/2000	(357)	19:49.2	39.69	273.3
SLM	7/1/2000	(183)	10:33.7	51.91	271.7	RND	6/6/2000	(158)	06:31.2	59.41	275.4
SLM	8/19/2000	(232)	33:29.5	40.48	272.3	RND	6/6/2000	(158)	25:16.4	51.34	276.7
SLM	6/15/2000	(167)	20:17.0	59.18	274.8	RND	10/6/2000	(280)	39:09.6	53.52	277.7
SLM	6/6/2000	(158)	06:31.3	59.43	275.4	RND	6/14/2000	(166)	55:32.5	74.98	278.8
SLM	6/25/2000	(177)	44:04.9	58.01	276.6	RND	9/22/1999	(265)	25:11.5	68.90	281.1
SLM	6/6/2000	(158)	25:16.5	51.36	276.7	RND	6/10/2000	(162)	33:59.7	68.77	281.1
SLM	6/19/2000	(171)	46:11.5	77.78	276.9	RND	8/4/2000	(217)	19:57.1	38.84	281.5
SLM	6/14/2000	(166)	55:32.6	74.99	278.8	RND	6/7/2000	(159)	58:08.8	75.99	302.8
SLM	6/10/2000	(162)	33:59.7	68.78	281.1	RND	1/26/2001	(026)	28:58.8	87.90	324.6
SLM	8/4/2000	(217)	19:57.1	38.85	281.4	RND	2/25/2001	(056)	32:49.8	75.29	327.9
SLM	6/7/2000	(159)	58:08.6	75.95	302.8	RND	12/6/2000	(341)	22:16.4	75.32	341.4
SLM	6/6/2000	(158)	53:05.2	75.79	358.6	RND	11/25/2000	(330)	21:57.1	75.35	345.2
RND	8/28/1999	(240)	51:38.7	82.92	107.4	RND	6/6/2000	(158)	53:05.7	75.89	358.6
RND	8/20/1999	(232)	13:05.8	70.76	109.0	GOO	6/17/2000	(169)	48:44.4	47.28	27.8
RND	7/11/1999	(192)	24:12.5	62.93	109.8	GOO	9/28/2000	(272)	35:24.6	80.77	109.3
RND	7/21/2000	(203)	04:12.9	69.93	109.9	GOO	6/23/2001	(174)	46:17.5	98.21	110.0
RND	6/23/2001	(174)	46:17.0	98.10	110.4	GOO	7/4/2001	(185)	18:28.4	87.66	205.4
RND	1/13/2001	(013)	43:37.3	65.25	111.4	GOO	4/28/2001	(118)	01:15.2	84.12	206.3
RND	5/20/2001	(140)	30:32.0	53.77	124.8	GOO	8/27/2000	(240)	33:29.9	84.03	208.5
RND	6/3/2001	(154)	54:33.7	96.02	205.7	GOO	6/14/2000	(166)	13:18.5	85.49	212.8
RND	7/4/2001	(185)	18:29.6	87.90	205.7	GOO	2/28/2001	(059)	18:05.3	91.00	217.1
RND	4/28/2001	(118)	01:16.4	84.36	206.7	GOO	1/9/2001	(009)	01:22.4	85.10	221.9
RND	5/19/2001	(139)	47:56.0	86.28	206.9	GOO	5/9/2001	(129)	50:12.0	82.65	229.0
RND	5/26/2001	(146)	08:55.2	86.72	207.1	GOO	4/19/2001	(109)	52:25.2	81.81	234.9
RND	12/18/2000	(353)	30:35.1	87.85	208.1	GOO	11/16/2000	(321)	53:57.1	80.87	238.4
RND	9/2/2000	(246)	13:23.1	86.78	208.3	GOO	11/18/2000	(323)	06:41.4	81.38	239.7
RND	9/14/2000	(258)	11:47.8	82.80	210.3	GOO	11/16/2000	(321)	06:32.4	80.07	239.8
RND	8/9/2000	(222)	20:47.2	85.84	221.3	GOO	6/30/2001	(181)	46:27.0	84.44	243.8
RND	10/4/2000	(278)	10:52.0	85.90	222.4	GOO	7/22/2001	(203)	27:32.4	89.42	257.3
RND	4/19/2001	(109)	55:31.6	82.09	235.4	GOO	8/7/2000	(220)	45:40.3	95.08	264.5
RND	6/1/2001	(152)	48:44.0	82.25	236.3	GOO	6/25/2000	(177)	44:03.6	57.84	276.4
RND	12/6/2000	(341)	09:18.1	80.32	239.5	GOO	3/24/2001	(083)	36:47.6	54.79	277.1
RND	7/26/1999	(207)	44:59.7	81.49	239.9	GOO	10/6/2000	(280)	39:08.5	53.37	277.5
RND	11/17/2000	(322)	13:42.0	81.87	239.9	GOO	7/18/2000	(200)	10:18.5	74.05	278.2
RND	11/16/2000	(321)	06:33.7	80.32	240.1	GOO	7/16/2000	(198)	32:31.9	71.41	278.3
RND	8/26/1999	(238)	51:17.3	82.50	246.3	GOO	6/10/2000	(162)	33:58.8	68.63	280.8
RND	8/12/2000	(225)	38:22.6	86.13	255.2	GOO	8/4/2000	(217)	19:55.9	38.70	281.4
RND	6/15/2001	(166)	27:30.1	61.75	255.2	GOO	6/6/2000	(158)	09:15.0	64.36	302.1

sta	date	ordinal day	time	delta	seaz	sta	date	ordinal day	time	delta	seaz
GOO	1/26/2001	(026)	28:59.0	87.94	324.3	HURN	6/5/2001	(156)	12:09.6	84.79	243.6
GOO	2/25/2001	(056)	32:50.1	75.34	327.6	HURN	6/5/2001	(156)	26:02.2	84.72	243.7
GOO	12/6/2000	(341)	22:17.0	75.43	341.0	HURN	8/26/1999	(238)	51:14.8	82.03	245.7
GOO	11/25/2000	(330)	20:19.3	75.40	345.0	HURN	3/3/2000	(063)	34:49.6	85.79	246.0
HURN	6/7/1999	(158)	43:14.5	42.90	10.4	HURN	12/19/2000	(354)	22:16.6	68.59	253.3
HURN	6/7/1999	(158)	18:01.8	42.93	10.5	HURN	6/14/2001	(165)	41:10.6	61.38	254.9
HURN	5/21/2000	(142)	06:17.9	43.19	17.1	HURN	6/4/2001	(155)	50:51.4	63.37	254.9
HURN	7/13/2001	(194)	59:09.8	71.48	62.6	HURN	10/10/1999	(283)	15:08.7	85.53	256.7
HURN	8/28/1999	(240)	51:39.8	83.12	106.7	HURN	8/27/2000	(240)	28:30.4	59.76	259.6
HURN	8/20/1999	(232)	13:07.0	70.95	108.1	HURN	9/10/2000	(254)	18:26.7	86.95	261.5
HURN	7/21/2000	(203)	04:14.0	70.11	109.1	HURN	8/28/2000	(241)	18:18.0	90.50	261.9
HURN	1/13/2001	(013)	43:38.4	65.42	110.5	HURN	8/28/2000	(241)	42:01.2	90.67	262.2
HURN	3/12/2000	(072)	31:14.2	62.09	113.3	HURN	1/28/2000	(028)	29:46.3	95.63	264.6
HURN	7/21/2000	(203)	22:43.5	56.34	118.1	HURN	2/24/2001	(055)	45:50.4	85.88	265.3
HURN	12/29/1999	(363)	28:43.6	55.50	120.8	HURN	6/23/2000	(175)	13:58.2	86.20	265.3
HURN	8/9/2000	(222)	50:44.5	55.13	122.0	HURN	2/24/2001	(055)	35:55.8	86.21	265.4
HURN	4/29/2001	(119)	35:47.0	53.85	123.9	HURN	5/4/2000	(125)	33:41.0	89.54	266.7
HURN	8/21/1999	(233)	10:09.7	85.53	202.6	HURN	1/1/2001	(001)	08:45.6	81.05	267.6
HURN	4/16/2000	(107)	37:40.5	83.86	202.9	HURN	7/30/2000	(212)	34:22.3	51.72	270.9
HURN	6/16/2001	(167)	25:17.9	80.05	203.3	HURN	7/8/2000	(190)	06:21.1	51.70	271.3
HURN	8/17/2000	(230)	16:41.9	87.20	203.3	HURN	8/18/2000	(231)	00:56.5	51.62	271.3
HURN	9/26/2000	(270)	29:38.1	82.41	203.4	HURN	7/15/2000	(197)	39:05.0	51.42	271.3
HURN	1/26/2000	(026)	38:39.4	82.51	203.4	HURN	6/24/2001	(175)	25:46.2	39.24	271.4
HURN	5/7/2000	(128)	59:17.4	80.44	203.5	HURN	6/15/2000	(167)	20:14.8	58.86	274.4
HURN	12/7/1999	(341)	41:19.3	81.18	203.7	HURN	6/6/2000	(158)	06:29.1	59.11	275.0
HURN	1/8/2000	(008)	58:50.6	82.22	203.7	HURN	6/25/2000	(177)	44:02.7	57.71	276.3
HURN	7/19/2001	(200)	23:41.4	82.34	204.1	HURN	6/6/2000	(158)	25:14.3	51.06	276.4
HURN	7/4/2001	(185)	18:27.1	87.38	205.1	HURN	3/24/2001	(083)	36:46.7	54.67	277.0
HURN	6/3/2001	(154)	54:31.4	95.51	205.1	HURN	10/6/2000	(280)	39:07.6	53.24	277.4
HURN	8/15/2000	(228)	42:32.2	97.63	206.0	HURN	2/26/2001	(057)	04:42.6	39.04	277.5
HURN	4/28/2001	(118)	01:13.8	83.85	206.0	HURN	7/18/2000	(200)	10:17.9	73.93	278.0
HURN	5/19/2001	(139)	47:53.5	85.76	206.2	HURN	7/16/2000	(198)	32:31.2	71.30	278.1
HURN	1/17/2000	(017)	29:42.8	80.51	207.4	HURN	1/28/2000	(028)	49:13.9	65.11	279.0
HURN	9/2/2000	(246)	13:20.7	86.26	207.6	HURN	6/14/2001	(165)	45:48.3	67.57	280.3
HURN	9/14/2000	(258)	11:45.1	82.28	209.6	HURN	6/10/2000	(162)	33:58.1	68.52	280.6
HURN	7/31/2000	(213)	56:32.9	84.46	214.3	HURN	8/4/2000	(217)	19:55.0	38.59	281.4
HURN	11/26/1999	(330)	33:21.7	85.94	220.2	HURN	6/7/2000	(159)	58:08.4	75.92	302.3
HURN	8/22/1999	(234)	52:50.5	85.70	220.5	HURN	1/26/2001	(026)	28:59.5	88.04	324.0
HURN	8/9/2000	(222)	20:44.6	85.31	220.7	HURN	11/8/1999	(312)	56:30.9	75.27	327.1
HURN	10/4/2000	(278)	10:49.4	85.38	221.7	HURN	7/17/2000	(199)	04:46.1	75.58	327.3
HURN	7/16/2000	(198)	37:13.0	82.64	223.1	HURN	5/12/2000	(133)	21:33.9	75.93	327.4
HURN	6/10/2000	(162)	29:38.7	81.81	223.6	HURN	12/6/2000	(341)	22:17.9	75.59	340.8
HURN	5/6/2000	(127)	56:02.5	81.92	224.4	HURN	11/25/2000	(330)	21:58.8	75.65	344.7
HURN	1/5/2000	(005)	52:26.7	82.01	224.4	HURN	6/6/2000	(158)	53:08.0	76.29	358.0
HURN	5/9/2001	(129)	50:10.6	82.39	228.7	PYY	7/9/2000	(191)	54:14.1	82.09	207.1
HURN	4/19/2001	(109)	10:11.7	81.45	234.7	PYY	6/14/2000	(166)	27:00.5	92.06	208.8
HURN	4/19/2001	(109)	55:28.9	81.59	234.7	PYY	6/9/2000	(161)	40:01.7	55.30	270.1
HURN	5/29/2001	(149)	49:06.1	81.53	235.6	PYY	6/3/2000	(155)	03:05.3	49.80	271.1
HURN	6/1/2001	(152)	48:41.3	81.74	235.7	PYY	7/15/2000	(197)	39:04.7	51.38	271.3
HURN	8/14/2000	(227)	23:17.4	84.16	235.8	PYY	6/15/2000	(167)	20:14.5	58.82	274.3
HURN	10/29/2000	(303)	48:41.3	79.86	237.5	PYY	6/6/2000	(158)	25:14.0	51.02	276.4
HURN	7/8/2001	(189)	06:09.9	82.32	238.5	PYY	7/16/2000	(198)	32:31.0	71.26	278.0
HURN	6/9/2000	(161)	38:54.8	80.70	238.8	PYY	6/10/2000	(162)	33:57.9	68.49	280.6
HURN	11/17/2000	(322)	13:39.4	81.37	239.3	PYY	6/7/2000	(159)	58:08.4	75.93	302.2
HURN	11/18/2000	(323)	06:40.1	81.13	239.4	PYY	7/17/2000	(199)	04:46.4	75.63	327.2
HURN	11/16/2000	(321)	06:31.1	79.83	239.5	MHR	11/8/2000	(313)	11:11.9	75.60	102.9
HURN	2/6/2000	(037)	45:38.9	82.05	240.0	MHR	12/12/2000	(347)	37:53.1	74.39	107.9
HURN	11/17/1999	(321)	39:32.1	82.98	241.8	MHR	1/13/2001	(013)	43:38.8	65.48	110.2
HURN	6/30/2001	(181)	46:25.8	84.21	243.5	MHR	6/10/2000	(162)	01:35.7	82.39	201.8

sta	date	ordinal day	time	delta	seaz	sta	date	ordinal day	time	delta	seaz
MHR	11/9/2000	(314)	57:29.9	80.42	203.0	BYR	7/13/2001	(194)	59:12.2	71.87	62.0
MHR	8/17/2000	(230)	16:41.0	87.02	203.0	BYR	8/20/1999	(232)	13:08.1	71.13	107.5
MHR	9/26/2000	(270)	29:37.2	82.23	203.2	BYR	7/11/1999	(192)	24:14.9	63.28	108.1
MHR	7/19/2001	(200)	23:40.5	82.17	203.9	BYR	1/13/2001	(013)	43:39.4	65.58	109.8
MHR	6/3/2001	(154)	54:30.6	95.34	204.8	BYR	6/6/1999	(157)	18:04.6	63.92	111.4
MHR	7/31/2001	(212)	08:40.0	83.70	207.7	BYR	6/15/1999	(166)	51:13.8	57.08	115.8
MHR	9/14/2000	(258)	11:44.2	82.10	209.4	BYR	9/30/1999	(273)	40:41.0	59.38	116.5
MHR	6/14/2000	(166)	13:16.2	85.03	212.2	BYR	12/29/1999	(363)	28:44.2	55.58	120.0
MHR	11/16/2000	(321)	53:54.8	80.44	237.9	BYR	6/21/1999	(172)	52:01.5	55.47	120.1
MHR	6/9/2000	(161)	38:53.9	80.53	238.5	BYR	4/29/2001	(119)	35:47.5	53.92	123.0
MHR	12/7/2000	(342)	42:53.3	79.68	238.6	BYR	6/10/2000	(162)	01:34.5	82.17	201.5
MHR	12/6/2000	(341)	09:14.4	79.66	238.7	BYR	11/4/1999	(308)	02:02.0	80.38	201.8
MHR	11/17/2000	(322)	13:38.4	81.20	239.0	BYR	8/21/1999	(233)	10:07.7	85.14	202.1
MHR	11/16/2000	(321)	06:30.1	79.65	239.3	BYR	4/16/2000	(107)	37:38.5	83.47	202.3
MHR	6/21/2000	(173)	35:12.0	66.25	254.1	BYR	6/16/1999	(167)	47:39.6	81.77	202.3
MHR	6/14/2001	(165)	41:09.6	61.23	254.7	BYR	1/2/2000	(002)	28:37.0	85.60	202.4
MHR	10/27/2000	(301)	30:31.8	57.60	264.9	BYR	6/16/2001	(167)	25:15.7	79.66	202.7
MHR	2/24/2001	(055)	35:55.1	86.08	265.1	BYR	9/26/2000	(270)	29:36.0	82.01	202.8
MHR	7/4/2001	(185)	56:28.3	52.99	269.5	BYR	9/11/2000	(255)	29:23.2	80.69	202.8
MHR	6/9/2000	(161)	40:01.2	55.23	270.0	BYR	12/7/1999	(341)	41:17.2	80.78	203.1
MHR	2/24/2001	(055)	01:56.5	47.59	270.8	BYR	7/19/1999	(200)	29:46.3	93.91	203.9
MHR	6/29/2000	(181)	38:57.7	51.51	270.9	BYR	7/4/2001	(185)	18:25.2	86.98	204.5
MHR	6/3/2000	(155)	03:04.8	49.73	271.0	BYR	4/28/2001	(118)	01:11.8	83.45	205.5
MHR	7/2/2000	(184)	12:09.8	51.53	271.1	BYR	5/19/2001	(139)	47:51.5	85.36	205.6
MHR	7/1/2000	(183)	10:30.2	51.45	271.3	BYR	6/26/1999	(177)	16:25.1	83.59	206.7
MHR	8/19/2000	(232)	33:25.7	40.03	272.1	BYR	12/18/2000	(353)	30:30.8	86.93	206.8
MHR	10/3/2000	(277)	21:09.4	44.66	272.4	BYR	1/17/2000	(017)	29:40.6	80.11	206.9
MHR	6/15/2000	(167)	20:14.1	58.75	274.2	BYR	1/15/2000	(015)	00:54.7	86.99	206.9
MHR	6/6/2000	(158)	06:28.4	59.01	274.9	BYR	9/2/2000	(246)	13:18.8	85.85	207.1
MHR	6/25/2000	(177)	44:02.0	57.61	276.1	BYR	8/27/2000	(240)	33:26.6	83.35	207.6
MHR	6/6/2000	(158)	25:13.5	50.95	276.3	BYR	7/18/1999	(199)	45:23.7	88.57	207.8
MHR	10/6/2000	(280)	39:06.9	53.15	277.3	BYR	9/14/2000	(258)	11:43.0	81.87	209.1
MHR	2/26/2001	(057)	04:41.8	38.94	277.4	BYR	11/26/1999	(330)	33:19.6	85.52	219.7
MHR	6/13/2001	(164)	28:11.9	67.36	279.8	BYR	8/22/1999	(234)	52:48.4	85.28	219.9
MHR	6/7/2000	(159)	58:08.2	75.90	302.1	BYR	8/9/2000	(222)	20:42.5	84.89	220.1
MHR	1/26/2001	(026)	28:59.7	88.08	323.8	BYR	10/4/2000	(278)	10:47.3	84.95	221.2
MHR	2/25/2001	(056)	32:51.0	75.51	327.2	BYR	5/6/2000	(127)	56:00.3	81.50	223.9
MHR	12/6/2000	(341)	22:18.5	75.68	340.6	BYR	5/9/2001	(129)	50:08.4	81.97	228.1
FID	6/17/2000	(169)	48:48.9	47.86	27.1	BYR	4/19/2001	(109)	10:09.5	81.04	234.1
FID	8/9/2000	(222)	50:44.9	55.19	121.3	BYR	4/19/2001	(109)	55:26.7	81.17	234.2
FID	8/17/2000	(230)	16:40.4	86.90	202.9	BYR	5/29/2001	(149)	49:03.9	81.12	235.1
FID	8/27/2000	(240)	33:27.1	83.45	207.7	BYR	6/1/2001	(152)	48:39.1	81.33	235.1
FID	8/9/2000	(222)	07:57.5	84.30	214.1	BYR	8/14/2000	(227)	23:15.3	83.75	235.3
FID	8/9/2000	(222)	20:43.0	85.00	220.2	BYR	7/9/1999	(190)	16:22.3	80.69	235.4
FID	6/9/2000	(161)	38:53.2	80.40	238.4	BYR	10/29/2000	(303)	48:39.1	79.45	237.0
FID	8/27/2000	(240)	28:28.6	59.51	259.3	BYR	11/16/2000	(321)	53:53.6	80.21	237.6
FID	6/23/2000	(175)	13:57.0	85.97	265.0	BYR	7/8/2001	(189)	06:07.8	81.91	238.0
FID	6/9/2000	(161)	40:00.6	55.13	269.9	BYR	6/9/2000	(161)	38:52.6	80.30	238.2
FID	7/27/2000	(209)	58:26.8	51.26	270.9	BYR	12/6/2000	(341)	09:13.2	79.42	238.4
FID	6/3/2000	(155)	03:04.1	49.64	270.9	BYR	7/26/1999	(207)	44:54.9	80.59	238.7
FID	7/8/2000	(190)	06:19.6	51.50	271.0	BYR	11/18/2000	(323)	06:37.9	80.73	238.8
FID	7/27/2000	(209)	21:24.2	51.32	271.0	BYR	11/16/2000	(321)	06:28.9	79.42	239.0
FID	8/18/2000	(231)	00:55.0	51.41	271.0	BYR	2/6/2000	(037)	45:36.8	81.64	239.4
FID	6/25/2000	(177)	44:01.4	57.53	276.0	BYR	6/30/2001	(181)	46:23.8	83.81	243.0
FID	6/6/2000	(158)	25:12.9	50.87	276.2	BYR	6/5/2001	(156)	26:00.2	84.33	243.1
FID	6/7/2000	(159)	58:08.1	75.87	301.9	BYR	8/26/1999	(238)	51:12.8	81.64	245.2
BYR	6/7/1999	(158)	18:04.7	43.29	10.2	BYR	12/19/2000	(354)	22:14.3	68.23	252.8
BYR	5/21/2000	(142)	06:20.9	43.57	16.8	BYR	6/29/2000	(181)	09:24.6	67.19	253.7
BYR	6/21/2000	(173)	59:54.1	47.89	27.2	BYR	6/21/2000	(173)	35:10.7	66.04	253.8

sta	date	ordinal day	time	delta	seaz	sta	date	ordinal day	time	delta	seaz
BYR	8/12/2000	(225)	38:18.7	85.34	254.0	WOLF	6/21/2000	(173)	35:10.5	66.02	253.9
BYR	6/15/2001	(166)	27:24.8	60.96	254.3	WOLF	8/12/2000	(225)	38:18.6	85.31	254.1
BYR	6/21/1999	(172)	46:41.9	72.91	254.4	WOLF	7/15/2000	(197)	25:58.2	92.06	258.7
BYR	6/14/2001	(165)	41:08.2	61.02	254.5	WOLF	8/7/2000	(220)	45:38.1	94.59	263.6
BYR	6/4/2001	(155)	50:49.1	63.01	254.5	WOLF	6/14/2000	(166)	12:29.8	82.32	265.1
BYR	7/22/2001	(203)	27:29.8	88.87	256.5	WOLF	6/9/2000	(161)	40:00.1	55.07	269.9
BYR	3/28/2000	(088)	09:40.5	59.33	259.3	WOLF	6/3/2000	(155)	03:03.7	49.58	271.0
BYR	7/3/2001	(184)	19:50.3	60.28	259.6	WOLF	7/8/2000	(190)	06:19.2	51.44	271.1
BYR	9/10/2000	(254)	18:25.1	86.62	261.0	WOLF	8/18/2000	(231)	00:54.5	51.35	271.1
BYR	8/28/2000	(241)	18:16.5	90.17	261.3	WOLF	7/1/2000	(183)	10:29.1	51.30	271.2
BYR	8/7/2000	(220)	45:38.1	94.59	263.6	WOLF	6/15/2000	(167)	20:13.1	58.62	274.1
BYR	7/3/1999	(184)	38:45.4	57.35	264.7	WOLF	6/6/2000	(158)	06:27.5	58.88	274.7
BYR	7/31/2001	(212)	23:22.9	85.58	264.8	WOLF	6/6/2000	(158)	25:12.6	50.83	276.3
BYR	2/24/2001	(055)	35:54.2	85.90	264.8	WOLF	6/10/2000	(162)	33:56.9	68.33	280.3
BYR	8/4/2001	(216)	56:51.0	84.19	264.9	WOLF	6/7/2000	(159)	58:08.4	75.92	301.9
BYR	6/14/2000	(166)	12:29.8	82.32	265.0	TCE	6/17/2000	(169)	48:52.4	48.31	26.8
BYR	8/6/2000	(219)	35:38.3	55.61	267.1	TCE	6/21/2000	(173)	59:56.8	48.24	27.0
BYR	1/1/2001	(001)	08:44.1	80.75	267.1	TCE	7/21/2000	(203)	04:14.5	70.20	108.2
BYR	6/9/2000	(161)	40:00.1	55.06	269.8	TCE	8/9/2000	(222)	50:43.9	55.05	120.8
BYR	7/30/2000	(212)	34:20.1	51.44	270.6	TCE	8/17/2000	(230)	16:38.2	86.44	202.6
BYR	7/30/2000	(212)	26:35.0	51.42	270.7	TCE	8/2/2000	(215)	48:47.5	82.57	203.5
BYR	7/27/2000	(209)	58:26.2	51.18	270.8	TCE	9/3/2000	(247)	32:51.7	85.69	205.7
BYR	7/7/1999	(188)	58:50.0	31.99	270.9	TCE	8/27/2000	(240)	33:24.8	83.00	207.5
BYR	7/8/2000	(190)	06:19.1	51.43	271.0	TCE	6/14/2000	(166)	13:13.3	84.46	211.8
BYR	7/27/2000	(209)	21:23.7	51.24	271.0	TCE	8/9/2000	(222)	07:55.3	83.87	213.9
BYR	7/15/2000	(197)	39:02.9	51.14	271.0	TCE	8/9/2000	(222)	20:40.9	84.58	220.0
BYR	7/1/2000	(183)	10:29.0	51.28	271.1	TCE	7/16/2000	(198)	37:09.2	81.91	222.5
BYR	7/20/2000	(202)	47:26.3	48.54	271.1	TCE	8/12/2000	(225)	38:18.0	85.20	254.0
BYR	6/24/2001	(175)	25:43.8	38.97	271.2	TCE	6/9/2000	(161)	39:59.8	55.02	270.0
BYR	5/25/2001	(145)	47:42.8	38.96	271.4	TCE	7/30/2000	(212)	34:19.9	51.40	270.8
BYR	1/28/2000	(028)	28:10.7	40.62	271.6	TCE	7/30/2000	(212)	26:34.8	51.39	270.9
BYR	8/15/2000	(228)	27:49.8	40.65	271.6	TCE	6/29/2000	(181)	38:56.2	51.31	271.0
BYR	9/18/1999	(261)	34:03.2	29.70	271.9	TCE	7/27/2000	(209)	58:26.0	51.15	271.1
BYR	8/19/2000	(232)	33:24.4	39.87	272.0	TCE	6/3/2000	(155)	03:03.3	49.54	271.1
BYR	6/15/2000	(167)	20:13.0	58.60	274.0	TCE	7/8/2000	(190)	06:18.8	51.39	271.2
BYR	8/7/2000	(220)	33:08.4	59.29	274.6	TCE	7/15/2000	(197)	39:02.7	51.11	271.3
BYR	6/6/2000	(158)	06:27.3	58.85	274.6	TCE	7/1/2000	(183)	10:28.8	51.25	271.3
BYR	6/6/2000	(158)	25:12.4	50.81	276.1	TCE	7/20/2000	(202)	47:26.0	48.51	271.4
BYR	10/6/2000	(280)	39:05.8	53.00	277.1	TCE	9/3/2000	(247)	08:35.7	40.64	272.0
BYR	12/11/1999	(345)	14:50.1	76.04	277.4	TCE	8/19/2000	(232)	33:24.2	39.85	272.4
BYR	7/16/2000	(198)	32:29.7	71.06	277.6	TCE	6/15/2000	(167)	20:12.9	58.59	274.2
BYR	8/26/1999	(238)	49:04.1	72.45	277.8	TCE	6/6/2000	(158)	06:27.3	58.85	274.8
BYR	6/13/2001	(164)	28:11.0	67.23	279.6	TCE	6/6/2000	(158)	25:12.4	50.81	276.4
BYR	11/1/1999	(305)	03:29.4	68.57	279.7	TCE	7/16/2000	(198)	32:29.8	71.07	277.7
BYR	9/26/1999	(269)	03:18.8	68.42	280.2	TCE	6/14/2000	(166)	55:29.7	74.48	277.8
BYR	6/10/2000	(162)	33:56.7	68.29	280.2	TCE	6/10/2000	(162)	33:56.9	68.32	280.3
BYR	7/28/2000	(210)	38:43.2	68.86	280.2	TCE	6/7/2000	(159)	58:08.9	76.01	301.8
BYR	8/4/2000	(217)	19:53.2	38.37	281.3	TCE	6/6/2000	(158)	53:11.8	76.96	357.4
BYR	6/7/2000	(159)	58:07.9	75.85	301.8	PVE	6/9/2000	(161)	39:58.6	54.86	269.6
BYR	1/26/2001	(026)	28:59.8	88.12	323.4	PVE	6/29/2000	(181)	38:54.9	51.14	270.6
BYR	7/17/2000	(199)	04:46.7	75.68	326.8	PVE	6/3/2000	(155)	03:02.1	49.37	270.8
BYR	2/25/2001	(056)	32:51.3	75.56	326.9	PVE	7/1/2000	(183)	10:27.5	51.09	271.0
BYR	5/12/2000	(133)	21:34.5	76.04	326.9	PVE	6/15/2000	(167)	20:11.7	58.42	273.9
BYR	12/6/2000	(341)	22:19.1	75.79	340.3	PVE	6/6/2000	(158)	06:26.1	58.68	274.5
WOLF	6/21/2000	(173)	59:55.0	48.00	27.1	PVE	6/6/2000	(158)	25:11.2	50.64	276.0
WOLF	9/28/2000	(272)	35:25.6	80.96	108.3	PVE	6/10/2000	(162)	33:55.9	68.16	280.0
WOLF	8/17/2000	(230)	16:39.4	86.69	202.7	PVW	7/21/2000	(203)	57:09.4	70.67	107.7
WOLF	6/14/2000	(166)	13:14.5	84.69	211.9	PVW	7/21/2000	(203)	04:16.3	70.48	107.8
WOLF	8/9/2000	(222)	20:42.0	84.80	220.1	PVW	1/13/2001	(013)	43:40.7	65.78	109.2

sta	date	ordinal day	time	delta	seaz	sta	date	ordinal day	time	delta	seaz
PVW	7/21/2000	(203)	22:45.4	56.61	116.6	SBL	8/9/2000	(222)	50:47.9	55.61	121.6
PVW	8/9/2000	(222)	50:46.1	55.36	120.4	SBL	6/16/2001	(167)	25:19.6	80.38	202.7
PVW	9/26/2000	(270)	29:34.7	81.76	202.3	SBL	7/8/2001	(189)	06:10.0	82.34	237.9
PVW	7/4/2001	(185)	18:24.0	86.73	204.0	SBL	6/15/2001	(166)	27:26.3	61.19	253.9
PVW	8/9/2000	(222)	07:55.6	83.92	213.4	SBL	6/14/2001	(165)	41:09.7	61.24	254.1
PVW	10/4/2000	(278)	10:45.8	84.66	220.7	SBL	10/6/2000	(280)	39:05.2	52.92	276.6
PVW	10/29/2000	(303)	48:37.4	79.15	236.5	EFS	5/20/2001	(140)	30:35.1	54.19	123.9
PVW	7/8/2001	(189)	06:06.1	81.60	237.4	EFS	9/14/2000	(258)	11:47.4	82.72	209.4
PVW	12/6/2000	(341)	09:11.5	79.11	237.8	EFS	5/9/2001	(129)	50:12.2	82.70	228.5
PVW	6/29/2000	(181)	09:22.7	66.90	253.2	SAN	6/21/2000	(173)	59:45.8	46.82	28.0
PVW	6/21/2000	(173)	35:08.8	65.75	253.3	SAN	11/8/2000	(313)	11:12.1	75.63	103.5
PVW	8/12/2000	(225)	38:17.2	85.04	253.5	SAN	8/13/2000	(226)	14:41.1	68.91	105.9
PVW	7/22/2001	(203)	27:28.4	88.58	256.0	SAN	9/28/2000	(272)	35:26.0	81.02	109.2
PVW	8/27/2000	(240)	28:26.1	59.13	258.8	SAN	7/21/2000	(203)	57:08.2	70.48	109.4
PVW	7/3/2001	(184)	19:48.3	59.99	259.2	SAN	7/21/2000	(203)	04:15.1	70.30	109.4
PVW	9/10/2000	(254)	18:23.7	86.33	260.5	SAN	6/23/2001	(174)	46:18.7	98.46	109.8
PVW	8/28/2000	(241)	18:15.1	89.88	260.8	SAN	7/21/2000	(203)	22:45.6	56.63	118.7
PVW	8/28/2000	(241)	41:58.4	90.06	261.2	SAN	8/9/2000	(222)	50:46.9	55.47	122.5
PVW	8/7/2000	(220)	45:36.9	94.31	263.1	SAN	5/20/2001	(140)	30:35.0	54.17	124.3
PVW	2/24/2001	(055)	35:52.9	85.62	264.3	SAN	4/29/2001	(119)	35:49.7	54.21	124.5
PVW	8/4/2001	(216)	56:49.6	83.92	264.4	SAN	6/16/2001	(167)	25:21.6	80.74	203.3
PVW	1/1/2001	(001)	08:42.6	80.48	266.6	SAN	6/3/2001	(154)	54:34.5	96.19	205.2
PVW	8/6/2000	(219)	35:36.4	55.34	266.7	SAN	8/9/2000	(222)	20:47.5	85.90	220.7
PVW	7/4/2001	(185)	56:25.1	52.55	268.9	SAN	10/4/2000	(278)	10:52.3	85.95	221.8
PVW	7/30/2000	(212)	34:18.2	51.17	270.2	SAN	6/1/2001	(152)	48:43.7	82.20	235.7
PVW	2/24/2001	(055)	01:53.1	47.17	270.3	SAN	10/29/2000	(303)	48:43.6	80.30	237.5
PVW	7/30/2000	(212)	26:33.1	51.16	270.3	SAN	11/17/2000	(322)	13:41.6	81.79	239.3
PVW	6/29/2000	(181)	38:54.5	51.08	270.4	SAN	8/12/2000	(225)	38:21.7	85.94	254.6
PVW	7/8/2000	(190)	06:17.1	51.16	270.6	SAN	6/14/2001	(165)	41:12.3	61.62	254.7
PVW	8/18/2000	(231)	00:52.4	51.08	270.6	SAN	8/7/2000	(220)	45:40.1	95.04	264.4
PVW	7/1/2000	(183)	10:27.0	51.02	270.7	SAN	2/24/2001	(055)	35:56.3	86.33	265.4
PVW	7/20/2000	(202)	47:24.2	48.28	270.8	SAN	7/8/2000	(190)	06:21.5	51.75	270.8
PVW	6/19/2000	(171)	10:38.9	74.44	277.0	SAN	8/18/2000	(231)	00:56.8	51.66	270.8
PVW	7/16/2000	(198)	32:28.3	70.82	277.2	SAN	5/25/2001	(145)	47:45.4	39.28	270.8
PVW	8/4/2000	(217)	19:51.2	38.15	281.0	SAN	7/23/2000	(205)	01:21.1	51.69	270.9
PVW	8/5/2001	(217)	28:36.9	90.50	298.4	SAN	1/3/2001	(003)	54:48.8	39.80	271.0
PVW	1/26/2001	(026)	28:59.7	88.09	322.9	SAN	11/13/2000	(318)	04:41.3	42.30	272.4
PVW	7/17/2000	(199)	04:46.7	75.67	326.4	SAN	10/6/2000	(280)	39:07.3	53.21	277.0
PVW	12/6/2000	(341)	22:19.4	75.85	339.9	SAN	7/16/2000	(198)	32:30.9	71.25	278.0
WON	6/21/2000	(173)	59:49.8	47.33	27.2	DH1	7/21/2000	(203)	04:11.6	69.72	110.4
WON	9/26/2000	(270)	29:39.2	82.62	202.2	DH1	2/13/2001	(044)	32:11.0	64.36	111.9
WON	9/11/2000	(255)	29:26.5	81.30	202.2	DH1	1/13/2001	(013)	43:35.9	65.04	111.9
WON	8/2/2000	(215)	48:52.4	83.53	202.9	DH1	7/21/2000	(203)	22:41.4	56.03	119.6
WON	4/28/2001	(118)	01:14.7	84.03	204.9	DH1	5/20/2001	(140)	30:30.6	53.57	125.3
WON	1/9/2001	(009)	01:20.9	84.81	220.5	DH1	4/29/2001	(119)	35:45.3	53.61	125.4
WON	4/19/2001	(109)	55:27.9	81.40	233.5	DH1	9/11/2000	(255)	29:28.3	81.65	204.6
WON	11/16/2000	(321)	53:54.6	80.39	236.9	DH1	7/19/2001	(200)	23:44.4	82.91	205.3
WON	11/16/2000	(321)	06:29.8	79.58	238.3	DH1	6/3/2001	(154)	54:34.0	96.09	206.1
WON	6/14/2001	(165)	41:07.8	60.96	253.5	DH1	4/28/2001	(118)	01:16.7	84.43	207.2
WON	7/3/2001	(184)	19:49.4	60.15	258.6	DH1	5/19/2001	(139)	47:56.3	86.34	207.3
WON	8/7/2000	(220)	45:37.3	94.40	263.1	DH1	5/26/2001	(146)	08:55.5	86.79	207.5
WON	6/24/2001	(175)	25:41.4	38.68	269.7	DH1	9/2/2000	(246)	13:23.5	86.85	208.8
WON	9/3/2000	(247)	08:33.5	40.37	270.1	DH1	9/14/2000	(258)	11:48.2	82.88	210.8
WON	8/15/2000	(228)	27:47.4	40.36	270.2	DH1	2/14/2001	(045)	29:15.8	87.27	212.0
WON	8/19/2000	(232)	33:21.9	39.57	270.5	DH1	1/9/2001	(009)	01:24.2	85.48	222.7
WON	8/13/2001	(225)	18:56.1	43.94	272.3	DH1	10/4/2000	(278)	10:52.6	86.02	222.8
WON	8/4/2000	(217)	19:49.6	37.96	279.8	DH1	11/15/2000	(320)	39:17.7	85.33	223.3
SBL	6/21/2000	(173)	59:48.7	47.19	27.5	DH1	7/16/2000	(198)	37:16.3	83.29	224.2
SBL	7/21/2000	(203)	22:46.7	56.79	117.8	DH1	8/3/2000	(216)	21:29.7	82.96	224.3

sta	date	ordinal day	time	delta	seaz
DH1	12/22/2000	(357)	42:27.1	82.28	226.9
DH1	5/9/2001	(129)	50:14.0	83.05	229.8
DH1	4/19/2001	(109)	52:27.4	82.22	235.7
DH1	4/19/2001	(109)	10:15.2	82.12	235.8
DH1	4/19/2001	(109)	55:32.4	82.25	235.8
DH1	8/14/2000	(227)	23:20.7	84.82	236.9
DH1	10/29/2000	(303)	48:44.9	80.53	238.6
DH1	11/18/2000	(323)	17:30.1	81.13	239.2
DH1	11/16/2000	(321)	53:59.3	81.28	239.2
DH1	7/8/2001	(189)	06:13.4	82.98	239.6
DH1	11/21/2000	(326)	45:20.0	81.88	240.0
DH1	11/17/2000	(322)	13:42.9	82.04	240.3
DH1	11/18/2000	(323)	06:43.6	81.79	240.5
DH1	11/16/2000	(321)	06:34.7	80.49	240.6
DH1	6/30/2001	(181)	46:29.1	84.87	244.6
DH1	7/3/2001	(184)	19:56.6	61.22	261.0
DH1	9/10/2000	(254)	18:29.5	87.55	262.6
DH1	8/7/2000	(220)	45:42.2	95.49	265.3
DH1	10/27/2000	(301)	30:36.6	58.30	265.9
DH1	2/24/2001	(055)	35:58.6	86.79	266.4
DH1	6/14/2000	(166)	12:34.4	83.21	266.6
DH1	4/14/2001	(104)	36:23.2	54.42	267.1
DH1	8/6/2000	(219)	35:44.4	56.47	268.3
DH1	1/1/2001	(001)	08:48.6	81.61	268.7
DH1	7/4/2001	(185)	56:33.2	53.66	270.4
DH1	7/30/2000	(212)	34:26.3	52.26	271.7
DH1	7/30/2000	(212)	26:41.2	52.25	271.8
DH1	6/29/2000	(181)	39:02.6	52.16	271.8
DH1	7/27/2000	(209)	58:32.4	52.01	271.9
DH1	7/8/2000	(190)	06:25.2	52.25	272.0
DH1	8/18/2000	(231)	01:00.5	52.16	272.0
DH1	7/23/2000	(205)	01:24.8	52.19	272.1
DH1	7/15/2000	(197)	39:09.1	51.96	272.1
DH1	7/20/2000	(202)	47:32.5	49.36	272.1
DH1	7/1/2000	(183)	10:35.1	52.10	272.2
DH1	8/13/2001	(225)	19:04.9	45.05	274.6
DH1	6/15/2000	(167)	20:18.4	59.38	275.2
DH1	6/25/2000	(177)	44:06.3	58.22	277.1
DH1	6/6/2000	(158)	25:18.1	51.56	277.1
DH1	3/24/2001	(083)	36:50.3	55.17	277.8
DH1	10/6/2000	(280)	39:11.2	53.74	278.2
DH1	7/18/2000	(200)	10:20.7	74.42	279.0
DH1	7/16/2000	(198)	32:34.2	71.79	279.0
DH1	6/13/2001	(164)	28:15.5	67.93	280.9
DH1	7/28/2000	(210)	38:47.5	69.55	281.6
DH1	1/26/2001	(026)	28:59.5	88.05	325.0
DH2	6/17/2000	(169)	48:41.8	46.95	28.5
DH2	6/21/2000	(173)	59:46.2	46.88	28.6
DH2	8/9/2000	(222)	50:40.8	54.61	124.0
DH2	6/14/2000	(166)	13:20.3	85.87	214.1
DH2	6/15/2000	(167)	20:20.1	59.63	275.7
DH2	6/6/2000	(158)	06:34.4	59.87	276.4
DH2	6/6/2000	(158)	25:19.9	51.81	277.7
DH2	6/10/2000	(162)	34:02.6	69.24	282.0
DH2	6/7/2000	(159)	58:11.3	76.44	303.7
DH3	6/21/2000	(173)	59:46.6	46.93	28.9
DH3	7/21/2000	(203)	04:07.6	69.08	111.4
DH3	6/23/2001	(174)	46:13.2	97.24	111.9
DH3	1/13/2001	(013)	43:31.7	64.40	112.9
DH3	8/17/2000	(230)	16:44.2	87.69	205.5
DH3	9/26/2000	(270)	29:40.7	82.91	205.7
DH3	6/3/2001	(154)	54:33.8	96.04	207.2
DH3	5/26/2001	(146)	08:55.4	86.76	208.7
DH3	12/18/2000	(353)	30:35.3	87.90	209.6
DH3	9/14/2000	(258)	11:48.2	82.88	211.9
DH3	5/29/2001	(149)	49:11.1	82.49	237.9
DH3	6/1/2001	(152)	48:46.3	82.70	238.0
DH3	8/14/2000	(227)	23:22.2	85.11	238.1
DH3	7/16/2000	(198)	50:27.8	86.57	253.8
DH3	6/21/2000	(173)	35:19.9	67.49	256.6
DH3	7/22/2001	(203)	27:36.6	90.32	259.2
DH3	9/10/2000	(254)	18:32.0	88.06	263.7
DH3	8/28/2000	(241)	42:06.4	91.79	264.4
DH3	6/29/2000	(181)	39:06.8	52.74	273.2
DH3	5/25/2001	(145)	47:54.3	40.35	273.7
DH3	3/23/2001	(082)	37:16.9	40.66	273.8
DH3	10/3/2000	(277)	21:19.1	45.89	274.6
DH3	11/13/2000	(318)	04:50.1	43.38	275.1
DH3	7/16/2000	(198)	32:37.8	72.39	280.2
DH3	1/26/2001	(026)	29:02.3	88.65	326.1
DH3	2/25/2001	(056)	32:53.8	76.01	329.3
DH3	12/6/2000	(341)	22:19.7	75.91	342.7
CZN	6/6/2000	(158)	53:07.5	76.20	0.3
CZN	9/2/2000	(246)	13:24.2	87.00	210.4
CZN	7/31/2000	(213)	56:37.3	85.33	217.0
CZN	8/9/2000	(222)	08:03.5	85.48	217.2
CZN	8/9/2000	(222)	20:49.4	86.29	223.4
CZN	7/16/2000	(198)	37:18.2	83.65	225.8
CZN	8/3/2000	(216)	21:31.5	83.32	226.0
CZN	6/10/2000	(162)	29:44.0	82.84	226.4
CZN	8/14/2000	(227)	23:23.3	85.34	238.5
CZN	6/9/2000	(161)	39:01.2	81.92	241.5
CZN	8/12/2000	(225)	38:27.0	87.02	257.2
CZN	9/10/2000	(254)	18:33.1	88.29	264.2
CZN	8/28/2000	(241)	18:24.2	91.84	264.5
CZN	8/28/2000	(241)	42:07.4	92.02	264.9
CZN	8/7/2000	(220)	45:45.6	96.26	266.8
CZN	6/14/2000	(166)	12:38.3	83.98	268.2